

#22

IN THE UNITED STATES PATENT AND TRADEMARK OFFICE

In re PATENT APPLICATION of
Inventor(s): Mills

Appln. No.: 09/008,947

Filing Date: 1/20/1998

Title: HYDRIDE BATTERY AND FUEL CELL

Group Art Unit: 1745

Examiner: Kalafut



RECEIVED
JUN 11 2001
TC 1700

June 8, 2001

**SUBMISSION OF EXPERIMENTAL EVIDENCE FURTHER DEMONSTRATING THE
EXISTENCE OF LOWER-ENERGY HYDROGEN**

Hon. Asst. Commissioner
of Patents and Trademarks
Washington, D.C. 20231

Sir:

Attached is a Rule 132 Declaration of Applicant submitting additional experimental evidence that conclusively demonstrates the existence of lower-energy hydrogen.

Applicant maintains that the Secret Committee of Examiners assigned to prosecute this application has utterly failed to present a prima facie case of non-enablement and/or lack of utility under 35 U.S.C. §§ 101 and 112. To the extent that the Secret Committee raises even a coherent argument addressing these issues, those arguments are completely rebutted by the extensive experimental evidence already of record.

With the present submission, Applicant now goes even further by presenting novel spectral data from hydrogen atoms undergoing a catalyzed transition to lower-energy states. The use of spectral lines to identify hydrogen atoms has been well known for over 100 years. Indeed, spectral data from hydrogen atoms is a basis for

the atomic theories of Bohr, Schrodinger, and Heisenberg. Therefore, Applicant's reliance on such spectral data from hydrogen atoms to confirm the presence of lower-energy hydrogen cannot be summarily dismissed. Applicant demands that this evidence be considered and assigned the same high level of credibility given to the spectral lines used to identify the uncatalyzed energy states of hydrogen.

Applicant's declaration includes an article entitled "Spectral Emission of Fractional Quantum Energy Levels of Atomic Hydrogen from a Helium-Hydrogen Plasma and the Implications for Dark Matter." The extreme ultraviolet spectroscopic data presented in the article conclusively confirm the existence of lower-energy hydrogen having fractional quantum states $H(1/p)$, where p is an integer. The reaction vessel only contained hydrogen atoms and helium catalyst. All of the spectral lines for helium and ordinary hydrogen are well known and documented. The new emission lines shown in the figures included in the article were identified at energies of q 13.6eV, where $q = 1, 2, 3, 4, 6, 7, 8, 9$ and 11. Note that the intensity of the new emission lines increased over time as the concentration of lower-energy hydrogen increased during the reaction in the reaction vessel, thus further confirming the formation of lower-energy hydrogen.

From Table 1 in the article, it is remarkable how closely Applicant's predicted peaks for the energy of reaction for formation of lower-energy hydrogen matched the experimentally observed peaks to three significant figures. From Table 8 in the article, it is remarkable how closely Applicant's predicted peaks for the energy of reaction for formation of lower-energy hydrogen matched the peaks observed from the sun.

The Rule 132 Declaration of Applicant also includes an article entitled "Spectroscopic Identification of a Novel Catalytic Reaction of Potassium and Atomic Hydrogen and the Hydride Ion Product." This article conclusively demonstrates the formation of a hydride ion $H^-(1/4)$, also referred to as a lower-energy hydrogen ion. The novel hydride ion is identified spectroscopically at 110 nm corresponding to its predicted binding energy of 11.2 eV using a highly sophisticated extreme ultraviolet radiation spectrometer. Remarkably, Applicant's predicted binding energy of 11.2 eV

for $H(1/4)$ matched the experimentally measured value to three significant figures.

The extreme ultraviolet spectroscopic data presented and shown in Figure 3 of the article conclusively demonstrates that (1) intense extreme ultraviolet (EUV) emission was observed from atomic hydrogen; and (2) an atomized catalyst formed a plasma in a cell that was only heated to moderate temperatures with no high voltage source. The plasma was fueled by Applicant's novel method of forming lower-energy hydrogen. No emission or plasma was observed in the case of the control noncatalysts.

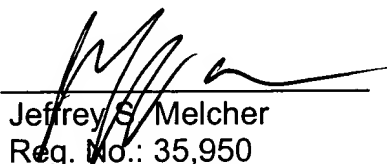
Also enclosed are new chapters for Applicant's textbook, which was previously made of record. The new chapters are "Magnetic Parameters of the electron (Bohr Magneton)," pp. 70-119, and "Atomic Coulomb Field Collapse - Hydrino Theory Blacklight Process," pp. 165-189. These new chapters further demonstrate the accuracy of Applicant's theory, which is a true theory in the sense that an atomic parameter is derived from first principles and then experimentally verified to a high degree of accuracy.

In view of the overwhelming evidence already of record and the conclusive experimental evidence submitted herewith demonstrating the existence of lower-energy hydrogen, it is sincerely believed that the subject application is once again in condition for allowance and Notice to that effect is respectfully requested.

Respectfully submitted,

Manelli Denison & Selter, PLLC

By


Jeffrey S. Melcher
Reg. No.: 35,950
Tel. No.: 202.261.1045
Fax. No.: 202.887.0336

#22.

DECLARATION OF Dr. Randell L. Mills

I, Randell L. Mills, declare and state as follows:

1. I am the founder and CEO of BlackLight Power, Inc., located at 493 Old Trenton Road, Cranbury, New Jersey 08512.
2. I majored in chemistry and received my bachelor of arts degree, *summa cum laude* and Phi Beta Kappa, from Franklin & Marshall College in 1982. I received a medical degree from Harvard Medical School in 1986. While attending Harvard Medical School, I consecutively spent a year taking courses in advanced electrical engineering at the Massachusetts Institute of Technology. I have had significant academic training in biology, chemistry, mathematics and physics.
3. I began my research in the field of energy technology over ten years ago. I have authored, co-authored or collaborated on numerous publications, reports and presentations at scientific meetings in the field of energy technology and novel hydrogen chemistry, as shown in the attachment hereto.
4. I am fully qualified to conduct the research that led to the discovery and development of BlackLight's lower-energy hydrogen technology.
5. I personally conducted and/or supervised the experiments shown in the attached article entitled "Spectral Emission of Fractional Quantum Energy Levels of Atomic Hydrogen from a Helium-Hydrogen Plasma and the Implications for Dark Matter." Dr. Paresh Ray, Dr. Ying Lu, and T. Onuma assisted me in preparing the spectroscopy.

6. Spectral lines have been used for over 100 years to confirm the energy states of the hydrogen atom, which led to the atomic theories of Bohr, Schrodinger, and Heisenberg. The extreme ultraviolet spectroscopic data presented in the attached article conclusively confirm the existence of lower-energy hydrogen having fractional quantum states $H(1/p)$, where p is an integer. The reaction vessel only contained hydrogen and helium catalyst. All of the spectral lines for helium and ordinary hydrogen are well known and documented. The new emission lines shown in the figures included in the article were identified at energies of $q \cdot 13.6\text{eV}$, where $q = 1, 2, 3, 4, 6, 7, 8, 9$ and 11 . The intensity of the new emission lines increased over time as the concentration of lower-energy hydrogen increased during the reaction in the reaction vessel, which again conclusively confirm the existence lower-energy hydrogen.
7. As shown in Table 1 of the attached article, my predicted peaks for the energy of reaction for formation of lower-energy hydrogen closely matched the experimentally observed peaks to a remarkable three significant figures.
8. As shown in Table 8 of the attached article, my predicted peaks for the energy of reaction for formation of lower-energy hydrogen and other such transitions closely matched the peaks observed from the interstellar medium and Sun.
9. I also personally conducted and/or supervised the experiments shown in the attached article entitled "Spectroscopic Identification of a Novel Catalytic Reaction of Potassium and Atomic Hydrogen and the Hydride Ion Product." Dr. Paresh Ray, Dr. Ying Lu, and T. Onuma assisted me in preparing the spectroscopy.

10. The extreme ultraviolet spectroscopic data presented in the attached article and shown in Figure 3 conclusively show that intense extreme ultraviolet (EUV) emission was observed from atomic hydrogen and an atomized catalyst that remarkably formed a plasma in a cell that was only heated to moderate temperatures with no high voltage source. No emission was observed in the case of the control noncatalysts.
11. The extreme ultraviolet spectroscopic data presented in the attached article and shown in Figure 4 conclusively show that emission was observed from K^{3+} that confirmed the resonant nonradiative energy transfer of $3 \cdot 27.2 \text{ eV}$ from atomic hydrogen to atomic potassium catalyst which ionized to K^{3+} .
12. The extreme ultraviolet spectroscopic data presented in the attached article and shown in Figure 8 conclusively show the spectroscopic observation of the predicted $H^-(1/4)$ hydride ion of hydrogen catalysis by potassium catalyst at 110 nm corresponding to its predicted binding energy of 11.2 eV which matches to three significant figures.
13. I declare further that all statements made herein of my own knowledge are true and that all statements made on information and belief are believed to be true; and further that these statements were made with the knowledge that willful false statements and the like so made are punishable by fine or imprisonment, or both, under Section 1001 of Title 18 of the United States Code and that such willful false statements may jeopardize the validity of the application or any patent issuing thereon.

By 
Dr. Randell L. Mills

Date: 6/8/01

Publications:

1. R. Mills, P. Ray, Spectral Emission of Fractional Quantum Energy Levels of Atomic Hydrogen from a Helium-Hydrogen Plasma and the Implications for Dark Matter, Int. J. Hydrogen Energy, submitted.
2. R. Mills, P. Ray, Spectroscopic Identification of a Novel Catalytic Reaction of Potassium and Atomic Hydrogen and the Hydride Ion Product, Int. J. Hydrogen Energy, submitted.
3. R. Mills, "BlackLight Power Technology-A New Clean Hydrogen Energy Source with the Potential for Direct Conversion to Electricity", Proceedings of the National Hydrogen Association, 12 th Annual U.S. Hydrogen Meeting and Exposition, *Hydrogen: The Common Thread*, The Washington Hilton and Towers, Washington DC, (March 6-8, 2001), pp. 671-697.
- ✓ 4. R. Mills, W. Good, A. Voigt, Jinquan Dong, "Minimum Heat of Formation of Potassium Iodo Hydride", Int. J. Hydrogen Energy, in press.
- ✓ 5. R. Mills, "Spectroscopic Identification of a Novel Catalytic Reaction of Atomic Hydrogen and the Hydride Ion Product", Int. J. Hydrogen Energy, in press.
- ✓ 6. R. Mills, N. Greenig, S. Hicks, "Optically Measured Power Balances of Anomalous Discharges of Mixtures of Argon, Hydrogen, and Potassium, Rubidium, Cesium, or Strontium Vapor", Int. J. Hydrogen Energy, in progress.
7. R. Mills, "The Grand Unified Theory of Classical Quantum Mechanics", Global Foundation, Inc. Orbis Scientiae entitled *The Role of Attractive and Repulsive Gravitational Forces in Cosmic Acceleration of Particles The Origin of the Cosmic Gamma Ray Bursts*, (29th Conference on High Energy Physics and Cosmology Since 1964) Dr. Behram N. Kursunoglu, Chairman, December 14-17, 2000, Lago Mar Resort, Fort Lauderdale, FL, in press.
8. R. Mills, "The Grand Unified Theory of Classical Quantum Mechanics", Int. J. Hydrogen Energy, submitted.
9. R. Mills and M. Nansteel, "Anomalous Argon-Hydrogen-Strontium Discharge", IEEE Transactions on Plasma Science, submitted.
- ✓ 10. R. Mills, B. Dhandapani, M. Nansteel, J. He, A. Voigt, "Identification of Compounds Containing Novel Hydride Ions by Nuclear Magnetic Resonance Spectroscopy", Int. J. Hydrogen Energy, in press.
11. R. Mills, "BlackLight Power Technology-A New Clean Energy Source with the Potential for Direct Conversion to Electricity", Global Foundation International Conference on "Global Warming and Energy Policy", Dr. Behram N. Kursunoglu, Chairman, Fort Lauderdale, FL, November 26-28, 2000, in press.

12. R. Mills, The Nature of Free Electrons in Superfluid Helium--a Test of Quantum Mechanics and a Basis to Review its Foundations and Make a Comparison to Classical Theory, Int. J. Hydrogen Energy, in press.
13. R. Mills, M. Nansteel, and Y. Lu, "Anomalous Hydrogen-Strontium Discharge", European Journal of Physics D, submitted.
14. R. Mills, J. Dong, Y. Lu, "Observation of Extreme Ultraviolet Hydrogen Emission from Incandescently Heated Hydrogen Gas with Certain Catalysts", Int. J. Hydrogen Energy, Vol. 25, (2000), pp. 919-943.
- ✓ 15. R. Mills, "Observation of Extreme Ultraviolet Emission from Hydrogen-KI Plasmas Produced by a Hollow Cathode Discharge", Int. J. Hydrogen Energy, Vol. 26, No. 6, (2001), pp. 579-592.
- ✓ 16. R. Mills, "Temporal Behavior of Light-Emission in the Visible Spectral Range from a Ti-K₂CO₃-H-Cell", Int. J. Hydrogen Energy, Vol. 26, No. 4, (2001), pp. 327-332.
- ✓ 17. R. Mills, T. Onuma, and Y. Lu, "Formation of a Hydrogen Plasma from an Incandescently Heated Hydrogen-Catalyst Gas Mixture with an Anomalous Afterglow Duration", Int. J. Hydrogen Energy, in press.
- ✓ 18. R. Mills, M. Nansteel, and Y. Lu, "Observation of Extreme Ultraviolet Hydrogen Emission from Incandescently Heated Hydrogen Gas with Strontium that Produced an Anomalous Optically Measured Power Balance", Int. J. Hydrogen Energy, Vol. 26, No. 4, (2001), pp. 309-326.
19. R. Mills, *The Grand Unified Theory of Classical Quantum Mechanics*, January 2000 Edition, BlackLight Power, Inc., Cranbury, New Jersey, Distributed by Amazon.com.
- ✓ 20. R. Mills, B. Dhandapani, N. Greenig, J. He, "Synthesis and Characterization of Potassium Iodo Hydride", Int. J. of Hydrogen Energy, Vol. 25, Issue 12, December, (2000), pp. 1185-1203.
- ✓ 21. R. Mills, "Novel Inorganic Hydride", Int. J. of Hydrogen Energy, Vol. 25, (2000), pp. 669-683.
- ✓ 22. R. Mills, B. Dhandapani, M. Nansteel, J. He, T. Shannon, A. Echezuria, "Synthesis and Characterization of Novel Hydride Compounds", Int. J. of Hydrogen Energy, Vol. 26, No. 4, (2001), pp. 339-367.
- ✓ 23. R. Mills, "Highly Stable Novel Inorganic Hydrides", Journal of Materials Research, submitted.
- ✓ 24. R. Mills, "Novel Hydrogen Compounds from a Potassium Carbonate Electrolytic Cell", Fusion Technology, Vol. 37, No. 2, March, (2000), pp. 157-182.
25. R. Mills, "The Hydrogen Atom Revisited", Int. J. of Hydrogen Energy, Vol. 25, Issue 12, December, (2000), pp. 1171-1183.
- ✓ 26. Mills, R., Good, W., "Fractional Quantum Energy Levels of Hydrogen", Fusion Technology, Vol. 28, No. 4, November, (1995), pp. 1697-1719.
- ✓ 27. Mills, R., Good, W., Shaubach, R., "Dihydrino Molecule Identification", Fusion Technology, Vol. 25, 103 (1994).

28. R. Mills and S. Kneizys, Fusion Technol. Vol. 20, 65 (1991).

Test Reports:

Numerous test reports are available from BlackLight Power (e.g. V. Noninski, Fusion Technol., Vol. 21, 163 (1992); Niedra, J., Meyers, I., Fralick, G. C., and Baldwin, R., "Replication of the Apparent Excess Heat Effect in a Light Water-Potassium Carbonate-Nickel Electrolytic Cell, NASA Technical Memorandum 107167, February, (1996). pp. 1-20.; Niedra, J., Baldwin, R., Meyers, I., NASA Presentation of Light Water Electrolytic Tests, May 15, 1994; Haldeman, C. W., Savoye, G. W., Iseler, G. W., Clark, H. R., MIT Lincoln Laboratories Excess Energy Cell Final report ACC Project 174 (3), April 25, 1995; Peterson, S., H., Evaluation of Heat Production from Light Water Electrolysis Cells of HydroCatalysis Power Corporation, Report from Westinghouse STC, 1310 Beulah Road, Pittsburgh, PA, February 25, 1994; Craw-Ivanco, M. T.; Tremblay, R. P.; Boniface, H. A.; Hilborn, J. W.; "Calorimetry for a Ni/K₂CO₃ Cell", Atomic Energy Canada Limited, Chemical Engineering Branch, Chalk River Laboratories, Chalk River, Ontario, June 1994; Nesterov, S. B., Kryukov, A. P., Moscow Power Engineering Institute Affidavit, February, 26, 1993; Jacox, M. G., Watts, G. R., "The Search for Excess Heat in the Mills Electrolytic Cell", Idaho National Engineering Laboratory, EG&G Idaho, Inc., Idaho Falls, Idaho, 83415, January 7, 1993; Gernert, N., Shaubach, R. M., Mills, R., Good, W., "Nascent Hydrogen: An Energy Source," Final Report prepared by Thermacore, Inc., for the Aero Propulsion and Power Directorate, Wright Laboratory, Air Force Material Command (ASC), Wright-Patterson Air Force Base, Contract Number F33615-93-C-2326, May, (1994); Phillips, J., Smith, J., Kurtz, S., "Report On Calorimetric Investigations Of Gas-Phase Catalyzed Hydrino Formation" Final report for Period October-December 1996", January 1, 1997, A Confidential Report submitted to BlackLight Power, Inc. provided by BlackLight Power, Inc., Great Valley Corporate Center, 41 Great Valley Parkway, Malvern, PA 19355; B. N. Popov, "Electrochemical Characterization of BlackLight Power, Inc. MH as Electrodes for Li-ion Batteries, Dept. of Chemical Engineering, University of South Carolina, February 6, 2000; Scores of Independent Tests of BlackLight Power's Novel Hydride Compounds from over 20 Independent Testing Laboratories.)

Meetings:

1. R. Mills, J. He, "Spectroscopic Identification of a Novel Catalytic Reaction of Atomic Hydrogen and the Hydride Ion Product", National Hydrogen Association, 12 th Annual U.S. Hydrogen Meeting

- and Exposition, *Hydrogen: The Common Thread*, The Washington Hilton and Towers, Washington DC, (March 6-8, 2001).
2. R. Mills, B. Dhandapani, M. Nansteel, N. Greenig, S. Hicks, J. Dong, "Optically Measured Power Balances of Anomalous Discharges of Mixtures of Argon, Hydrogen, and Potassium, Rubidium, Cesium, or Strontium Vapor", National Hydrogen Association, 12 th Annual U.S. Hydrogen Meeting and Exposition, *Hydrogen: The Common Thread*, The Washington Hilton and Towers, Washington DC, (March 6-8, 2001).
 3. R. Mills, M. Nansteel, N. Greenig, S. Hicks, "BlackLight Power Technology-A New Clean Energy Source with the Potential for Direct Conversion to Electricity", National Hydrogen Association, 12 th Annual U.S. Hydrogen Meeting and Exposition, *Hydrogen: The Common Thread*, The Washington Hilton and Towers, Washington DC, (March 6-8, 2001).
 4. R. Mills, B. Dhandapani, M. Nansteel, J. He, A. Voigt, "Identification of Compounds Containing Novel Hydride Ions by Nuclear Magnetic Resonance Spectroscopy", National Hydrogen Association, 12 th Annual U.S. Hydrogen Meeting and Exposition, *Hydrogen: The Common Thread*, The Washington Hilton and Towers, Washington DC, (March 6-8, 2001).
 5. R. Mills, "BlackLight Power Technology-A New Clean Energy Source with the Potential for Direct Conversion to Electricity", *The 8 th Annual Emerald Groundhog Day Investment Forum*, February 1, 2001, Wyndham Franklin Plaza Hotel, Philadelphia, PA, Organized by Emerald Asset Management, Lancaster, PA.
 6. R. Mills, "The Grand Unified Theory of Classical Quantum Mechanics", Global Foundation, Inc. Orbis Scientiae entitled *The Role of Attractive and Repulsive Gravitational Forces in Cosmic Acceleration of Particles The Origin of the Cosmic Gamma Ray Bursts*, (29th Conference on High Energy Physics and Cosmology Since 1964) Dr. Behram N. Kursunoglu, Chairman, December 14-17, 2000, Lago Mar Resort, Fort Lauderdale, FL.
 7. R. Mills, "BlackLight Power Technology-A New Clean Energy Source with the Potential for Direct Conversion to Electricity", Global Foundation, Inc. conference entitled *Global Warming and Energy Policy*, Fort Lauderdale, FL, November 26-28, 2000.
 8. R. Mills, B. Dhandapani, N. Greenig, J. He, J. Dong, Y. Lu, and H. Conrads, "Formation of an Energetic Plasma and Novel Hydrides from Incandescently Heated Hydrogen Gas with Certain Catalysts", August National ACS Meeting (220th ACS National Meeting, Washington, DC, (August 20-24, 2000)).
 9. R. Mills, J. He, and B. Dhandapani, "Novel Alkali and Alkaline Earth Hydrides", August National ACS Meeting (220th ACS National Meeting, Washington, DC, (August 20-24, 2000)).
 10. R. Mills, B. Dhandapani, N. Greenig, J. He, J. Dong, Y. Lu, and H. Conrads, "Formation of an Energetic Plasma and Novel Hydrides from Incandescently Heated Hydrogen Gas with Certain

- Catalysts", June ACS Meeting (29th Northeast Regional Meeting, University of Connecticut, Storrs, CT, (June 18-21, 2000)).
11. Mills, J. Dong, N. Greenig, and Y. Lu, "Observation of Extreme Ultraviolet Hydrogen Emission from Incandescently Heated Hydrogen Gas with Certain Catalysts", 219 th National ACS Meeting, San Francisco, California, (March 26-30, 2000).
 12. R. Mills, B. Dhandapani, N. Greenig, J. He, J. Dong, Y. Lu, and H. Conrads, "Formation of an Energetic Plasma and Novel Hydrides from Incandescently Heated Hydrogen Gas with Certain Catalysts", 219 th National ACS Meeting, San Francisco, California, (March 26-30, 2000).
 13. R. Mills, "Novel Hydride Compound", 219 th National ACS Meeting, San Francisco, California, (March 26-30, 2000).
 14. R. Mills, J. He, and B. Dhandapani, "Novel Alkali and Alkaline Earth Hydrides", 219 th National ACS Meeting, San Francisco, California, (March 26-30, 2000).
 15. R. Mills, J. Dong, N. Greenig, and Y. Lu, "Observation of Extreme Ultraviolet Hydrogen Emission from Incandescently Heated Hydrogen Gas with Certain Catalysts", National Hydrogen Association, 11 th Annual U.S. Hydrogen Meeting, Vienna, VA, (February 29-March 2, 2000).
 16. R. Mills, B. Dhandapani, N. Greenig, J. He, J. Dong, Y. Lu, and H. Conrads, "Formation of an Energetic Plasma and Novel Hydrides from Incandescently Heated Hydrogen Gas with Certain Catalysts", National Hydrogen Association, 11 th Annual U.S. Hydrogen Meeting, Vienna, VA, (February 29-March 2, 2000).
 17. R. Mills, "Novel Hydride Compound", National Hydrogen Association, 11 th Annual U.S. Hydrogen Meeting, Vienna, VA, (February 29-March 2, 2000).
 18. R. Mills, J. He, and B. Dhandapani, "Novel Alkali and Alkaline Earth Hydrides", National Hydrogen Association, 11 th Annual U.S. Hydrogen Meeting, Vienna, VA, (February 29-March 2, 2000).
 19. R. Mills, J. Dong, Y. Lu, J. Conrads, "Observation of Extreme Ultraviolet Hydrogen Emission from Incandescently Heated Hydrogen Gas with Certain Catalysts", 1999 Pacific Conference on Chemistry and Spectroscopy and the 35th ACS Western Regional Meeting, Ontario Convention Center, California, (October 6-8, 1999).
 20. R. Mills, "Novel Hydride Compound", 1999 Pacific Conference on Chemistry and Spectroscopy and the 35th ACS Western Regional Meeting, Ontario Convention Center, California, (October 6-8, 1999).
 21. R. Mills, B. Dhandapani, N. Greenig, J. He, "Synthesis and Characterization of Potassium Iodo Hydride", 1999 Pacific Conference on Chemistry and Spectroscopy and the 35th ACS Western Regional Meeting, Ontario Convention Center, California, (October 6-8, 1999).

22. R. Mills, J. He, and B. Dhandapani, "Novel Hydrogen Compounds", 1999 Pacific Conference on Chemistry and Spectroscopy and the 35th ACS Western Regional Meeting, Ontario Convention Center, California, (October 6-8, 1999).
23. R. Mills, "Excess Heat Production by the Electrolysis of an Aqueous Potassium Carbonate Electrolyte", August 1991 meeting of the American Chemical Society, NY, NY.

Other Mills publications:

A Novel Cancer Therapy Using a Mossbauer-Isotope Compound, Randell L. Mills, Carl W. Walter, Lata Venkataraman, Kevin Pang, John Farrell, *Nature*, 336,787, (1988).

On the Potentialities of Nuclear Gamma Resonance (Mossbauer Effect) Spectroscopy as a New, Low Dose Approach to Cancer Radiation Therapy, W.M. Reiff, R.L. Mills, J.J. Farrell, The Proceedings of the International Conference on the Applications of the Mossbauer Effect, ICAME 1989, Budapest, Hungary (Hyperfine Interactions 1990).

Spectral Emission of Fractional Quantum Energy Levels of Atomic Hydrogen from a Helium-Hydrogen Plasma and the Implications for Dark Matter

Randell L. Mills

Paresh Ray

BlackLight Power, Inc.

493 Old Trenton Road

Cranbury, NJ 08512

ABSTRACT

From a solution of a Schrödinger-type wave equation with a nonradiative boundary condition based on Maxwell's equations, Mills predicts that atomic hydrogen may undergo a catalytic reaction with certain atomized elements and ions which singly or multiply ionize at integer multiples of the potential energy of atomic hydrogen, $m \cdot 27.2 \text{ eV}$ wherein m is an integer. The reaction involves a nonradiative energy transfer to form a hydrogen atom that is lower in energy than unreacted atomic hydrogen that corresponds to a fraction principal quantum number ($n = \frac{1}{p} = \frac{1}{\text{integer}}$ replaces the well known parameter $n = \text{integer}$ in the Rydberg equation for hydrogen excited states). One such atomic catalytic system involves helium ions. The second ionization energy of helium is 54.4 eV ; thus, the ionization reaction of He^+ to He^{2+} has a net enthalpy of reaction of 54.4 eV which is equivalent to $2 \cdot 27.2 \text{ eV}$. Since the products of the catalysis reaction have binding energies of $m \cdot 27.2 \text{ eV}$, they may further serve as catalysts. Extreme ultraviolet (EUV) spectroscopy was recorded on microwave and glow discharges of helium with 2% hydrogen. Novel emission lines were observed with energies of $q \cdot 13.6 \text{ eV}$ where $q = 1, 2, 3, 4, 6, 7, 8, 9, \text{ or } 11$ or these lines inelastically scattered by helium atoms wherein 21.2 eV was absorbed in the excitation of $\text{He} (1s^2)$ to $\text{He} (1s^1 2p^1)$. These lines were identified as hydrogen transitions to electronic energy levels below the "ground" state corresponding to fractional quantum numbers. Furthermore, astrophysical data was reviewed and such transitions were found to match the spectral lines of the extreme ultraviolet background of interstellar space. They may resolve the paradox of the identity of dark matter and account for many celestial observations such as: diffuse $\text{H}\alpha$ emission is ubiquitous throughout the Galaxy and widespread sources of flux shortward of 912 \AA are required. Fractional hydrogen transitions were also assigned to unidentified lines in the Solar EUV spectrum which may resolve the solar neutrino problem, the mystery of the cause of sunspots and other solar activity, and why the Sun emits X-rays.

I. INTRODUCTION

A. Background

J. J. Balmer showed in 1885 that the frequencies for some of the lines observed in the emission spectrum of atomic hydrogen could be expressed with a completely empirical relationship. This approach was later extended by J. R. Rydberg, who showed that all of the spectral lines of atomic hydrogen were given by the equation:

$$\bar{\nu} = R \left(\frac{1}{n_f^2} - \frac{1}{n_i^2} \right) \quad (1)$$

where $R = 109,677 \text{ cm}^{-1}$, $n_f = 1, 2, 3, \dots$, $n_i = 2, 3, 4, \dots$, and $n_i > n_f$.

Niels Bohr, in 1913, developed a theory for atomic hydrogen that gave energy levels in agreement with Rydberg's equation. An identical equation, based on a totally different theory for the hydrogen atom, was developed by E. Schrödinger, and independently by W. Heisenberg, in 1926.

$$E_n = -\frac{e^2}{n^2 8\pi\epsilon_0 a_H} = -\frac{13.598 \text{ eV}}{n^2} \quad (2a)$$

$$n = 1, 2, 3, \dots \quad (2b)$$

where a_H is the Bohr radius for the hydrogen atom (52.947 pm), e is the magnitude of the charge of the electron, and ϵ_0 is the vacuum permittivity. Based on the solution of a Schrödinger-type wave equation with a nonradiative boundary condition based on Maxwell's equations, Mills [1-40] predicts that atomic hydrogen may undergo a catalytic reaction with certain atomized elements or certain gaseous ions which singly or multiply ionize at integer multiples of the potential energy of atomic hydrogen, 27.2 eV. The reaction involves a nonradiative energy transfer to form a hydrogen atom that is lower in energy than unreacted atomic hydrogen that corresponds to a fraction principal quantum number where Eq. (2b), should be replaced by Eq. (2c).

$$n = 1, 2, 3, \dots, \text{ and, } n = \frac{1}{2}, \frac{1}{3}, \frac{1}{4}, \dots \quad (2c)$$

A number of independent experimental observations lead to the conclusion that atomic hydrogen can exist in fractional quantum states that are at lower energies than the traditional "ground" ($n=1$) state.

B. Experimental Data of Lower-Energy Hydrogen

Observation of intense extreme ultraviolet (EUV) emission at low temperatures (e.g. $\approx 10^3 K$) from atomic hydrogen and certain atomized elements or certain gaseous ions [7-23] has been reported previously. The only pure elements that were observed to emit EUV were those wherein the ionization of t electrons from an atom to a continuum energy level is such that the sum of the ionization energies of the t electrons is approximately $m \cdot 27.2 eV$ where t and m are each an integer. Potassium, cesium, and strontium atoms and Rb^+ ion ionize at integer multiples of the potential energy of atomic hydrogen and caused emission. Whereas, the chemically similar atoms, sodium, magnesium and barium, do not ionize at integer multiples of the potential energy of atomic hydrogen and caused no emission. Additional prior studies that support the possibility of a novel reaction of atomic hydrogen which produces an anomalous discharge and produces novel hydride compounds [7-38] include:

- 1.) the recent analysis of mobility and spectroscopy data of individual electrons in liquid helium which shows direct experimental confirmation that electrons may have fractional principal quantum energy levels [6],
- 2.) the observation of continuum state emission of Cs^{2+} and Ar^{2+} at 533 Å and 456 Å, respectively, with the absence of the other corresponding Rydberg series of lines from these species which confirmed the resonant nonradiative energy transfer of 27.2 eV from atomic hydrogen to the catalysts atomic cesium or Ar^+ [8],
- 3.) the spectroscopic observation of the predicted hydride ion $H^-(1/2)$ of hydrogen catalysis by either cesium atom or Ar^+ catalyst at 4070 Å corresponding to its predicted binding energy of 3.05 eV [8],
- 4.) the observation of characteristic emission from K^{3+} which confirmed the resonant nonradiative energy transfer of 3·27.2 eV from atomic hydrogen to atomic potassium [7],
- 5.) the spectroscopic observation of the predicted $H^-(1/4)$ hydride

ion of hydrogen catalysis by potassium catalyst at 1100 Å corresponding to its predicted binding energy of 11.2 eV [7],

6.) the identification of transitions of atomic hydrogen to lower energy levels corresponding to fractional principal quantum numbers in the extreme ultraviolet emission spectrum from interstellar medium [1, 5],

7.) the EUV spectroscopic observation of lines by the Institut für Niedertemperatur-Plasmaphysik e.V. that could be assigned to transitions of atomic hydrogen to lower energy levels corresponding to fractional principal quantum numbers and the emission from the excitation of the corresponding hydride ions [13],

8.) the observation by the Institut für Niedertemperatur-Plasmaphysik e.V. of an anomalous plasma and plasma afterglow duration formed with hydrogen-potassium mixtures [14],

9.) the observation of anomalous afterglow durations of plasmas formed by catalysts providing a net enthalpy of reaction within thermal energies of $m \cdot 27.28 \text{ eV}$ [14-15],

10.) the observation of Lyman series in the EUV that represents an energy release 10 times hydrogen combustion which is greater than that of any possible known chemical reaction [7-23],

11.) the observation of line emission by the Institut für Niedertemperatur-Plasmaphysik e.V. with a 4 ° grazing incidence EUV spectrometer that was 100 times more energetic than the combustion of hydrogen [13],

12.) the observation of anomalous plasmas formed with strontium and argon catalysts at 1% of the theoretical or prior known voltage requirement with a light output for power input up to 8600 times that of the control standard light source [10-11, 16],

13.) the observation that the optically measured output power of gas cells for power supplied to the glow discharge increased by over two orders of magnitude depending on the presence of less than 1% partial pressure of certain catalysts in hydrogen gas or argon-hydrogen gas mixtures [9],

14.) the isolation of novel hydrogen compounds as products of the reaction of atomic hydrogen with atoms and ions which formed an anomalous plasma as reported in the EUV studies [19, 21-38],

15.) the identification of novel hydride compounds by i.) time of flight secondary ion mass spectroscopy which showed a dominant hydride ion in the negative ion spectrum, ii.) X-ray photoelectron spectroscopy which showed novel hydride peaks and significant shifts of the core levels of the primary elements bound to the novel hydride ions, iii.) ^1H nuclear magnetic resonance spectroscopy (NMR) which showed extraordinary upfield chemical shifts compared to the NMR of the corresponding ordinary hydrides, and iv.) thermal decomposition with analysis by gas chromatography, and mass spectroscopy which identified the compounds as hydrides [19, 21-38],

16.) the NMR identification of novel hydride compounds MH^*X wherein M is the metal, X , is a halide, and H^* comprises a novel high binding energy hydride ion identified by a large distinct upfield resonance [24-25, 28],

17.) the replication of the NMR results of the identification of novel hydride compounds by large distinct upfield resonances at Spectral Data Services, University of Massachusetts Amherst, University of Delaware, Grace Davison, and National Research Council of Canada [24],

18.) the NMR identification of novel hydride compounds MH^* and MH_2^* wherein M is the metal and H^* comprises a novel high binding energy hydride ion identified by a large distinct upfield resonance that proves the hydride ion is different from the hydride ion of the corresponding known compound of the same composition [24], and

19.) minimum heats of formation of KHI by the catalytic reaction of potassium with atomic hydrogen and KI were over $-2000 \text{ kJ/mole } H_2$ compared to the enthalpy of combustion of hydrogen of $-241.8 \text{ kJ/mole } H_2$ [38].

C. Mechanism of the Formation of Lower-Energy Hydrogen

The mechanism of EUV emission, formation of novel hydrides, and certain EUV lines from interstellar medium can not be explained by the conventional energy levels of hydrogen, but it is predicted by a solution of the Schrödinger equation with a nonradiative boundary constraint put forward by Mills [1]. Mills predicts that certain atoms or ions serve as catalysts to release energy from hydrogen to produce an increased

binding energy hydrogen atom called a *hydrino atom* having a binding energy given by Eq. (2a) where

$$n = \frac{1}{2}, \frac{1}{3}, \frac{1}{4}, \dots, \frac{1}{p} \quad (3)$$

and p is an integer greater than 1, designated as $H\left[\frac{a_H}{p}\right]$ where a_H is the radius of the hydrogen atom. Hydrinos are predicted to form by reacting an ordinary hydrogen atom with a catalyst having a net enthalpy of reaction of about

$$m \cdot 27.2 \text{ eV} \quad (4)$$

where m is an integer. This catalysis releases energy from the hydrogen atom with a commensurate decrease in size of the hydrogen atom, $r_n = na_H$. For example, the catalysis of $H(n=1)$ to $H(n=1/2)$ releases 40.8 eV, and the hydrogen radius decreases from a_H to $\frac{1}{2}a_H$.

The excited energy states of atomic hydrogen are also given by Eq. (2a) except with Eq. (2b). The $n=1$ state is the "ground" state for "pure" photon transitions (the $n=1$ state can absorb a photon and go to an excited electronic state, but it cannot release a photon and go to a lower-energy electronic state). However, an electron transition from the ground state to a lower-energy state is possible by a nonradiative energy transfer such as multipole coupling or a resonant collision mechanism.

These lower-energy states have fractional quantum numbers, $n = \frac{1}{\text{integer}}$.

Processes that occur without photons and that require collisions are common. For example, the exothermic chemical reaction of $H+H$ to form H_2 does not occur with the emission of a photon. Rather, the reaction requires a collision with a third body, M , to remove the bond energy- $H+H+M \rightarrow H_2+M^*$ [41]. The third body distributes the energy from the exothermic reaction, and the end result is the H_2 molecule and an increase in the temperature of the system. Some commercial phosphors are based on nonradiative energy transfer involving multipole coupling. For example, the strong absorption strength of Sb^{3+} ions along with the efficient nonradiative transfer of excitation from Sb^{3+} to Mn^{2+} , are responsible for the strong manganese luminescence from phosphors containing these ions [42]. Similarly, the $n=1$ state of hydrogen and the

$n = \frac{1}{\text{integer}}$ states of hydrogen are nonradiative, but a transition between two nonradiative states is possible via a nonradiative energy transfer, say $n=1$ to $n=1/2$. In these cases, during the transition the electron couples to another electron transition, electron transfer reaction, or inelastic scattering reaction which can absorb the exact amount of energy that must be removed from the hydrogen atom. Thus, a catalyst provides a net positive enthalpy of reaction of $m \cdot 27.2 \text{ eV}$ (i.e. it absorbs $m \cdot 27.2 \text{ eV}$ where m is an integer). Certain atoms or ions serve as catalysts which resonantly accept energy from hydrogen atoms and release the energy to the surroundings to effect electronic transitions to fractional quantum energy levels. Recent analysis of mobility and spectroscopy data of individual electrons in liquid helium show direct experimental evidence that electrons may have fractional principal quantum energy levels [6].

The catalysis of hydrogen involves the nonradiative transfer of energy from atomic hydrogen to a catalyst which may then release the transferred energy by radiative and nonradiative mechanisms. As a consequence of the nonradiative energy transfer, the hydrogen atom becomes unstable and emits further energy until it achieves a lower-energy nonradiative state having a principal energy level given by Eqs. (2a) and (3).

D. Catalysts

According to Mills [1], a catalytic system is provided by the ionization of t electrons from an atom or ion to a continuum energy level such that the sum of the ionization energies of the t electrons is approximately $m \times 27.2 \text{ eV}$ where m is an integer.

a. Helium Ion

Helium ion (He^+) is such a catalyst because the second ionization energy of helium is 54.417 eV , which is equivalent to $m=2$ in Eq. (4). In this case, the catalysis reaction is

$$54.417 \text{ eV} + \text{He}^+ + \text{H}[a_H] \rightarrow \text{He}^{2+} + e^- + \text{H}\left[\frac{a_H}{3}\right] + 108.8 \text{ eV} \quad (5)$$

$$\text{He}^{2+} + e^- \rightarrow \text{He}^+ + 54.417 \text{ eV} \quad (6)$$

And, the overall reaction is

$$\text{H}[a_H] \rightarrow \text{H}\left[\frac{a_H}{3}\right] + 54.4 \text{ eV} + 54.4 \text{ eV} \quad (7)$$

The energy given off during catalysis is much greater than the energy lost to the catalyst. The energy released is large as compared to conventional chemical reactions. For example, when hydrogen and oxygen gases undergo combustion to form water



the known enthalpy of formation of water is $\Delta H_f = -286 \text{ kJ/mole}$ or 1.48 eV per hydrogen atom. By contrast, each ($n=1$) ordinary hydrogen atom undergoing catalysis releases a net of 40.8 eV . Moreover, further catalytic transitions may occur: $n = \frac{1}{2} \rightarrow \frac{1}{3}, \frac{1}{3} \rightarrow \frac{1}{4}, \frac{1}{4} \rightarrow \frac{1}{5}$, and so on. Once catalysis begins, hydrinos autocatalyze further in a process called *disproportionation*. This mechanism is similar to that of an inorganic ion catalysis. But, hydrino catalysis should have a higher reaction rate than that of the inorganic ion catalyst due to the better match of the enthalpy to $m \cdot 27.2 \text{ eV}$.

b. Hydrino Catalysts

In a process called *disproportionation*, lower-energy hydrogen atoms, *hydrinos*, can act as catalysts because each of the metastable excitation, resonance excitation, and ionization energy of a hydrino atom is $m \times 27.2 \text{ eV}$ (Eq. (4)). The transition reaction mechanism of a first hydrino atom affected by a second hydrino atom involves the resonant coupling between the atoms of m degenerate multipoles each having 27.21 eV of potential energy [1]. The energy transfer of $m \times 27.2 \text{ eV}$ from

the first hydrino atom to the second hydrino atom causes the central field of the first atom to increase by m and its electron to drop m levels lower from a radius of $\frac{a_H}{p}$ to a radius of $\frac{a_H}{p+m}$. The second interacting lower-energy hydrogen is either excited to a metastable state, excited to a resonance state, or ionized by the resonant energy transfer. The resonant transfer may occur in multiple stages. For example, a nonradiative transfer by multipole coupling may occur wherein the central field of the first increases by m , then the electron of the first drops m levels lower from a radius of $\frac{a_H}{p}$ to a radius of $\frac{a_H}{p+m}$ with further resonant energy transfer. The energy transferred by multipole coupling may occur by a mechanism that is analogous to photon absorption involving an excitation to a virtual level. Or, the energy transferred by multipole coupling during the electron transition of the first hydrino atom may occur by a mechanism that is analogous to two photon absorption involving a first excitation to a virtual level and a second excitation to a resonant or continuum level [43-45]. The transition energy greater than the energy transferred to the second hydrino atom may appear as a photon in a vacuum medium.

The transition of $H\left[\frac{a_H}{p}\right]$ to $H\left[\frac{a_H}{p+m}\right]$ induced by a multipole resonance transfer of $m \cdot 27.21 \text{ eV}$ (Eq. (4)) and a transfer of $[(p')^2 - (p' - m')^2] X 13.6 \text{ eV} - m \cdot 27.2 \text{ eV}$ with a resonance state of $H\left[\frac{a_H}{p' - m'}\right]$ excited in $H\left[\frac{a_H}{p'}\right]$ is represented by

$$H\left[\frac{a_H}{p'}\right] + H\left[\frac{a_H}{p}\right] \rightarrow H\left[\frac{a_H}{p' - m'}\right] + H\left[\frac{a_H}{p+m}\right] + [(p+m)^2 - p^2 - (p'^2 - (p' - m')^2)] X 13.6 \text{ eV} \quad (9)$$

where p , p' , m , and m' are integers.

Hydrinos may be ionized during a disproportionation reaction by the resonant energy transfer. A hydrino atom with the initial lower-energy state quantum number p and radius $\frac{a_H}{p}$ may undergo a transition to the state with lower-energy state quantum number $(p+m)$ and radius

$\frac{a_H}{(p+m)}$ by reaction with a hydrino atom with the initial lower-energy state quantum number m' , initial radius $\frac{a_H}{m'}$, and final radius a_H that provides a net enthalpy of $m \times 27.2 \text{ eV}$ (Eq.(4)). Thus, reaction of hydrogen-type atom, $H\left[\frac{a_H}{p}\right]$, with the hydrogen-type atom, $H\left[\frac{a_H}{m'}\right]$, that is ionized by the resonant energy transfer to cause a transition reaction is represented by

$$m \times 27.21 \text{ eV} + H\left[\frac{a_H}{m'}\right] + H\left[\frac{a_H}{p}\right] \rightarrow H^+ + e^- + H\left[\frac{a_H}{(p+m)}\right] + [(p+m)^2 - p^2 - (m'^2 - 2m)] \times 13.6 \text{ eV} \quad (10)$$

$$H^+ + e^- \rightarrow H\left[\frac{a_H}{1}\right] + 13.6 \text{ eV} \quad (11)$$

And, the overall reaction is

$$H\left[\frac{a_H}{m'}\right] + H\left[\frac{a_H}{p}\right] \rightarrow H\left[\frac{a_H}{1}\right] + H\left[\frac{a_H}{(p+m)}\right] + [2pm + m^2 - m'^2] \times 13.6 \text{ eV} + 13.6 \text{ eV} \quad (12)$$

Helium ion catalyzes $H[a_H]$ to $H\left[\frac{a_H}{3}\right]$ as shown in Eqs. (5-7). Further disproportionation reactions may then proceed:

$$H\left[\frac{a_H}{3}\right] + H\left[\frac{a_H}{3}\right] \rightarrow H\left[\frac{a_H}{4}\right] + H\left[\frac{a_H}{2}\right] + 27.2 \text{ eV} \quad (13)$$

$$H[a_H] + H\left[\frac{a_H}{2}\right] \rightarrow H\left[\frac{a_H}{3}\right] + H^+ + e^- + 54.4 \text{ eV} \quad (14)$$

$$H\left[\frac{a_H}{2}\right] + H\left[\frac{a_H}{2}\right] \rightarrow H\left[\frac{a_H}{3}\right] + H^+ + e^- + 13.6 \text{ eV} \quad (15)$$

$$H\left[\frac{a_H}{2}\right] + H\left[\frac{a_H}{2}\right] \rightarrow H\left[\frac{a_H}{3}\right] + H[a_H] + 27.2 \text{ eV} \quad (16)$$

$$H\left[\frac{a_H}{2}\right] + H\left[\frac{a_H}{2}\right] \rightarrow H\left[\frac{a_H}{4}\right] + H^+ + e^- + 108.8 \text{ eV} \quad (17)$$

$$H\left[\frac{a_H}{2}\right] + H\left[\frac{a_H}{2}\right] \rightarrow H\left[\frac{a_H}{4}\right] + H[a_H] + 122.4 \text{ eV} \quad (18)$$

$$H\left[\frac{a_H}{3}\right] + H\left[\frac{a_H}{2}\right] \rightarrow H\left[\frac{a_H}{4}\right] + H^+ + e^- + 40.8 \text{ eV} \quad (19)$$

$$H\left[\frac{a_H}{3}\right] + H\left[\frac{a_H}{2}\right] \rightarrow H\left[\frac{a_H}{4}\right] + H[a_H] + 54.4 \text{ eV} \quad (20)$$

$$H\left[\frac{a_H}{4}\right] + H\left[\frac{a_H}{2}\right] \rightarrow H\left[\frac{a_H}{5}\right] + H^+ + e^- + 68 \text{ eV} \quad (21)$$

$$H\left[\frac{a_H}{4}\right] + H\left[\frac{a_H}{2}\right] \rightarrow H\left[\frac{a_H}{5}\right] + H[a_H] + 81.6 \text{ eV} \quad (22)$$

$$H\left[\frac{a_H}{2}\right] + He^+ \rightarrow H\left[\frac{a_H}{4}\right] + He^{2+} + e^- + 108.8 \text{ eV} \quad (23)$$

$$H[a_H] + H\left[\frac{a_H}{3}\right] \rightarrow H\left[\frac{a_H}{4}\right] + H^+ + e^- + 81.6 \text{ eV} \quad (24)$$

$$H\left[\frac{a_H}{3}\right] + H\left[\frac{a_H}{3}\right] \rightarrow H\left[\frac{a_H}{5}\right] + H\left[\frac{a_H}{2}\right] + 149.6 \text{ eV} \quad (25)$$

$$H\left[\frac{a_H}{3}\right] + H\left[\frac{a_H}{3}\right] \rightarrow H\left[\frac{a_H}{5}\right] + H[a_H] + 108.8 \text{ eV} \quad (26)$$

$$H\left[\frac{a_H}{3}\right] + H\left[\frac{a_H}{3}\right] \rightarrow H\left[\frac{a_H}{5}\right] + H^+ + e^- + 95.2 \text{ eV} \quad (27)$$

$$H\left[\frac{a_H}{4}\right] + H\left[\frac{a_H}{3}\right] \rightarrow H\left[\frac{a_H}{5}\right] + H\left[\frac{a_H}{2}\right] + 54.4 \text{ eV} \quad (28)$$

$$H\left[\frac{a_H}{4}\right] + H\left[\frac{a_H}{3}\right] \rightarrow H\left[\frac{a_H}{5}\right] + H[a_H] + 13.6 \text{ eV} \quad (29)$$

$$H\left[\frac{a_H}{5}\right] + H\left[\frac{a_H}{2}\right] \rightarrow H\left[\frac{a_H}{6}\right] + H^+ + e^- + 95.2 \text{ eV} \quad (30)$$

$$H\left[\frac{a_H}{5}\right] + H\left[\frac{a_H}{2}\right] \rightarrow H\left[\frac{a_H}{6}\right] + H[a_H] + 108.8 \text{ eV} \quad (31)$$

$$H\left[\frac{a_H}{6}\right] + H\left[\frac{a_H}{2}\right] \rightarrow H\left[\frac{a_H}{7}\right] + H^+ + e^- + 122.4 \text{ eV} \quad (32)$$

$$H\left[\frac{a_H}{6}\right] + H\left[\frac{a_H}{2}\right] \rightarrow H\left[\frac{a_H}{7}\right] + H[a_H] + 136 \text{ eV} \quad (33)$$

$$H\left[\frac{a_H}{7}\right] + H\left[\frac{a_H}{2}\right] \rightarrow H\left[\frac{a_H}{8}\right] + H^+ + e^- + 149.6 \text{ eV} \quad (34)$$

$$H\left[\frac{a_H}{7}\right] + H\left[\frac{a_H}{2}\right] \rightarrow H\left[\frac{a_H}{8}\right] + H[a_H] + 163.2 \text{ eV} \quad (35)$$

c. Inelastic Scattering by Atomic Helium

It is proposed that the photons that arise from hydrogen catalysis may undergo inelastic helium scattering. That is, the catalytic reaction

$$H[a_H] \xrightarrow{He^*} H\left[\frac{a_H}{3}\right] + 54.4 \text{ eV} + 54.4 \text{ eV} \quad (36)$$

yields two 54.4 eV photons (228 Å). When each of these photons strikes $He(1s^2)$, 21.2 eV is absorbed in the excitation to $He(1s^1 2p^1)$. This leaves a 33.19 eV (374 Å) photon peak shown in Table 1. Thus, for helium the inelastic scattered peak of 54.4 eV photons from Eqs. (7), (14), (20), and (28) is given by

$$E = 54.4 \text{ eV} - 21.21 \text{ eV} = 33.19 \text{ eV} \text{ (374 Å)} \quad (37)$$

For helium, the inelastic scattered peak of 27.2 eV photons from Eqs. (13) and (16) is given by

$$E = 27.2 \text{ eV} - 21.21 \text{ eV} = 5.99 \text{ eV} \text{ (2071 Å)} \quad (38)$$

For helium, the inelastic scattered peak of 40.8 eV photons from Eq. (19) is given by

$$E = 40.8 \text{ eV} - 21.21 \text{ eV} = 19.59 \text{ eV} \text{ (633 Å)} \quad (39)$$

For helium, the inelastic scattered peak of 68 eV photons from Eq. (21) is

given by

$$E = 68 \text{ eV} - 21.21 \text{ eV} = 46.79 \text{ eV} \text{ (265 \AA)} \quad (40)$$

For helium, the inelastic scattered peak of 81.6 eV photons from Eqs. (22) and (24) is given by

$$E = 81.6 \text{ eV} - 21.21 \text{ eV} = 60.39 \text{ eV} \text{ (205 \AA)} \quad (41)$$

For helium, the inelastic scattered peak of 95.2 eV photons from Eqs. (27) and (30) is given by

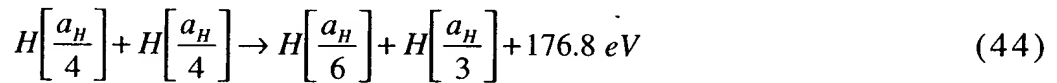
$$E = 95.2 \text{ eV} - 21.21 \text{ eV} = 73.99 \text{ eV} \text{ (167.6 \AA)} \quad (42)$$

For helium, the inelastic scattered peak of 108.8 eV photons from Eqs. (17), (23), (26), and (31) is given by

$$E = 108.8 \text{ eV} - 21.21 \text{ eV} = 87.59 \text{ eV} \text{ (141.6 \AA)} \quad (43)$$

E. EUV Spectroscopy Detects Lower-Energy Hydrogen

Previously reported lines observed at the Institut für Niedertemperatur-Plasmaphysik e.V. by EUV spectroscopy could be assigned to transitions of atomic hydrogen to lower energy levels corresponding to hydrinos and the emission from the excitation of the corresponding hydride ions [13]. For example, the product of the catalysis of atomic hydrogen with potassium metal, $H\left[\frac{a_H}{4}\right]$ may serve as both a catalyst and a reactant to form $H\left[\frac{a_H}{3}\right]$ and $H\left[\frac{a_H}{6}\right]$. The transition of $H\left[\frac{a_H}{4}\right]$ to $H\left[\frac{a_H}{6}\right]$ induced by a multipole resonance transfer of 54.4 eV (2·27.2 eV) and a transfer of 40.8 eV with a resonance state of $H\left[\frac{a_H}{3}\right]$ excited in $H\left[\frac{a_H}{4}\right]$ is represented by



The predicted 176.8 eV (70.2 Å) photon is a close match with the observed 73.0 Å line. The energy of this line emission corresponds to an equivalent temperature of 1,000,000 °C and an energy over 100 times the energy of combustion of hydrogen.

Since the Sun and stars contain significant amounts of He^+ and atomic hydrogen, catalysis of atomic hydrogen by He^+ as given by Eqs. (5-7) may occur. Also, the simultaneous ionization of two hydrogen atoms may provide a net enthalpy given by Eq. (4) to catalyze hydrino formation. Once formed, hydrinos have binding energies given by Eqs. (2a) and (3); thus, they may serve as reactants which provide a net enthalpy of reaction given by Eq. (4). Characteristic emissions from the Sun corresponding to these reactions may be observed, and stellar production may be a source of hydrinos in interstellar space where further transitions may occur with corresponding emission of characteristic EUV lines.

The detection of atomic hydrogen in fractional quantum energy levels below the traditional "ground" state—hydrinos—was previously reported [1, 5] by the assignment of soft x-ray emissions from the interstellar medium, the Sun, and stellar flares, and by assignment of certain lines obtained by the far-infrared absolute spectrometer (FIRAS) on the Cosmic Background Explorer. The detection of a new molecular species—the diatomic hydrino molecule—was reported by the assignment of certain infrared line emissions from the Sun. The detection of a new hydride species—hydrino hydride ion—was reported by the assignment of certain soft X-ray, ultraviolet (UV), and visible emissions from the Sun. This has implications for several unresolved astrophysical problems such as the identity of dark matter and the Solar neutrino paradox.

We report that extreme ultraviolet (EUV) spectroscopy was recorded on microwave and glow discharges of helium with 2% hydrogen. Novel emission lines were observed with energies of $q \cdot 13.6 \text{ eV}$ where $q = 1, 2, 3, 4, 6, 7, 8, 9, \text{ or } 11$ or these lines inelastically scattered by helium atoms wherein 21.2 eV was absorbed in the excitation of $He(1s^2)$ to $He(1s^1 2p^1)$. These lines were identified as hydrogen transitions to electronic energy levels below the "ground" state corresponding to fractional quantum numbers. A comparison was made between the plasma results and astrophysical data. Similar lower-energy-hydrogen transitions were found that matched the spectral lines of the extreme ultraviolet background of interstellar space and Solar lines.

II. EXPERIMENTAL

A. EUV Spectroscopy

Extreme ultraviolet (EUV) spectroscopy was recorded on microwave and discharge cell light sources. Due to the extremely short wavelength of this radiation, "transparent" optics do not exist. Therefore, a windowless arrangement was used wherein the microwave or discharge cell was connected to the same vacuum vessel as the grating and detectors of the extreme ultraviolet (EUV) spectrometer. Differential pumping permitted a high pressure in the cell as compared to that in the spectrometer. This was achieved by pumping on the cell outlet and pumping on the grating side of the collimator that served as a pin-hole inlet to the optics. The spectrometer was continuously evacuated to 10^{-4} – 10^{-6} torr by a turbomolecular pump with the pressure read by a cold cathode pressure gauge. The EUV spectrometer was connected to the cell light source with a 1.5 mm X 5 mm collimator which provided a light path to the slits of the EUV spectrometer. The collimator also served as a flow constrictor of gas from the cell. The cell was operated under gas flow conditions while maintaining a constant gas pressure in the cell.

EUV spectroscopy was recorded on a helium-hydrogen (98/2%) plasma. The mixture was made from ultrahigh purity gases by addition of hydrogen to helium to achieve a 98/2% mixture based on the individual gas partial pressures. The plasma source was a microwave plasma or a glow discharge cell. The microwave EUV spectrum and the discharge EUV spectrum were recorded with a normal incidence and grazing incidence EUV spectrometer, respectively. To demonstrate that neither spectrometer produced any spectral artifacts, a control hydrogen discharge was recorded with the normal incidence EUV spectrometer, and a control xenon discharge plasma was recorded with the grazing incidence EUV spectrometer.

The light emission from a microwave plasma was introduced to an EUV spectrometer for spectral measurement. The spectrometer was a normal incidence McPherson 0.2 meter monochromator (Model 302, Seya-Namioka type) equipped with a 1200 lines/mm holographic grating with a platinum coating. The wavelength region covered by the

monochromator was 50–5600 Å. The EUV spectrum was recorded with a channel electron multiplier (CEM) at 2500–3000 V. The wavelength resolution was about 0.2 Å (FWHM) with an entrance and exit slit width of 50 μm . The increment was 2 Å and the dwell time was 500 ms.

To achieve higher sensitivity at the shorter EUV wavelengths, the light emission of a glow discharge cell was recorded with a McPherson 4° grazing incidence EUV spectrometer (Model 248/310G) equipped with a grating having 600 G/mm with a radius of curvature of $\approx 1\text{ m}$. The angle of incidence was 87°. The wavelength region covered by the monochromator was 50–650 Å. The wavelength resolution was about 0.4 Å (FWHM) with an entrance and exit slit width of 300 μm . A channel electron multiplier (CEM) at 2400 V was used to detect the EUV light. The increment was 1 Å and the dwell time was 1 s.

B. Helium-Hydrogen Microwave Emission Spectrum

The extreme ultraviolet emission spectrum was obtained on a helium/hydrogen (98/2%) plasma with a microwave discharge system and an EUV spectrometer. The microwave generator was a Opthos model MPG-4M generator (Frequency: 2450 MHz). The output power was set at 85 watts. Gas was flowed through a half inch diameter quartz tube at 1 torr, 20 torr, or 760 torr. The gas pressure inside the cell was maintained by flowing a helium-hydrogen (98/2%) while monitoring the pressure with a 10 torr and 1000 torr MKS Baratron absolute pressure gauge. The tube was fitted with an Opthos coaxial microwave cavity (Evenson cavity). The EUV spectrometer was a McPherson model 302 (Seya-Namioka type) normal incidence monochromator. (See EUV-Spectroscopy Section).

C. Helium-Hydrogen Glow Discharge Emission Spectrum

A diagram of the discharge plasma source is given in Figure 1. The hollow cathode and EUV spectrograph were aligned on a common optical axis using a laser. The experimental setup for the discharge measurements is illustrated in Figure 2. The extreme ultraviolet emission spectrum was obtained on each of a control hydrogen, control

xenon, and helium/hydrogen (98/2%) plasma with a gas discharge cell that comprised a five-way stainless steel cross that served as the anode with a hollow stainless steel cathode. The plasma was generated at the hollow cathode inside the discharge cell. The hollow cathode was constructed of a stainless steel rod inserted into a steel tube, and this assembly was inserted into an Alumina tube. A flange opposite the end of the hollow cathode connected the spectrometer with the cell. It had a small hole that permitted radiation to pass to the spectrometer. An AC power supply ($U = 0 - 1$ kV, $I = 0 - 100$ mA) was connected to the hollow cathode to generate a discharge. The AC voltage and current at the time the EUV spectrum was recorded were 200 V and 40 mA, respectively. A Swagelok adapter at the very end of the steel cross provided a gas inlet and a connection with the pumping system, and the cell was pumped with a mechanical pump. Valves were between the cell and the mechanical pump, the cell and the monochromator, and the monochromator and its turbo pump. The five-way cross was pressurized with 400 mtorr of gas which was maintained by flowing a helium-hydrogen (98/2%) while monitoring the pressure with a 1 torr MKS Baratron absolute pressure gauge.

III. RESULTS AND DISCUSSION

A. EUV Spectroscopy

The EUV emission was recorded from microwave and glow discharge plasmas of hydrogen, xenon, and helium with 2% hydrogen over the wavelength range 50-1250 Å. The EUV spectrum (200–1250 Å) of the control hydrogen discharge cell emission is shown in Figure 3. The EUV spectrum (200–645 Å) of the control xenon discharge cell emission is shown in Figure 4. In either case, no spurious peaks or artifacts due to the grating or the spectrometer were observed.

The EUV spectrum (150–650 Å) of the helium-hydrogen mixture (98/2%) microwave cell emission that was recorded at 1, 24, and 72 hours is shown in Figure 5. Ordinary hydrogen has no emission in these regions as shown in Figure 3. Peaks observed at 205 Å, 374 Å, and 456 Å which do not correspond to helium and increased with time were

assigned to lower-energy hydrogen transitions in Table 1. The pressure was increased from 20 torr to 760 torr, and the corresponding spectra were compared in Figure 6. The peaks appeared slightly more intense at the lower pressure; so, the pressure was decreased to 1 torr and spectra were recorded.

At the 1 torr condition, additional novel peaks were observed in the short wavelength region. The short wavelength EUV spectrum (50-200 Å) of the control hydrogen discharge cell emission is shown in Figure 7. No spectrometer artifacts were observed at the short wavelengths. The short wavelength EUV spectrum (50-460 Å) of the helium-hydrogen mixture (98/2%) microwave cell emission with a pressure of 1 torr is shown in Figure 8. Peaks observed at 82.9 Å, 101.3 Å, 130.3 Å, and 141.5 Å which do not correspond to helium were assigned to lower-energy hydrogen transitions in Table 1. It is also proposed that the 304 Å peak shown in Figures 5, 6, and 8 was not entirely due to the He II transition. Conspicuously absent was the 256 Å (48.3 eV) line of He II which implies only a minor He II transition contribution to the 304 Å peak.

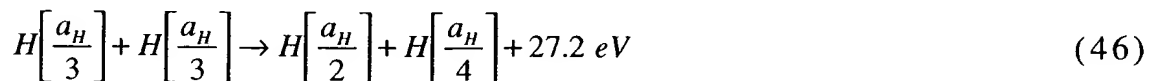
The EUV spectrum (500-650 Å) of the helium-hydrogen mixture (98/2%) discharge cell emission is shown in Figure 9. It is proposed that the 633 Å peak shown in Figure 9 arises from inelastic helium scattering of the 304 Å peak. That is, the $\frac{1}{3} \rightarrow \frac{1}{4}$ transition yields a 40.8 eV photon (304 Å). When this photon strikes $He(1s^2)$, 21.2 eV is absorbed in the excitation to $He(1s^1 2p^1)$. This leaves a 19.6 eV (633 Å) photon and a 21.2 eV (584 Å) photon from $He(1s^1 2p^1)$. The intensity of the 584 Å shown in Figure 9 is off-scale with 56,771 photons/sec. Thus, the transition $He(1s^2) \rightarrow He(1s^1 2p^1)$ dominated the inelastic scattering of EUV peaks. For the first nine peaks assigned as lower-energy hydrogen transitions or such transitions inelastically scattered by helium, the agreement between the predicted values and the experimental values shown in Table 1 is remarkable. It is also remarkable that the hydrino lines are moderately intense based on the low grating efficiency at these short wavelengths.

The EUV spectrum (880-1250 Å) of the helium-hydrogen mixture (98/2%) microwave cell emission is shown in Figure 10. The EUV spectrum (800-1050 Å) of the control hydrogen discharge cell emission is shown in Figure 11. The ratio of the Lβ peak to the 912 Å peak of the

helium-hydrogen plasma shown in Figure 10 was 2; whereas, the ratio of the L β peak to the 912 Å peak of the control hydrogen plasma shown in Figure 11, was 8 which indicates that the majority of the 912 Å peak was due to a transition other than the binding of an electron by a proton. Based on the intensity, it is proposed that the majority of the 912 Å peak shown in Figure 10 was due to the $\frac{1}{2} \rightarrow \frac{1}{4}$ and $\frac{1}{4} \rightarrow \frac{1}{5}$ transitions given in Table 1.

The energies for the hydrogen transitions given in Table 1 in order of energy are 13.6 eV, 27.2 eV, 40.8 eV, 54.4 eV, 81.6 eV, 95.2 eV, 108.8 eV, 122.4 eV and 149.6 eV. The corresponding peaks are 912 Å, 456 Å, 304 Å with 633 Å, 374 Å, 205 Å, 130.3 Å, 141.5 Å, 101.3 Å, and 82.9 Å, respectively. Thus, the lines identified in Figures 5-10 as hydrogen transitions to electronic energy levels below the "ground" state corresponding to fractional quantum numbers correspond to energies of $q \cdot 13.6 \text{ eV}$ where $q=1,2,3,4,6,7,8,9$, or 11 or these lines inelastically scattered by helium atoms wherein 21.2 eV was absorbed in the excitation of $\text{He}(1s^2)$ to $\text{He}(1s^1 2p^1)$. The absence of the series members corresponding to $q=5$ and $q=10$ may be due to a slow reaction rate due to selection rules, low cross section, or low relative reactant concentrations with only one dominant reaction pathway given by Eqs. (21) and (33), respectively. For example, the data is consistent with the reaction given by Eq. (22) which gives rise to the helium scattered peak at 205 Å being favored over that given by Eq. (21) corresponding to $q=5$. And, the reaction cross section and concentration of $H\left[\frac{a_H}{6}\right]$ required in the case of the reaction given by Eq. (33) corresponding to $q=10$ may have been relatively lower.

The disproportionation reaction assignments given in Table 1 start with the product of the catalysis of atomic hydrogen by He^+ given by Eqs. (5-7). One cascade of reactions which gives rise to the peaks assigned in Table 1 is:



$$H\left[\frac{a_H}{2}\right] + H\left[\frac{a_H}{2}\right] \rightarrow H^+ + e^- + H\left[\frac{a_H}{3}\right] + 13.6 \text{ eV} \quad (47)$$

$$H\left[\frac{a_H}{3}\right] + H\left[\frac{a_H}{2}\right] \rightarrow H^+ + e^- + H\left[\frac{a_H}{4}\right] + 40.8 \text{ eV} \quad (48)$$

$$H\left[\frac{a_H}{4}\right] + H\left[\frac{a_H}{2}\right] \rightarrow H[a_H] + H\left[\frac{a_H}{5}\right] + 81.6 \text{ eV} \quad (49)$$

$$H\left[\frac{a_H}{3}\right] + H\left[\frac{a_H}{3}\right] \rightarrow H\left[\frac{a_H}{5}\right] + H^+ + e^- + 95.2 \text{ eV} \quad (50)$$

$$H\left[\frac{a_H}{3}\right] + H\left[\frac{a_H}{3}\right] \rightarrow H\left[\frac{a_H}{5}\right] + H[a_H] + 108.8 \text{ eV} \quad (51)$$

$$H\left[\frac{a_H}{2}\right] + H\left[\frac{a_H}{2}\right] \rightarrow H\left[\frac{a_H}{4}\right] + H[a_H] + 122.4 \text{ eV} \quad (52)$$

$$H\left[\frac{a_H}{3}\right] + H\left[\frac{a_H}{3}\right] \rightarrow H\left[\frac{a_H}{5}\right] + H\left[\frac{a_H}{2}\right] + 149.6 \text{ eV} \quad (53)$$

wherein peaks inelastically scattered by helium are given by

$$\text{photon } (h\nu) + \text{He } (1s^2) \rightarrow \text{He } (1s^1 2p^1) + \text{photon } (h\nu - 21.21 \text{ eV}) \quad (54)$$

All other peaks besides those assigned to lower-energy hydrogen transitions could be assigned to He I (e.g. 524 Å, 536 Å, 591 Å, 602 Å, 625 Å, 628 Å, 639 Å, 641 Å, 645 Å,), He II (assigned in Figures), second order lines (608 Å, 615 Å, 886 Å, 1046 Å, 1073.6 Å, 1135 Å, 1164 Å, 1245 Å), or atomic (e.g. 1216 Å, 1026 Å, 973 Å) or molecular hydrogen (e.g. 907 Å, 918 Å, 1067 Å, 1100 Å) emission [46-47]. No known lines of helium or hydrogen explain the $q \cdot 13.6 \text{ eV}$ related set of peaks. Given that these spectra are readily repeatable, these peaks may have been overlooked in the past without considering the role of the helium scattering. The 633 Å peak which arises from the helium scattered 304 Å peak has significant astrophysical importance as discussed in the Identification of Lower-Energy Hydrogen by Soft X-rays from Dark Interstellar Medium section.

B. Identification of Lower-Energy Hydrogen by Soft X-rays from Dark Interstellar Medium

a. Dark Matter

The Universe is predominantly comprised of hydrogen and a small amount of helium. These elements exist in interstellar regions of space, and they are expected to comprise the majority of interstellar matter. However, the observed constant angular velocity of many galaxies as the distance from the luminous galactic center increases can only be accounted for by the existence of nonluminous weakly interacting matter, dark matter. Dark matter exists at the cold fringes of galaxies and in cold interstellar space. It may account for the majority of the universal mass.

The identity of dark matter has been a cosmological mystery. Postulated assignments include τ neutrinos, but a detailed search for signature emissions has yielded nil [48]. The search for signatures by the Cryogenic Dark Matter Search (CDMS) developed to detect theorized weakly Interacting Massive Particles (WIMPs) has similarly yielded nil [49-50]. WIMP theory's main competitor known as MACHO theory which assigns the Dark Matter to Massive Compact Halo Objects (MACHOs) which rather than elusive subatomic particles comprises ordinary baryonic matter in the form of burned-out dark stars, stray planets, and other large, heavy, but dark objects that must be ubiquitous throughout the universe. However, MACHO theory has also recently been ruled out based on lack of evidence of these dark objects observable by the brief ellipses caused by them moving in front of distant stars. Only a few such objects have been observed after exhaustively searching for over five years [49, 51].

It is anticipated that the emission spectrum of the extreme ultraviolet background of interstellar matter possesses the spectral signature of dark matter. Labov and Bowyer designed a grazing incidence spectrometer to measure and record the diffuse extreme ultraviolet background [52]. The instrument was carried aboard a sounding rocket, and data were obtained between 80 Å and 650 Å (data points approximately every 1.5 Å). Several lines including an intense

635 Å emission associated with dark matter were observed [52] which has considerable astrophysical importance as indicated by the authors:

"Regardless of the origin, the 635 Å emission observed could be a major source of ionization. Reynolds (1983, 1984, 1985) has shown that diffuse H α emission is ubiquitous throughout the Galaxy, and widespread sources of flux shortward of 912 Å are required. Pulsar dispersion measures (Reynolds 1989) indicate a high scale height for the associated ionized material. Since the path length for radiation shortward of 912 Å is low, this implies that the ionizing source must also have a large scale height and be widespread. Transient heating appears unlikely, and the steady state ionization rate is more than can be provided by cosmic rays, the soft X-ray background, B stars, or hot white dwarfs (Reynolds 1986; Brushweiler & Cheng 1988). Sciama (1990) and Salucci & Sciama (1990) have argued that a variety of observations can be explained by the presence of dark matter in the galaxy which decays with the emission of radiation below 912 Å.

The flux of 635 Å radiation required to produce hydrogen ionization is given by $F = \zeta_H / \sigma_\lambda = 4.3 \times 10^4 \zeta_{-13} \text{ photons cm}^{-2} \text{ s}^{-1}$, where ζ_{-13} is the ionizing rate in units of 10^{-13} s^{-1} per H atom. Reynolds (1986) estimates that in the immediate vicinity of the Sun, a steady state ionizing rate of ζ_{-13} between 0.4 and 3.0 is required. To produce this range of ionization, the 635 Å intensity we observe would have to be distributed over 7% - 54% of the sky."

The first soft X-ray background was detected and reported [53] about 25 years ago. Quite naturally, it was assumed that these soft X-ray emissions were from ionized atoms within hot gases. Labov and Bowyer also interpreted the data as emissions from hot gases. However, the authors left the door open for some other interpretation with the following statement from their introduction:

"It is now generally believed that this diffuse soft X-ray background is produced by a high-temperature component of the interstellar medium. However, evidence of the thermal nature of this emission is indirect in that it is based not on observations of line

emission, but on indirect evidence that no plausible non-thermal mechanism has been suggested which does not conflict with some component of the observational evidence."

The authors also state that "if this interpretation is correct, gas at several temperatures is present." Specifically, emissions were attributed to gases in three ranges: $5.5 < \log T < 5.7$; $\log T = 6$; $6.6 < \log T < 6.8$.

The explanation proposed herein of the observed dark interstellar medium spectrum hinges on the possibility of energy states below the $n=1$ state, as given by Eqs. (2a) and (3). A number of experimental observations discussed in the Introduction section lead to the conclusion that atomic hydrogen can exist in fractional quantum states that are at lower energies than the traditional "ground" ($n=1$) state. The existence of fractional quantum states of hydrogen atoms explains the spectral observations of the extreme ultraviolet background emission from interstellar space [52], which may characterize dark matter as demonstrated in Table 3. (In these cases, a hydrogen atom in a fractional quantum state, $H(n_i)$, collides, for example, with a $n=\frac{1}{2}$ hydrogen atom, $H(\frac{1}{2})$, and the result is an even lower-energy hydrogen atom, $H(n_f)$, and $H(\frac{1}{2})$ is ionized,

$$H(n_i) + H\left(\frac{1}{2}\right) \rightarrow H(n_f) + H^+ + e^- + \text{photon} \quad (55)$$

The energy released, as a photon, is the difference between the energies of the initial and final states given by Eqs. (2a) and (3) minus the ionization energy of $H(\frac{1}{2})$, 54.4 eV.

Thus, lower-energy transitions of the type,

$$\Delta E = \left(\frac{1}{n_f^2} - \frac{1}{n_i^2} \right) \times 13.6 \text{ eV} - 54.4 \text{ eV} \quad n = 1, \frac{1}{2}, \frac{1}{3}, \frac{1}{4}, \dots, \text{ and } n_i > n_f \quad (56)$$

induced by a disproportionation reaction with $H\left[\frac{a_H}{2}\right]$ ought to occur. The wavelength is related to ΔE by

$$\lambda \text{ (in } \text{\AA}) = \frac{1.240 \times 10^4}{\Delta E \text{ (in eV)}} \quad (57)$$

The energies and wavelengths of several of these proposed transitions are shown in Table 2. Note that the lower energy transitions are in the soft X-ray region.

b. The Data And Its Interpretation

In their analysis of the data, Labov and Bowyer [52] established several tests to separate emission features from the background. There were seven features (peaks) that passed their criteria. The wavelengths and other aspects of these peaks are shown in Table 3. Peaks 2 and 5 were interpreted by Labov and Bowyer as instrumental second-order images of peaks 4 and 7, respectively. Peak 3, the strongest feature, is clearly a helium resonance line: $\text{He}(1s^1 2p^1 \rightarrow 1s^2)$. At issue here, is the interpretation of peaks 1, 4, 6, and 7. It is proposed that peaks 4, 6, and 7 arise from the $\frac{1}{3} \rightarrow \frac{1}{4}$, $\frac{1}{4} \rightarrow \frac{1}{5}$, and $\frac{1}{6} \rightarrow \frac{1}{7}$ hydrogen atoms transitions given by Eq. (55). It is also proposed that peak 1 arises from inelastic helium scattering of peak 4. That is, the $\frac{1}{3} \rightarrow \frac{1}{4}$ transition yields a 40.8 eV photon (303.9 Å). Conspicuously absent is the 256 Å (48.3 eV) line of He II which eliminates the assignment of the majority of the 303 Å line to the He II transition. When this photon strikes $\text{He}(1s^2)$, 21.2 eV is absorbed in the excitation to $\text{He}(1s^1 2p^1)$. This leaves a 19.6 eV photon (632.6 Å), peak 1. For these four peaks, the agreement between the predicted values (Table 2) and the experimental values (Table 3) is remarkable.

One argument against this new interpretation of the data is that the transition $\frac{1}{5} \rightarrow \frac{1}{6}$ is missing—predicted at 130.2 Å by Eqs. (56-57). This missing peak cannot be explained into existence, but a reasonable rationale can be provided for why it might be missing from these data. The data obtained by Labov and Bowyer are outstanding when the region of the spectrum, the time allotted for data collection, and the logistics are considered. Nonetheless, it is clear that the signal-to-noise ratio is low and that considerable effort had to be expended to differentiate emission features from the background. This particular peak, $\frac{1}{5} \rightarrow \frac{1}{6}$, is likely to

be only slightly stronger than the $\frac{1}{6} \rightarrow \frac{1}{7}$ peak (the intensities, Table 3, appear to decrease as n decreases), which has low intensity. Labov and Bowyer provided their data (wavelength, count, count error, background, and background error). The counts minus background values for the region of interest, $130.2 \pm 5 \text{ \AA}$, are shown in Table 4 (the confidence limits for the wavelength of about $\pm 5 \text{ \AA}$ are the single-side 1 confidence levels and include both the uncertainties in the fitting procedure and uncertainties in the wavelength calibration). Note that the largest peak (count – background) is at 129.64 \AA and has a *counts – background* = 8.72. The *counts – background* for the strongest signal of the other hydrino transitions are: $n=1/3$ to $n=1/4$, 20.05; $n=1/4$ to $n=1/5$, 11.36; $n=1/6$ to $n=1/7$, 10.40. Thus, there is fair agreement with the wavelength and the strength of the signal. This, of course, does not mean that there is a peak at 130.2 \AA . However, it is not unreasonable to conclude that a spectrum with a better signal-to-noise ratio might uncover the missing peak. With the assignment of the $1/5 \rightarrow 1/6$ transition, all of the hydrogen transitions $1/3 \rightarrow 1/4$, $1/4 \rightarrow 1/5$, $1/5 \rightarrow 1/6$, and $1/6 \rightarrow 1/7$ are observed over the recorded spectral range, and the 632.6 \AA peak is identified.

B. Identification of Lower-Energy Hydrogen by Soft X-rays from the Sun

a. Solar Neutrino Problem

Another cosmological mystery unresolved for over two-decades is the discrepancy between solar neutrino flux observed with the Homestake detector, $2.1 \pm 0.03 \text{ SNU}$, and that predicted based on the Standard Solar Model, $7.9 \pm 2.6 \text{ SNU}$ [54-56]. According to the Standard Solar Model, the pp chain is the predominant energy source of main-sequence stars which commences with proton-proton fusion according to the following reaction [54];



And, according to this model, strong coupling exists between luminosity and neutrino flux because they are both based on nuclear reactions. An experiment with a radioactive solar surrogate at the Gallex solar neutrino

detector in Italy supports the results that over the past several years the Gallex and Russia's SAGE, the other large gallium detector, see only about 60% of the solar neutrino signal predicted to within 1 to 2% by astrophysical models [57].

The paradox of the paucity of solar neutrinos to account for the solar energy output by the pp chain is resolved by assigning a major portion of the solar output to hydrogen transitions. Hydrogen transitions to electronic energy levels below the "ground" state corresponding to fractional quantum numbers can yield energies comparable to nuclear energies. For example, all transitions to the $n = \frac{1}{100}$ state of hydrogen taken together release 136 keV. Data strongly supporting this tenant is the observation by Labov and Bowyer of an intense 304 Å (40.8 eV) solar emission line corresponding to the transition given by Eq. (55),

$$H\left[\frac{a_H}{3}\right] \xrightarrow{H\left[\frac{a_H}{2}\right]} H\left[\frac{a_H}{4}\right] \quad (59)$$

in the absence of the 256 Å (48.3 eV) line of He II which challenges the assignment of the 304 Å line to the He II transition. Solar lines which match lower-energy hydrogen transitions shown in Table 5 are also observed on the Sun which is consistent with a stellar origin of lower-energy hydrogen in interstellar space.

b. Temperature of the Solar Corona Problem

In addition to the questions of what powers the Sun and why the solar neutrino flux is significantly deficient, there exists no satisfactory answer to two additional solar questions: The cause of sunspots and other solar activity and why the Sun emits X-rays is unknown [62]. In fact, a possible anticorrelation exists between the abundance of sunspots and the solar neutrino flux observed with the Homestake detector [63]. The photosphere of the Sun is 6000 K; whereas, the temperature of the corona based on the assignment of the emitted X-rays to highly ionized heavy elements is in excess of 10^6 K. No satisfactory power transfer mechanism is known which explains the excessive temperature of the corona relative to that of the photosphere. The mechanism must explain the constant transfer over time of energy from the photosphere at 6000 K

to the corona at 10^6 K which radiates energy into cold space. Further compounding the temperature mystery is the observation of a strong coronal hydrogen Lyman series, beginning with $L\alpha$ at 1216 \AA and ending at 912 \AA , corresponding to unionized hydrogen atoms. The hydrogen lines would indicate that the corona is less than 10^4 K. The paradox is resolved by the existence of a power source associated with the corona.

The cause of sunspots and other solar activity, and why the Sun emits X-rays can be explained by energy releasing transitions of hydrogen to lower energy levels. The energy which maintains the corona at a temperature that appears in excess of 10^6 K may be that released by disproportionation reactions of lower-energy hydrogen as given by Eqs. (10-12). Hydrogen transitions to electronic energy levels below the "ground" state corresponding to fractional quantum numbers match lines of the solar emission spectrum in the extreme ultraviolet and X-ray regions. The solar lines that match the energy of disproportionation reactions of lower-energy hydrogen given by Eqs. (10-12) are given in Table 5.

The agreement between the calculated and the experimental values is remarkable, and several match those identified by EUV spectroscopy of the helium-hydrogen plasma as shown in Table 1. Furthermore, many of the lines of Table 5 had no previous assignment, or the assignment was unsatisfactory. Some lines assigned in the literature may have been assigned incorrectly by trying to fit the spectrum to known lines. But, inconsistencies arise. For example, the intensity of the peak assigned to He II by Thomas [58] is extremely strong ($I=62,200$). The laboratory He II transition intensities are: $I(303.780) = 1000$; $I(303.786) = 500$; $I(256) = 300$. Therefore, the predicted peak intensity of the 256 \AA (48.3 eV) line of He II is $I=12,440$; whereas, the observed intensity is too weak ($I=1580$) which challenges the assignment of the 304 \AA line solely to the He II transition.

Temporal variation in the disproportionation line intensities may reflect solar activity. For example, the coronal power is $\cong 0.01 \%$ of the solar power in the case of a quiet Sun and as high as 100% of the solar power in the case of an active Sun [64]. Emission lines corresponding to lower energy hydrogen transitions and assigned as such in Table 5 greatly increase in intensity during flare events [1, 65-67] which is

evidence that lower-energy hydrogen transitions are the cause of solar flares.

V. CONCLUSION

Transitions to fractional quantum energy levels were previously recorded at the Institut für Niedertemperatur-Plasmaphysik e.V. We report that extreme ultraviolet (EUV) spectroscopy was recorded on microwave and glow discharges of helium with 2% hydrogen. Novel emission lines were observed with energies of $q \cdot 13.6 \text{ eV}$ where $q = 1, 2, 3, 4, 6, 7, 8, 9, \text{ or } 11$ or these lines inelastically scattered by helium atoms wherein 21.2 eV was absorbed in the excitation of $\text{He}(1s^2)$ to $\text{He}(1s^1 2p^1)$. These lines were identified as hydrogen transitions to electronic energy levels below the "ground" state corresponding to fractional quantum numbers. Furthermore, astrophysical data was reviewed, and such transitions were found to match the spectral lines of the extreme ultraviolet background of interstellar space. These transitions may resolve the paradox of the identity of dark matter and account for many celestial observations such as: diffuse $\text{H}\alpha$ emission is ubiquitous throughout the Galaxy and widespread sources of flux shortward of 912 \AA are required. The origin of the 633 \AA emission observed by Låbov and others [52] that could be a major source of ionization of interstellar hydrogen was also observed in our helium-hydrogen plasma. We assigned the 633 \AA emission to atomic helium scattered 304 \AA emission from the $H\left[\frac{a_H}{3}\right] \xrightarrow{H\left[\frac{a_H}{2}\right]} \left[\frac{a_H}{4}\right]$ hydrogen transition. Furthermore, fractional hydrogen transitions were also assigned to lines in the Solar EUV spectrum which may resolve the solar neutrino problem, the mystery of the cause of sunspots and other solar activity, and why the Sun emits X-rays. In addition to producing power on the Sun, the catalysis of hydrogen represents a new powerful energy source with the potential for direct conversion of plasma to electricity with the production of novel compounds [39-40].

ACKNOWLEDGMENT

Special thanks to Y. Lu and T. Onuma for recording some spectra and B. Dhandapani for assisting with logistics and reviewing this manuscript. Special thanks to S. Labov and S. Bowyer for providing their raw digitized spectroscopic data and W. Good for bringing this paper to my attention. Special thanks to J. Farrell for contributions to the analysis of the interstellar and solar spectral data.

REFERENCES

1. R. Mills, *The Grand Unified Theory of Classical Quantum Mechanics*, January 2000 Edition, BlackLight Power, Inc., Cranbury, New Jersey, Distributed by Amazon.com.
2. R. Mills, "The Grand Unified Theory of Classical Quantum Mechanics", Global Foundation, Inc. Orbis Scientiae entitled *The Role of Attractive and Repulsive Gravitational Forces in Cosmic Acceleration of Particles The Origin of the Cosmic Gamma Ray Bursts*, (29th Conference on High Energy Physics and Cosmology Since 1964) Dr. Behram N. Kursunoglu, Chairman,. December 14-17, 2000, Lago Mar Resort, Fort Lauderdale, FL.
3. R. Mills, "The Grand Unified Theory of Classical Quantum Mechanics", Global Foundation, Inc. Orbis Scientiae entitled *The Role of Attractive and Repulsive Gravitational Forces in Cosmic Acceleration of Particles The Origin of the Cosmic Gamma Ray Bursts*, (29th Conference on High Energy Physics and Cosmology Since 1964) Dr. Behram N. Kursunoglu, Chairman,. December 14-17, 2000, Lago Mar Resort, Fort Lauderdale, FL, in press.
4. R. Mills, "The Grand Unified Theory of Classical Quantum Mechanics", II Nuovo Cimento, submitted.
5. R. Mills, "The Hydrogen Atom Revisited", Int. J. of Hydrogen Energy, Vol. 25, Issue 12, December, (2000), pp. 1171-1183.
6. R. Mills, The Nature of Free Electrons in Superfluid Helium--a Test of Quantum Mechanics and a Basis to Review its Foundations and Make a Comparison to Classical Theory, Int. J. Hydrogen Energy, in press.
7. R. Mills, P. Ray, Spectroscopic Identification of a Novel Catalytic

- Reaction of Potassium and Atomic Hydrogen and the Hydride Ion Product, *Int. J. Hydrogen Energy*, submitted.
8. R. Mills, "Spectroscopic Identification of a Novel Catalytic Reaction of Atomic Hydrogen and the Hydride Ion Product", *Int. J. Hydrogen Energy*, in press.
 9. R. Mills, N. Greenig, S. Hicks, "Optically Measured Power Balances of Anomalous Discharges of Mixtures of Argon, Hydrogen, and Potassium, Rubidium, Cesium, or Strontium Vapor", *Int. J. Hydrogen Energy*, submitted.
 10. R. Mills and M. Nansteel, "Anomalous Argon-Hydrogen-Strontium Discharge", *IEEE Transactions on Plasma Science*, submitted.
 11. R. Mills, M. Nansteel, and Y. Lu, "Anomalous Hydrogen-Strontium Discharge", *European Journal of Physics D*, submitted.
 12. R. Mills, J. Dong, Y. Lu, "Observation of Extreme Ultraviolet Hydrogen Emission from Incandescently Heated Hydrogen Gas with Certain Catalysts", *Int. J. Hydrogen Energy*, Vol. 25, (2000), pp. 919-943.
 13. R. Mills, "Observation of Extreme Ultraviolet Emission from Hydrogen-KI Plasmas Produced by a Hollow Cathode Discharge", *Int. J. Hydrogen Energy*, Vol. 26, No. 6, (2001), pp. 579-592.
 14. R. Mills, "Temporal Behavior of Light-Emission in the Visible Spectral Range from a Ti-K₂CO₃-H-Cell", *Int. J. Hydrogen Energy*, Vol. 26, No. 4, (2001), pp. 327-332.
 15. R. Mills, T. Onuma, and Y. Lu, "Formation of a Hydrogen Plasma from an Incandescently Heated Hydrogen-Catalyst Gas Mixture with an Anomalous Afterglow Duration", *Int. J. Hydrogen Energy*, in press.
 16. R. Mills, M. Nansteel, and Y. Lu, "Observation of Extreme Ultraviolet Hydrogen Emission from Incandescently Heated Hydrogen Gas with Strontium that Produced an Anomalous Optically Measured Power Balance", *Int. J. Hydrogen Energy*, Vol. 26, No. 4, (2001), pp. 309-326.
 17. R. Mills, J. Dong, Y. Lu, J. Conrads, "Observation of Extreme Ultraviolet Hydrogen Emission from Incandescently Heated Hydrogen Gas with Certain Catalysts", 1999 Pacific Conference on Chemistry and Spectroscopy and the 35th ACS Western Regional Meeting, Ontario Convention Center, California, (October 6-8, 1999).
 18. R. Mills, J. Dong, N. Greenig, and Y. Lu, "Observation of Extreme Ultraviolet Hydrogen Emission from Incandescently Heated Hydrogen

- Gas with Certain Catalysts", National Hydrogen Association, 11 th Annual U.S. Hydrogen Meeting, Vienna, VA, (February 29-March 2, 2000).
19. R. Mills, B. Dhandapani, N. Greenig, J. He, J. Dong, Y. Lu, and H. Conrads, "Formation of an Energetic Plasma and Novel Hydrides from Incandescently Heated Hydrogen Gas with Certain Catalysts", National Hydrogen Association, 11 th Annual U.S. Hydrogen Meeting, Vienna, VA, (February 29-March 2, 2000).
 20. Mills, J. Dong, N. Greenig, and Y. Lu, "Observation of Extreme Ultraviolet Hydrogen Emission from Incandescently Heated Hydrogen Gas with Certain Catalysts", 219 th National ACS Meeting, San Francisco, California, (March 26-30, 2000).
 21. R. Mills, B. Dhandapani, N. Greenig, J. He, J. Dong, Y. Lu, and H. Conrads, "Formation of an Energetic Plasma and Novel Hydrides from Incandescently Heated Hydrogen Gas with Certain Catalysts", 219 th National ACS Meeting, San Francisco, California, (March 26-30, 2000).
 22. R. Mills, B. Dhandapani, N. Greenig, J. He, J. Dong, Y. Lu, and H. Conrads, "Formation of an Energetic Plasma and Novel Hydrides from Incandescently Heated Hydrogen Gas with Certain Catalysts", June ACS Meeting (29th Northeast Regional Meeting, University of Connecticut, Storrs, CT, (June 18-21, 2000)).
 23. R. Mills, B. Dhandapani, N. Greenig, J. He, J. Dong, Y. Lu, and H. Conrads, "Formation of an Energetic Plasma and Novel Hydrides from Incandescently Heated Hydrogen Gas with Certain Catalysts", August National ACS Meeting (220th ACS National Meeting, Washington, DC, (August 20-24, 2000)).
 24. R. Mills, B. Dhandapani, M. Nansteel, J. He, A. Voigt, "Identification of Compounds Containing Novel Hydride Ions by Nuclear Magnetic Resonance Spectroscopy", Int. J. Hydrogen Energy, in press.
 25. R. Mills, B. Dhandapani, N. Greenig, J. He, "Synthesis and Characterization of Potassium Iodo Hydride", Int. J. of Hydrogen Energy, Vol. 25, Issue 12, December, (2000), pp. 1185-1203.
 26. R. Mills, "Novel Inorganic Hydride", Int. J. of Hydrogen Energy, Vol. 25, (2000), pp. 669-683.
 27. R. Mills, "Novel Hydrogen Compounds from a Potassium Carbonate Electrolytic Cell", Fusion Technology, Vol. 37, No. 2, March, (2000), pp.

157-182.

28. R. Mills, B. Dhandapani, M. Nansteel, J. He, T. Shannon, A. Echezuria, "Synthesis and Characterization of Novel Hydride Compounds", *Int. J. of Hydrogen Energy*, Vol. 26, No. 4, (2001), pp. 339-367.
29. R. Mills, "Highly Stable Novel Inorganic Hydrides", *Journal of Materials Research*, submitted.
30. R. Mills, "Novel Hydride Compound", 1999 Pacific Conference on Chemistry and Spectroscopy and the 35th ACS Western Regional Meeting, Ontario Convention Center, California, (October 6-8, 1999).
31. R. Mills, B. Dhandapani, N. Greenig, J. He, "Synthesis and Characterization of Potassium Iodo Hydride", 1999 Pacific Conference on Chemistry and Spectroscopy and the 35th ACS Western Regional Meeting, Ontario Convention Center, California, (October 6-8, 1999).
32. R. Mills, J. He, and B. Dhandapani, "Novel Hydrogen Compounds", 1999 Pacific Conference on Chemistry and Spectroscopy and the 35th ACS Western Regional Meeting, Ontario Convention Center, California, (October 6-8, 1999).
33. R. Mills, "Novel Hydride Compound", National Hydrogen Association, 11 th Annual U.S. Hydrogen Meeting, Vienna, VA, (February 29-March 2, 2000).
34. R. Mills, J. He, and B. Dhandapani, "Novel Alkali and Alkaline Earth Hydrides", National Hydrogen Association, 11 th Annual U.S. Hydrogen Meeting, Vienna, VA, (February 29-March 2, 2000).
35. R. Mills, "Novel Hydride Compound", 219 th National ACS Meeting, San Francisco, California, (March 26-30, 2000).
36. R. Mills, J. He, and B. Dhandapani, "Novel Alkali and Alkaline Earth Hydrides", 219 th National ACS Meeting, San Francisco, California, (March 26-30, 2000).
37. R. Mills, J. He, and B. Dhandapani, "Novel Alkali and Alkaline Earth Hydrides", August National ACS Meeting (220th ACS National Meeting, Washington, DC, (August 20-24, 2000)).
38. R. Mills, W. Good, A. Voigt, Jinqun Dong, "Minimum Heat of Formation of Potassium Iodo Hydride", *Int. J. Hydrogen Energy*, in press.
39. R. Mills, "BlackLight Power Technology-A New Clean Hydrogen Energy Source with the Potential for Direct Conversion to Electricity", *Proceedings of the National Hydrogen Association*, 12 th Annual U.S.

- Hydrogen Meeting and Exposition, *Hydrogen: The Common Thread*, The Washington Hilton and Towers, Washington DC, (March 6-8, 2001), in press.
40. R. Mills, "BlackLight Power Technology-A New Clean Energy Source with the Potential for Direct Conversion to Electricity", Global Foundation International Conference on "Global Warming and Energy Policy", Dr. Behram N. Kursunoglu, Chairman, Fort Lauderdale, FL, November 26-28, 2000, in press.
 41. N. V. Sidgwick, *The Chemical Elements and Their Compounds*, Volume I, Oxford, Clarendon Press, (1950), p.17.
 42. M. D. Lamb, *Luminescence Spectroscopy*, Academic Press, London, (1978), p. 68.
 43. B. J. Thompson, *Handbook of Nonlinear Optics*, Marcel Dekker, Inc., New York, (1996), pp. 497-548.
 44. Y. R. Shen, *The Principles of Nonlinear Optics*, John Wiley & Sons, New York, (1984), pp. 203-210.
 45. B. de Beauvoir, F. Nez, L. Julien, B. Cagnac, F. Biraben, D. Touahri, L. Hilico, O. Acef, A. Clairon, and J. J. Zondy, *Physical Review Letters*, Vol. 78, No. 3, (1997), pp. 440-443.
 46. R. Kelly, *Journal of Physical and Chemical Reference Data*. "Atomic and Ionic Spectrum Lines below 2000 Angstroms: Hydrogen through Krypton", Part I (H-Cr), Volume 16, (1987), Supplement No. 1, Published by the American Chemical Society and the American Institute of Physics for the National Bureau of Standards, pp. 20-21.
 47. NIST Atomic Spectra Database, www.physics.nist.gov/cgi-bin/AtData/display.ksh.
 48. A. Davidsen, et al., "Test of the decaying dark matter hypothesis using the Hopkins ultraviolet telescope", *Nature*, 351, (1991), pp. 128-130.
 49. W. Milan, "Shall the WIMPs Inherit the Universe", *SPACE.com*, 28, February, 2000, http://space.com/scienceastronomy/generalscience/dark_matter_000228.html.
 50. R. Abusaidi, et al., "Exclusion limits on the WIMP-nucleon cross section from the cryogenic dark matter search", *Physical Review Letters*, Vol. 84, No. 25, 19, June, (2000), pp. 5699-5703.
 51. B. R. Oppenheimer, N. C. Hambly, A. P. Digby, S. T. Hodgkin, and D.

- Saumon, "Direct detection of galactic halo dark matter," *Science*, Vol. 292, 27, April, (2000), pp. 698-702.
52. S. Labov, S. Bowyer, "Spectral observations of the extreme ultraviolet background", *The Astrophysical Journal*, 371, (1991), pp. 810-819.
 53. S. Bower, G. Field, and J. Mack, "Detection of an Anisotropic Soft X-ray Background Flux," *Nature*, Vol. 217, (1968), p. 32.
 54. J. Bahcall, et al., "Solar neutrinos: a field in transition", *Nature*, 334, 11, (1988), pp. 487-493.
 55. G. Taubes, *Science*, 256, (1992), pp. 1512-1513.
 56. G. Taubes, *Science*, 256, (1992), pp. 731-733.
 57. B. Schwarzschild, *Physics Today*, April, (1995), pp.19-21.
 58. R. J. Thomas, W. M. Neupert, *Astrophysical Journal Supplement Series*, Vol. 91, (1994), pp. 461-482.
 59. M. Malinovsky, L. Heroux, *Astrophysical Journal*, Vol. 181, (1973), pp. 1009-1030.
 60. R. Noyes, *The Sun, Our Star*, Harvard University Press, Cambridge, MA, (1982), p.172.
 61. J. H. Phillips, *Guide to the Sun*, Cambridge University Press, Cambridge, Great Britain, (1992), pp. 118-119; 120-121; 144-145.
 62. J. Harvey, *Physics Today*, October, (1995), pp. 32-38.
 63. B. Schwarzschild, *Physics Today*, October, (1990), pp. 17-20.
 64. M. Stix, *The Sun*, Springer-Verlag, Berlin, (1991), pp. 351-356.
 65. R. Cowen, *Science News*, 141, (1992), pp. 344-346.
 66. S. Bowyer, *Science*, Vol. 263, (1994), pp. 55-59.
 67. B. C. M. Fossi, et al., *Astrophysical Journal*, 449, (1995), pp. 376-385.

Table 1. Observed line emission from helium-hydrogen plasmas assigned to the disproportionation reactions given by Eqs. (9-12) and helium inelastic scattered peaks of hydrogen transitions, wherein the photon strikes $He(1s^2)$ and 21.2 eV is absorbed in the excitation to $He(1s^1 2p^1)$.

Observed Line (Å)	Predicted (Mills) (Å)	Assignment (Mills)	Equation #	Figure #
82.9	82.9	$H\left[\frac{a_H}{3}\right] + H\left[\frac{a_H}{3}\right] \rightarrow H\left[\frac{a_H}{5}\right] + H\left[\frac{a_H}{2}\right] + 149.6 \text{ eV}$	25	8
		$H\left[\frac{a_H}{7}\right] + H\left[\frac{a_H}{2}\right] \rightarrow H\left[\frac{a_H}{8}\right] + H^+ + e^- + 149.6 \text{ eV}$	34	
101.3	101.3	$H\left[\frac{a_H}{2}\right] + H\left[\frac{a_H}{2}\right] \rightarrow H\left[\frac{a_H}{4}\right] + H[a_H] + 122.4 \text{ eV}$	18	8
		$H\left[\frac{a_H}{6}\right] + H\left[\frac{a_H}{2}\right] \rightarrow H\left[\frac{a_H}{7}\right] + H^+ + e^- + 122.4 \text{ eV}$	32	
130.3 ^a	130.3	$H\left[\frac{a_H}{3}\right] + H\left[\frac{a_H}{3}\right] \rightarrow H\left[\frac{a_H}{5}\right] + H^+ + e^- + 95.2 \text{ eV}$	27	8
		$H\left[\frac{a_H}{5}\right] + H\left[\frac{a_H}{2}\right] \rightarrow H\left[\frac{a_H}{6}\right] + H^+ + e^- + 95.2 \text{ eV}$	30	
141.5	141.5	$H\left[\frac{a_H}{2}\right] + H\left[\frac{a_H}{2}\right] \rightarrow H\left[\frac{a_H}{4}\right] + H^+ + e^- + 108.8 \text{ eV}$	17	8
		$H\left[\frac{a_H}{2}\right] + He^+ \rightarrow H\left[\frac{a_H}{4}\right] + He^{2+} + e^- + 108.8 \text{ eV}$	23	
		$H\left[\frac{a_H}{3}\right] + H\left[\frac{a_H}{3}\right] \rightarrow H\left[\frac{a_H}{5}\right] + H[a_H] + 108.8 \text{ eV}$	26	
		$H\left[\frac{a_H}{5}\right] + H\left[\frac{a_H}{2}\right] \rightarrow H\left[\frac{a_H}{6}\right] + H[a_H] + 108.8 \text{ eV}$	31	
		$108.8 \text{ eV} + He(1s^2) \rightarrow He(1s^1 2p^1) \rightarrow +87.59 \text{ eV}$	43	

205	205	$H\left[\frac{a_H}{4}\right] + H\left[\frac{a_H}{2}\right] \rightarrow H\left[\frac{a_H}{5}\right] + H[a_H] + 81.6 \text{ eV}$	22	5, 6, 8
		$H[a_H] + H\left[\frac{a_H}{3}\right] \rightarrow H\left[\frac{a_H}{4}\right] + H^+ + e^- + 81.6 \text{ eV}$	24	
		$81.6 \text{ eV} + He (1s^2) \rightarrow He (1s^1 2p^1) \rightarrow +60.39 \text{ eV}$	41	
304	304	$H\left[\frac{a_H}{3}\right] + H\left[\frac{a_H}{2}\right] \rightarrow H\left[\frac{a_H}{4}\right] + H^+ + e^- + 40.8 \text{ eV}$	19	5, 6, 8
304	304	$He^+(n=2) \rightarrow He^+(n=1) + 40.8 \text{ eV}^b$		5, 6, 8
374	374	$H[a_H] \xrightarrow{He^+} H\left[\frac{a_H}{3}\right] + 54.4 \text{ eV} + 54.4 \text{ eV}$	5-7	5, 6, 8
		$H[a_H] + H\left[\frac{a_H}{2}\right] \rightarrow H\left[\frac{a_H}{3}\right] + H^+ + e^- + 54.4 \text{ eV}$	14	
		$H\left[\frac{a_H}{3}\right] + H\left[\frac{a_H}{2}\right] \rightarrow H\left[\frac{a_H}{4}\right] + H[a_H] + 54.4 \text{ eV}$	20	
		$H\left[\frac{a_H}{4}\right] + H\left[\frac{a_H}{3}\right] \rightarrow H\left[\frac{a_H}{5}\right] + H\left[\frac{a_H}{2}\right] + 54.4 \text{ eV}$	28	
		$54.4 \text{ eV} + He (1s^2) \rightarrow He (1s^1 2p^1) \rightarrow +33.19 \text{ eV}$	37	
456	456	$H\left[\frac{a_H}{3}\right] + H\left[\frac{a_H}{3}\right] \rightarrow H\left[\frac{a_H}{4}\right] + H\left[\frac{a_H}{2}\right] + 27.2 \text{ eV}$	13	5, 6, 8
		$H\left[\frac{a_H}{2}\right] + H\left[\frac{a_H}{2}\right] \rightarrow H\left[\frac{a_H}{3}\right] + H[a_H] + 27.2 \text{ eV}$	16	
584	584	$He (1s^1 2p^1) \rightarrow He (1s^2) + 21.2 \text{ eV}^c$		5, 6, 9
633	633	$H\left[\frac{a_H}{3}\right] + H\left[\frac{a_H}{2}\right] \rightarrow H\left[\frac{a_H}{4}\right] + H^+ + e^- + 40.8 \text{ eV}$	19	9
		$40.8 \text{ eV} + He (1s^2) \rightarrow He (1s^1 2p^1) \rightarrow +19.59 \text{ eV}$	39	

633	633	$He^+(n=2) \rightarrow He^+(n=1) + 40.8 \text{ eV}^b$	9
		$40.8 \text{ eV} + He(1s^2) \rightarrow He(1s^1 2p^1) \rightarrow +19.59 \text{ eV}$	39
912	912	$H\left[\frac{a_H}{2}\right] + H\left[\frac{a_H}{2}\right] \rightarrow H\left[\frac{a_H}{3}\right] + H^+ + e^- + 13.6 \text{ eV}$	15 10
		$H\left[\frac{a_H}{4}\right] + H\left[\frac{a_H}{3}\right] \rightarrow H\left[\frac{a_H}{5}\right] + H[a_H] + 13.6 \text{ eV}$	29
912	912	$H^+ + e^- \rightarrow H[a_H] + 13.6 \text{ eV}^d$	11

^a Weak shoulder on the 141.5 Å peak.

^b In Figures 5, 6, and 8, the peak corresponding to $He^+(n=3) \rightarrow He^+(n=1) + 48.35 \text{ eV}$ (256 Å) was absent which makes this assignment difficult.

^c The intensity which is off-scale in Figure 9 was 56,771 photons/sec; thus, the transition $He(1s^2) \rightarrow He(1s^1 2p^1)$ dominated the inelastic scattering of EUV peaks.

^d The ratio of the Lβ peak to the 912 Å peak of the helium-hydrogen plasma shown in Figure 10 was 2; whereas, the ratio of the Lβ peak to the 912 Å peak of the control hydrogen plasma shown in Figure 11, was 8 which makes this assignment difficult.

Table 2. Energies (Eq. (56)) of several fractional-state transitions catalyzed by $H\left[\frac{a_H}{2}\right]$.

n_i	n_f	ΔE (eV)	λ (Å)
$\frac{1}{2}$	$\frac{1}{3}$	13.6	912
$\frac{1}{3}$	$\frac{1}{4}$	40.80	303.9
$\frac{1}{4}$	$\frac{1}{5}$	68.00	182.4
$\frac{1}{5}$	$\frac{1}{6}$	95.20	130.2
$\frac{1}{6}$	$\frac{1}{7}$	122.4	101.3
$\frac{1}{7}$	$\frac{1}{8}$	149.6	82.9

Table 3. Emission features of the Labov and Bowyer spectrum and their interpretation.

peak	λ (Å)	confidence limit (Å)	intensity photons cm ⁻² s ⁻¹ sr ⁻¹	assignment (Labov & Bowyer)	assignment (Mills)	predicted λ (Eq. (56-57)) (Å)
1	633.0	-4.7 to +4.7	19,000	O^{+} ; Log T = 5.5	He scattering of 303.9 line (peak 4)	633.0
2	607.5	-4.9 to +4.9	second order	second order of 302.5 line	second order of 303.9 line	607.8
3	584	-4.5 to +4.5	70,400	He resonance ($1s^1 2p^1 \rightarrow 1s^2$)	He resonance ($1s^1 2p^1 \rightarrow 1s^2$)	584
4	302.5	-6.0 to +5.9	2,080	He^{+} ; ($2p^1$ to $1s^1$)	n = 1/3 to n = 1/4	303.9
5	200.6	-4.4 to +5.3	second order	second order of 101.5 line	second order of 101.3 line	202.6
6	181.7	-4.6 to +5.1	1,030	Fe^{9+} and Fe^{10+} ; Log T = 6	n = 1/4 to n = 1/5	182.3
7	101.5	-5.3 to +4.2	790	Fe^{17+} and Fe^{18+} ; Log T = 6.6-6.8	n = 1/6 to n = 1/7	101.3

Table 4. Data (Labov & Bowyer) near the predicted $\frac{1}{5} \rightarrow \frac{1}{6}$ transition (130.2 Å).

λ (Å)	counts	background	counts – background
125.82	26	21.58	4.42
127.10	22	21.32	0.68
128.37	18	19.50	–1.50
129.64	29	20.28	8.72
130.90	18	19.76	–1.76
132.15	20	19.50	0.50
133.41	19	19.50	–0.50
134.65	19	20.80	–1.80

Table 5. Observed solar line emission assigned to the disproportionation reactions given by Eqs. (10-12). (Raw extreme ultraviolet solar spectral data taken from Figures 3a-k of [58], Figures 1a-d (observed lines from Table 1) of [59]; Figure 7.5 of [60], and Figure 4.10 of Phillips [61].)

Observed Line (Å)	^b Predicted (Mills) (Å)	<i>m, m'</i> <i>f</i>	Assignment (Mills)	Ref	Assignment (Other)
1215.7	1215.67	d	$H(2p^1) \rightarrow H(1s^1) + 10.2 \text{ eV}$	57, 58	Collisional Excitation, L α scattering
911.8	911.78	1, 1; 1; ^c	1 \rightarrow 1/2 H transition	57, 58	$H^+ + e^- \rightarrow H$ + 13.6 eV at $T > 20,000 \text{ K}$
		1, 2	1/2 \rightarrow 1/3 H transition		
584.5	584.5	e	$He(1s^1 2p^1) \rightarrow He(1s^2)$ + 21.2 eV	57, 58	Collisional Excitation
373.7	373.73	2, 2	Inelastic Scattering (He) of 1 \rightarrow 1/3 H transition	55	None
303.784	303.92	1, 2	1/3 \rightarrow 1/4 transition	55	He II
280.2 ^a 280.8 ^a	280.54	2, 2	Inelastic Scattering (H) of 1 \rightarrow 1/3 H transition	56	None
264.80	265.08	1, 2	Inelastic Scattering (He) of 1/4 \rightarrow 1/5 H transition	56	Fe XIV
228 ^a	227.95	2, 2	1 \rightarrow 1/3 H transition	56	None
215.16	214.54	1, 2	Inelastic Scattering (H) of 1/4 \rightarrow 1/5 H transition	56	S XII
182.16	182.36	1, 2	1/4 \rightarrow 1/5 H transition	56	Fe XI
167.50	167.62	1, 2	Inelastic Scattering (He) of 1/5 \rightarrow 1/6 H transition	56	Fe VIII
152.15	151.97	3, 3	1 \rightarrow 1/4 H transition	56	Ni XII
145.9 ^a	145.88	1, 2	Inelastic Scattering (H) of 1/5 \rightarrow 1/6 H transition	56	None

141 ^a	141.59	2, 2	Inelastic Scattering (He) of 56 1/2 → 1/4 H transition	None
129.87	130.26	1, 2	1/5 → 1/6 H transition 56	O VI
125.5 ^a	125.76	2, 2	Inelastic Scattering (H) of 56 1/2 → 1/4 H transition	None
122.2 ^a	122.56	1, 2	Inelastic Scattering (He) of 56 1/6 → 1/7 H transition	None
114 ^a	113.97	2, 2	1/2 → 1/4 H transition 56	None
110.5 ^a	110.52	1, 2	Inelastic Scattering (H) of 56 1/6 → 1/7 H transition	None
101.3 ^a	101.31	1, 2	1/6 → 1/7 H transition 56	None
96.7 ^a	96.59	1, 2	Inelastic Scattering (He) of 56 1/7 → 1/8 H transition	None
88.8	88.95	1, 2	Inelastic Scattering (H) of 56 1/7 → 1/8 H transition	None
87.0 ^a	87.34	2, 2	Inelastic Scattering (He) of 56 1/3 → 1/5 H transition	None
82.9 ^a	82.89	1, 2	1/7 → 1/8 H transition 56	None
81.1 ^a	81.05	2, 2	Inelastic Scattering (H) of 56 1/3 → 1/5 H transition	None
79.58	79.70	1, 2	Inelastic Scattering (He) of 56 1/8 → 1/9 H transition	Fe XII
76.0 ^a	75.98	2, 2	1/3 → 1/5 H transition 56	None
70.1 ^a	70.14	1, 2	1/8 → 1/9 H transition 56	None
67.5 ^a	67.84	1, 2	Inelastic Scattering (He) of 56 1/9 → 1/10 H transition	None
63.12	63.14	2, 2	Inelastic Scattering (He) of 56 1/4 → 1/6 H transition	Mg X
61.0 ^a	60.78	1, 2	1/9 → 1/10 H transition 56	None
59.7 ^a	59.79	2, 2	Inelastic Scattering (H) of 56 1/4 → 1/6 H transition	None

^a Wavelength read from Figure 1 of [59]; wavelength not given in Table of [59];

^b For lower-energy transitions, $n = 1, \frac{1}{2}, \frac{1}{3}, \frac{1}{4}, \dots$, and $n_i > n_f$ induced by a disproportionation reaction with $H\left[\frac{a_H}{2}\right]$, $E = \left(\frac{1}{n_f^2} - \frac{1}{n_i^2}\right) X 13.6 \text{ eV} - m'^2 X 13.6 \text{ eV}$;

^b For helium inelastic scattered peaks of hydrogen transitions, $n_i \rightarrow n_f$,
 $E = \left(\frac{1}{n_f^2} - \frac{1}{n_i^2}\right) X 13.6 \text{ eV} - m'^2 X 13.6 \text{ eV} - 21.21 \text{ eV}$ (when this photon strikes $He(1s^2)$,
 21.2 eV is absorbed in the excitation to $He(1s^1 2p^1)$);

^b For hydrogen inelastic scattered peaks of hydrogen transitions, $n_i \rightarrow n_f$,
 $E = \left(\frac{1}{n_f^2} - \frac{1}{n_i^2}\right) X 13.6 \text{ eV} - m'^2 X 13.6 \text{ eV} - 10.2 \text{ eV}$ (when this photon strikes $H(1s^1)$,
 10.2 eV is absorbed in the excitation to $H(2p^1)$);

^c $H[n=1] \xrightarrow{2H} H\left[n=\frac{1}{2}\right] + h\nu (911.8 \text{ \AA})$;

^d $H(2p^1) \rightarrow H(1s^1) + 10.2 \text{ eV}$ (excitation by emission of lower-energy hydrogen transitions);

^e $He(1s^1 2p^1) \rightarrow He(1s^2) + 21.2 \text{ eV}$ (excitation by emission of lower-energy hydrogen transitions);

^f Eqs. (10-12).

Figure Captions

Figure 1. Cross sectional view of the discharge cell.

Figure 2. The experimental set up comprising a discharge gas cell light source and an EUV spectrometer which was differentially pumped.

Figure 3. The EUV spectrum (200-1250 Å) of the control hydrogen discharge cell emission that was recorded with a normal incidence EUV spectrometer and a CEM.

Figure 4. The EUV spectrum (200–645 Å) of the control xenon discharge cell emission that was recorded with a 4° grazing incidence EUV spectrometer and a CEM.

Figure 5. The EUV spectrum (150–650 Å) of the helium-hydrogen mixture (98/2%) microwave cell emission that was recorded at 1, 24, and 72 hours with a normal incidence EUV spectrometer and a CEM. The pressure was maintained at 20 torr.

Figure 6. The EUV spectrum (150–650 Å) of the helium-hydrogen mixture (98/2%) microwave cell emission that was recorded with a normal incidence EUV spectrometer and a CEM. The pressure was maintained at 20 torr and 760 torr for the top and bottom curves, respectively.

Figure 7. The short wavelength EUV spectrum (50-200 Å) of the control hydrogen discharge cell emission that was recorded with a normal incidence EUV spectrometer and a CEM.

Figure 8. The short wavelength EUV spectrum (50–460 Å) of the helium-hydrogen mixture (98/2%) microwave cell emission that was recorded with a normal incidence EUV spectrometer and a CEM. The pressure was maintained at 1 torr.

Figure 9. The EUV spectrum (500–650 Å) of the helium-hydrogen mixture (98/2%) discharge cell emission that was recorded with a 4° grazing incidence EUV spectrometer and a CEM. The pressure was maintained at 400 mtorr.

Figure 10. The EUV spectrum (880–1250 Å) of the helium-hydrogen mixture (98/2%) microwave cell emission that was recorded with a normal incidence EUV spectrometer and a CEM. The pressure was maintained at 20 torr.

Figure 11. The EUV spectrum (800–1050 Å) of the control hydrogen discharge cell emission that was recorded with a normal incidence EUV spectrometer and a CEM.

Fig. 1

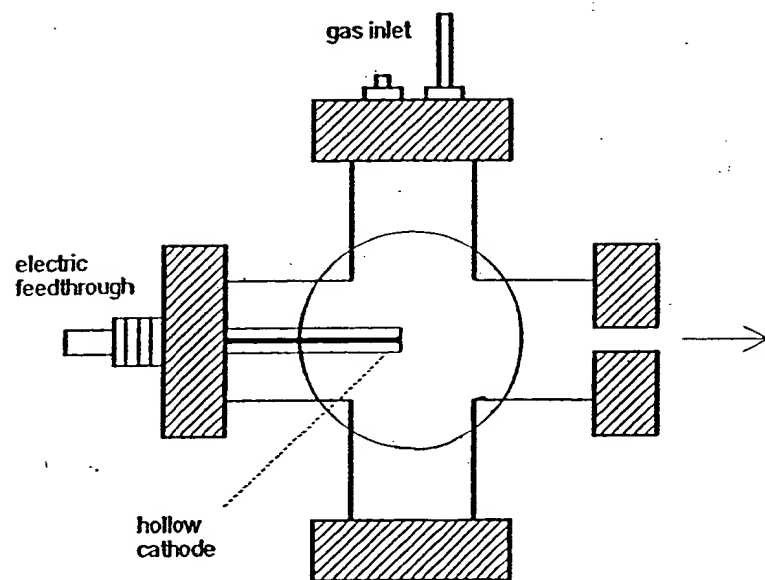
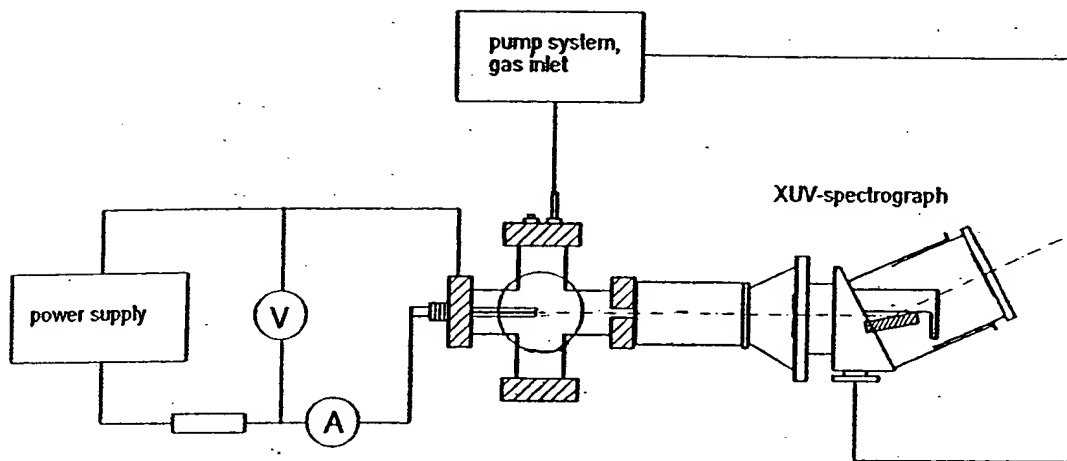


Fig. 2



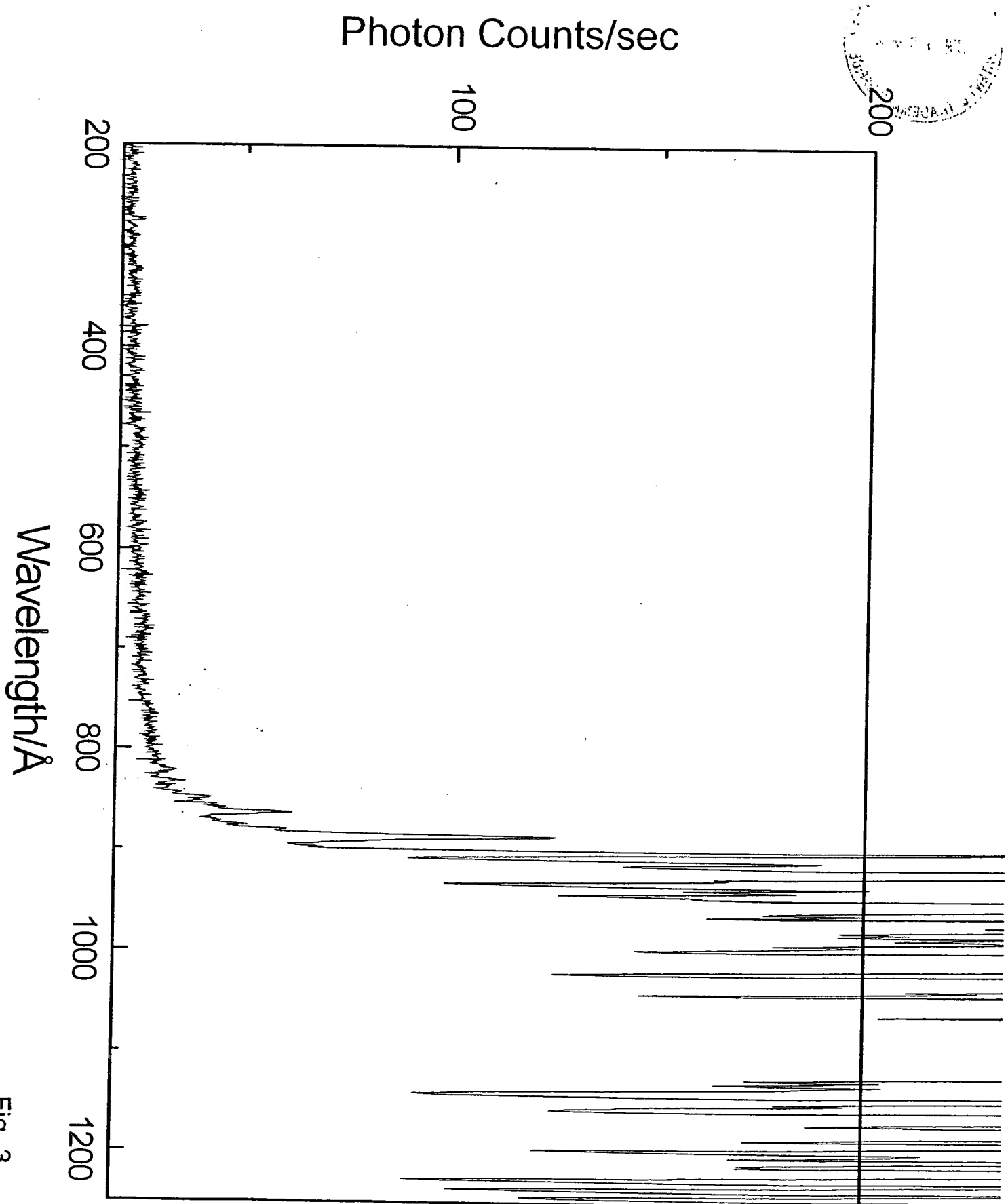
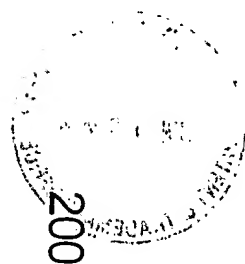


Fig. 3

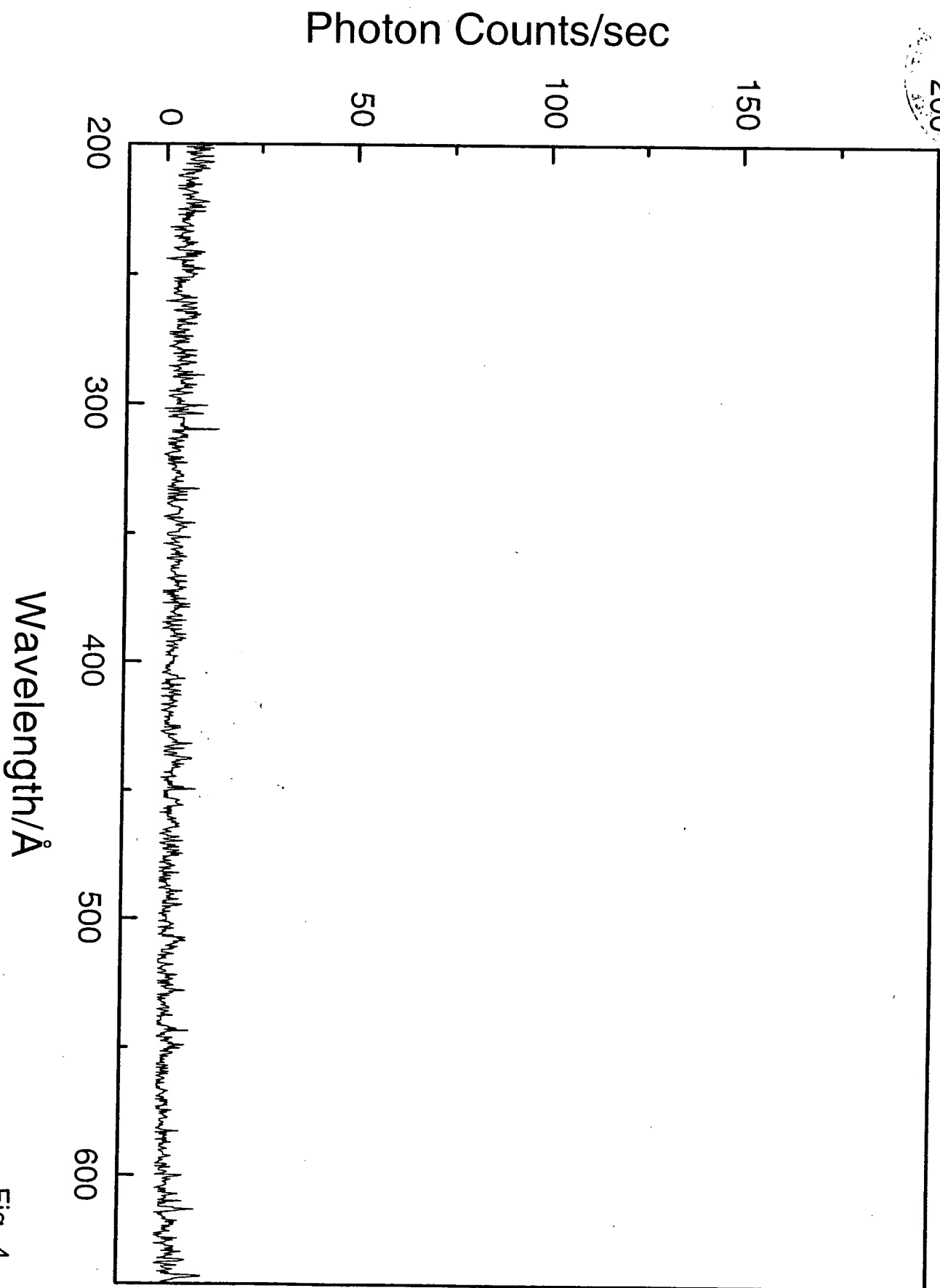


Fig. 4

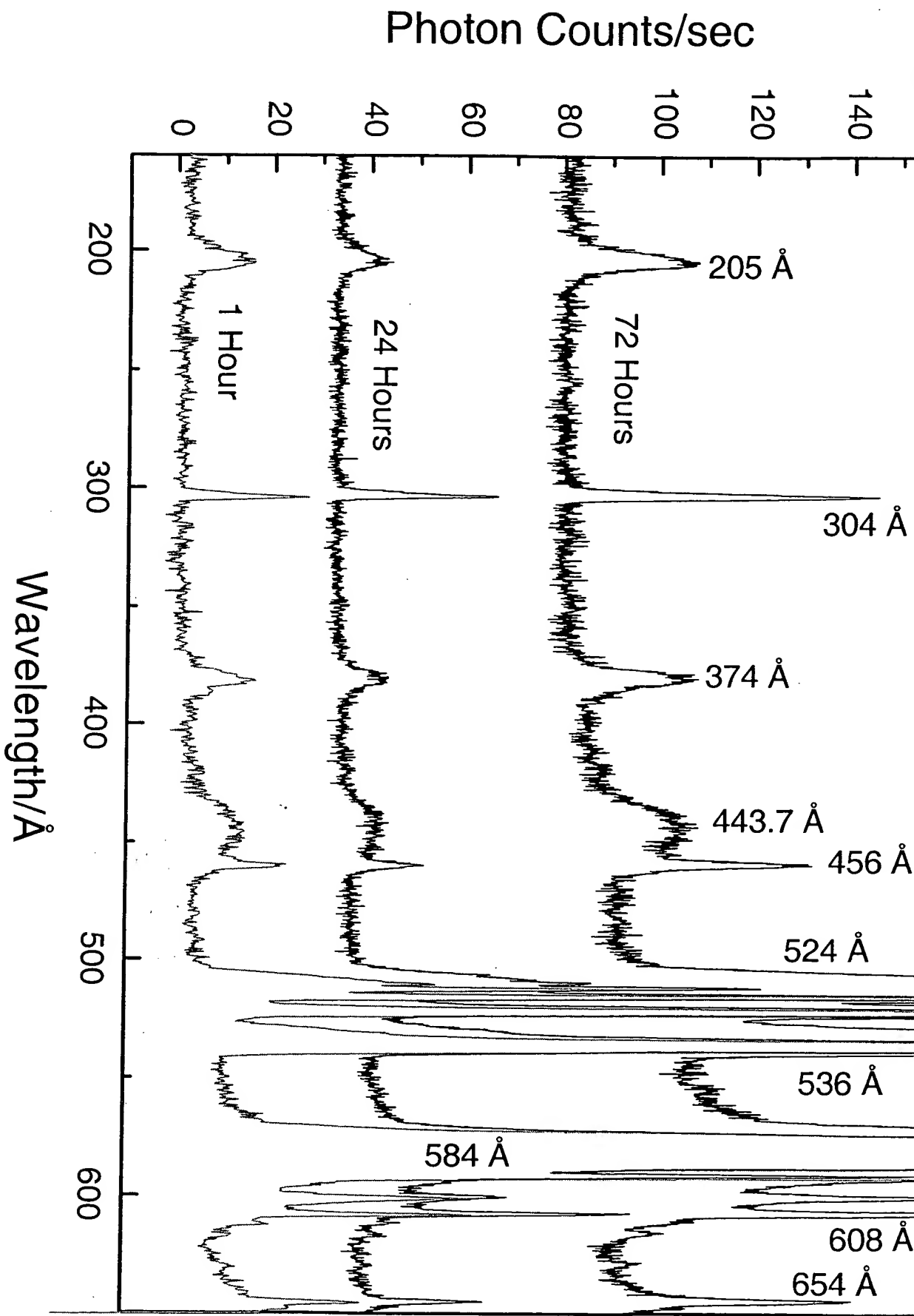


Fig. 5

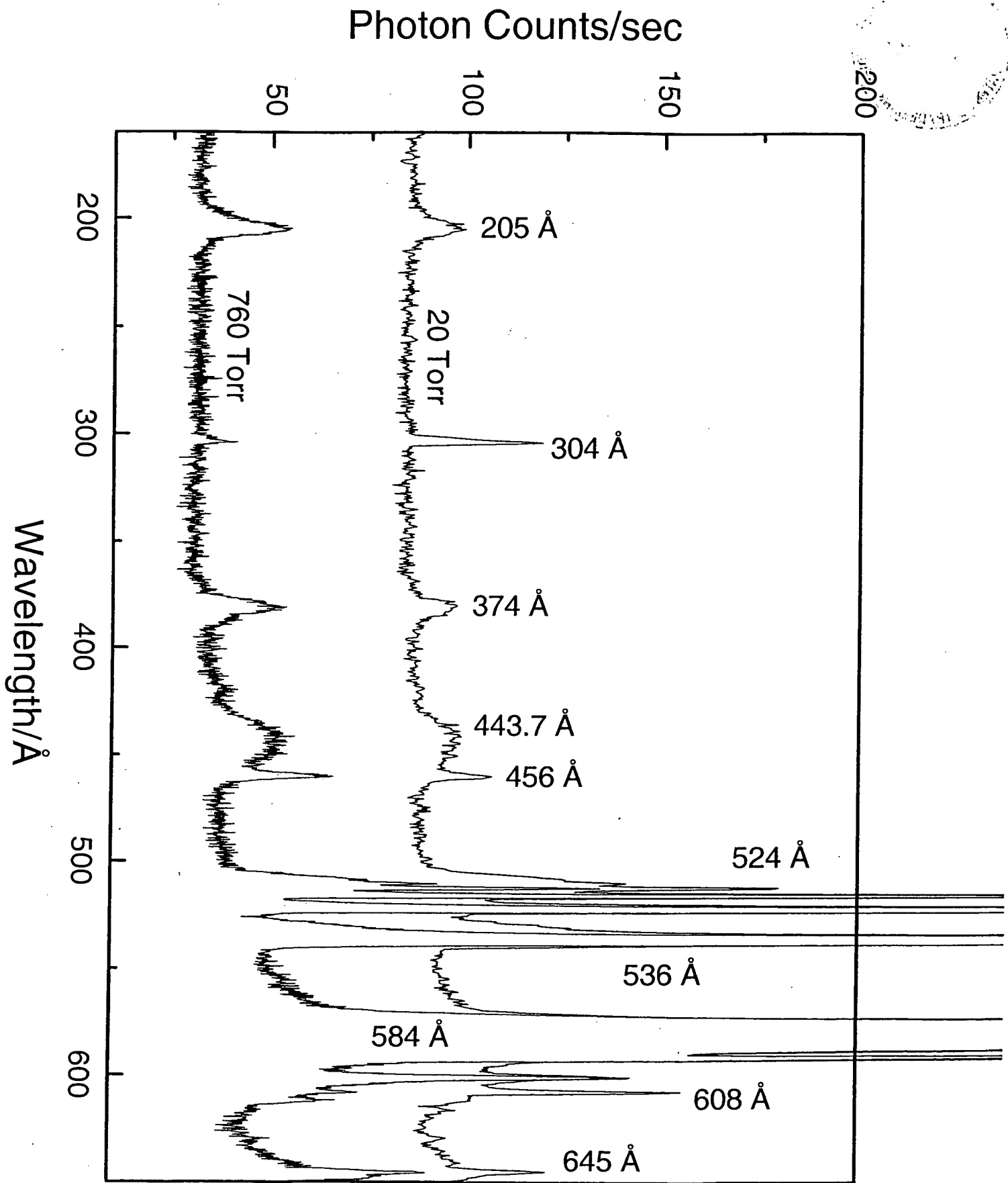


Fig. 6

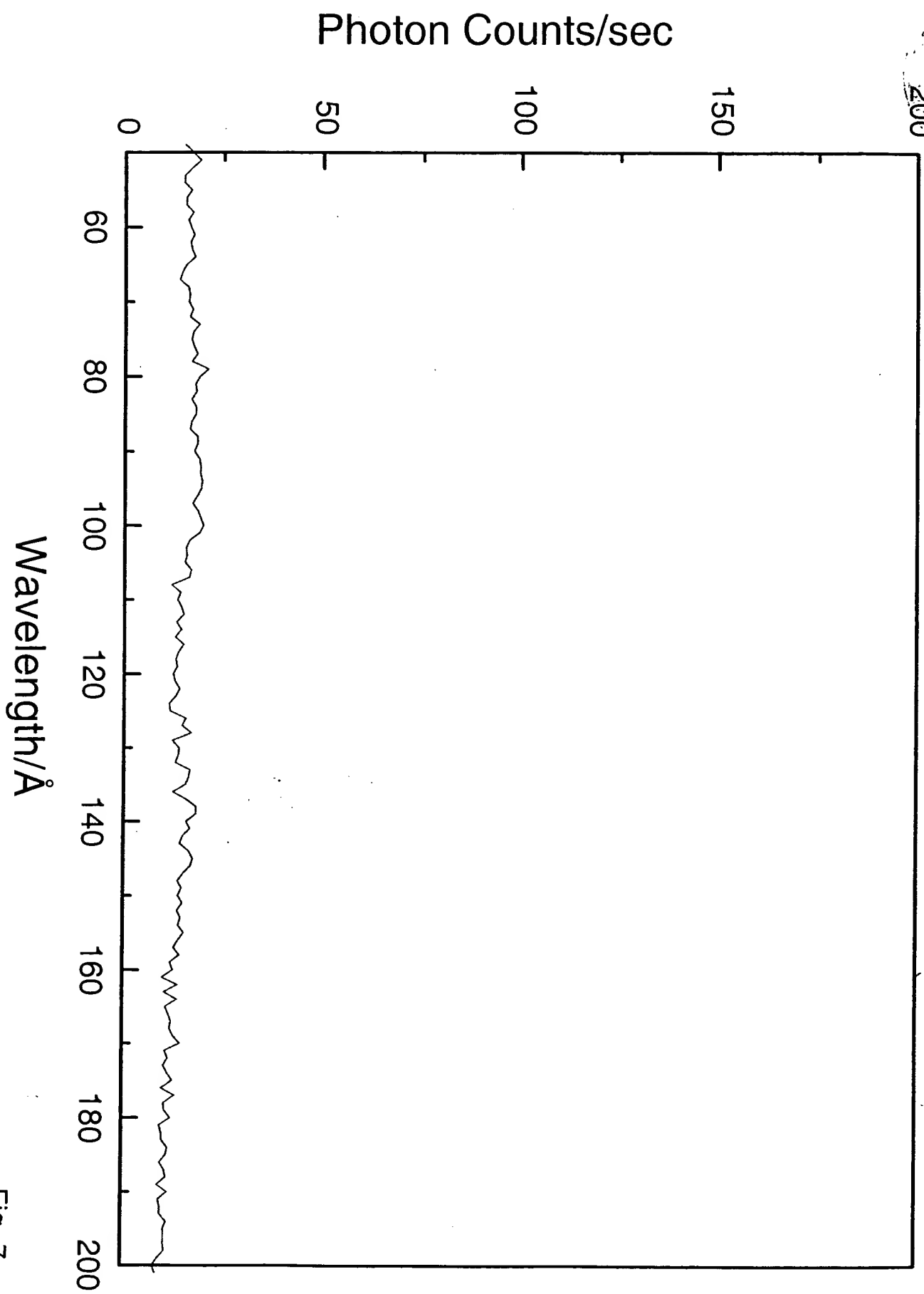


Fig. 7

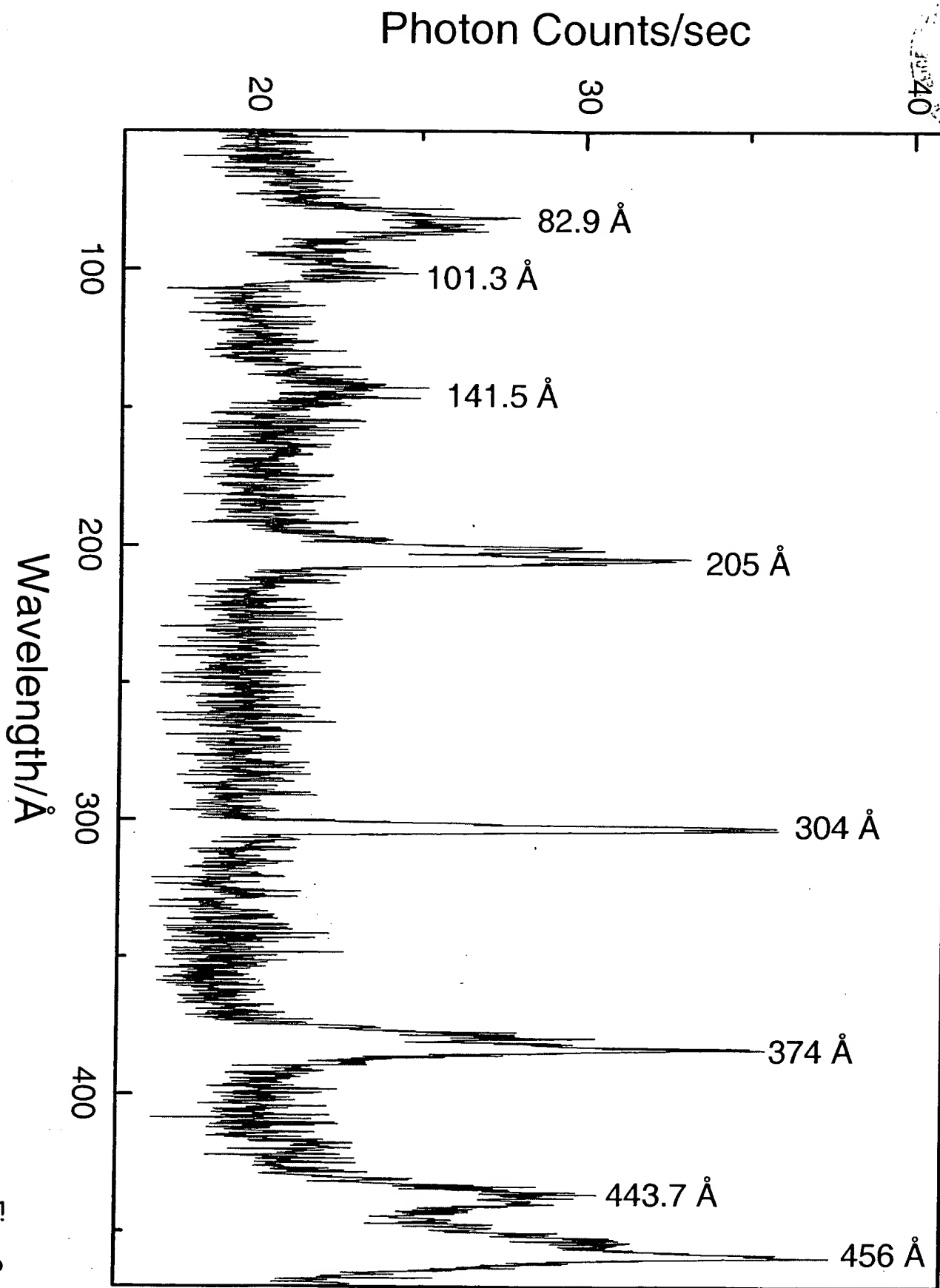


Fig. 8

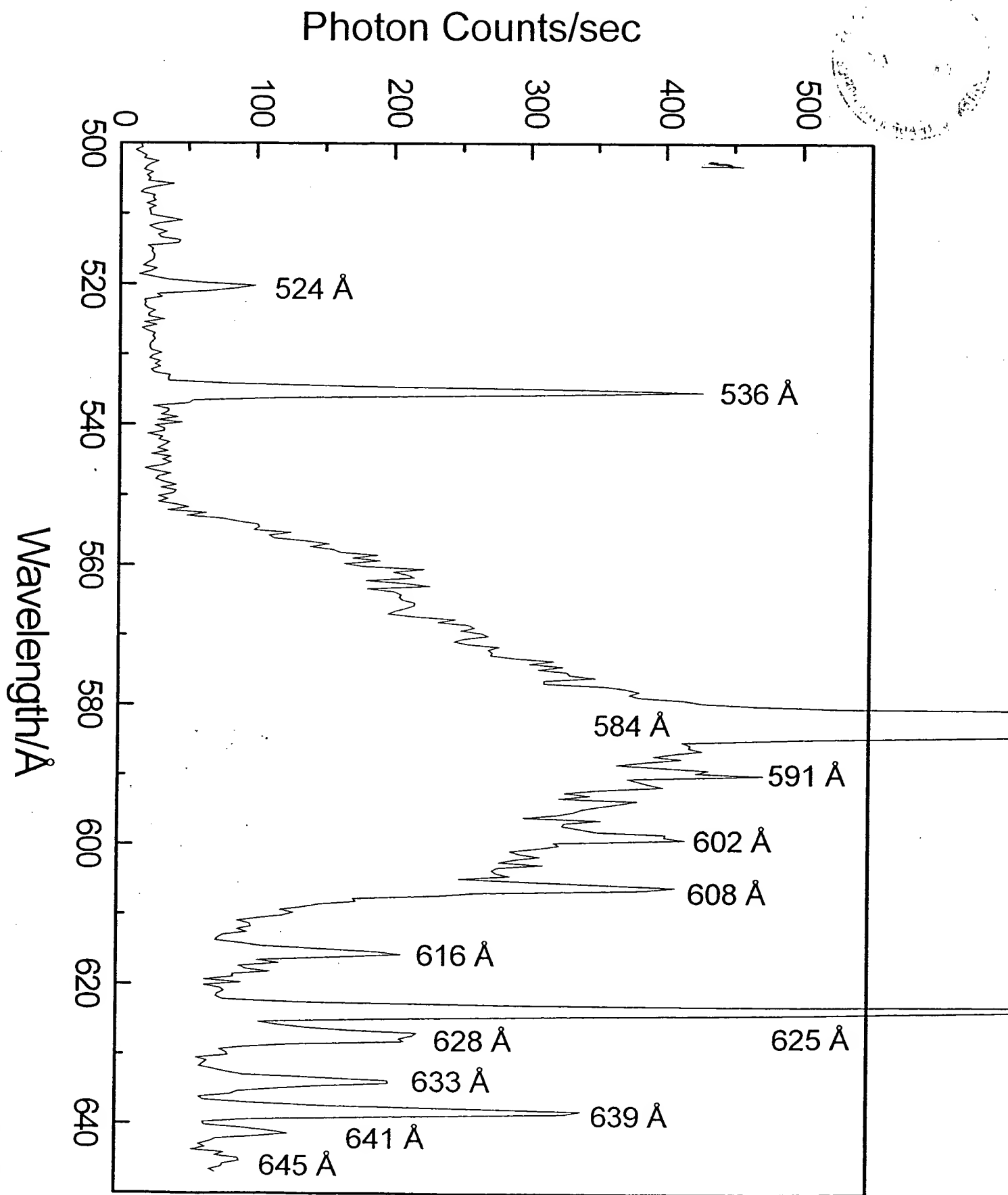


Fig. 9

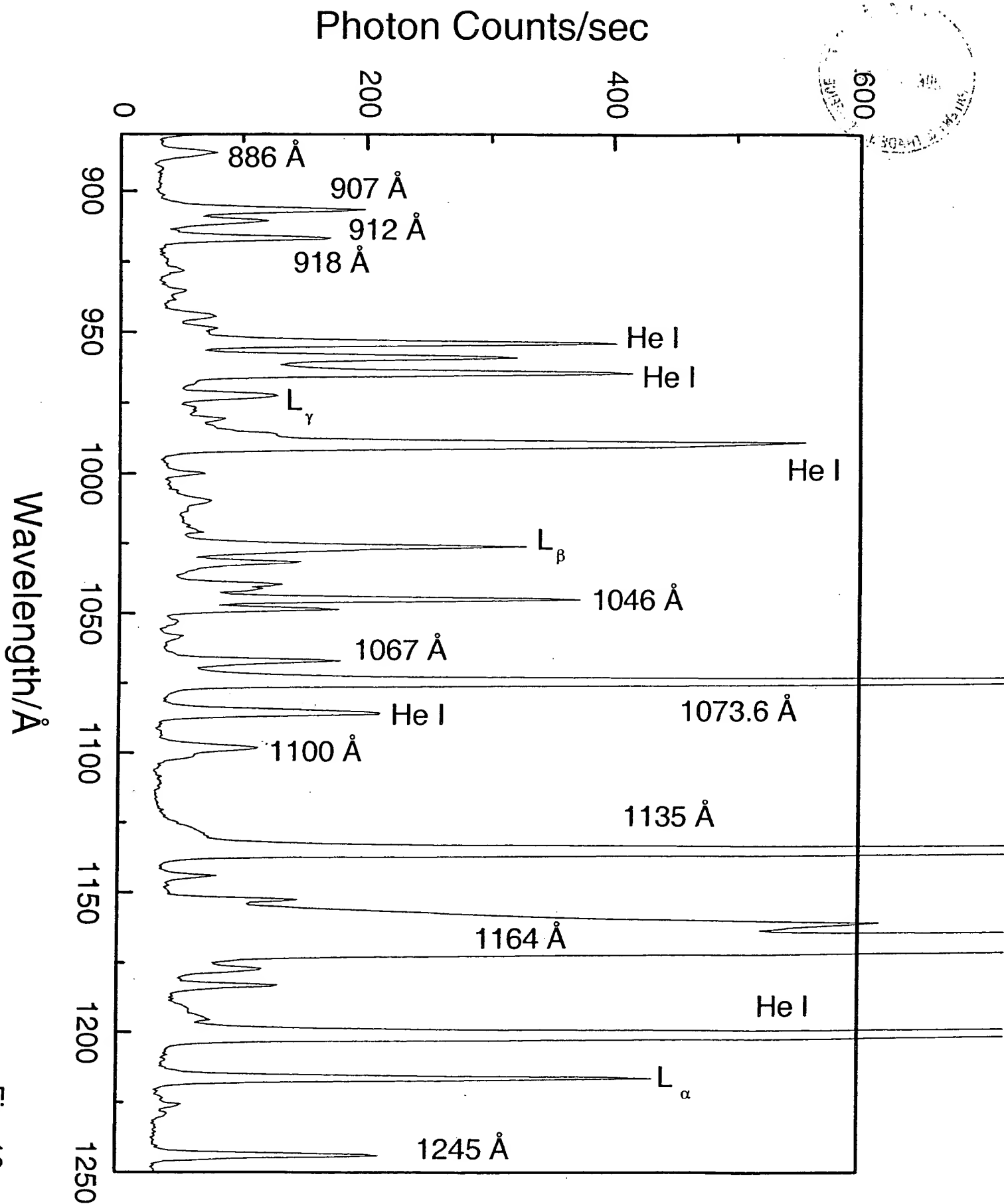


Fig. 10

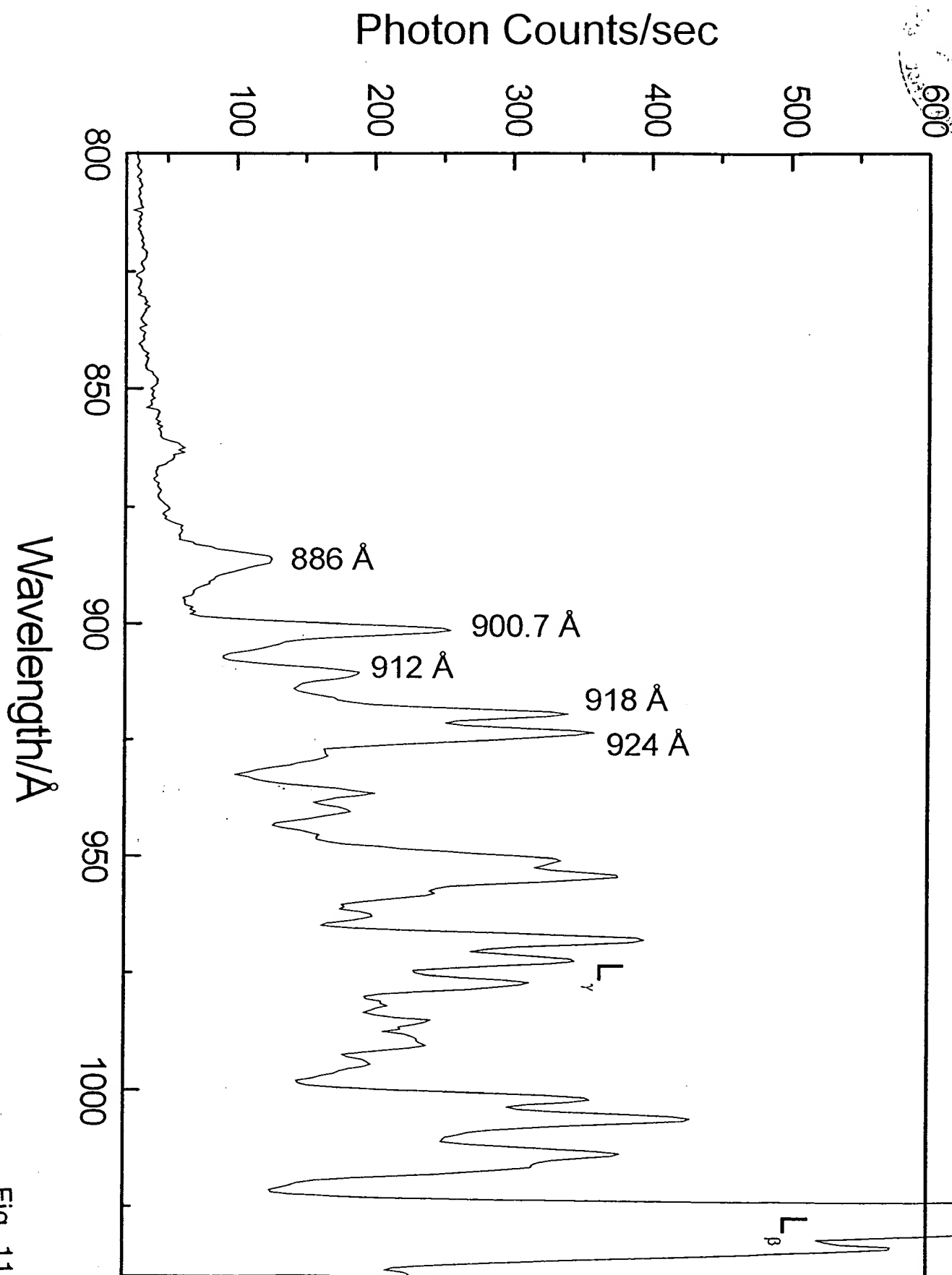


Fig. 11

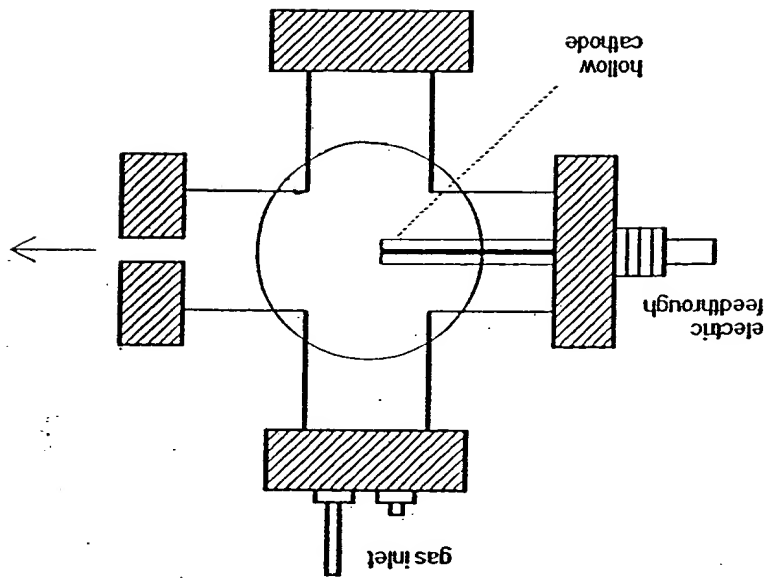


Fig. 1

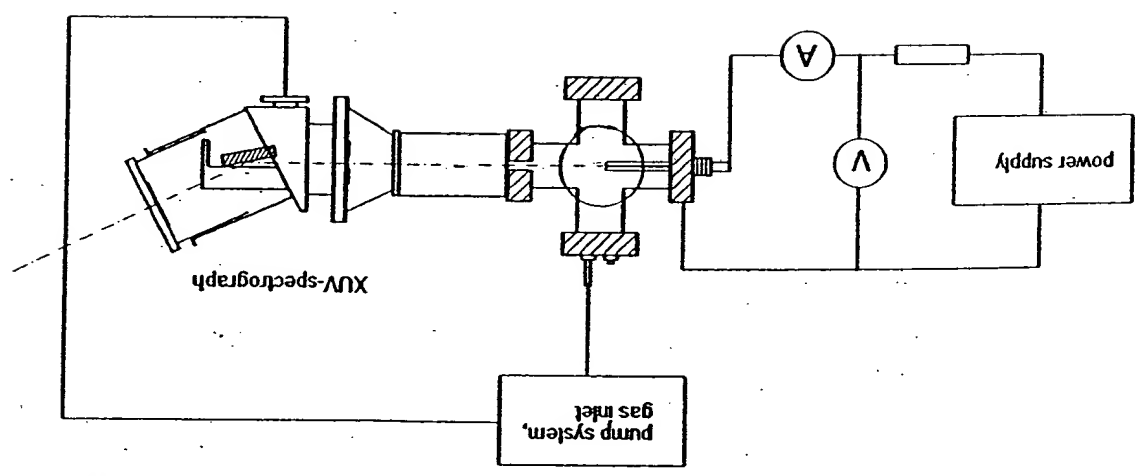


Fig. 2

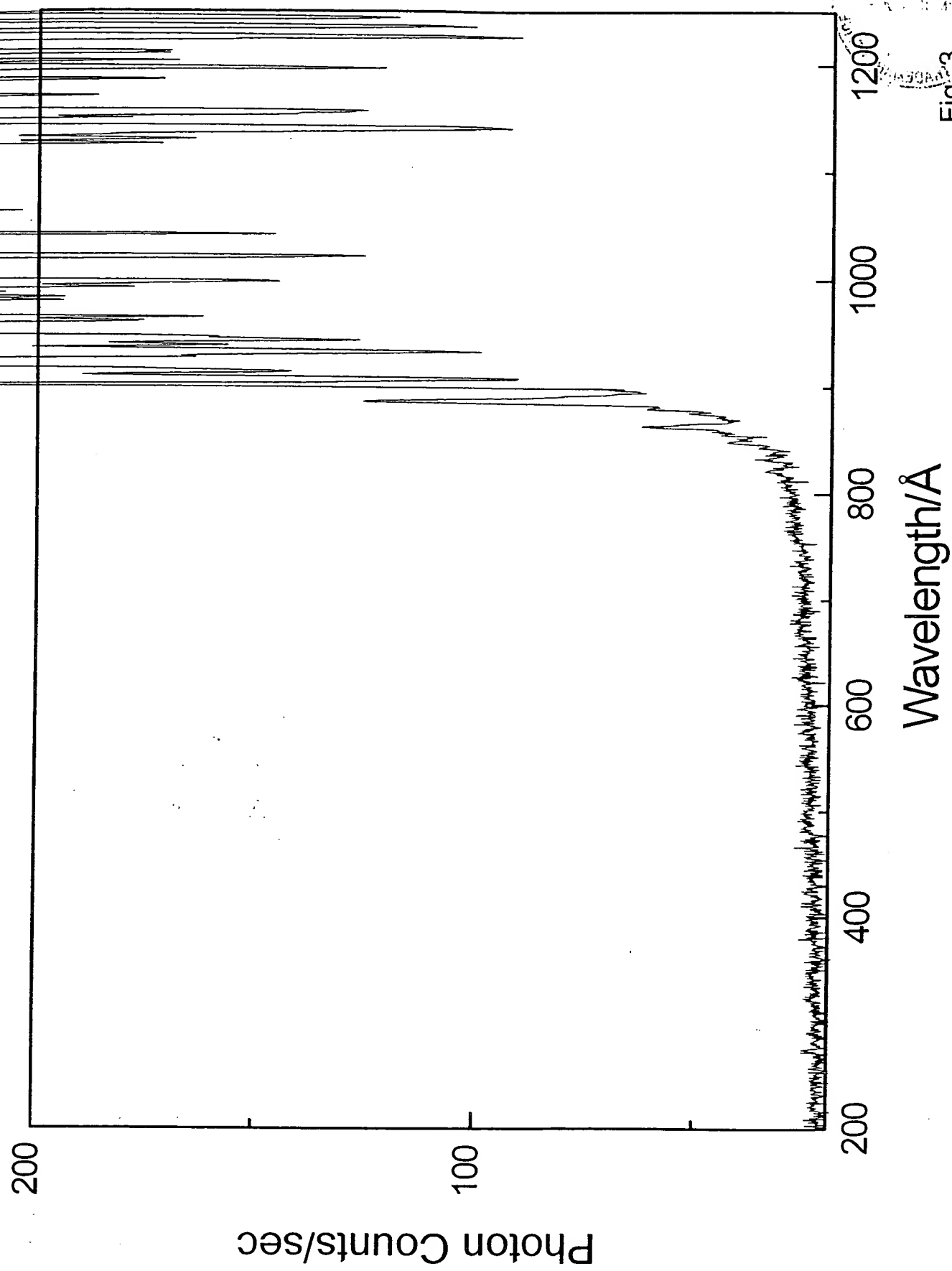


Fig. 3

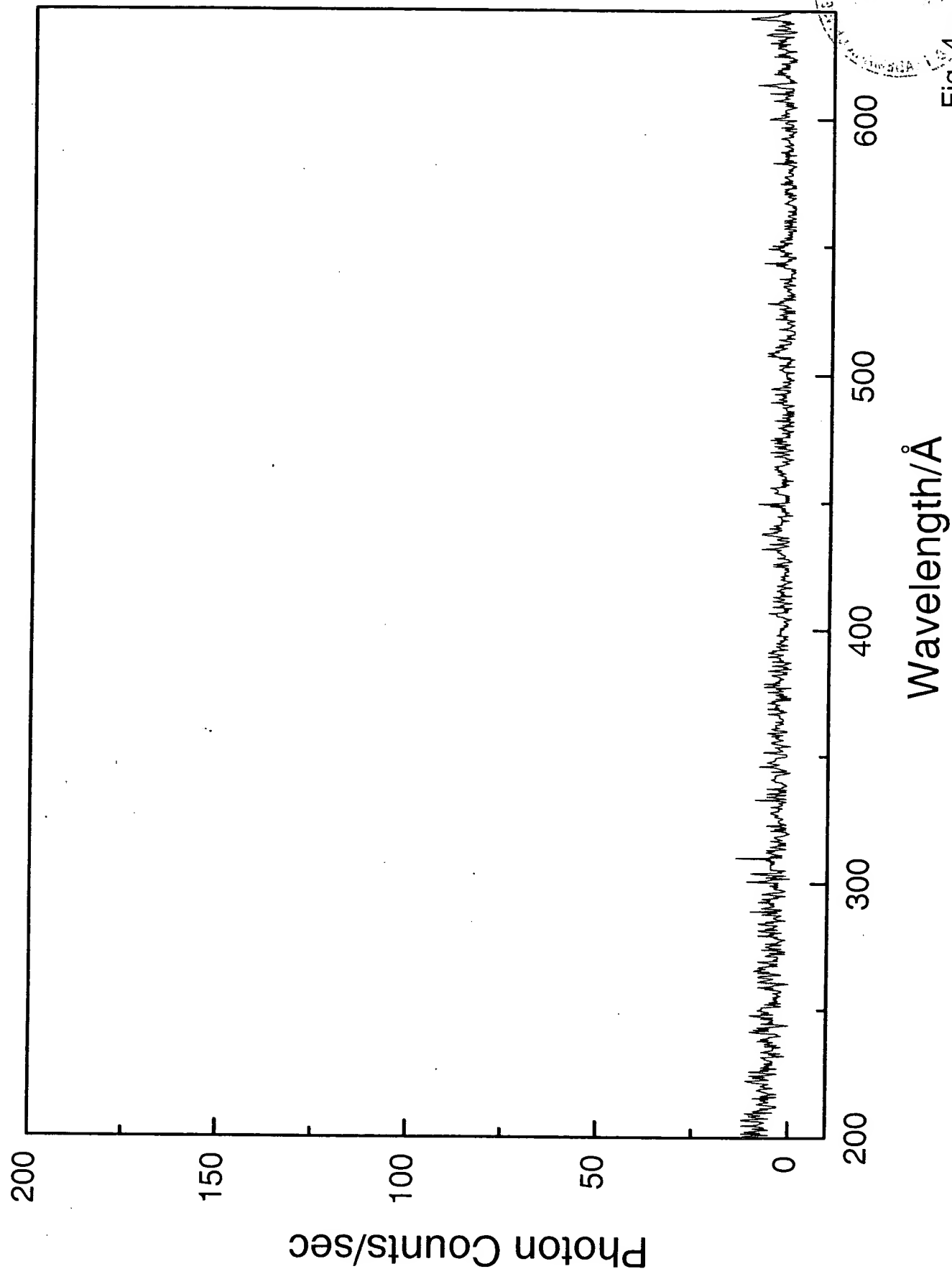


Fig. 4

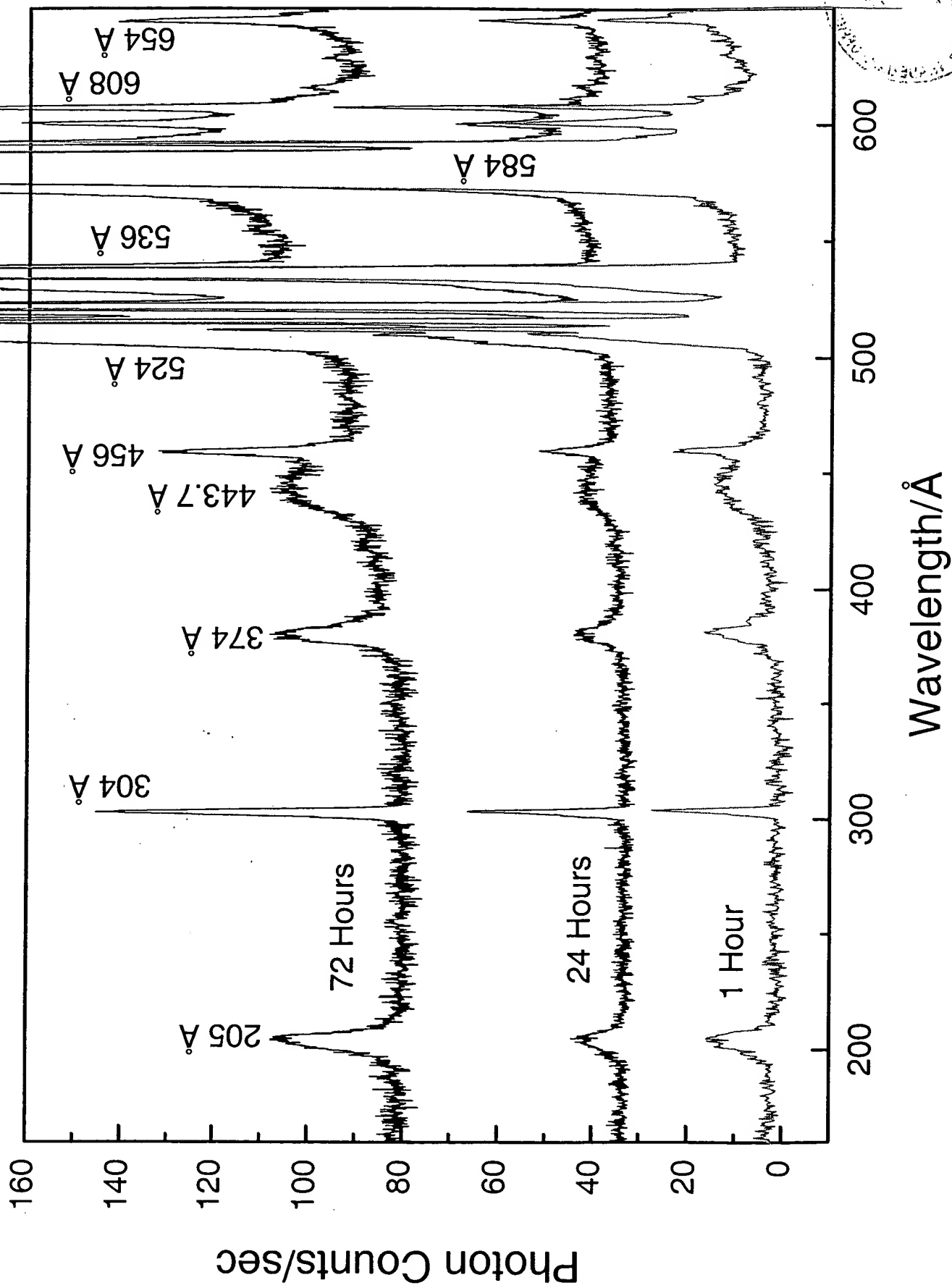


Fig. 5

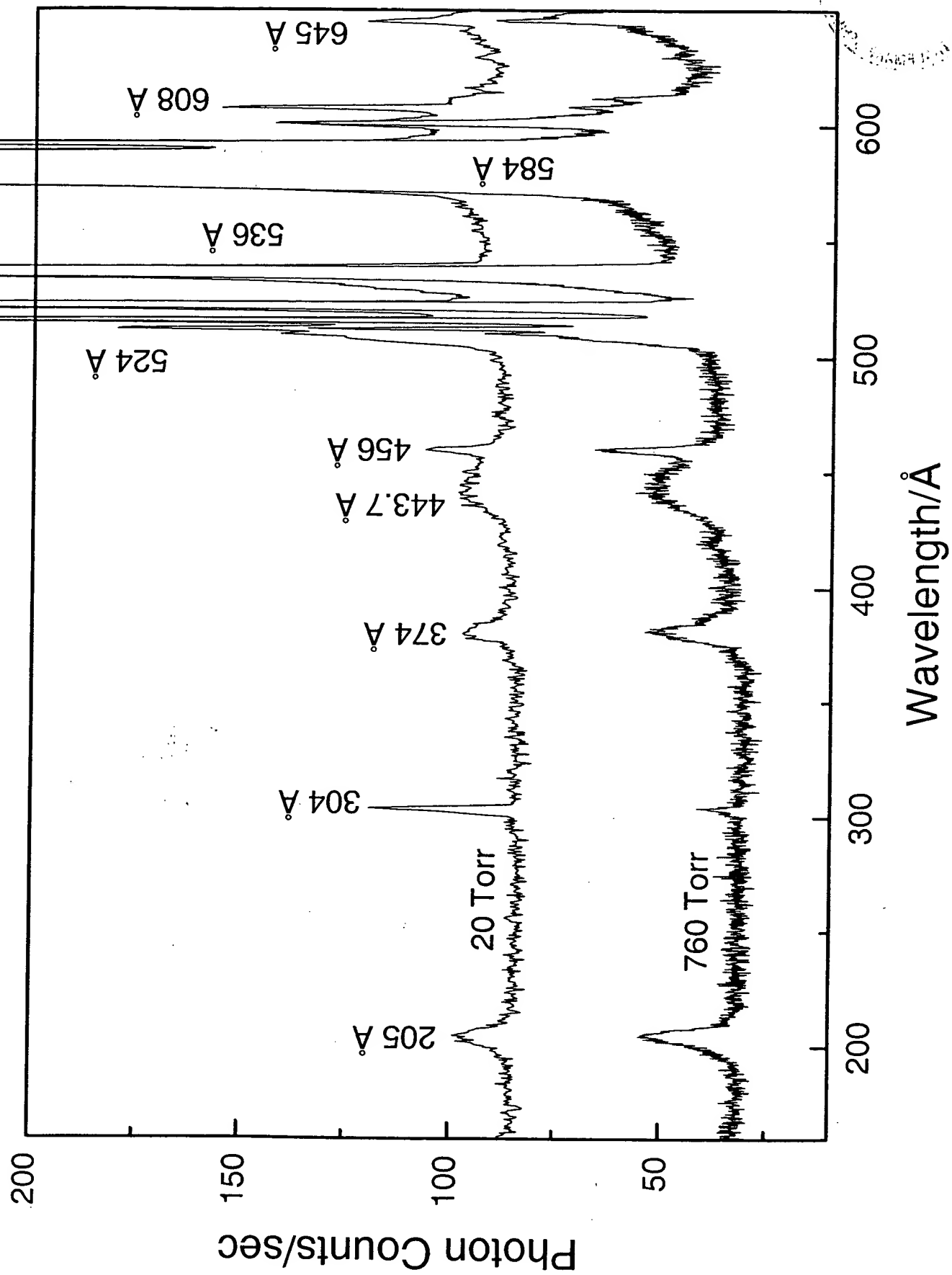


Fig. 6

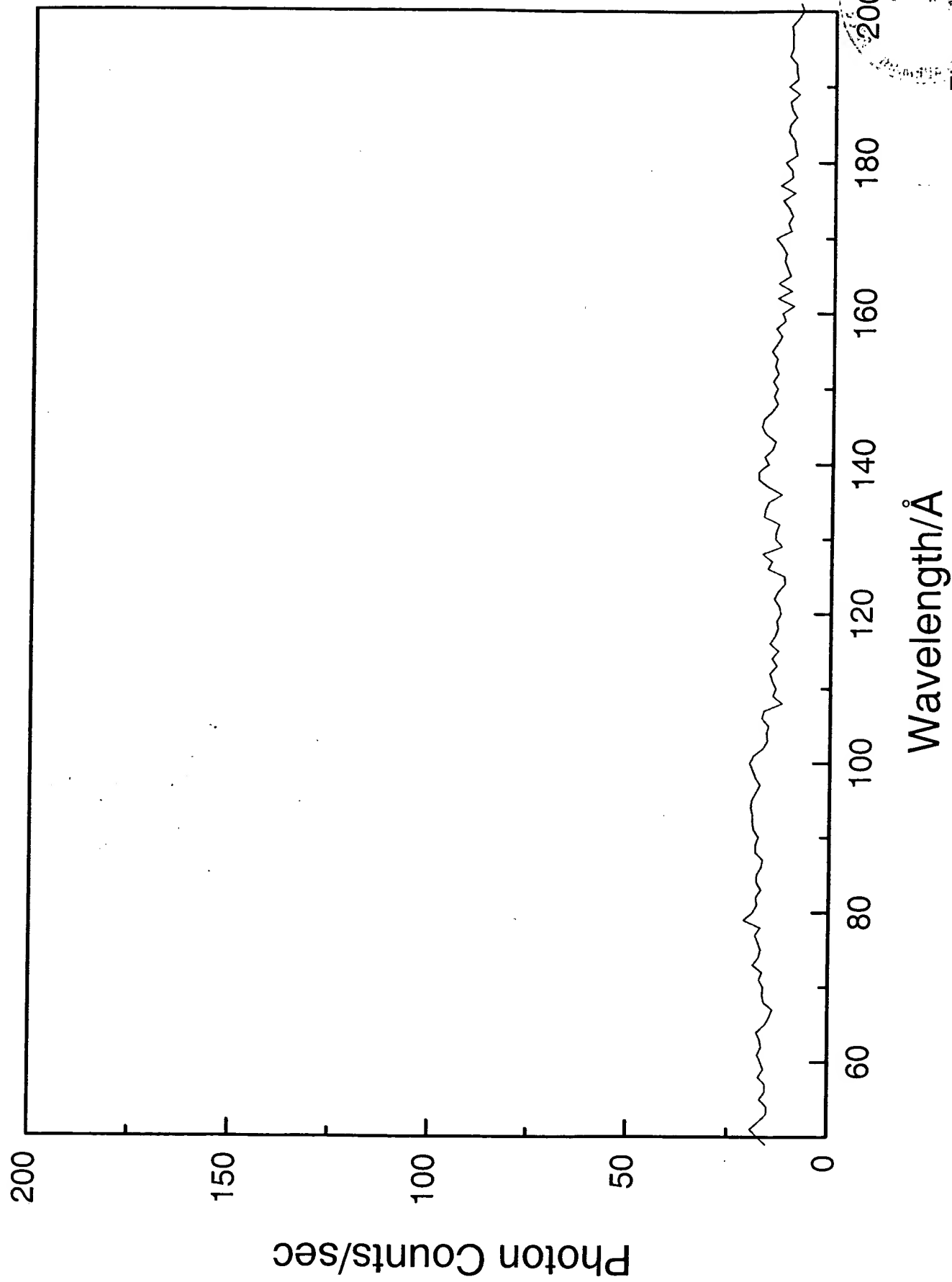


Fig. 7

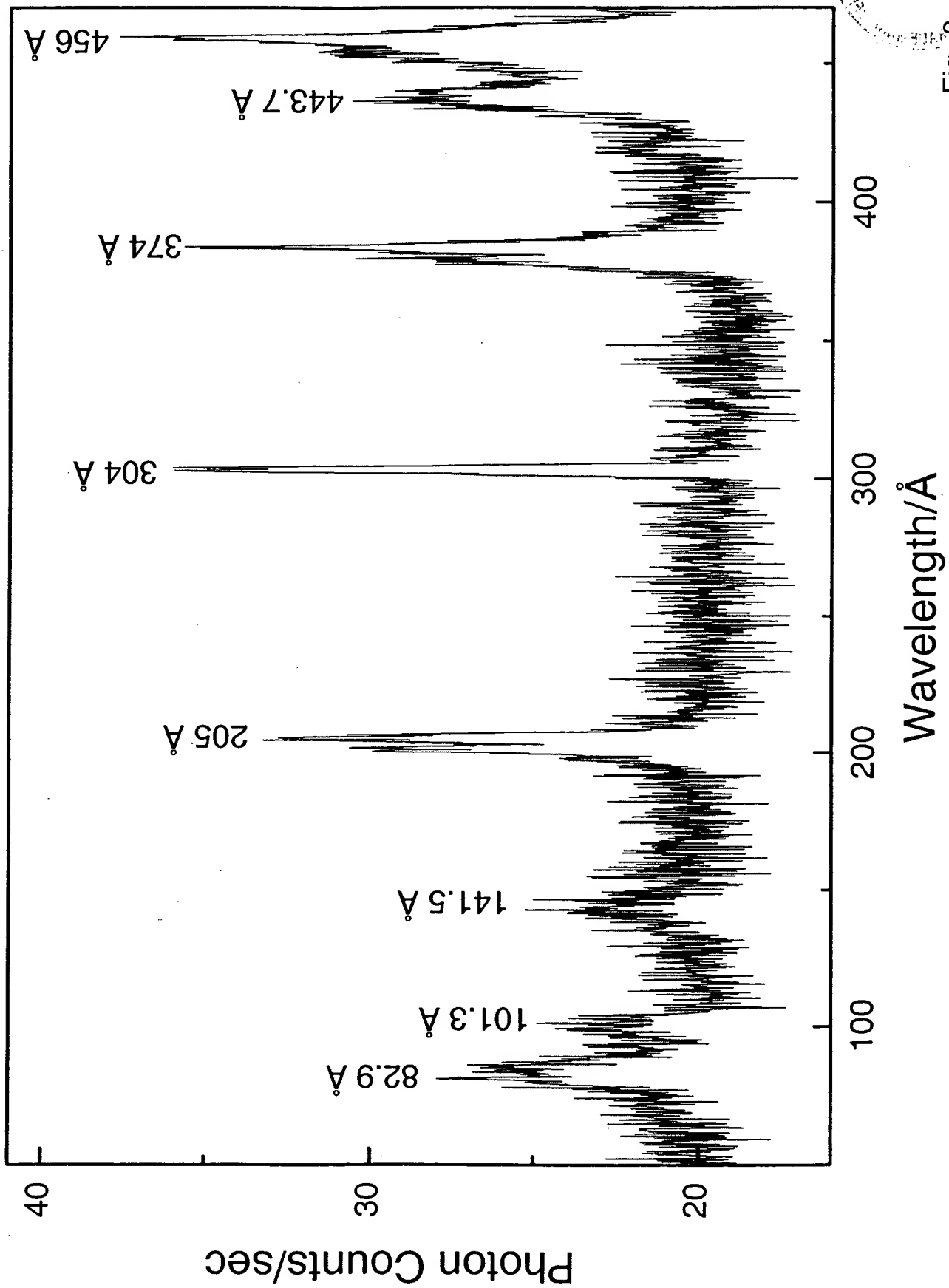


Fig. 8

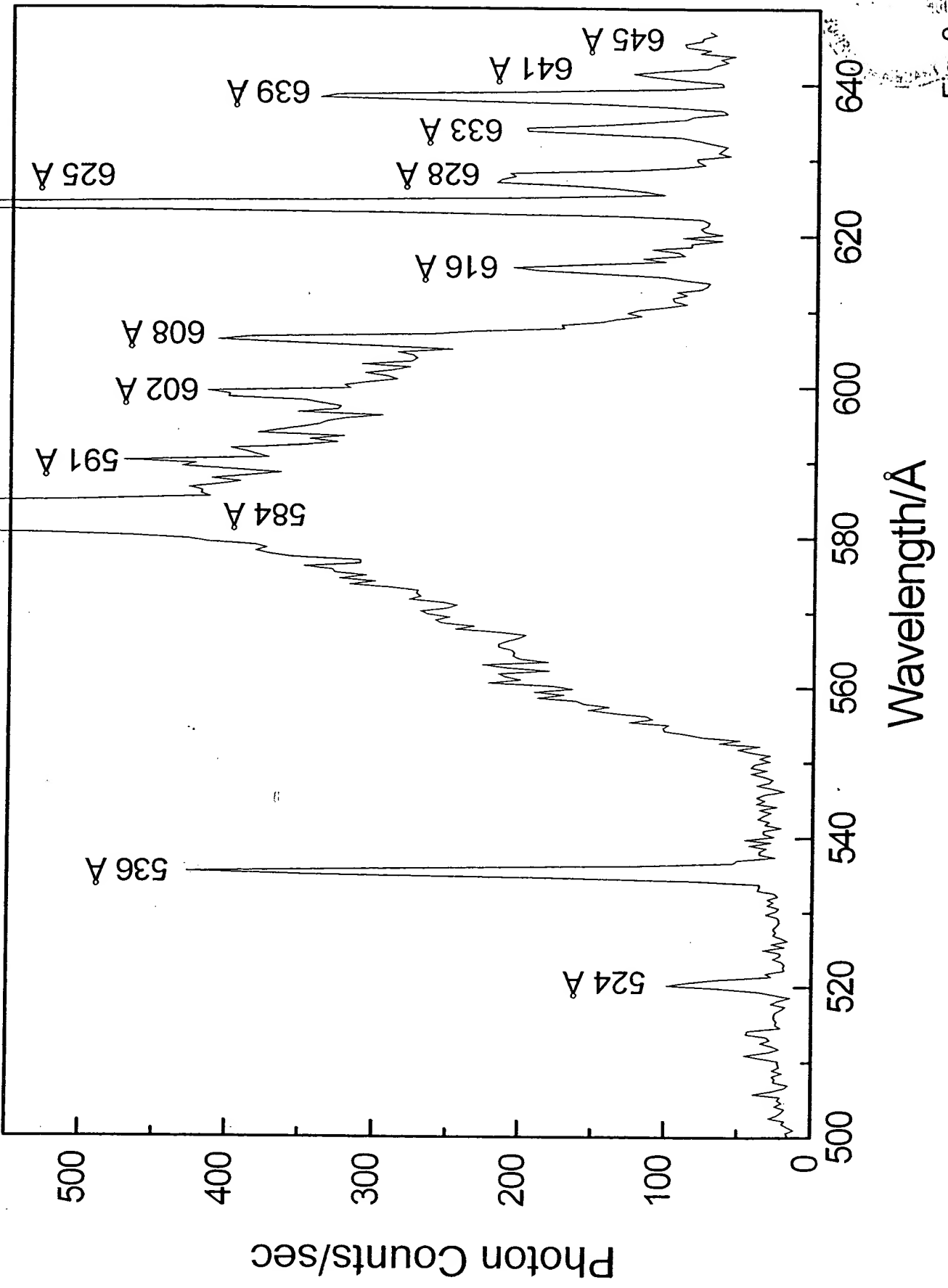


Fig. 9

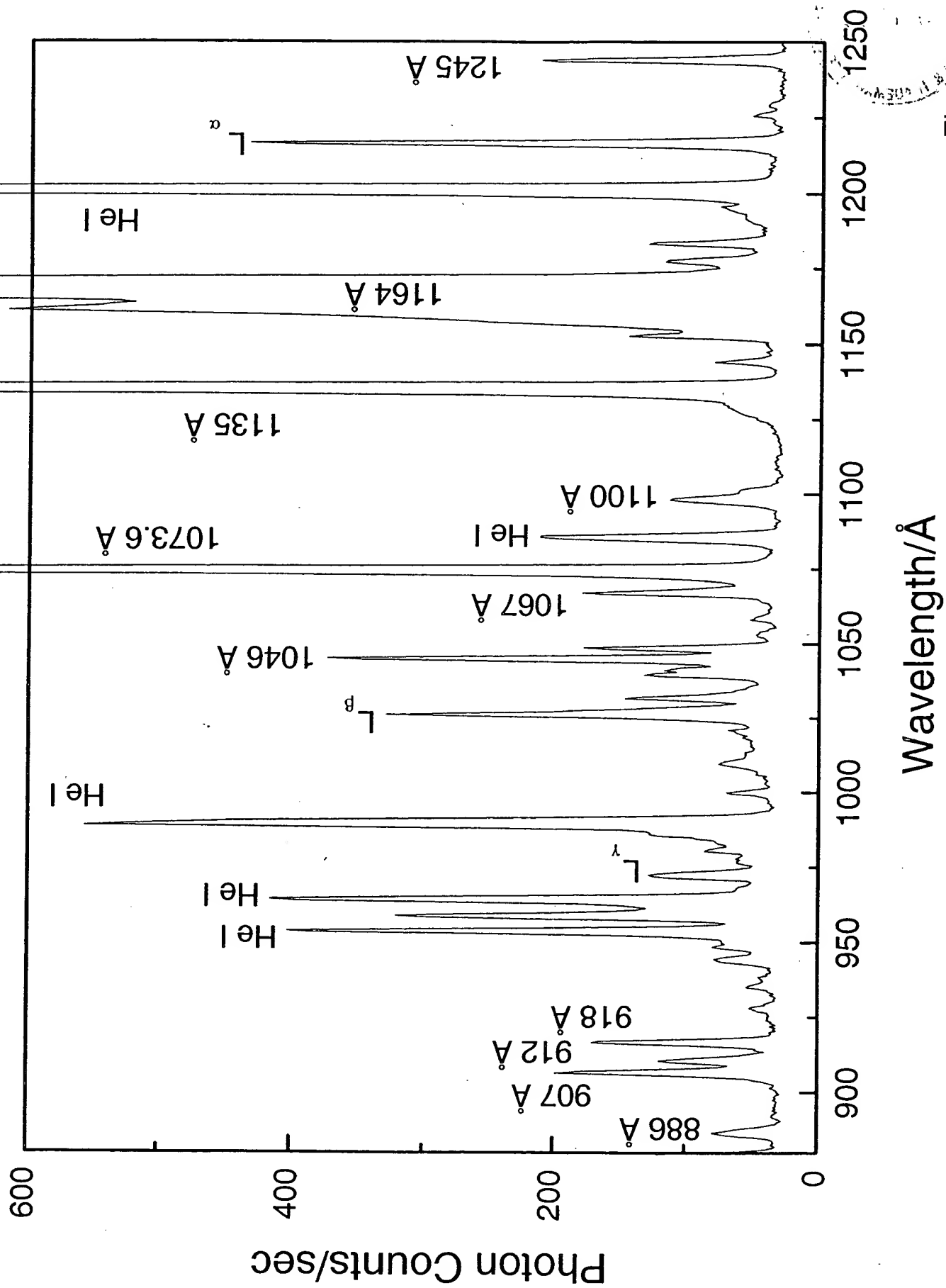


Fig. 10

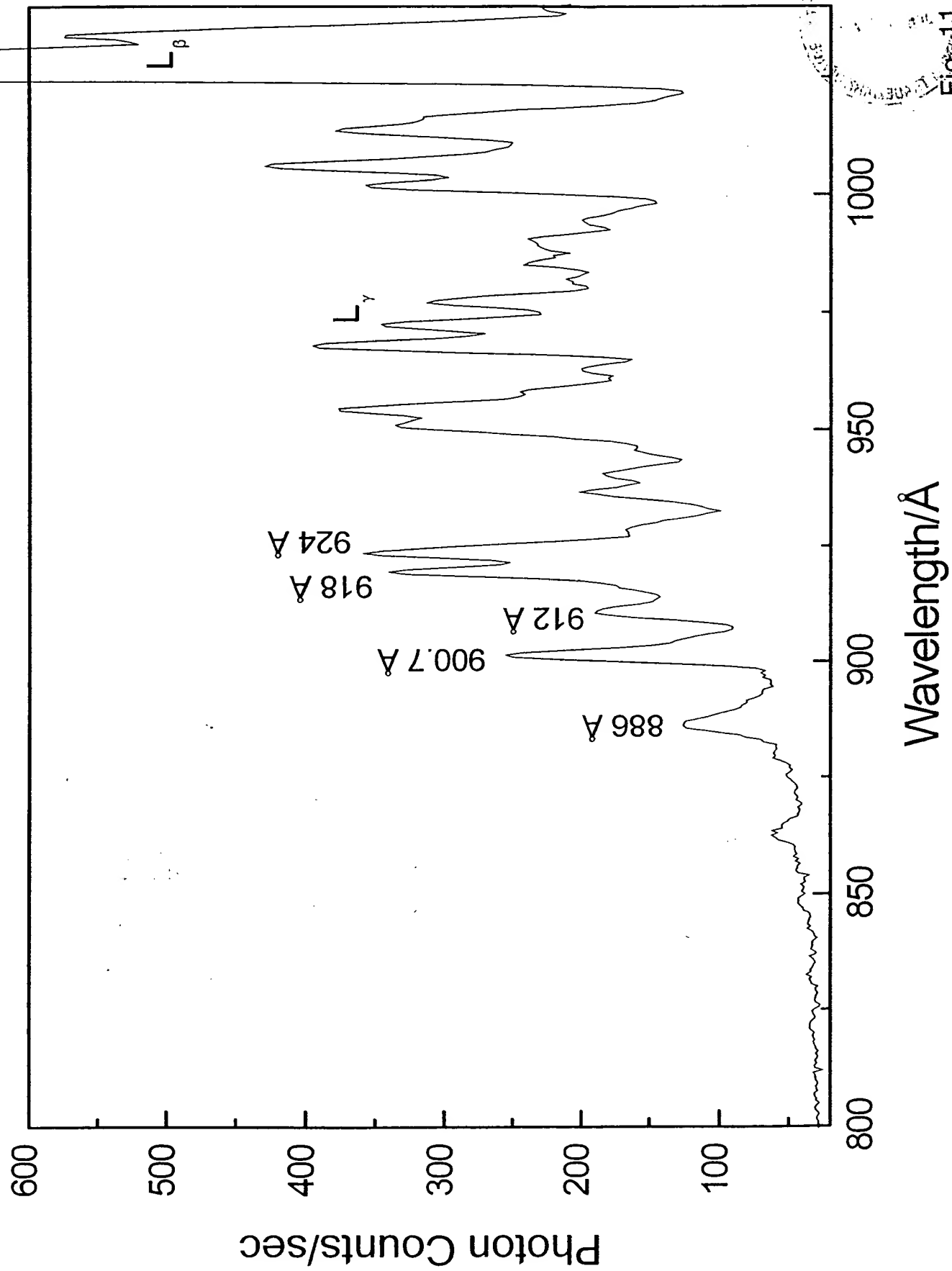


Fig 3.11

Spectroscopic Identification of a Novel Catalytic Reaction of Potassium and Atomic Hydrogen and the Hydride Ion Product

Randell L. Mills

Paresh Ray

BlackLight Power, Inc.

493 Old Trenton Road

Cranbury, NJ 08512

ABSTRACT

From a solution of a Schrödinger-type wave equation with a nonradiative boundary condition based on Maxwell's equations, Mills predicts that atomic hydrogen may undergo a catalytic reaction with certain atomized elements and ions which singly or multiply ionize at integer multiples of the potential energy of atomic hydrogen, 27.2 eV , $m \cdot 27.2\text{ eV}$ wherein m is an integer. The reaction involves a nonradiative energy transfer to form a hydrogen atom that is lower in energy than unreacted atomic hydrogen with the release of energy. One such atomic catalytic system involves potassium atoms. The first, second, and third ionization energies of potassium are 4.34066 eV , 31.63 eV , and 45.806 eV , respectively. The triple ionization ($t=3$) reaction of K to K^{3+} , then, has a net enthalpy of reaction of 81.7766 eV , which is equivalent to $3 \cdot 27.2\text{ eV}$. Intense extreme ultraviolet (EUV) emission was observed from incandescently heated atomic hydrogen and the atomized potassium catalyst that generated an anomalous plasma at low temperatures (e.g. $\approx 10^3\text{ K}$) and an extraordinary low field strength of about $1\text{--}2\text{ V/cm}$. No emission was observed with potassium or hydrogen alone or when sodium replaced potassium with hydrogen. Emission was observed from K^{3+} that confirmed the resonant nonradiative energy transfer of $3 \cdot 27.2\text{ eV}$ from atomic hydrogen to atomic potassium. The catalysis product, a lower-energy hydrogen atom, was predicted to be a highly reactive intermediate which further reacts to form a novel hydride ion. The predicted hydride ion of hydrogen catalysis by atomic potassium is the hydride ion $H^-(1/4)$. This ion was observed spectroscopically at 110 nm corresponding to its predicted binding energy of 11.2 eV .

I. INTRODUCTION

Based on the solution of a Schrödinger-type wave equation with a nonradiative boundary condition based on Maxwell's equations, Mills [1-39] predicts that atomic hydrogen may undergo a catalytic reaction with certain atomized elements or certain gaseous ions which singly or multiply ionize at integer multiples of the potential energy of atomic hydrogen, 27.2 eV . For example, cesium atoms ionize at an integer multiple of the potential energy of atomic hydrogen, $m \cdot 27.2\text{ eV}$. The enthalpy of ionization of Cs to Cs^{2+} has a net enthalpy of reaction of 27.05135 eV , which is equivalent to $m=1$ [40]. And, the reaction Ar^+ to Ar^{2+} has a net enthalpy of reaction of 27.63 eV , which is equivalent to $m=1$ [40]. In each case, the reaction involves a nonradiative energy transfer to form a hydrogen atom that is lower in energy than unreacted atomic hydrogen. The product hydrogen atom has an energy state that corresponds to a fractional principal quantum number. Recent analysis of mobility and spectroscopy data of individual electrons in liquid helium show direct experimental confirmation that electrons may have fractional principal quantum energy levels [36]. The lower-energy hydrogen atom is a highly reactive intermediate which further reacts to form a novel hydride ion. Emission was observed previously from a continuum state of Cs^{2+} and Ar^{2+} at 53.3 nm and 45.6 nm , respectively [6]. The single emission feature with the absence of the other corresponding Rydberg series of lines from these species confirmed the resonant nonradiative energy transfer of 27.2 eV from atomic hydrogen to atomic cesium or Ar^+ . The catalysis product, a lower-energy hydrogen atom, was predicted to be a highly reactive intermediate which further reacts to form a novel hydride ion. The predicted hydride ion of hydrogen catalysis by either cesium atom or Ar^+ catalyst is the hydride ion $\text{H}^-(1/2)$. This ion was observed spectroscopically at 407 nm corresponding to its predicted binding energy of 3.05 eV . The catalytic reactions with the formation of the hydride ions are given in the Appendix.

Additional prior studies that support the possibility of a novel reaction of atomic hydrogen which produces an anomalous discharge and produces novel hydride compounds include extreme ultraviolet (EUV) spectroscopy [6, 8-21], plasma formation [6-21], power generation [7-9,

14, 37], and analysis of chemical compounds [17, 19-35]. Typically the emission of extreme ultraviolet light from hydrogen gas is achieved via a discharge at high voltage, a high power inductively coupled plasma, or a plasma created and heated to extreme temperatures by RF coupling (e.g. $>10^6$ K) with confinement provided by a toroidal magnetic field. Observation of intense extreme ultraviolet (EUV) emission at low temperatures (e.g. $\approx 10^3$ K) from atomic hydrogen and certain atomized elements or certain gaseous ions has been reported previously [6, 8-21]. The only pure elements that were observed to emit EUV were those predicted [1-39] wherein the ionization of t electrons from an atom or ion to a continuum energy level is such that the sum of the ionization energies of the t electrons is approximately $m \cdot 27.2$ eV where t and m are each an integer.

The observed EUV emission could not be explained by conventional chemistry; rather it must have been due to a novel chemical reaction between catalyst and atomic hydrogen. The catalysis of hydrogen involves the nonradiative transfer of energy from atomic hydrogen to a catalyst which may then release the transferred energy by radiative and nonradiative mechanisms. As a consequence of the nonradiative energy transfer, the hydrogen atom becomes unstable and emits further energy until it achieves a lower-energy nonradiative state having a principal energy level given by Eqs. (1-2) of the Appendix.

The energy released during catalysis may undergo internal conversion and ionize or excite molecular and atomic hydrogen resulting in hydrogen emission which includes well characterized ultraviolet lines such as the Lyman series. Lyman series emission, emission due to the catalyst mechanism, and emission of the hydride ion product were measured by EUV spectroscopy. The catalytic reactions and binding energies of the product hydride ions are given in the Appendix.

Potassium, cesium, and strontium atoms and Rb^+ ion ionize at integer multiples of the potential energy of atomic hydrogen. In prior studies [6, 8-21] and in the current experiments, these catalysts caused intense extreme ultraviolet (EUV) emission from incandescently heated atomic hydrogen and the atomized catalyst that generated a plasma at low temperatures (e.g. $\approx 10^3$ K). Whereas, the chemically similar noncatalyst atoms, sodium, magnesium and barium, do not ionize at

integer multiples of the potential energy of atomic hydrogen, did not generate a plasma, and caused no emission. In the case of atomic potassium catalyst, the first, second, and third ionization energies are 4.34066 eV, 31.63 eV, 45.806 eV, respectively. The triple ionization ($t=3$) reaction of K to K^{3+} , then, has a net enthalpy of reaction of 81.7766 eV, which is equivalent to 3·27.2 eV. Emission was observed from K^{3+} that confirmed the resonant nonradiative energy transfer of 3·27.2 eV from atomic hydrogen to atomic potassium. The predicted hydride ion of hydrogen catalysis by atomic potassium is the hydride ion $H^-(1/4)$. This ion was observed spectroscopically at 110 nm corresponding to its predicted binding energy of 11.2 eV.

II. EXPERIMENTAL

A. EUV Spectroscopy

Due to the extremely short wavelength of this radiation, "transparent" optics do not exist. Therefore, a windowless arrangement was used wherein the source was connected to the same vacuum vessel as the grating and detectors of the EUV spectrometer. Windowless EUV spectroscopy was performed with an extreme ultraviolet spectrometer that was mated with the cell. Differential pumping permitted a high pressure in the cell as compared to that in the spectrometer. This was achieved by pumping on the cell outlet and pumping on the grating side of the collimator that served as a pin-hole inlet to the optics. The cell was operated under hydrogen flow conditions while maintaining a constant hydrogen pressure in the cell with a mass flow controller.

The experimental set up shown in Figure 1 comprised a quartz cell which was 500 mm in length and 50 mm in diameter. Three ports for gas inlet, outlet, and photon detection were on the cap of the cell. The cell pump was a mechanical pump. The spectrometer was continuously evacuated to 10^{-4} – 10^{-6} torr by a turbomolecular pump with the pressure read by a cold cathode pressure gauge. The EUV spectrometer was connected to the cell light source with a 1.5 mm X 5 mm collimator which provided a light path to the slits of the EUV spectrometer. The collimator also served as a flow constrictor of gas from the cell. Valves were

between the cell and the mechanical pump, the cell and the monochromator, and the monochromator and its turbo pump.

A tungsten filament (0.508 mm in diameter and 800 cm in length, total resistance ~2.5 ohm) and a titanium cylindrical screen (300 mm long and 40 mm in diameter) that performed as a hydrogen dissociator were inside the quartz cell. A new dissociator was used for each experiment. The filament was coiled on a grooved ceramic support to maintain its shape when heated. The return lead ran through the middle of the ceramic support. The filament leads were covered by an Alumina sheath. The titanium screen was electrically floated. The power was applied to the filament by a power supply (Sorensen 80-13) which was controlled by a constant power controller. For the catalysts, the cell was operated with a maximum of 300 W of input power which corresponded to a cell wall temperature of about 700 °C. The temperature of the tungsten filament was estimated to be about 1500 °C. In the case of the noncatalysts, the cell power was increased to the maximum of 500 W. The gas was ultrahigh purity hydrogen. The gas pressure inside the cell was maintained at about 300 mtorr with a hydrogen flow rate of 5.5 sccm controlled by a 0-20 sccm range mass flow controller (MKS 1179A21CS1BB) with a readout (MKS type 246). The entire quartz cell was enclosed inside an insulation package (Zircar AL-30). Several K type thermocouples were placed in the insulation to measure key temperatures of the cell and insulation. The thermocouples were read with a multichannel computer data acquisition system.

In the present study, the light emission phenomena was studied for 1.) hydrogen, argon, neon, and helium alone, 2.) sodium, rubidium, magnesium, strontium, and barium metals, and 3.) Na_2CO_3 , K_2CO_3 , and Cs_2CO_3 . The inorganic test materials were coated on a titanium screen dissociator by the method of wet impregnation. The screen was coated by dipping it in a 0.6 M Na_2CO_3 /10% H_2O_2 , 0.6 M K_2CO_3 /10% H_2O_2 , or 0.6 M Cs_2CO_3 /10% H_2O_2 solution, and the crystalline material was dried on the surface by heating for 12 hours in a drying oven at 130 °C. A new dissociator was used for each experiment. The metals were placed in the bottom of the cell and volatilized by the filament heater.

The light emission was introduced to an EUV spectrometer for spectral measurement. The spectrometer was a McPherson 0.2 meter

monochromator (Model 302, Seya-Namioka type) equipped with a 1200 lines/mm holographic grating with a platinum coating. The wavelength region covered by the monochromator was 30–560 nm. The vacuum inside the monochromator was maintained below 5×10^{-4} torr by a turbo pump.

The EUV spectrum (40–160 nm) of the cell emission was recorded with a channel electron multiplier (CEM). The wavelength resolution was about 1 nm (FWHM) with an entrance and exit slit width of 300 μm .

The EUV/UV/VIS spectrum (40–560 nm) of the cell emission with hydrogen alone was recorded with a photomultiplier tube (PMT) and a sodium salicylate scintillator. The PMT (Model R1527P, Hamamatsu) used has a spectral response in the range of 185–680 nm with a peak efficiency at about 400 nm. The scan interval was 0.4 nm. The inlet and outlet slit were 500 μm with a corresponding wavelength resolution of 2 nm.

B. Standard Potassium Emission Spectrum

The standard extreme ultraviolet emission spectrum of potassium was obtained with a gas discharge cell comprised a five-way stainless steel cross that served as the anode with a hollow stainless steel cathode that was coated with K_2CO_3 by the same procedure used to coat the titanium dissociator. The five-way cross was pressurized with 1 torr of hydrogen to initiate the discharge. The hydrogen was then evacuated so that only potassium lines were observed. The DC voltage at the time the EUV spectrum was recorded was 300 V.

III. RESULTS

A. EUV Spectroscopy

The intensity of the Lyman α emission as a function of time from the gas cell at a cell temperature of 700 °C comprising a tungsten filament, a titanium dissociator, and 300 mtorr hydrogen with a flow rate of 5.5 sccm was tested for several controls and catalysts. The cell was run with hydrogen but without any test material present to establish the

baseline of the spectrometer. The intensity of the Lyman α emission as a function of time was measured for three hours, and no emission was observed. The corresponding UV/VIS spectrum (40–560 nm) is shown in Figure 2. The spectrum was recorded with a photomultiplier tube (PMT) and a sodium salicylate scintillator. No emission was observed except for the blackbody filament radiation at the longer wavelengths. No emission was also observed for the pure elements alone or when argon, neon, or helium replaced hydrogen. Sodium, magnesium, or barium metal was vaporized by filament heating. Sodium metal was also vaporized from Na_2CO_3 as the source. No emission was observed in any case. The maximum filament power was greater than 500 W. A metal coating formed in the cap of the cell over the course of the experiment in all cases.

The intensity of the Lyman α emission as a function of time with each of vaporized cesium from Cs_2CO_3 , potassium from K_2CO_3 , Rb^+ from rubidium metal, and strontium from strontium metal was recorded. In all cases, strong EUV emission was observed from vaporized catalyst with hydrogen. The superposition of the EUV spectra (80–130 nm) of the cell emission recorded at about the point of the maximum Lyman α emission for each of the catalysts is shown in Figure 3. In each case, no emission was observed in the absence of hydrogen, and no emission occurred until the catalyst was vaporized as indicated by the appearance of a metal coating in the cap of the cell over the course of the experiment.

E. EUV Emission of Potassium Catalyst

The EUV spectrum (45–80 nm) of the emission of the potassium-hydrogen gas cell and a replication experiment are shown in Figures 4 & 5. Line emission corresponding to K^{3+} was observed at 65–67 nm and 74–76 nm. K^{2+} was observed at 51 nm and 55 nm, and K^+ was observed at 62 nm. A large K^{3+} peak not shown in Figures 4 & 5 was also observed at 89.2 nm. The assignments of the K^{3+} , K^{2+} , and K^+ lines were confirmed by the standard potassium plasma spectrum shown in Figure 6 and NIST tables [41–42].

F. 110 nm Emission with Potassium Catalyst

The EUV spectrum (80–130 nm) of the cell emission from the potassium gas cell and a replication experiment are shown in Figures 7 & 8. The EUV spectrum (80–130 nm) of the cell emission from the cesium, potassium, rubidium, and strontium gas cells are superimposed in Figure 3. Only potassium is predicted to form a hydride with emission at 110 nm as shown in the Appendix and Table 1. From the comparison, a novel continuum feature is observed at 110 nm which was not due to hydrogen or potassium emission. The novel 110 nm continuum peak was observed only with potassium and atomic hydrogen present over an extended reaction time. As shown in Figures 7 & 3, the Lyman β and Lyman δ lines of the potassium gas cell at 102.6 nm and 97.3 nm, respectively, have a greater intensity relative to Lyman α line at 121.6 nm than the other catalysts which indicates a high plasma temperature. These results are consistent with the formation of $H^-(1/4)$ from the catalysis of atomic hydrogen by $K(m)$.

IV. DISCUSSION

A plasma that emitted intense EUV formed at low temperatures (e.g. $\approx 10^3$ K) from atomic hydrogen and each of Rb^+ , cesium, potassium, and strontium catalyst which was vaporized by heating. No possible chemical reactions of the tungsten filament, the dissociator, the vaporized test material, and 300 mtorr hydrogen at a cell temperature of 700 °C could be found which accounted for the hydrogen Lyman α line emission. In fact, no known chemical reaction releases enough energy to excite Lyman α emission from hydrogen. The emission was not observed with catalyst or hydrogen alone. Intense emission was observed for catalyst with hydrogen gas, but no emission was observed when sodium, magnesium, or barium replaced a catalyst with hydrogen. This result indicates that the emission was due to a reaction of the catalyst with hydrogen.

The only pure elements that were observed to emit EUV were those wherein the ionization of i electrons from an atom or ion to a continuum energy level is such that the sum of the ionization energies of the i

electrons is approximately $m \cdot 27.2 \text{ eV}$ where t and m are each an integer. Rubidium ions and potassium, cesium, and strontium atoms ionize at an integer multiple of the potential energy of atomic hydrogen, $m \cdot 27.2 \text{ eV}$. The triple ionization ($t=3$) reaction of K to K^{3+} has a net enthalpy of reaction of 81.7766 eV , which is equivalent to $m=3$. The reaction Rb^+ to Rb^{2+} has a net enthalpy of reaction of 27.28 eV , which is equivalent to $m=1$. The double ionization ($t=2$) of Cs to Cs^{2+} has a net enthalpy of reaction of 27.05135 eV , which is equivalent to $m=1$ [40]. The ionization reaction of Sr to Sr^{5+} , ($t=5$) has a net enthalpy of reaction of 188.2 eV , which is equivalent to $m=7$. In each case, the reaction involves a nonradiative energy transfer to form a hydrogen atom that is lower in energy than unreacted atomic hydrogen.

Characteristic emission was observed from K^{3+} which confirmed the resonant nonradiative energy transfer of $3 \cdot 27.2 \text{ eV}$ from atomic hydrogen to atomic potassium (Eq. (5)). With a highly conductive plasma, the voltage of the cell was about 20 V, and the field strength was about 1-2 V/cm which was too low to ionize potassium to K^{3+} which requires at least 81.7766 eV . The K^{3+} lines generated in the incandescently heated cell and due to the catalyst reaction of atomic hydrogen were confirmed by a high voltage discharge and NIST tables [41-42].

$K(m)$ is predicted to catalyze hydrogen to form $H\left[\frac{a_H}{4}\right]$ which reacts with an electron to form $H^-(1/4)$. The predicted $H^-(1/4)$ hydride ion of hydrogen catalysis by potassium was observed spectroscopically at 110 nm corresponding to its predicted binding energy of 11.2 eV . The hydride reaction product formed over time.

The release of energy from hydrogen as evidenced by the EUV emission must result in a lower-energy state of hydrogen. The present study identified the formation of a novel hydride ion. The formation of novel compounds based on novel hydride ions would be substantial evidence supporting catalysis of hydrogen as the mechanism of the observed EUV emission and further support the present spectroscopic identification of $H^-(1/4)$. Compounds containing novel hydride ions have been isolated as products of the reaction of atomic hydrogen with atoms and ions identified as catalysts in the present study and previously reported EUV studies [6, 8-35, 37]. The novel hydride compounds were

identified analytically by techniques such as time of flight secondary ion mass spectroscopy, X-ray photoelectron spectroscopy, and ^1H nuclear magnetic resonance spectroscopy. For example, the time of flight secondary ion mass spectroscopy showed a large hydride peak in the negative spectrum. The X-ray photoelectron spectrum showed large metal core level shifts due to binding with the hydride as well as novel hydride peaks. The ^1H nuclear magnetic resonance spectrum showed significantly upfield shifted peaks which corresponded to and identified novel hydride ions.

The hydride ion $\text{H}^-(1/4)$ has been reported previously [23]. KHI containing $\text{H}^-(1/4)$ was synthesized by reaction of potassium metal, atomic hydrogen, and KI . The XPS spectrum of the product blue crystals differed from that of KI by having additional features at 9.1 eV and 11.1 eV. The XPS peaks centered at 9.0 eV and 11.1 eV that did not correspond to any other primary element peaks were assigned to the $\text{H}^-(n=1/4) E_b = 11.2 \text{ eV}$ hydride ion (Eq. (18)) in two different chemical environments where E_b is the predicted vacuum binding energy. Furthermore, the reported minimum heats of formation of KHI by the catalytic reaction of potassium with atomic hydrogen and KI were over $-2000 \text{ kJ/mole } \text{H}_2$ compared to the enthalpy of combustion of hydrogen of $-241.8 \text{ kJ/mole } \text{H}_2$ [37]. From Eq. (1), Eq. (18), and the bond energy of molecular hydrogen of $-435.99 \text{ kJ/mole } \text{H}_2$ [43], the heat of formation of $\text{H}^-(1/4)$ from hydrogen is $-41.1 \text{ MJ/mole } \text{H}_2$. The implications are that a new field of novel hydrogen chemistry has been discovered that represents a new source of energy with the potential for direct conversion of plasma to electricity [38-39].

V. CONCLUSION

Characteristic emission was observed from K^{3+} which confirmed the resonant nonradiative energy transfer of 3.272 eV from atomic hydrogen to atomic potassium (Eq. (5)). The predicted $\text{H}^-(1/4)$ hydride ion of hydrogen catalysis by potassium catalyst given by Eqs. (5-7) and Eq. (18) was observed spectroscopically at 110 nm corresponding to its predicted binding energy of 11.2 eV .

APPENDIX

A. Catalysts

The mechanism of EUV emission and formation of novel hydrides can not be explained by the conventional chemistry of hydrogen; rather it must have been due to a novel chemical reaction between catalyst and atomic hydrogen. Mills [1-39] predicts that certain atoms or ions serve as catalysts to release energy from hydrogen to produce an increased binding energy hydrogen atom called a *hydrino atom* having a binding energy of

$$\text{Binding Energy} = \frac{13.6 \text{ eV}}{n^2} \quad (1)$$

where

$$n = \frac{1}{2}, \frac{1}{3}, \frac{1}{4}, \dots, \frac{1}{p} \quad (2)$$

and p is an integer greater than 1, designated as $H\left[\frac{a_H}{p}\right]$ where a_H is the radius of the hydrogen atom. Hydrinos are predicted to form by reacting an ordinary hydrogen atom with a catalyst having a net enthalpy of reaction of about

$$m \cdot 27.2 \text{ eV} \quad (3)$$

where m is an integer. This catalysis releases energy from the hydrogen atom with a commensurate decrease in size of the hydrogen atom, $r_n = na_H$. For example, the catalysis of $H(n=1)$ to $H(n=1/2)$ releases 40.8 eV, and the hydrogen radius decreases from a_H to $\frac{1}{2}a_H$.

The excited energy states of atomic hydrogen are also given by Eq. (1) except that

$$n = 1, 2, 3, \dots \quad (4)$$

The $n=1$ state is the "ground" state for "pure" photon transitions (the $n=1$ state can absorb a photon and go to an excited electronic state, but it cannot release a photon and go to a lower-energy electronic state). However, an electron transition from the ground state to a lower-energy state is possible by a nonradiative energy transfer such as multipole coupling or a resonant collision mechanism. These lower-energy states

have fractional quantum numbers, $n = \frac{1}{\text{integer}}$. Processes that occur without photons and that require collisions are common. For example, the exothermic chemical reaction of $H+H$ to form H_2 does not occur with the emission of a photon. Rather, the reaction requires a collision with a third body, M , to remove the bond energy- $H+H+M \rightarrow H_2+M^*$ [44]. The third body distributes the energy from the exothermic reaction, and the end result is the H_2 molecule and an increase in the temperature of the system. Some commercial phosphors are based on nonradiative energy transfer involving multipole coupling. For example, the strong absorption strength of Sb^{3+} ions along with the efficient nonradiative transfer of excitation from Sb^{3+} to Mn^{2+} , are responsible for the strong manganese luminescence from phosphors containing these ions [45]. Similarly, the $n=1$ state of hydrogen and the $n = \frac{1}{\text{integer}}$ states of hydrogen are

nonradiative, but a transition between two nonradiative states is possible via a nonradiative energy transfer, say $n=1$ to $n=1/2$. In these cases, during the transition the electron couples to another electron transition, electron transfer reaction, or inelastic scattering reaction which can absorb the exact amount of energy that must be removed from the hydrogen atom. Thus, a catalyst provides a net positive enthalpy of reaction of $m \cdot 27.2 \text{ eV}$ (i.e. it absorbs $m \cdot 27.2 \text{ eV}$ where m is an integer). Certain atoms or ions serve as catalysts which resonantly accept energy from hydrogen atoms and release the energy to the surroundings to effect electronic transitions to fractional quantum energy levels. Recent analysis of mobility and spectroscopy data of individual electrons in liquid helium show direct experimental evidence that electrons may have fractional principal quantum energy levels [36].

According to Mills [1-39], a catalytic system is provided by the ionization of t electrons from an atom or ion to a continuum energy level such that the sum of the ionization energies of the t electrons is approximately $m \times 27.2 \text{ eV}$ where m is an integer.

Potassium

One such atomic catalytic system involves potassium atoms. The first, second, and third ionization energies of potassium are 4.34066 eV ,

31.63 eV, 45.806 eV, respectively [40]. The triple ionization ($t=3$) reaction of K to K^{3+} , then, has a net enthalpy of reaction of 81.7766 eV, which is equivalent to $m=3$ in Eq. (3).

$$81.7766 \text{ eV} + K(m) + H\left[\frac{a_H}{p}\right] \rightarrow K^{3+} + 3e^- + H\left[\frac{a_H}{(p+3)}\right] + [(p+3)^2 - p^2] \times 13.6 \text{ eV} \quad (5)$$

$$K^{3+} + 3e^- \rightarrow K(m) + 81.7766 \text{ eV} \quad (6)$$

And, the overall reaction is

$$H\left[\frac{a_H}{p}\right] \rightarrow H\left[\frac{a_H}{(p+3)}\right] + [(p+3)^2 - p^2] \times 13.6 \text{ eV} \quad (7)$$

Vaporized atomic potassium was formed by hydrogen reduction and thermal decomposition of potassium carbonate.

Rubidium Ion

Rubidium ions can also provide a net enthalpy of a multiple of that of the potential energy of the hydrogen atom. The second ionization energy of rubidium is 27.28 eV. The reaction Rb^+ to Rb^{2+} has a net enthalpy of reaction of 27.28 eV, which is equivalent to $m=1$ in Eq. (3).

$$27.28 \text{ eV} + Rb^+ + H\left[\frac{a_H}{p}\right] \rightarrow Rb^{2+} + e^- + H\left[\frac{a_H}{(p+1)}\right] + [(p+1)^2 - p^2] \times 13.6 \text{ eV} \quad (8)$$

$$Rb^{2+} + e^- \rightarrow Rb^+ + 27.28 \text{ eV} \quad (9)$$

The overall reaction is

$$H\left[\frac{a_H}{p}\right] \rightarrow H\left[\frac{a_H}{(p+1)}\right] + [(p+1)^2 - p^2] \times 13.6 \text{ eV} \quad (10)$$

Rubidium metal may form RbH which may provide gas phase Rb^+ ions, or rubidium metal may be ionized to provide gas phase Rb^+ ions. Rb^+ ion emission was observed in the EUV spectrum of rubidium metal.

Cesium

A catalytic system is provided by the ionization of two electrons from a cesium atom each to a continuum energy level such that the sum of the ionization energies of the two electrons is approximately 27.2 eV. The first and second ionization energies of cesium are 3.89390 eV and

23.15745 eV, respectively [40]. The double ionization ($t=2$) reaction of Cs to Cs^{2+} , then, has a net enthalpy of reaction of 27.05135 eV, which is equivalent to $m=1$ in Eq. (3).

$$27.05135 \text{ eV} + Cs(m) + H\left[\frac{a_H}{p}\right] \rightarrow Cs^{2+} + 2e^- + H\left[\frac{a_H}{(p+1)}\right] + [(p+1)^2 - p^2]X13.6 \text{ eV} \quad (11)$$

$$Cs^{2+} + 2e^- \rightarrow Cs(m) + 27.05135 \text{ eV} \quad (12)$$

And, the overall reaction is

$$H\left[\frac{a_H}{p}\right] \rightarrow H\left[\frac{a_H}{(p+1)}\right] + [(p+1)^2 - p^2]X13.6 \text{ eV} \quad (13)$$

Vaporized atomic cesium was formed by hydrogen reduction and thermal decomposition of the carbonate.

Strontium

One such catalytic system involves strontium. The first through the fifth ionization energies of strontium are 5.69484 eV, 11.03013 eV, 42.89 eV, 57 eV, and 71.6 eV, respectively [40]. The ionization reaction of Sr to Sr^{5+} , ($t=5$), then, has a net enthalpy of reaction of 188.2 eV, which is equivalent to $m=7$ in Eq. (3).

$$188.2 \text{ eV} + Sr(m) + H\left[\frac{a_H}{p}\right] \rightarrow Sr^{5+} + 5e^- + H\left[\frac{a_H}{(p+7)}\right] + [(p+7)^2 - p^2]X13.6 \text{ eV} \quad (14)$$

$$Sr^{5+} + 5e^- \rightarrow Sr(m) + 188.2 \text{ eV} \quad (15)$$

And, the overall reaction is

$$H\left[\frac{a_H}{p}\right] \rightarrow H\left[\frac{a_H}{(p+7)}\right] + [(p+7)^2 - p^2]X13.6 \text{ eV} \quad (16)$$

Vaporized atomic strontium was formed by heating the metal to 700 °C.

B. Hydride Ion

A novel hydride ion having extraordinary chemical properties given by Mills [1] is predicted to form by the reaction of an electron with a hydrino (Eq. (17)). The resulting hydride ion is referred to as a hydrino hydride ion, designated as $H^-(1/p)$.



The hydrino hydride ion is distinguished from an ordinary hydride ion having a binding energy of 0.8 eV. The hydrino hydride ion is predicted [1] to comprise a hydrogen nucleus and two indistinguishable electrons at a binding energy according to the following formula:

$$\text{Binding Energy} = \frac{\hbar^2 \sqrt{s(s+1)}}{8\mu_e a_0^2 \left[\frac{1 + \sqrt{s(s+1)}}{p} \right]^2} - \frac{\pi\mu_0 e^2 \hbar^2}{m_e^2 a_0^3} \left(1 + \frac{2^2}{\left[\frac{1 + \sqrt{s(s+1)}}{p} \right]^3} \right) \quad (18)$$

where p is an integer greater than one, $s=1/2$, \hbar is Planck's constant bar, μ_0 is the permeability of vacuum, m_e is the mass of the electron, μ_e is the reduced electron mass, a_0 is the Bohr radius, and e is the elementary charge. The ionic radius is

$$r_1 = \frac{a_0}{p} \left(1 + \sqrt{s(s+1)} \right); s = \frac{1}{2} \quad (19)$$

From Eq. (19), the radius of the hydrino hydride ion $H^-(1/p)$; $p = \text{integer}$ is $\frac{1}{p}$ that of ordinary hydride ion, $H^-(1/1)$. Compounds containing hydrino hydride ions have been isolated as products of the reaction of atomic hydrogen with atoms and ions identified as catalysts by EUV emission [6, 8-35, 37].

ACKNOWLEDGMENT

Special thanks to Ying Lu, Takeyoshi Onuma, and Jiliang He for recording some spectra and Bala Dhandapani for assisting with logistics and reviewing this manuscript.

REFERENCES

1. R. Mills, *The Grand Unified Theory of Classical Quantum Mechanics*, January 2000 Edition, BlackLight Power, Inc., Cranbury, New Jersey, Distributed by Amazon.com.
2. R. Mills, "The Grand Unified Theory of Classical Quantum Mechanics", Global Foundation, Inc. Orbis Scientiae entitled *The Role of Attractive and Repulsive Gravitational Forces in Cosmic Acceleration of Particles The Origin of the Cosmic Gamma Ray Bursts*, (29th Conference on High Energy Physics and Cosmology Since 1964) Dr. Behram N. Kursunoglu, Chairman,. December 14-17, 2000, Lago Mar Resort, Fort Lauderdale, FL.
3. R. Mills, "The Grand Unified Theory of Classical Quantum Mechanics", Global Foundation, Inc. Orbis Scientiae entitled *The Role of Attractive and Repulsive Gravitational Forces in Cosmic Acceleration of Particles The Origin of the Cosmic Gamma Ray Bursts*, (29th Conference on High Energy Physics and Cosmology Since 1964) Dr. Behram N. Kursunoglu, Chairman,. December 14-17, 2000, Lago Mar Resort, Fort Lauderdale, FL, in press.
4. R. Mills, "The Grand Unified Theory of Classical Quantum Mechanics", II Nuovo Cimento, submitted.
5. R. Mills, "The Hydrogen Atom Revisited", Int. J. of Hydrogen Energy, Vol. 25, Issue 12, December, (2000), pp. 1171-1183.
6. R. Mills, "Spectroscopic Identification of a Novel Catalytic Reaction of Atomic Hydrogen and the Hydride Ion Product", Int. J. Hydrogen Energy, in press.
7. R. Mills, N. Greenig, S. Hicks, "Optically Measured Power Balances of Anomalous Discharges of Mixtures of Argon, Hydrogen, and Potassium, Rubidium, Cesium, or Strontium Vapor", Int. J. Hydrogen Energy, submitted.

8. R. Mills and M. Nansteel, "Anomalous Argon-Hydrogen-Strontium Discharge", IEEE Transactions on Plasma Science, submitted.
9. R. Mills, M. Nansteel, and Y. Lu, "Anomalous Hydrogen/Strontium Discharge", European Journal of Physics D, submitted.
10. R. Mills, J. Dong, Y. Lu, "Observation of Extreme Ultraviolet Hydrogen Emission from Incandescently Heated Hydrogen Gas with Certain Catalysts", Int. J. Hydrogen Energy, Vol. 25, (2000), pp. 919-943.
11. R. Mills, "Observation of Extreme Ultraviolet Emission from Hydrogen-KI Plasmas Produced by a Hollow Cathode Discharge", Int. J. Hydrogen Energy, in press.
12. R. Mills, "Temporal Behavior of Light-Emission in the Visible Spectral Range from a Ti-K₂CO₃-H-Cell", Int. J. Hydrogen Energy, Vol. 26, No. 4, (2001), pp. 327-332.
13. R. Mills, T. Onuma, and Y. Lu, "Formation of a Hydrogen Plasma from an Incandescently Heated Hydrogen-Catalyst Gas Mixture with an Anomalous Afterglow Duration", Int. J. Hydrogen Energy, in press.
14. R. Mills, M. Nansteel, and Y. Lu, "Observation of Extreme Ultraviolet Hydrogen Emission from Incandescently Heated Hydrogen Gas with Strontium that Produced an Anomalous Optically Measured Power Balance", Int. J. Hydrogen Energy, Vol. 26, No. 4, (2001), pp. 309-326.
15. R. Mills, J. Dong, Y. Lu, J. Conrads, "Observation of Extreme Ultraviolet Hydrogen Emission from Incandescently Heated Hydrogen Gas with Certain Catalysts", 1999 Pacific Conference on Chemistry and Spectroscopy and the 35th ACS Western Regional Meeting, Ontario Convention Center, California, (October 6-8, 1999).
16. R. Mills, J. Dong, N. Greenig, and Y. Lu, "Observation of Extreme Ultraviolet Hydrogen Emission from Incandescently Heated Hydrogen Gas with Certain Catalysts", National Hydrogen Association, 11 th Annual U.S. Hydrogen Meeting, Vienna, VA, (February 29-March 2, 2000).
17. R. Mills, B. Dhandapani, N. Greenig, J. He, J. Dong, Y. Lu, and H. Conrads, "Formation of an Energetic Plasma and Novel Hydrides from Incandescently Heated Hydrogen Gas with Certain Catalysts", National Hydrogen Association, 11 th Annual U.S. Hydrogen Meeting, Vienna, VA, (February 29-March 2, 2000).

18. Mills, J. Dong, N. Greenig, and Y. Lu, "Observation of Extreme Ultraviolet Hydrogen Emission from Incandescently Heated Hydrogen Gas with Certain Catalysts", 219 th National ACS Meeting, San Francisco, California, (March 26-30, 2000).
19. R. Mills, B. Dhandapani, N. Greenig, J. He, J. Dong, Y. Lu, and H. Conrads, "Formation of an Energetic Plasma and Novel Hydrides from Incandescently Heated Hydrogen Gas with Certain Catalysts", 219 th National ACS Meeting, San Francisco, California, (March 26-30, 2000).
20. R. Mills, B. Dhandapani, N. Greenig, J. He, J. Dong, Y. Lu, and H. Conrads, "Formation of an Energetic Plasma and Novel Hydrides from Incandescently Heated Hydrogen Gas with Certain Catalysts", June ACS Meeting (29th Northeast Regional Meeting, University of Connecticut, Storrs, CT, (June 18-21, 2000)).
21. R. Mills, B. Dhandapani, N. Greenig, J. He, J. Dong, Y. Lu, and H. Conrads, "Formation of an Energetic Plasma and Novel Hydrides from Incandescently Heated Hydrogen Gas with Certain Catalysts", August National ACS Meeting (220th ACS National Meeting, Washington, DC, (August 20-24, 2000)).
22. R. Mills, B. Dhandapani, M. Nansteel, J. He, A. Voigt, "Identification of Compounds Containing Novel Hydride Ions by Nuclear Magnetic Resonance Spectroscopy", Int. J. Hydrogen Energy, in press.
23. R. Mills, B. Dhandapani, N. Greenig, J. He, "Synthesis and Characterization of Potassium Iodo Hydride", Int. J. of Hydrogen Energy, Vol. 25, Issue 12, December, (2000), pp. 1185-1203.
24. R. Mills, "Novel Inorganic Hydride", Int. J. of Hydrogen Energy, Vol. 25, (2000), pp. 669-683.
25. R. Mills, "Novel Hydrogen Compounds from a Potassium Carbonate Electrolytic Cell", Fusion Technology, Vol. 37, No. 2, March, (2000), pp. 157-182.
26. R. Mills, B. Dhandapani, M. Nansteel, J. He, T. Shannon, A. Echezuria, "Synthesis and Characterization of Novel Hydride Compounds", Int. J. of Hydrogen Energy, Vol. 26, No. 4, (2001), pp. 339-367.
27. R. Mills, "Highly Stable Novel Inorganic Hydrides", Journal of Materials Research, submitted.

28. R. Mills, "Novel Hydride Compound", 1999 Pacific Conference on Chemistry and Spectroscopy and the 35th ACS Western Regional Meeting, Ontario Convention Center, California, (October 6-8, 1999).
29. R. Mills, B. Dhandapani, N. Greenig, J. He, "Synthesis and Characterization of Potassium Iodo Hydride", 1999 Pacific Conference on Chemistry and Spectroscopy and the 35th ACS Western Regional Meeting, Ontario Convention Center, California, (October 6-8, 1999).
30. R. Mills, J. He, and B. Dhandapani, "Novel Hydrogen Compounds", 1999 Pacific Conference on Chemistry and Spectroscopy and the 35th ACS Western Regional Meeting, Ontario Convention Center, California, (October 6-8, 1999).
31. R. Mills, "Novel Hydride Compound", National Hydrogen Association, 11 th Annual U.S. Hydrogen Meeting, Vienna, VA, (February 29-March 2, 2000).
32. R. Mills, J. He, and B. Dhandapani, "Novel Alkali and Alkaline Earth Hydrides", National Hydrogen Association, 11 th Annual U.S. Hydrogen Meeting, Vienna, VA, (February 29-March 2, 2000).
33. R. Mills, "Novel Hydride Compound", 219 th National ACS Meeting, San Francisco, California, (March 26-30, 2000).
34. R. Mills, J. He, and B. Dhandapani, "Novel Alkali and Alkaline Earth Hydrides", 219 th National ACS Meeting, San Francisco, California, (March 26-30, 2000).
35. R. Mills, J. He, and B. Dhandapani, "Novel Alkali and Alkaline Earth Hydrides", August National ACS Meeting (220th ACS National Meeting, Washington, DC, (August 20-24, 2000)).
36. R. Mills, The Nature of Free Electrons in Superfluid Helium--a Test of Quantum Mechanics and a Basis to Review its Foundations and Make a Comparison to Classical Theory, Int. J. Hydrogen Energy, in press.
37. R. Mills, W. Good, A. Voigt, Jinquan Dong, "Minimum Heat of Formation of Potassium Iodo Hydride", Int. J. Hydrogen Energy, in press.
38. R. Mills, "BlackLight Power Technology-A New Clean Hydrogen Energy Source with the Potential for Direct Conversion to Electricity", Proceedings of the National Hydrogen Association, 12 th Annual U.S. Hydrogen Meeting and Exposition, *Hydrogen: The Common Thread*, The Washington Hilton and Towers, Washington DC, (March 6-8, 2001), in press.

39. R. Mills, "BlackLight Power Technology-A New Clean Energy Source with the Potential for Direct Conversion to Electricity", Global Foundation International Conference on "Global Warming and Energy Policy", Dr. Behram N. Kursunoglu, Chairman, Fort Lauderdale, FL, November 26-28, 2000, in press.
40. David R. Linde, *CRC Handbook of Chemistry and Physics*, 79 th Edition, CRC Press, Boca Raton, Florida, (1998-9), p. 10-175 to p. 10-177.
41. R. Kelly, Journal of Physical and Chemical Reference Data. "Atomic and Ionic Spectrum Lines below 2000 Angstroms: Hydrogen through Krypton", Part I (H-Cr), Volume 16, (1987), Supplement No. 1, Published by the American Chemical Society and the American Institute of Physics for the National Bureau of Standards, pp. 418-422.
42. NIST Atomic Spectra Database, www.physics.nist.gov/cgi-bin/AtData/display.ksh.
43. D. R. Linde, *CRC Handbook of Chemistry and Physics*, 79 th Edition, CRC Press, Boca Raton, Florida, (1999), p. 9-51 to 9-69.
44. N. V. Sidgwick, *The Chemical Elements and Their Compounds*, Volume I, Oxford, Clarendon Press, (1950), p.17.
45. M. D. Lamb, *Luminescence Spectroscopy*, Academic Press, London, (1978), p. 68.

Table 1. The ionization energy of the hydrino hydride ion $H^-(n=1/p)$ as a function of p .

Hydride Ion	Catalyst	r_1 (a_0) ^a	Calculated Ionization Energy ^b (eV)	Calculated Wavelength (nm)
$H^-(n=1)$		1.8660	0.754	1645
$H^-(n=1/2)$	Rb^+, Cs	0.9330	3.047	407
$H^-(n=1/3)$		0.6220	6.610	188
$H^-(n=1/4)$	K	0.4665	11.23	110
$H^-(n=1/5)$		0.3732	16.70	74.2
$H^-(n=1/6)$	Sr	0.3110	22.81	54.4
$H^-(n=1/7)$		0.2666	29.34	42.3
$H^-(n=1/8)$		0.2333	36.08	34.4
$H^-(n=1/9)$		0.2073	42.83	28.9
$H^-(n=1/10)$		0.1866	49.37	25.1
$H^-(n=1/11)$		0.1696	55.49	22.34
$H^-(n=1/12)$		0.1555	60.98	20.33
$H^-(n=1/13)$		0.1435	65.62	18.89
$H^-(n=1/14)$		0.1333	69.21	17.91
$H^-(n=1/15)$		0.1244	71.53	17.33
$H^-(n=1/16)$		0.1166	72.38	17.13
$H^-(n=1/17)$		0.1098	71.54	17.33
$H^-(n=1/18)$		0.1037	68.80	18.02
$H^-(n=1/19)$		0.0982	63.95	19.39
$H^-(n=1/20)$		0.0933	56.78	21.83
$H^-(n=1/21)$		0.0889	47.08	26.33
$H^-(n=1/22)$		0.0848	34.63	35.80
$H^-(n=1/23)$		0.0811	19.22	64.49
$H^-(n=1/24)$		0.0778	0.6535	1897
$H^-(n=1/25)$			not stable	

^a from Equation (18)

^b from Equation (19)

Figure Captions

Figure 1. The experimental set up comprising a gas cell light source and an EUV spectrometer which was differentially pumped.

Figure 2. The UV/VIS spectrum (40–560 nm) of the cell emission from the gas cell at a cell temperature of 700 °C comprising a tungsten filament, a titanium dissociator, and 300 mtorr hydrogen that was recorded with a photomultiplier tube (PMT) and a sodium salicylate scintillator with an entrance and exit slit width of 500 μm .

Figure 3. The EUV spectrum (80–130 nm) of the cell emission recorded at about the point of the maximum Lyman α emission from the gas cell at a cell temperature of 700 °C comprising a tungsten filament, a titanium dissociator, 300 mtorr hydrogen, and each of vaporized cesium from Cs_2CO_3 , potassium from K_2CO_3 , Rb^+ from rubidium metal, and strontium from strontium metal that was recorded with a CEM.

Figure 4. The EUV spectrum (45–80 nm) of the cell emission recorded at about the point of the maximum Lyman α emission from the gas cell at a cell temperature of 700 °C comprising a tungsten filament, a titanium dissociator, 300 mtorr hydrogen, and vaporized potassium from K_2CO_3 that was recorded with a CEM.

Figure 5. The EUV spectrum (45–80 nm) of the cell emission recorded at about the point of the maximum Lyman α emission from a repeat gas cell at a cell temperature of 700 °C comprising a tungsten filament, a titanium dissociator, 300 mtorr hydrogen, and vaporized potassium from K_2CO_3 that was recorded with a CEM.

Figure 6. The EUV spectrum (50–90 nm) recorded of a standard potassium plasma excited by a discharge cell which comprised a five-way stainless steel cross that served as the anode with a hollow stainless steel cathode.

Figure 7. The EUV spectrum (80–130 nm) of the cell emission recorded at about the point of the maximum Lyman α emission from the gas cell at a cell temperature of 700 °C comprising a tungsten filament, a titanium dissociator, 300 mtorr hydrogen, and vaporized potassium from K_2CO_3 that was recorded with a CEM.

Figure 8. The EUV spectrum (80–130 nm) of the cell emission recorded at about the point of the maximum Lyman α emission from a

repeat gas cell at a cell temperature of 700 °C comprising a tungsten filament, a titanium dissociator, 300 mtorr hydrogen, and vaporized potassium from K_2CO_3 that was recorded with a CEM.

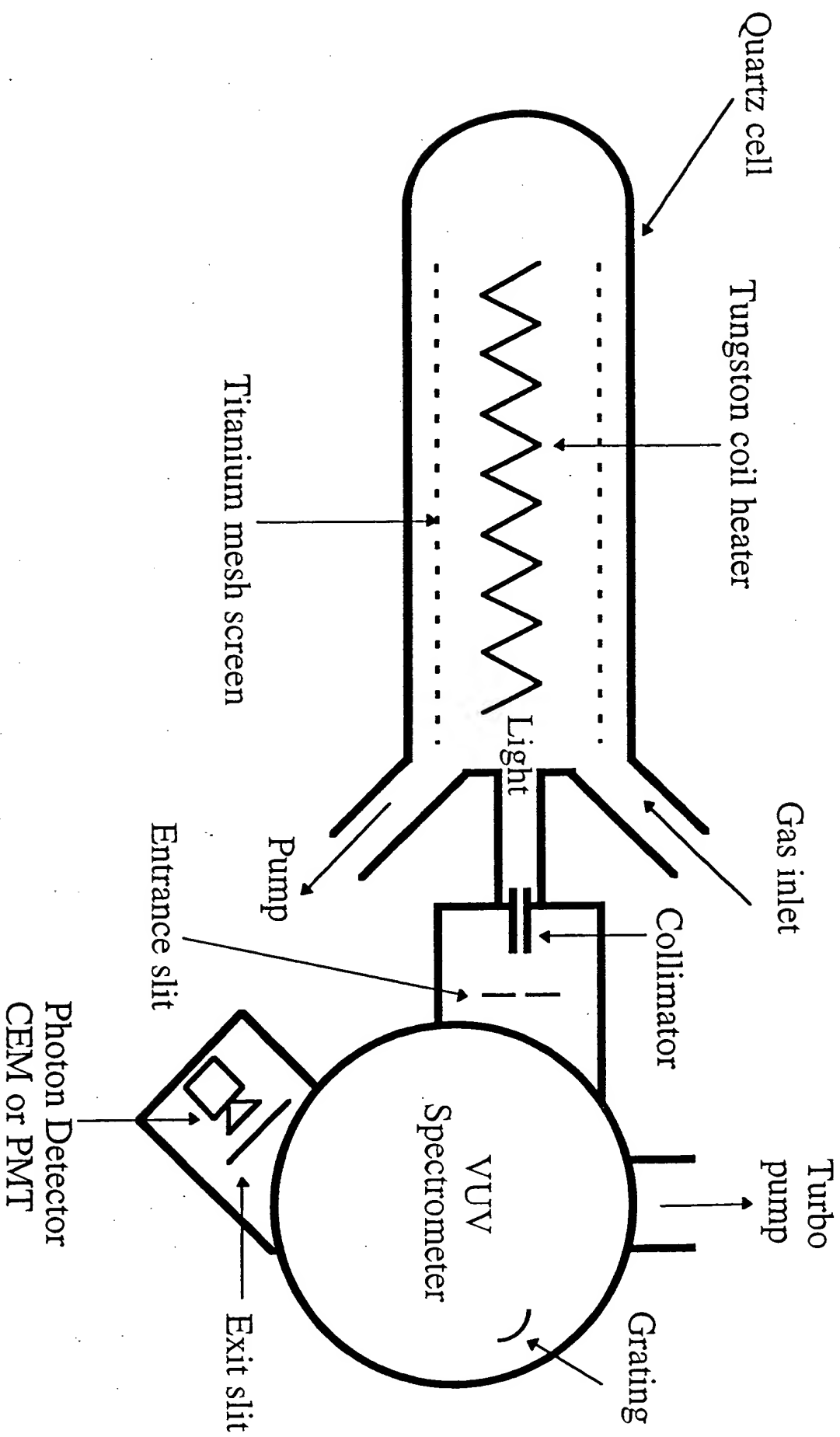
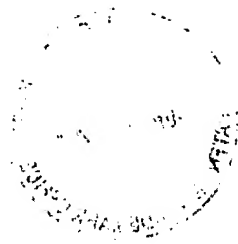


Fig. 1

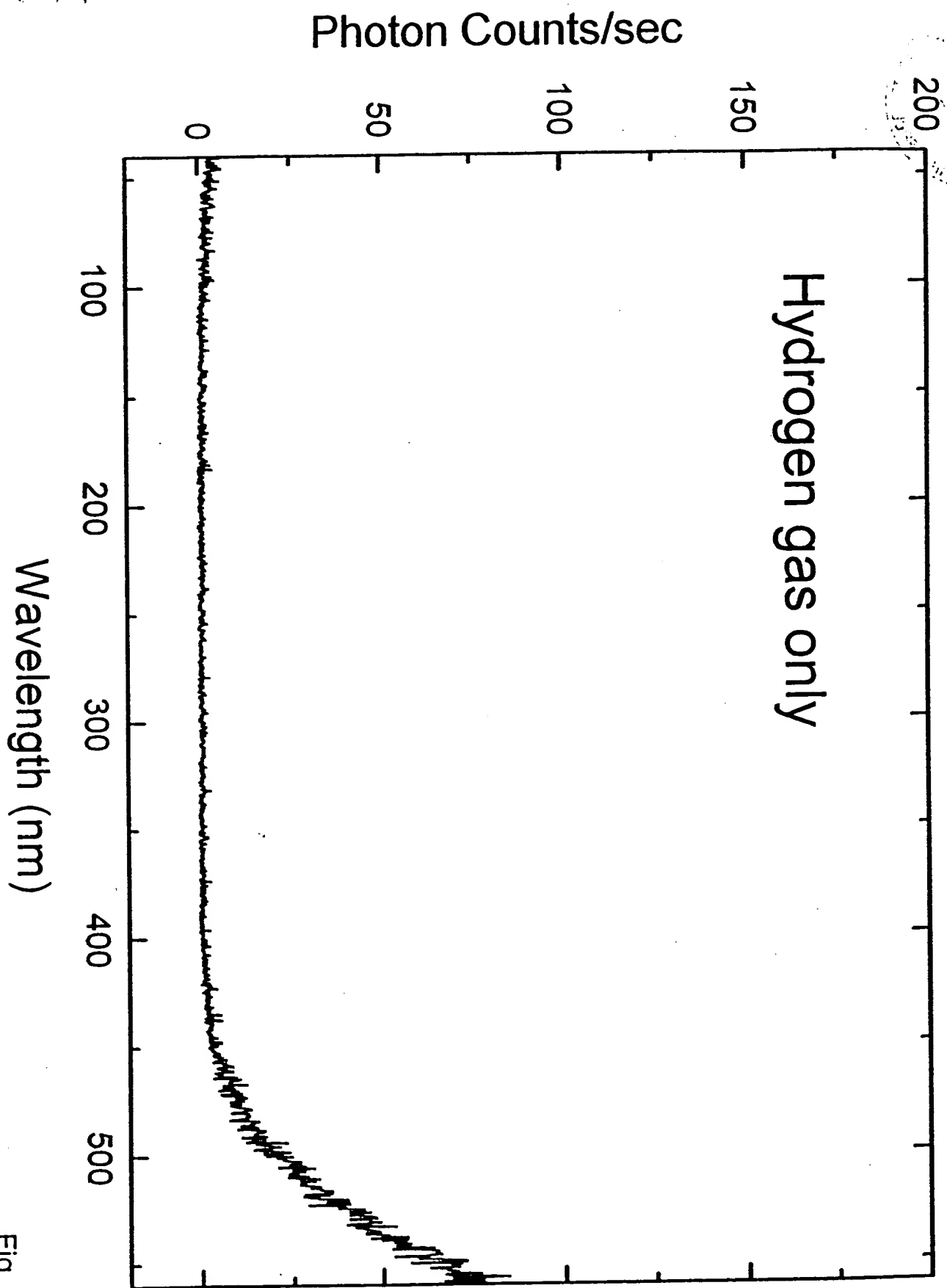


Fig. 2

PHOTON COUNTS / SEC

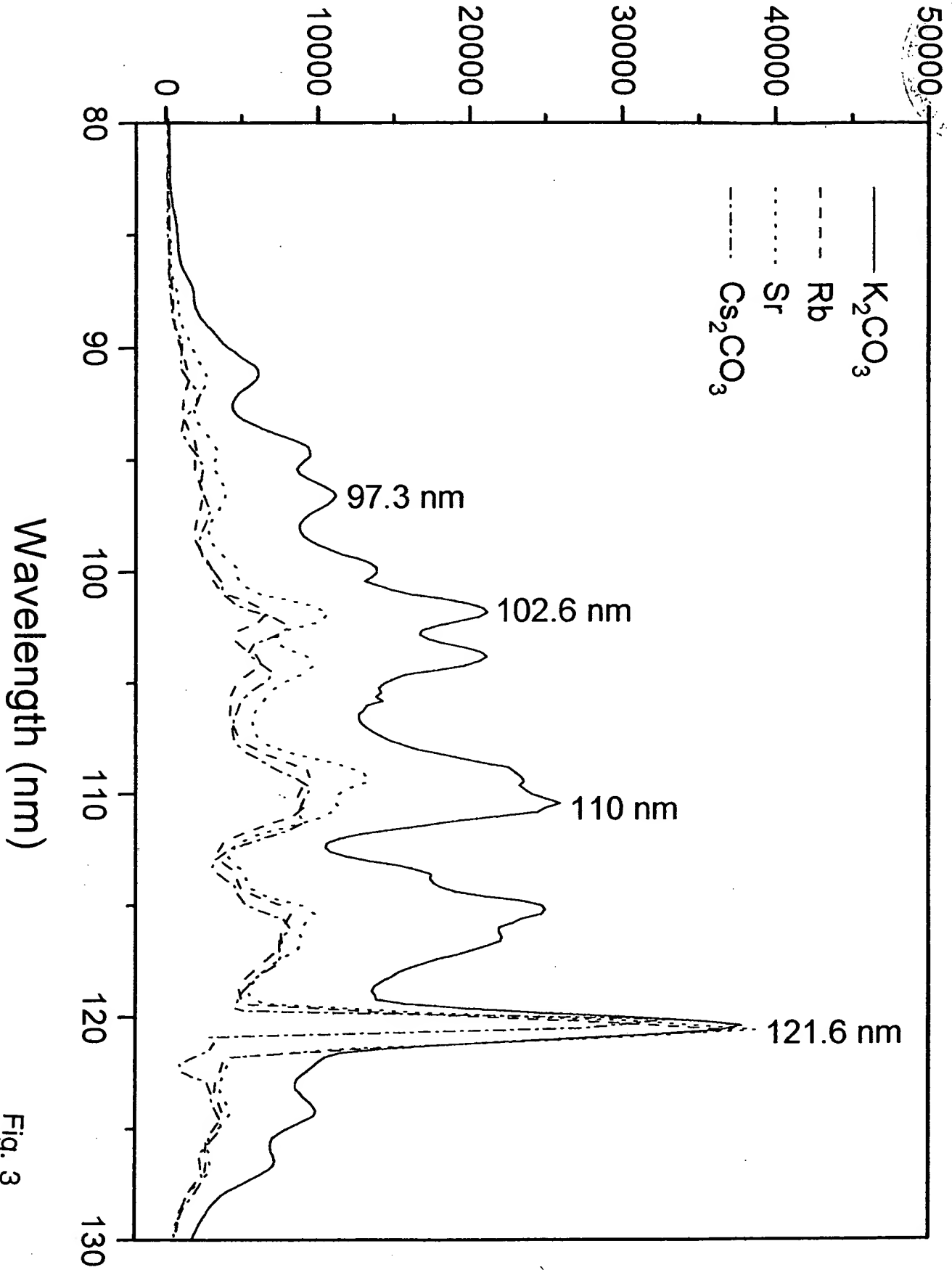
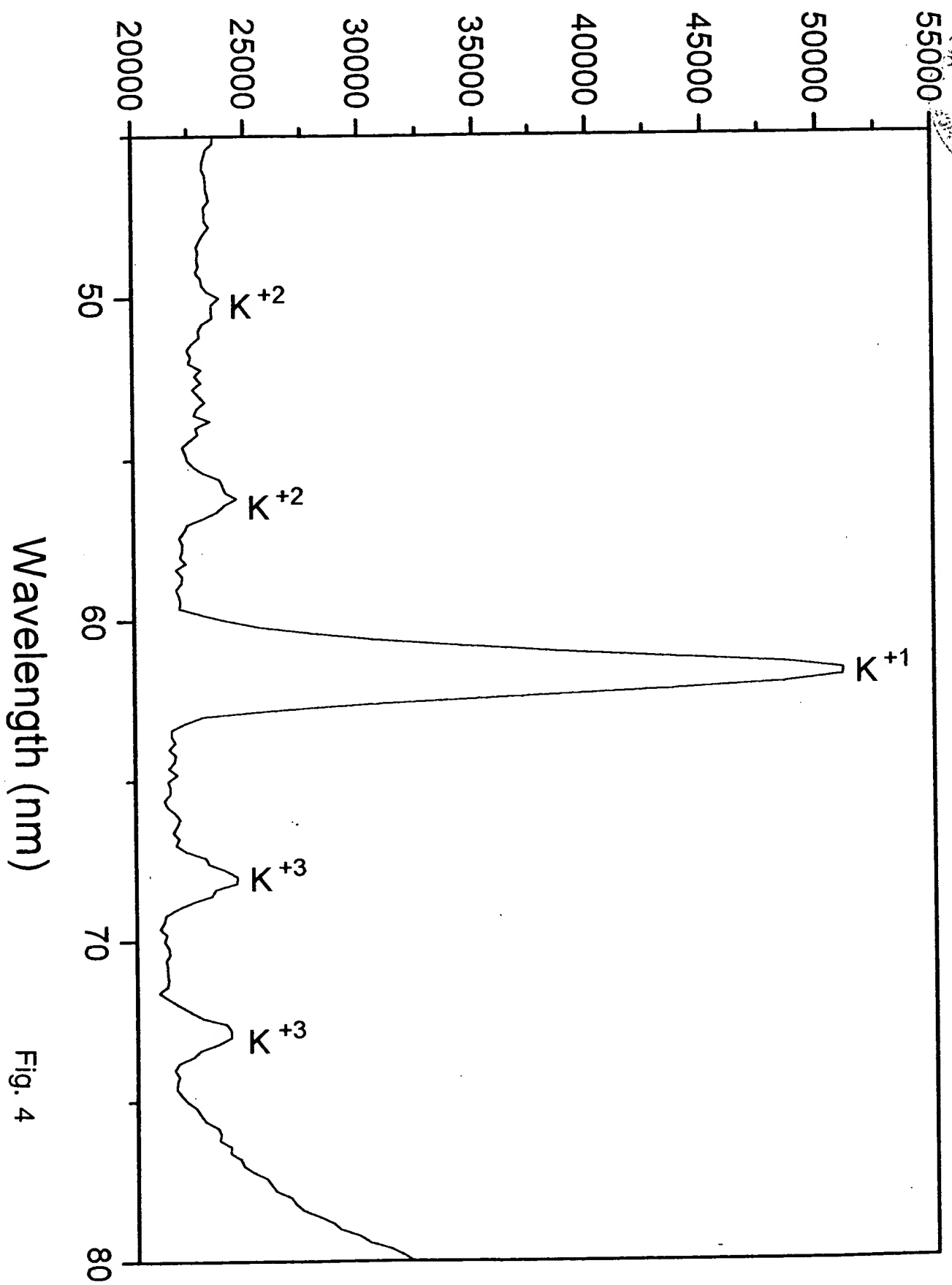


Fig. 3

PHOTON COUNTS / SEC



Wavelength (nm)

Fig. 4

PHOTON COUNTS / SEC

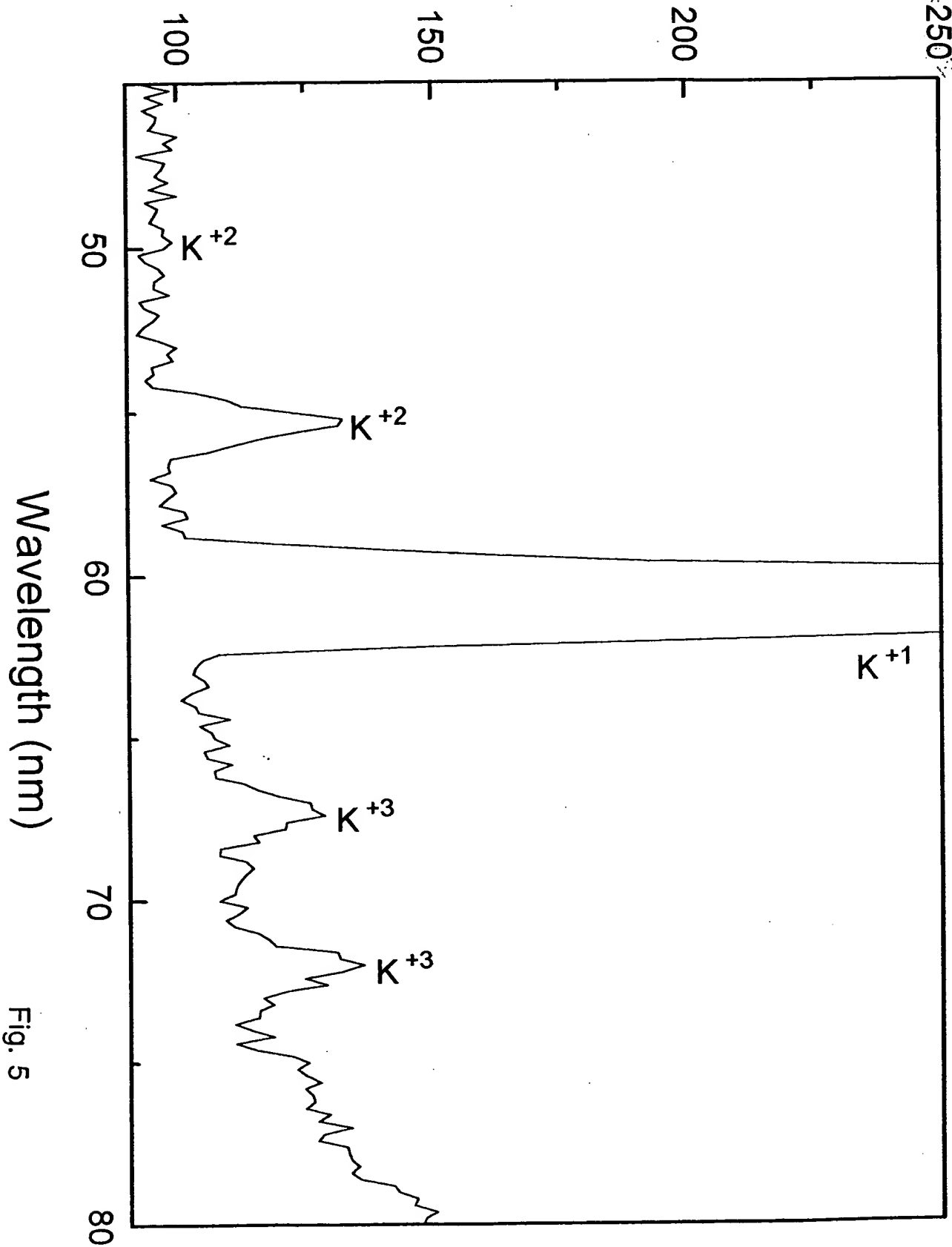
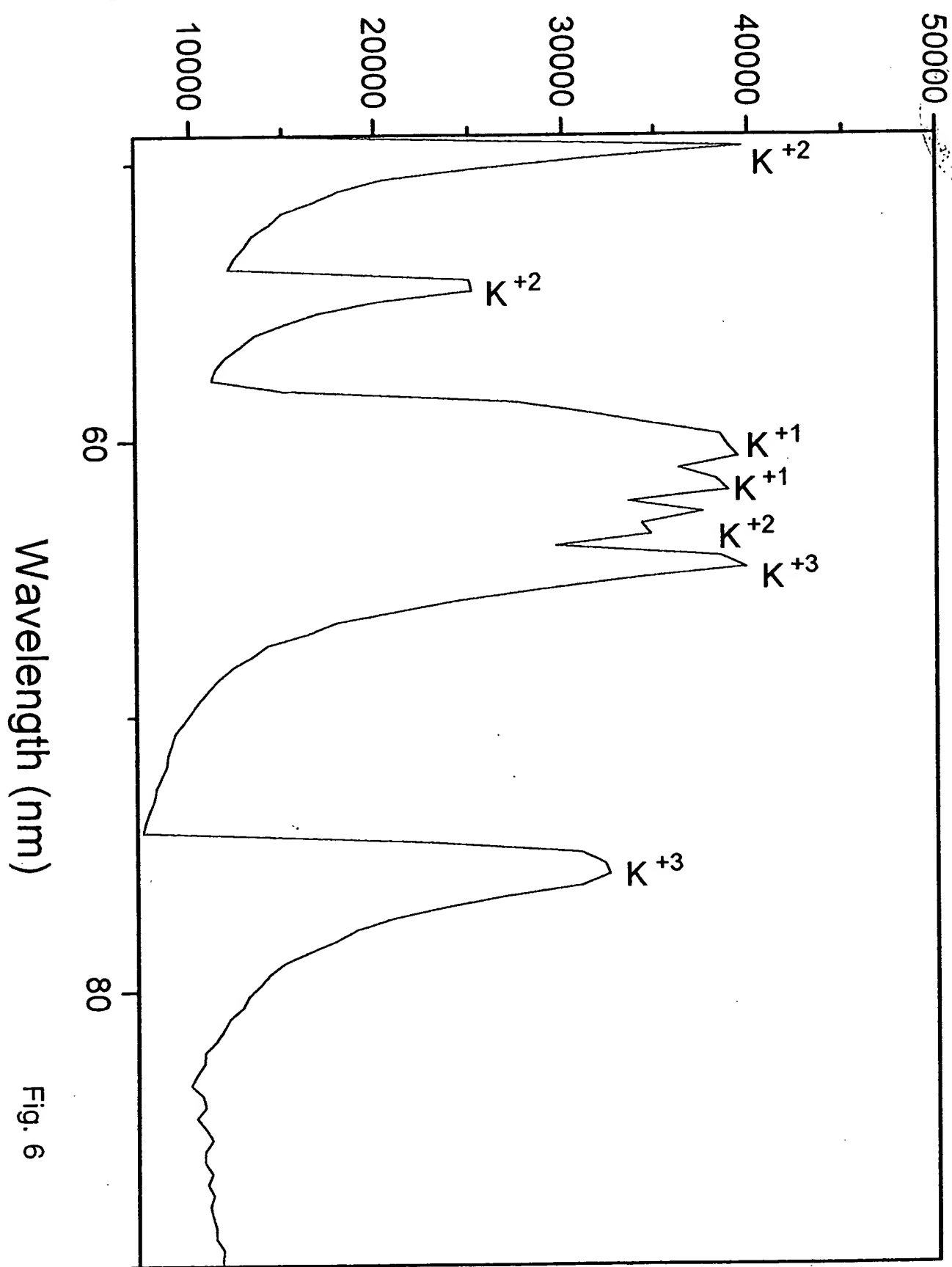


Fig. 5

PHOTON COUNTS / SEC



Wavelength (nm)

Fig. 6

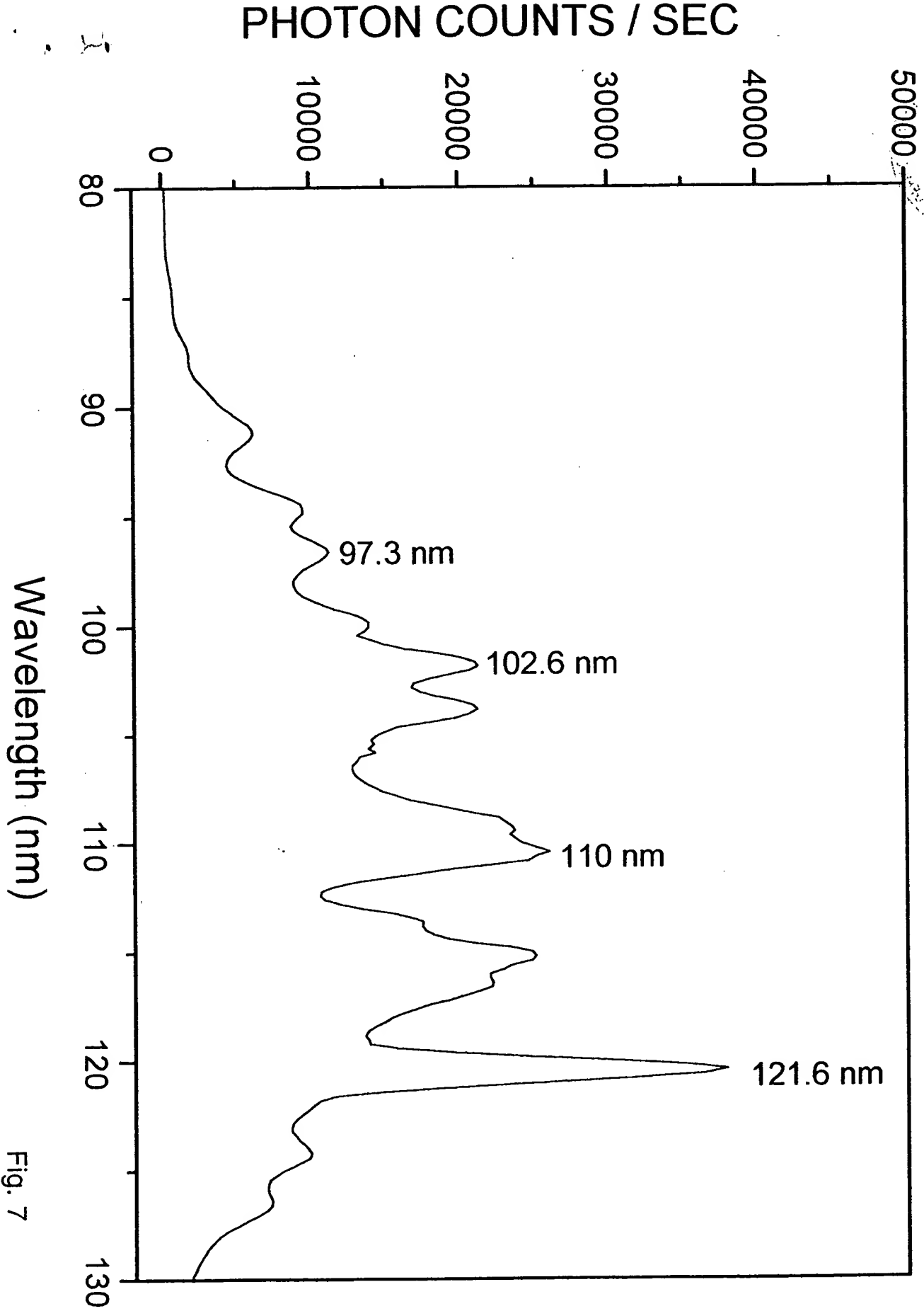


Fig. 7

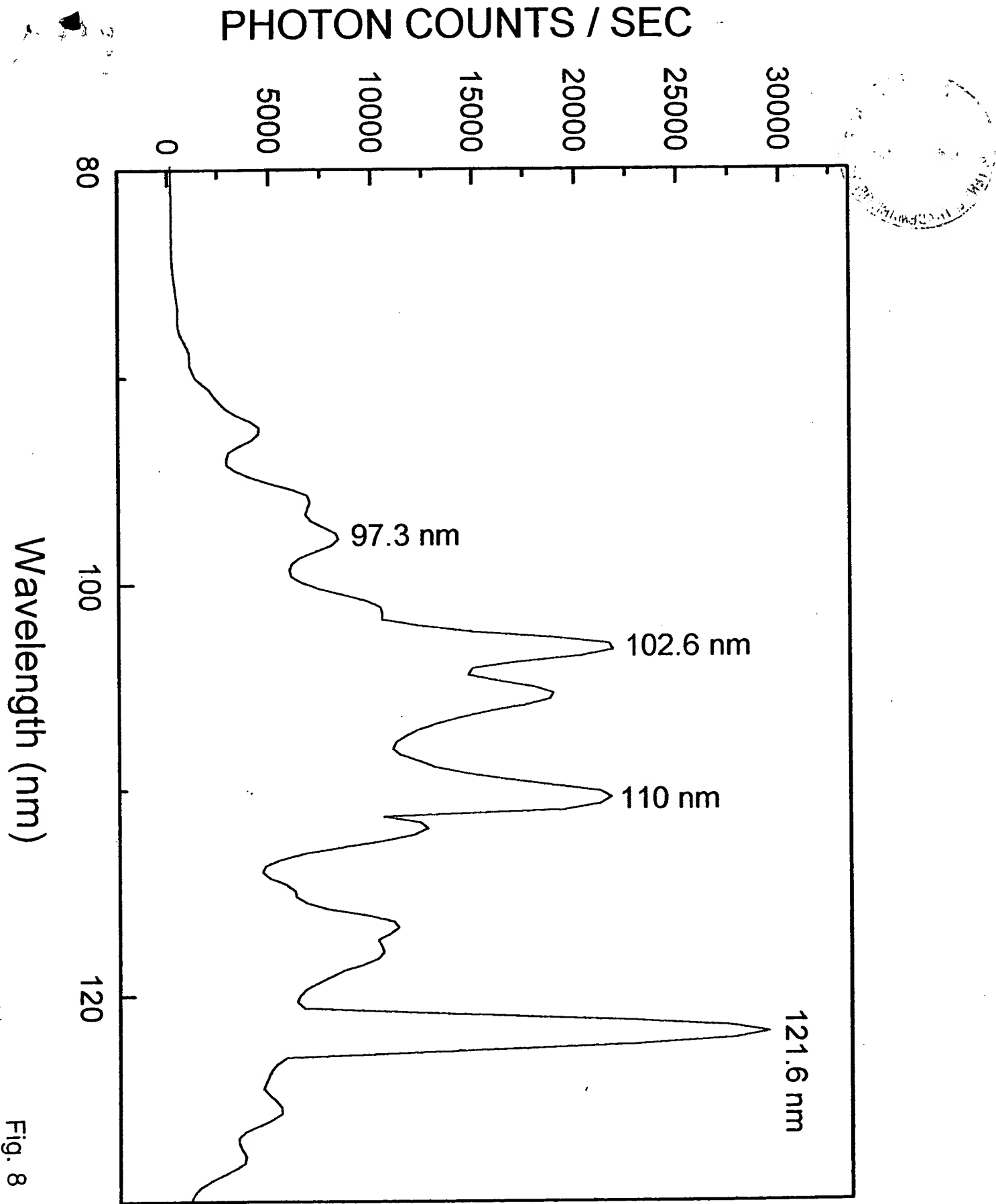


Fig. 8

$$v = \lambda \frac{\omega}{2\pi} \quad (22)$$

Whereas, Schrödinger derivation from the Helmholtz equation [1] with the substitution of

$$\lambda = \frac{h}{m_e v} \quad (23)$$

gives the rigid rotor equation with the paradox that

$$v^2 = \frac{h}{m_e} \frac{\omega}{2\pi} \quad (24)$$

which is not the wave relationship,

$$v = \lambda \frac{\omega}{2\pi} \quad (25)$$

References

1. McQuarrie, D. A., Quantum Chemistry, University Science Books, Mill Valley, CA, (1983), pp. 78-79.

MAGNETIC PARAMETERS OF THE ELECTRON (BOHR MAGNETON)

The Magnetic Field of an Orbitsphere from Spin

The orbitsphere is a shell of negative charge current comprising correlated charge motion along great circles. For $\mathbf{l} = 0$, the orbitsphere gives rise to a magnetic moment of 1 Bohr magneton [16] as shown in the Derivation of the Magnetic Field section,

$$\mu_B = \frac{e\hbar}{2m_e} = 9.274 \times 10^{-24} \text{ JT}^{-1}, \quad (1.99)$$

and a magnetic field derived below.

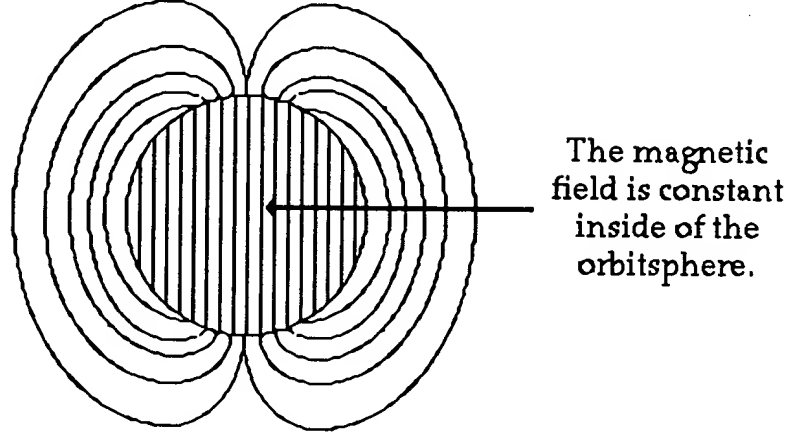
$$\mathbf{H} = \frac{e\hbar}{m_e r_n^3} (\mathbf{i}_r \cos \theta - \mathbf{i}_\theta \sin \theta) \quad \text{for } r < r_n \quad (1.100)$$

$$\mathbf{H} = \frac{e\hbar}{2m_e r^3} (\mathbf{i}_r 2 \cos \theta - \mathbf{i}_\theta \sin \theta) \quad \text{for } r > r_n \quad (1.101)$$

It follows from Eq. (1.99), the relationship for the Bohr magneton, and relationship between the magnetic dipole field and the magnetic moment \mathbf{m} [17] that Eqs. (1.100) and (1.101) are the equations for the magnetic field due to a magnetic moment of a Bohr magneton, $\mathbf{m} = \mu_B \mathbf{i}_z$ where $\mathbf{i}_z = \mathbf{i}_r \cos \theta - \mathbf{i}_\theta \sin \theta$. Note that the magnetic field is a constant for $r < r_n$. See Figure 1.6. It is shown in the Magnetic Parameters of the Electron (Bohr Magnetron) section that the energy stored in the magnetic field of the electron orbitsphere is

$$E_{mag,total} = \frac{\pi\mu_o e^2 \hbar^2}{m_e^2 r_1^3} \quad (1.102)$$

Figure 1.6. The magnetic field of an electron orbitsphere.



Derivation of the Magnetic Field

Consider Figure 1.6. The magnetic field must satisfy the following relationships:

$$\nabla \cdot \mathbf{H} = 0 \text{ in free space} \quad (1.103)$$

$$\mathbf{n} \times (\mathbf{H}_a - \mathbf{H}_b) = \mathbf{K} \quad (1.104)$$

$$\mathbf{n} \cdot (\mathbf{H}_a - \mathbf{H}_b) = 0 \quad (1.105)$$

$$\mathbf{H} = -\nabla \psi \quad (1.106)$$

The z component of the current, $|i|$, for a current loop of total charge, e , oriented at an angle θ with respect to the z-axis is given as the product of the charge, the angular velocity (The orbitsphere angular velocity is given by Eq. (1.55).), and $\sin \theta$.

$$|i| = \frac{e\hbar}{m_e r_n^2} \sin \theta \quad (1.107)$$

Consider the orbitsphere depicted in Figures 1.3, 1.4, and 1.5. The surface current-density function, $\mathbf{K}i_\phi$, is perpendicular to the angular momentum. As shown in the Spin Angular Momentum section, the vector projection of the orbitsphere angular momentum onto the xy-plane goes as $|\cos \Delta\alpha|$ as shown in Figure 1.5 B. It is periodic over the range of $\Sigma\Delta\alpha$

and $\Sigma\Delta\alpha'$ and varies in magnitude from a maximum of $\frac{\hbar}{\sqrt{2}}$ to zero to $\frac{\hbar}{\sqrt{2}}$ again. The projection of the charge-density of the orbitsphere onto the xy-plane (perpendicular to the z-axis) which carries the incremental current, i_ϕ , is a function of $\sin\theta$. The angular function of the current-density of the orbitsphere is normalized to that of one electron.

$$N = \frac{1}{\int_0^\pi \sin^2 \theta \sin \theta d\theta} = \frac{3}{4} \quad (1.108)$$

Due to the precession of the S-axis about the z axis, the time averaged projection of the angular momentum of the electron orbitsphere onto the xy-plane is zero. Therefore, the current corresponding to the total charge of the electron is about the z-axis, and the angular velocity of the spinning orbitsphere is twice that of a stationary orbitsphere. As shown in Figure 1.5 B, the projection of the angular momentum is only onto the negative z-axis of length r_n . Thus, the incremental current-density dKi_ϕ along the z-axis is given by dividing i_ϕ by the length, r_n . The current-density of the orbitsphere in the incremental length dz is

$$K(\rho, \phi, z) = i_\phi 2N \frac{e\hbar}{m_e r_n^3} = i_\phi \frac{3}{2} \frac{e\hbar}{m_e r_n^3} \quad (1.109)$$

Because

$$z = r \cos \theta \quad (1.110)$$

a differential length

$$dz = -\sin \theta r_n d\theta \quad (1.111)$$

and so the current-density in the differential length $r_n d\theta$ as measured along the periphery of the orbitsphere is a function of $\sin\theta$. Thus, the surface current-density function is given by

$$K(r, \theta, \phi) = i_\phi \frac{3}{2} \frac{e\hbar}{m_e r_n^3} \sin \theta \quad (1.112)$$

Substitution of Eq. (1.112) into Eq. (1.104) gives

$$H_\theta^a - H_\theta^b = \frac{3}{2} \frac{e\hbar}{m_e r_n^3} \sin \theta \quad (1.113)$$

To obtain H_θ , the derivative of Ψ with respect to θ must be taken, and this suggests that the θ dependence of Ψ be taken as $\cos\theta$. The field is finite at the origin and is zero at infinity; so, solutions of Laplace's equation in spherical coordinates are selected because they are consistent with these conditions [18].

$$\Psi = C \left[\frac{r}{r_n} \right] \cos \theta ; \quad r < r_n \quad (1.114)$$

$$\Psi = A \left[\frac{r_n}{r} \right]^2 \cos \theta ; \quad r > r_n \quad (1.115)$$

The negative gradient of these potentials is

$$\mathbf{H} = \frac{-C}{r_n} (\mathbf{i}_r \cos \theta - \mathbf{i}_\theta \sin \theta) \quad \text{for } r < r_n \quad (1.116)$$

$$\mathbf{H} = \frac{A}{r_n} \left[\frac{r_n}{r} \right]^3 (\mathbf{i}_r 2 \cos \theta + \mathbf{i}_\theta \sin \theta) \quad \text{for } r > r_n \quad (1.117)$$

The continuity conditions of Eqs. (1.104), (1.105), (1.112), and (1.113) and are applied to obtain the following relationships among the variables

$$\frac{-C}{r_n} = \frac{2A}{r_n} \quad (1.118)$$

$$\frac{A}{r_n} - \frac{C}{r_n} = \frac{3}{2} \frac{e\hbar}{m_e r_n^3} \quad (1.119)$$

Solving the variables algebraically gives the magnetic fields of an electron:

$$\mathbf{H} = \frac{e\hbar}{m_e r_n^3} (\mathbf{i}_r \cos \theta - \mathbf{i}_\theta \sin \theta) \quad \text{for } r < r_n \quad (1.120)$$

$$\mathbf{H} = \frac{e\hbar}{2m_e r^3} (\mathbf{i}_r 2 \cos \theta - \mathbf{i}_\theta \sin \theta) \quad \text{for } r > r_n \quad (1.121)$$

Derivation of the Energy

The energy stored in the magnetic field of the electron is

$$E_{mag} = \frac{1}{2} \mu_o \int_0^{2\pi} \int_0^\pi \int_0^\infty H^2 r^2 \sin \theta dr d\theta d\Phi \quad (1.122)$$

$$E_{mag \text{ total}} = E_{mag \text{ external}} + E_{mag \text{ internal}} \quad (1.123)$$

$$E_{mag \text{ internal}} = \frac{1}{2} \mu_o \int_0^{2\pi} \int_0^\pi \int_0^{r_1} \left[\frac{e\hbar}{m_e r^3} \right]^2 (\cos^2 \theta + \sin^2 \theta) r^2 \sin \theta dr d\theta d\Phi \quad (1.124)$$

$$= \frac{2\pi \mu_o e^2 \hbar^2}{3m_e^2 r_1^3} \quad (1.125)$$

$$E_{mag \text{ external}} = \frac{1}{2} \mu_o \int_0^{2\pi} \int_0^{\pi} \int_{r_1}^{\infty} \left[\frac{e\hbar}{2m_e r_1^3} \right]^2 (4 \cos^2 \theta + \sin^2 \theta) r^2 \sin \theta dr d\theta d\Phi \quad (1.126)$$

$$= \frac{\pi \mu_o e^2 \hbar^2}{3 m_e^2 r_1^3} \quad (1.127)$$

$$E_{mag \text{ total}} = \frac{2 \pi \mu_o e^2 \hbar^2}{3 m_e^2 r_1^3} + \frac{\pi \mu_o e^2 \hbar^2}{3 m_e^2 r_1^3} \quad (1.128)$$

$$E_{mag \text{ total}} = \frac{\pi \mu_o e^2 \hbar^2}{m_e^2 r_1^3} \quad (1.129)$$

STERN-GERLACH EXPERIMENT

The sum of the L_i , the magnitude of the angular momentum of each infinitesimal point of the orbitsphere of mass m_i , must be constant. The constant is \hbar .

$$\sum |L_i| = \sum |\mathbf{r} \times m_i \mathbf{v}| = m_e r_n \frac{\hbar}{m_e r_n} = \hbar \quad (1.130)$$

where the velocity is given by Eq. (1.47). Furthermore, it is known from the Stern-Gerlach experiment that a beam of silver atoms is split into two components when passed through an inhomogeneous magnetic field. The measured angular momentum in the direction of the applied field (spin axis) is $\pm \frac{\hbar}{2}$, and the magnitude of the angular momentum vector which

precesses about the spin axis is $\sqrt{\frac{3}{4}}\hbar$. As demonstrated in the Orbitsphere Equation of Motion section, the projection of the total orbitsphere angular momentum onto the spin axis is $\pm \frac{\hbar}{2}$, and the projection onto S, the axis

which precesses about the spin axis, is $\sqrt{\frac{3}{4}}\hbar$. The Stern-Gerlach experiment implies a magnetic moment of one Bohr magneton and an associated angular momentum quantum number of 1/2. Historically, this quantum number is called the spin quantum number, s ($s = \frac{1}{2}$; $m_s = \pm \frac{1}{2}$), and that designation is maintained.

ELECTRON g FACTOR

As demonstrated by Purcell [19], when a magnetic field is applied to an electron in a central field which comprises a current loop, the orbital radius does not change, but the velocity changes as follows:

$$\Delta v = \frac{erB}{2m_e} \quad (1.131)$$

The angular momentum of the electron orbitsphere is \hbar as given by Eq. (1.57), and as demonstrated in Figure 1.5, $\frac{\hbar}{2}$ of the orbitsphere angular momentum is in the plane perpendicular to any applied magnetic field. The angular momentum in the presence of an applied magnetic field is

$$\mathbf{L} = \mathbf{r} \times (m_e \mathbf{v} + e\mathbf{A}) \quad (1.132)$$

where \mathbf{A} is the vector potential of the external field evaluated at the location of the orbitsphere. Conservation of angular momentum of the orbitsphere permits a discrete change of its "kinetic angular momentum" ($\mathbf{r} \times m\mathbf{v}$) by the field of $\frac{\hbar}{2}$, and concomitantly the "potential angular momentum" ($\mathbf{r} \times e\mathbf{A}$) must change by $-\frac{\hbar}{2}$. The flux change, ϕ , of the orbitsphere for $r < r_n$ is determined as follows:

$$\Delta \mathbf{L} = \frac{\hbar}{2} - \mathbf{r} \times e\mathbf{A} \quad (1.133)$$

$$= \left[\frac{\hbar}{2} - \frac{e2\pi rA}{2\pi} \right] \hat{z} \quad (1.134)$$

$$= \left[\frac{\hbar}{2} - \frac{e\phi}{2\pi} \right] \hat{z} \quad (1.135)$$

In order that the change of angular momentum, $\Delta \mathbf{L}$, equals zero, ϕ must be $\Phi_0 = \frac{h}{2e}$, the magnetic flux quantum. Thus, to conserve angular momentum in the presence of an applied magnetic field, the orbitsphere magnetic moment can be parallel or antiparallel to an applied field as observed with the Stern-Gerlach experiment, and the flip between orientations (a rotation of $\frac{\pi}{2}$) is accompanied by the "capture" of the magnetic flux quantum by the orbitsphere "coils" comprising infinitesimal loops of charge moving along geodesics (great circles).

The energy to flip the orientation of the orbitsphere due to its magnetic moment of a Bohr magneton, μ_B , is

$$\Delta E_{mag}^{spin} = 2\mu_B B \quad (1.136)$$

where

$$\mu_B = \frac{e\hbar}{2m_e} \quad (1.137)$$

During the spin-flip transition, power must be conserved. Power flow is governed by the Poynting power theorem,

$$\nabla \cdot (\mathbf{E} \times \mathbf{H}) = -\frac{\partial}{\partial t} \left[\frac{1}{2} \mu_o \mathbf{H} \cdot \mathbf{H} \right] - \frac{\partial}{\partial t} \left[\frac{1}{2} \epsilon_o \mathbf{E} \cdot \mathbf{E} \right] - \mathbf{J} \cdot \mathbf{E} \quad (1.138)$$

Stored Magnetic Energy

Energy superimposes; thus, the calculation of the spin-flip energy is determined as a sum of contributions. The energy change corresponding to the "capture" of the magnetic flux quantum is derived below. From Eq. (1.129) for one electron,

$$\frac{1}{2} \mu_o \mathbf{H} \cdot \mathbf{H} = E_{mag}^{fluxon} = \frac{\pi \mu_o e^2 \hbar^2}{(m_e)^2 r_n^3} \quad (1.139)$$

is the energy stored in the magnetic field of the electron. The orbitsphere is equivalent to a Josephson junction which can trap integer numbers of fluxons where the quantum of magnetic flux is $\Phi_0 = \frac{h}{2e}$.

Consider Eq. (1.139). During the flip transition a fluxon treads the orbitsphere at the speed of light; therefore, the radius of the orbitsphere in the lab frame is 2π times the relativistic radius in the fluxon frame. Thus, the energy of the transition corresponding to the "capture" of a fluxon by the orbitsphere, E_{mag}^{fluxon} , is

$$E_{mag}^{fluxon} = \frac{\pi \mu_o e^2 \hbar^2}{(m_e)^2 (2\pi r_n)^3} \quad (1.140)$$

$$= \frac{\mu_o e^2}{4\pi^2 m_e r_n} \left(\frac{e\hbar}{2m_e} \right) \left(\frac{h}{2e\pi r_n^2} \right) \quad (1.141)$$

$$= \frac{\mu_o e^2}{4\pi^2 m_e r_n} \mu_B \left(\frac{\Phi_0}{A} \right) \quad (1.142)$$

where A is the area and Φ_0 is the magnetic flux quantum.

$$E_{mag}^{fluxon} = 2 \left[\frac{e^2 \mu_o}{2m_e r_n} \right] \frac{1}{4\pi^2} \mu_B B \quad (1.143)$$

where the n th fluxon treading through the area of the orbitsphere is equivalent to the applied magnetic flux. Furthermore, the term in brackets can be expressed in terms of the fine structure constant, α , as follows:

$$\frac{e^2 \mu_o}{2m_e r_n} = \frac{e^2 \mu_o c v}{2m_e v r_n c} \quad (1.144)$$

Substitution of Eq. (1.47) gives

$$\frac{e^2 \mu_o c v}{2\hbar c} \quad (1.145)$$

Substitution of

$$c = \sqrt{\frac{1}{\epsilon_o \mu_o}} \quad (1.146)$$

and

$$\alpha = \frac{\mu_o e^2 c}{2h} \quad (1.147)$$

gives

$$\frac{e^2 \mu_o c v}{2\hbar c} = 2\pi\alpha \frac{v}{c} \quad (1.148)$$

The fluxon treads the orbitsphere at $v=c$. Thus,

$$E_{mag}^{fluxon} = 2 \frac{\alpha}{2\pi} \mu_B B \quad (1.149)$$

Stored Electric Energy

S , the projection of the orbitsphere angular momentum that precesses about the z-axis called the spin axis is $|S| = \pm \sqrt{\frac{3}{4}} \hbar$ (Eq. (1.74)). S rotates about the z-axis at the Larmor frequency such that the time averaged projection of the orbitsphere angular momentum onto the axis of the applied magnetic field is $\pm \frac{\hbar}{2}$. The reorientation of S from parallel to antiparallel to the magnetic field applied along the z-axis gives rise to a current. The current is acted on by the flux corresponding to Φ_0 , the magnetic flux quantum, linked by the electron during the transition which gives rise to a Hall voltage. The electric field corresponding to the Hall voltage corresponds to the electric power term, $\frac{\delta}{\delta t} \left[\frac{1}{2} \epsilon_o \mathbf{E} \cdot \mathbf{E} \right]$, of the Poynting power theorem (Eq. (1.138)).

Consider a conductor in a uniform magnetic field and assume that it carries a current driven by an electric field perpendicular to the magnetic field. The current in this case is not parallel to the electric field, but is deflected at an angle to it by the magnetic field. This is the Hall Effect, and it occurs in most conductors.

A spin-flip transition is analogous to Quantum Hall Effect given in the corresponding section wherein the applied magnetic field quantizes the Hall conductance. The current is then precisely perpendicular to the magnetic field, so that no dissipation (that is no ohmic loss) occurs. This is seen in two-dimensional systems, at cryogenic temperatures, in quite high magnetic fields. Furthermore, the ratio of the total electric potential drop to the total current, the Hall resistance, R_H , is precisely equal to

$$R_H = \frac{h}{ne^2} \quad (1.150)$$

The factor n is an integer in the case of the Integral Quantum Hall Effect, and n is a small rational fraction in the case of the Fractional Quantum Hall Effect. In an experimental plot [20] as the function of the magnetic field, the Hall resistance exhibits flat steps precisely at these quantized

resistance values; whereas, the regular resistance vanishes (or is very small) at these Hall steps. Thus, the quantized Hall resistance steps occur for a transverse superconducting state.

Consider the case that an external magnetic field is applied along the x-axis to a two dimensional superconductor in the yz-plane which exhibits the Integral Quantum Hall Effect. (See Figure 1.7.) Conduction electrons align with the applied field in the x direction as the field permeates the material. The normal current carrying electrons experience a Lorentzian force, \mathbf{F}_L , due to the magnetic flux. The y directed Lorentzian force on an electron having a velocity \mathbf{v} in the z direction by an x directed applied flux, \mathbf{B} , is

$$\mathbf{F}_L = e\mathbf{v} \times \mathbf{B} \quad (1.151)$$

The electron motion is a cycloid where the center of mass experiences an $\mathbf{E} \times \mathbf{B}$ drift [21]. Consequently, the normal Hall Effect occurs. Conduction electron energy states are altered by the applied field and by the electric field corresponding to the Hall Effect. The electric force, \mathbf{F}_H , due to the Hall electric field, \mathbf{E}_y , is

$$\mathbf{F}_H = e\mathbf{E}_y \quad (1.152)$$

When these two forces are equal and opposite, conduction electrons propagate in the z direction alone. For this special case, it is demonstrated in Jackson [21] that the ratio of the corresponding Hall electric field E_H and the applied magnetic flux is

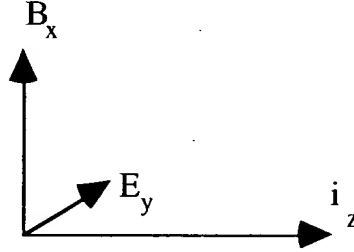
$$E_H/B = v \quad (1.153)$$

where v is the electron velocity. And, it is demonstrated in the Integral Quantum Hall Effect section that the Hall resistance, R_H , in the superconducting state is given by

$$R_H = \frac{h}{ne^2} \quad (1.154)$$

where n is an integer.

Figure 1.7. Coordinate system of crossed electric field, E_y , corresponding to the Hall voltage, magnetic flux, B_x , due to applied field, and superconducting current i_z .



Consider the case of the spin-flip transition of the electron. In the case of an exact balance between the Lorentzian force (Eq. (1.151)) and the electric force corresponding to the Hall voltage (Eq. (1.152)), each superconducting point mass of the electron propagates along a great circle where

$$E/B = v \quad (1.155)$$

where v is given by Eq. (1.47). Substitution of Eqs. (1.47) into Eq. (1.155) gives

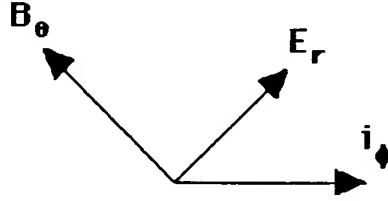
$$E/B = \frac{\hbar}{m_e r} \quad (1.156)$$

Eq. (1.156) is the condition for superconductivity in the presence of crossed electric and magnetic fields. The electric field corresponding to the Hall voltage corresponds to the electric energy term, E_{ele} , of the Poynting power theorem (Eq. (1.138)).

$$E_{ele} = \frac{1}{2} \int_0^{2\pi} \int_0^\pi \int_0^r \epsilon_o \mathbf{E} \cdot \mathbf{E} r^2 \sin \theta dr d\theta d\phi \quad (1.157)$$

The electric term for this superconducting state is derived as follows using the coordinate system shown in Figure 1.8.

Figure 1.8. Coordinate system of crossed electric field, E_r , corresponding to the Hall voltage, magnetic flux, B_θ , due to applied field, and superconducting current i_ϕ .



The current is perpendicular to E_r , thus there is no dissipation. This occurs when

$$e\mathbf{E} = e\mathbf{v} \times \mathbf{B} \quad (1.158)$$

or

$$E/B = v \quad (1.159)$$

The electric field corresponding to the Hall Voltage is

$$\mathbf{E} = \mathbf{v} \times \mathbf{B} \quad (1.160)$$

Substitution of Eq. (1.160) into Eq. (1.157) gives

$$E_{ele} = \frac{1}{2} \epsilon_o \int_0^{2\pi} \int_0^\pi \int_0^\eta (vB)^2 r^2 \sin\theta dr d\theta d\phi \quad (1.161)$$

The spin flip transition may be induced by the absorption of a resonant photon. The velocity is determined from the distance traversed by each point and the time of the transition due to capture of a photon resonant with the spin-flip transition energy. The current i_ϕ corresponding to the Hall voltage and E_r is given by the product of the electron charge and the frequency f of the photon where the correspondence principle holds as given in the Photon Absorption section.

$$i = ef \quad (1.162)$$

The resistance of free space for the propagation of a photon is the radiation resistance of free space η .

$$\eta = \sqrt{\frac{\mu_0}{\epsilon_0}} \quad (1.163)$$

The power P_r of the electron current induced by the photon as it transitions from free space to being captured by the electron is given by the product of the corresponding current and the resistance R which is given by Eq. (1.163).

$$P_r = i^2 R \quad (1.164)$$

Substitution of Eq. (1.162) and Eq. (1.163) gives

$$P_r = e^2 f^2 \sqrt{\frac{\mu_0}{\epsilon_0}} \quad (1.165)$$

It follows from the Poynting Power theorem (Eq. (1.138)) with spherical radiation that the transition time τ is given by the ratio of the energy and the power of the transition [22].

$$\tau = \frac{\text{energy}}{\text{power}} \quad (1.166)$$

The energy of the transition which is equal to the energy of the resonant photon is given by Planck's equation.

$$E = \hbar\omega = hf \quad (1.167)$$

Substitution of Eq. (1.165) and Eq. (1.167) into Eq. (1.166) gives

$$\tau = \frac{hf}{e^2 f^2 \sqrt{\frac{\mu_0}{\epsilon_0}}} \quad (1.168)$$

The distance traversed ℓ by the electron with an kinetic angular momentum change of $\frac{\hbar}{2}$ is

$$\ell = \frac{2\pi r}{2} = \frac{\lambda}{2} \quad (1.169)$$

where the wavelength is given by Eq. (1.43). The velocity is given by the distance traversed divided by the transition time. Eq. (1.168) and Eq. (1.169) give

$$v = \frac{\lambda/2}{\tau} = \frac{\lambda/2}{\frac{hf}{e^2 f^2 \sqrt{\frac{\mu_0}{\epsilon_0}}}} = \frac{\sqrt{\frac{\mu_0}{\epsilon_0}} e^2}{2h} \lambda f \quad (1.170)$$

The relationship for a photon in free space is

$$c = \lambda f \quad (1.171)$$

As shown in the Unification of Spacetime, the Forces, Matter, and Energy section, the fine structure constant given by Eqs. (1.147) is the dimensionless factor that corresponds to the relativistic invariance of charge.

$$\alpha = \frac{1}{4\pi} \sqrt{\frac{\mu_0}{\epsilon_0}} \frac{e^2}{\hbar} = \frac{1}{2} \frac{\sqrt{\frac{\mu_0}{\epsilon_0}}}{\frac{h}{e^2}} = \frac{\mu_0 e^2 c}{2h} \quad (1.172)$$

It is equivalent to one half the ratio of the radiation resistance of free

space, $\sqrt{\frac{\mu_0}{\epsilon_0}}$, and the hall resistance, $\frac{h}{e^2}$. The radiation resistance of free space is equal to the ratio of the electric field and the magnetic field of the photon (Eq. (4.10)). Substitution of Eq. (1.171) and Eq. (1.172) into Eq. (1.170) gives

$$\nu = \alpha c \quad (1.173)$$

Substitution of Eq. (1.173) into Eq. (1.161) gives

$$E_{ele} = \frac{1}{2} \epsilon_0 \int_0^{2\pi} \int_0^\pi \int_0^{\eta_1} (\alpha c \mu_0 H)^2 r^2 \sin \theta dr d\theta d\phi \quad (1.174)$$

where

$$B = \mu_0 H \quad (1.175)$$

The relationship between the speed of light, c , and the permittivity of free space, ϵ_0 , and the permeability of free space, μ_0 , is

$$c = \frac{1}{\sqrt{\mu_0 \epsilon_0}} \quad (1.176)$$

Thus, Eq. (1.174) may be written as

$$E_{ele} = \frac{1}{2} \alpha^2 \int_0^{2\pi} \int_0^\pi \int_0^{\eta_1} \mu_0 H^2 r^2 \sin \theta dr d\theta d\phi \quad (1.177)$$

Substitution of Eq. (1.125) gives

$$E_{ele} = \alpha^2 \frac{2\pi \mu_0 e^2 \hbar^2}{3m_e^2 r_1^3} \quad (1.178)$$

The magnetic flux, \mathbf{B} , is quantized in terms of the Bohr magneton because the electron links flux in units of the magnetic flux quantum,

$$\Phi_0 = \frac{h}{2e} \quad (1.179)$$

Substitution of Eqs. (1.139-1.149) gives

$$E_{ele} = 2 \left(\frac{2}{3} \alpha^2 \frac{\alpha}{2\pi} \mu_B B \right) \quad (1.180)$$

Dissipated Energy

The $\mathbf{J} \cdot \mathbf{E}$ energy over time is derived from the transient induced electric field and the magnetic field caused by the linkage of the fluxon. The magnetic field corresponds to a Lorentz force and a current density wherein the superconducting condition given by Eq. (1.155) is maintained with the transient induced electric field as the electron undergoes the spin-flip. The magnetic flux of the electron is given by

$$\mu_0 \mathbf{H} = \mathbf{B} = \frac{\mu_0 e \hbar}{2m_e r^3} (\mathbf{i}_r 2 \cos \theta - \mathbf{i}_\theta \sin \theta) \quad \text{for } r > r_n \quad (1.181)$$

From Eq. (1.149), the magnetic flux $B_{\mathbf{J} \cdot \mathbf{E}}$ of the fluxon is

$$B_{\mathbf{J} \cdot \mathbf{E}} = \frac{\alpha}{2\pi} B \quad (1.182)$$

The magnetic force on the electron due to the magnetic field of the fluxon is the Lorentzian force given by Eq. (1.151). Substitution of Eq. (1.47) for \mathbf{v} and Eq. (1.182) for $B_{\mathbf{J} \cdot \mathbf{E}}$ gives

$$\mathbf{F}_{mag} = \frac{\alpha}{2\pi} \frac{\mu_o e^2 \hbar^2}{2m_e^2 r_1^4} (\mathbf{i}_\theta 2 \cos \theta + \mathbf{i}_r \sin \theta) \quad (1.183)$$

The linking of a fluxon by an electron is equivalent to the contraction of the radius from ∞ to a finite value in the presence of the magnetic fluxon. The contraction of the orbitsphere of the electron produces a current.

The current over time $\Delta t \mathbf{J}$ is

$$\Delta t \mathbf{J} = \Delta t \sigma \mathbf{E}_f \quad (1.184)$$

where \mathbf{J} is the current-density, Δt is the time interval, σ is the conductivity, and \mathbf{E}_f is the effective electric field defined as follows:

$$\mathbf{F} = q \mathbf{E}_f \quad (1.185)$$

where \mathbf{F} is the magnetic force given by Eq. (1.183), and q is the charge-density given as follows:

$$q = \frac{e}{4\pi} \quad (1.186)$$

The orbit contracts in free space; thus, the relation for the conductivity is

$$\Delta t \sigma = \epsilon_o \quad (1.187)$$

The transient electric field of the contracting orbitsphere must have the same angular dependence as the Lorentzian force to maintain the superconducting condition given by Eq. (1.159).

$$\mathbf{E} = \frac{e}{4\pi \epsilon_o r_1^2} (\mathbf{i}_\theta 2 \cos \theta + \mathbf{i}_r \sin \theta) \quad (1.188)$$

where ϵ_o is the permittivity of free space ($8.854 \times 10^{-12} \text{ C}^2 / \text{N} \cdot \text{m}^2$). Using Eqs. (1.183-1.188), the $\mathbf{J} \cdot \mathbf{E}$ energy density over time for the contraction of the electron is

$$\Delta t (\mathbf{J} \cdot \mathbf{E}) = \frac{e}{4\pi \epsilon_o r_1^2} \frac{\alpha}{2\pi} \frac{\mu_o e^2 \hbar^2}{2m_e^2 r_1^4} \frac{4\pi \epsilon_o}{e} (4 \cos^2 \theta + \sin^2 \theta) \quad (1.189)$$

$$\Delta t (\mathbf{J} \cdot \mathbf{E}) = \frac{\alpha}{2\pi} \frac{\mu_o e^2 \hbar^2}{2m_e^2 r_1^6} (4 \cos^2 \theta + \sin^2 \theta) \quad (1.190)$$

The $\mathbf{J} \cdot \mathbf{E}$ energy over time is the volume integral of the energy density over time

$$[\Delta t (\mathbf{J} \cdot \mathbf{E})]_{\text{energy external}} = \frac{\alpha}{2\pi} \int_0^{2\pi} \int_0^\pi \int_0^\infty \frac{\mu_o e^2 \hbar^2}{2m_e^2 r_1^6} r^2 (4 \cos^2 \theta + \sin^2 \theta) \sin \theta dr d\theta d\Phi \quad (1.191)$$

$$[\Delta t (\mathbf{J} \cdot \mathbf{E})]_{\text{energy external}} = \frac{\alpha}{2\pi} \frac{4\pi \mu_o e^2 \hbar^2}{3m_e^2 r_1^3} \quad (1.192)$$

Substitution of Eq. (1.149) into Eq. (1.192) gives

$$[\Delta t(\mathbf{J} \cdot \mathbf{E})]_{\text{energy external}} = 2 \left(\frac{4}{3} \right) \left(\frac{\alpha}{2\pi} \right)^2 \mu_B B \quad (1.193)$$

Total Energy of Spin-Flip Transition

The principal energy of the transition corresponding to a reorientation of the orbitsphere is given by Eq. (1.136). And, the total energy of the flip transition is the sum of Eq. (1.136), and Eq. (1.149), (1.180), and (1.193) corresponding to the electric energy, the magnetic energy, and the dissipated energy of a fluxon treading the orbitsphere, respectively.

$$\Delta E_{\text{mag}}^{\text{spin}} = 2 \left(1 + \frac{\alpha}{2\pi} + \frac{2}{3} \alpha^2 \left(\frac{\alpha}{2\pi} \right) - \frac{4}{3} \left(\frac{\alpha}{2\pi} \right)^2 \right) \mu_B B \quad (1.194)$$

$$\Delta E_{\text{mag}}^{\text{spin}} = g \mu_B B \quad (1.195)$$

where the stored magnetic energy corresponding to the $\frac{\partial}{\partial t} \left[\frac{1}{2} \mu_o \mathbf{H} \cdot \mathbf{H} \right]$ term increases, the stored electric energy corresponding to the $\frac{\partial}{\partial t} \left[\frac{1}{2} \epsilon_o \mathbf{E} \cdot \mathbf{E} \right]$ term increases, and the $\mathbf{J} \cdot \mathbf{E}$ term is dissipative. The magnetic moment of Eq. (1.136) is twice that from the gyromagnetic ratio as given by Eq. (2.36) of the Orbital and Spin Splitting section. The magnetic moment of the electron is the sum of the component corresponding to the kinetic angular momentum, $\frac{\hbar}{2}$, and the component corresponding to the vector potential angular momentum, $\frac{\hbar}{2}$, (Eq. (1.132)). The spin-flip transition can be considered as involving a magnetic moment of g times that of a Bohr magneton. The g factor is redesignated the fluxon g factor as opposed to the anomalous g factor, and it is given by Eq. (1.194).

$$\frac{g}{2} = 1 + \frac{\alpha}{2\pi} + \frac{2}{3} \alpha^2 \left(\frac{\alpha}{2\pi} \right) - \frac{4}{3} \left(\frac{\alpha}{2\pi} \right)^2 \quad (1.196)$$

For $\alpha^{-1} = 137.03604(11)$ [23]

$$\frac{g}{2} = 1.001\,159\,652\,120 \quad (1.197)$$

The experimental value [24] is

$$\frac{g}{2} = 1.001\,159\,652\,188(4) \quad (1.198)$$

The calculated and experimental values are within the propagated error of the fine structure constant. Different values of the fine structure constant have been recorded from different experimental techniques, and α^{-1} depends on a circular argument between theory and experiment [25].

One measurement of the fine structure constant based on the electron g factor is $\alpha_e^{-1} = 137.036006(20)$ [26]. This value can be contrasted with equally precise measurements employing solid state techniques such as those based on the Josephson effect [27] ($\alpha_J^{-1} = 137.035963(15)$) or the quantized Hall effect [28] ($\alpha_H^{-1} = 137.035300(400)$). A method of the determination of α^{-1} that depends on the circular methodology between theory and experiment to a lesser extent is the substitution of the independently measured fundamental constants μ_0 , e , c , and h into Eq. (1.172). The following values of the fundamental constants are given by Weast [23]

$$\mu_0 = 4\pi \times 10^{-7} \text{ Hm}^{-1} \quad (1.199)$$

$$e = 1.6021892(46) \times 10^{-19} \text{ C} \quad (1.200)$$

$$c = 2.99792458(12) \times 10^8 \text{ ms}^{-1} \quad (1.201)$$

$$h = 6.626176(36) \times 10^{-34} \text{ JHz}^{-1} \quad (1.202)$$

For these constants,

$$\alpha^{-1} = 137.03603(82) \quad (1.203)$$

Substitution of the α^{-1} from Eq. (1.203) into Eq. (1.196) gives

$$\frac{g}{2} = 1.001\,159\,652\,137 \quad (1.204)$$

The experimental value [24] is

$$\frac{g}{2} = 1.001\,159\,652\,188(4) \quad (1.205)$$

The *postulated* quantum electrodynamics (QED) theory of $\frac{g}{2}$ is based on the determination of the terms of a *postulated* power series in α/π where each *postulated* virtual particle is a source of *postulated* vacuum polarization that gives rise to a *postulated* term. The algorithm involves scores of *postulated* Feynman diagrams corresponding to thousands of matrices with thousands of integrations per matrix requiring decades to reach a consensus on the "appropriate" *postulated* algorithm to remove the intrinsic infinities. The remarkable agreement

between Eqs. (1.204) and (1.205) demonstrates that $\frac{g}{2}$ may be derived in closed form from Maxwell's equations in a simple straight forward manner that yields a result with eleven figure agreement with experiment—the limit of the experimental capability of the measurement of the fundamental constants that determine α . In Appendix II: Quantum Electrodynamics is Purely Mathematical and Has No Basis in Reality, the Maxwellian result is contrast with the QED algorithm of invoking virtual particles, zero point fluctuations of the vacuum, and negative energy states of the vacuum.

The muon, like the electron, is a lepton with \hbar of angular momentum. The magnetic moment of the muon is given by Eq. (1.136) with the electron mass replaced by the muon mass. It is twice that from the gyromagnetic ratio as given by Eq. (2.36) of the Orbital and Spin Splitting section corresponding to the muon mass. As is the case with the electron, the magnetic moment of the muon is the sum of the component corresponding to the kinetic angular momentum, $\frac{\hbar}{2}$, and the component corresponding to the vector potential angular momentum, $\frac{\hbar}{2}$, (Eq. (1.132).

The spin-flip transition can be considered as involving a magnetic moment of g times that of a Bohr magneton of the muon. The g factor is equivalent to that of the electron given by Eq. (1.196).

The muon anomalous magnetic moment has been measured in a new experiment at Brookhaven National Laboratory (BNL) [29]. Polarized muons were stored in a superferric ring, and the angular frequency difference ω_a between the spin precession and orbital frequencies was determined by measuring the time distribution of high-energy decay positrons. The dependence of ω_a on the magnetic and electric fields is given by BMT equation which is the relativistic equation of motion for spin in uniform or slowly varying external fields [30]. The dependence on the electric field is eliminated by storing muons with the “magic” $\gamma=29.3$, which corresponds to a muon momentum $p=3.09 \text{ GeV}/c$. Hence measurement of ω_a and of B determines the anomalous magnetic moment.

The “magic” γ wherein the contribution to the change of the longitudinal polarization by the electric quadrapole focusing fields are eliminated occurs when

$$\frac{g_\mu \beta}{2} - \frac{1}{\beta} = 0 \quad (1.206)$$

where g_μ is the muon g factor which is required to be different from the electron g factor in the standard model due to the dependence of the

mass dependent interaction of each lepton with vacuum polarizations due to virtual particles. For example, the muon is much heavier than the electron, and so high energy (short distance) effects due to strong and weak interactions are more important here [26]. The BNL Muon (g-2) Collaboration [29] used a “magic” $\gamma=29.3$ which satisfied Eq. (1.206)

identically for $\frac{g_\mu}{2}$; however, their assumption that this condition eliminated the affect of the electrostatic field on ω_a is flawed as shown in Appendix III: Muon g Factor. Internal consistency was achieved during the determination of $\frac{g_\mu}{2}$ using the BMT equation with the flawed assumption that $\frac{g_\mu}{2} \neq \frac{g_e}{2}$. The parameter measured by Carey et al. [29] corresponding to $\frac{g_\mu}{2}$ was the sum of a finite electric term as well as a magnetic term. The calculated result based on the equivalence of the muon and electron g factors

$$\frac{g_\mu}{2} = 1.001\,165\,923 \quad (1.207)$$

is in agreement with the result of Carey et al. [29]:

$$\frac{g_\mu}{2} = 1.001\,165\,925 \quad (15) \quad (1.208)$$

Rather than indicating an expanded plethora of postulated supersymmetry virtual particles which make contributions such as smuon-neutralino and sneutrino-chargino loops as suggested by Brown et al.

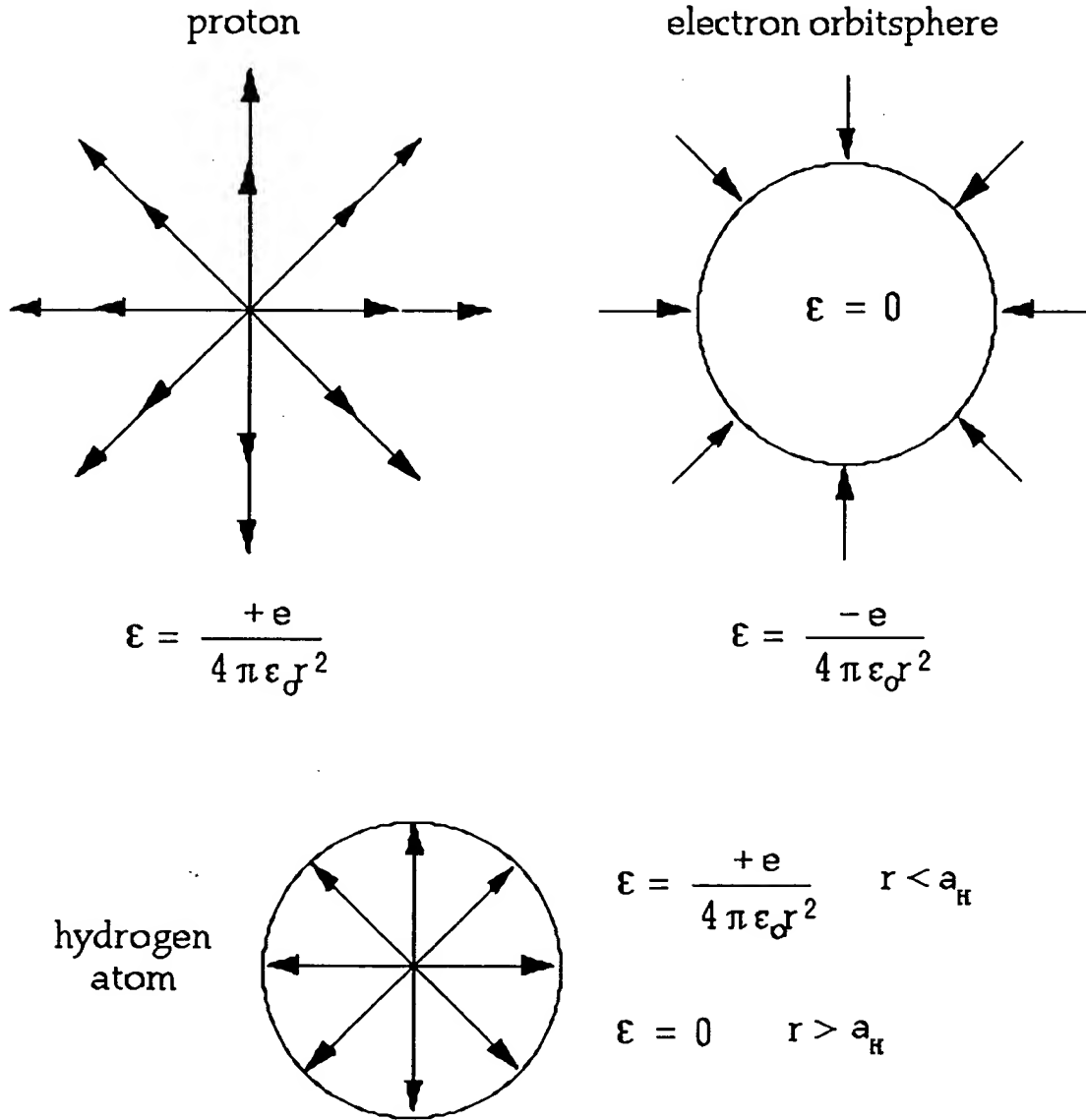
[31], the deviation of the experimental value of $\frac{g_\mu}{2}$ from that of the standard model prediction simply indicates that the muon g factor is identical to the electron g factor.

DETERMINATION OF ORBITSPIHERE RADII, r_n

The one-electron orbitsphere is a spherical shell of negative charge (total charge = $-e$) of zero thickness at a distance r_n from the nucleus (charge = $+Ze$). It is well known that the field of a spherical shell of charge is zero inside the shell and that of a point charge at the origin outside the shell [32]. See Figure 1.9.

Figure 1.9. The electric fields of a proton, an electron, and a hydrogen

atom.



Thus, for a nucleus of charge Z , the force balance equation for the electron orbitsphere is obtained by equating the forces on the mass and charge densities. For the ground state, $n=1$, the centrifugal force of the electron is given by

$$\mathbf{F}_{centrifugal} = \frac{m_e}{4\pi r_1^2} \frac{v_1^2}{r_1} \quad (1.209)$$

where $\frac{m_e}{4\pi r_1^2}$ is the mass density of the orbitsphere. The centripetal force is the electric force, \mathbf{F}_{ele} , between the electron and the nucleus.

$$\mathbf{F}_{ele} = \frac{e}{4\pi r_1^2} \frac{Ze}{4\pi\epsilon_0 r_1^2} \quad (1.210)$$

where ϵ_0 is the permittivity of free-space.

The second centripetal force is an electrodynamic force, a force dependent on the second derivative of charge position which respect to time, which arises between the electron and the nucleus. The motion of each point in the magnetic field of the nucleus will cause a relativistic central force, \mathbf{F}_{mag} , which acts on each point mass. The magnetic central force is derived as follows from the Lorentzian force which is relativistically corrected. Each infinitesimal point of the orbitsphere moves on a great circle, and each point charge has the charge-density $\frac{e}{4\pi r_n^2}$. As given in the Proton and Neutron section, the proton is

comprised of a linear combination of three constant functions and three orthogonal spherical harmonic quark/gluon functions. From the photon inertial reference frame at the radius of each infinitesimal point of the electron orbitsphere, the proton charge distribution is given as the product of the quark and gluon functions which gives rise to a uniform distribution. The magnetic flux of the proton in the $v=c$ inertial frame at the electron radius follows from McQuarrie [16]:

$$B = \frac{\mu_0 e \hbar}{2m_p r_n^3} \quad (1.211)$$

And, the magnetic flux due to a nucleus of charge Z and mass m is

$$B = \frac{\mu_0 Z e \hbar}{2m r_n^3} \quad (1.212)$$

The motion of each point will cause a relativistic central force, \mathbf{F}_{imag} , which acts on each point mass. The magnetic central force is derived as follows from the Lorentzian force which is relativistically corrected. The Lorentzian force density on each point moving at velocity v given by Eq. (1.47) is

$$\mathbf{F}_{mag} = \frac{e}{4\pi r_n^2} \mathbf{v} \times \mathbf{B} \quad (1.213)$$

Substitution of Eq. (1.47) for \mathbf{v} and Eq. (1.212) for \mathbf{B} gives

$$\mathbf{F}_{mag} = \frac{1}{4\pi r_1^2} \left[\frac{Z_1 e^2 \mu_0}{2m_e r_n} \right] \frac{\hbar^2}{m r_n^3} \quad (1.214)$$

The term in brackets can be expressed in terms α . From Eqs. (1.144-1.148)

$$\frac{Z_1 e^2 \mu_0}{2m_e r_n} = 2\pi\alpha Z_1 \frac{v}{c} \quad (1.215)$$

It can be shown that the relativistic correction to Eq. (1.214) is the reciprocal of Eq. (1.215). Consider an inertial frame following a great

circle of radius r_n with $v=c$. The motion is tangential to the radius; thus, r_n is Lorentzian invariant. But, the tangential distance along a great circle is $2\pi r_n$ in the laboratory frame and r_n in the $v=c$ frame. The charge is relativistically invariant, whereas, the mass is not. The relativistic correction to the laboratory frame mass relative to the $v=c$ frame is 2π . The correction follows from the Lorentz transformation of the electron's invariant angular momentum of \hbar . It is shown by Purcell [33] that the force on a moving charge due to a moving line of charge is a relativistic electric force due to Lorentzian contraction of the line charge density.

The force is proportional to $\frac{v}{c}$ where v is the electron's velocity. Thus, it follows that the electron mass in the laboratory frame relative to the $v=c$ inertial frame is which is also proportional to $\frac{v}{c}$. Following the derivation of Purcell with the substitution of the relativistic mass density for the charge density gives the electron mass correction to the electrodynamic force as

$$m_e = 2\pi \frac{v}{c} m_{e\text{Rest}} \quad (1.216)$$

Furthermore, due to invariance of charge under Gauss's Integral Law, the radius term in the brackets of Eq. (1.214) is relativistically corrected. The radius of the electron relative to the $v=c$ frame, r_α^* , is relativistically corrected as follows. From Eq. (1.43) the relationship between the radius and the electron wavelength is

$$2\pi r = \lambda \quad (1.217)$$

Using the de Broglie Eq. (1.46) with $v=c$

$$\lambda = \frac{h}{mv} = \frac{h}{mc} \quad (1.218)$$

With substitution of Eq. (1.217) into Eq. (1.218)

$$r_\alpha^* = \frac{\hbar}{mc} = \lambda_c = \alpha a_o \quad (1.219)$$

where λ_c is the Compton wavelength bar, and where a_o is the Bohr radius. The radius of the electron orbitsphere in the $v=c$ frame is λ_c , and the relativistic correction due to length contraction can be determined as a boundary value problem. Eq. (1.219) can be expressed in terms of a relativistic correction, n , which multiplies, r_1 , the radius of the electron orbitsphere in the lab frame. The lab frame electron radius is taken as $\frac{a_o}{Z_2}$ which is consistent with Eq. (1.227); thus, it is the solution of our boundary value problem as shown as follows.

$$r_\alpha^* = \frac{\hbar}{mc} = \lambda_c = \alpha a_o = \frac{n a_o}{Z_2} = n r_1 \quad (1.220)$$

It follows from Eq. (1.220) that the radius, r_n , of Eq. (1.214) must be corrected by the factor αZ_2 . By correcting the radius and the mass, the relativistic correction is $\frac{1}{2\pi\alpha Z_2 \frac{v}{c}}$. In this case, $Z_1 = Z_2$; thus, 1 is substituted

for the term in brackets in Eq. (1.214); therefore,

$$\mathbf{F}_{mag} = -\frac{1}{4\pi r_1^2} \frac{\hbar^2}{mr_n^3} \hat{r} \quad (1.221)$$

The force balance equation is given by equating the centrifugal and centripetal force densities:

$$\frac{m_e}{4\pi r_1^2} \frac{v_1^2}{r_1} = \frac{e}{4\pi r_1^2} \frac{Ze}{4\pi\epsilon_o r_1^2} - \frac{1}{4\pi r_1^2} \frac{\hbar^2}{mr_n^3} \quad (1.222)$$

Using Eq. (1.47),

$$r_1 = \frac{4\pi\epsilon_o \hbar^2}{Ze^2 \mu_e} \quad (1.223)$$

where the reduced electron mass, μ_e , is

$$\mu_e = \frac{m_e m}{m_e + m} \quad (1.224)$$

The Bohr radius is

$$a_o = \frac{4\pi\epsilon_o \hbar^2}{e^2 m_e} \quad (1.225)$$

And, the radius given by force balance between the centrifugal force and central electrostatic force alone is

$$r_1 = \frac{4\pi\epsilon_o \hbar^2}{Ze^2 m_e} = \frac{a_o}{Z} \quad (1.226)$$

And, for hydrogen, m of Eq. (1.224) is

$$m = m_p \quad (1.227)$$

Substitution of the reduced electron mass for the electron mass gives, a_H , the Bohr radius of the hydrogen atom.

$$a_H = \frac{4\pi\epsilon_o \hbar^2}{e^2 \mu_e} \quad (1.228)$$

Thus, Eq. (1.223) becomes

$$r_1 = \frac{a_H}{Z} \quad (1.229)$$

ENERGY CALCULATIONS

The potential energy V between the electron and the nucleus separated by the radial distance radius r_1 is,

$$V = \frac{-Ze^2}{4\pi\epsilon_0 r_1} = \frac{-Z^2 e^2}{4\pi\epsilon_0 a_H} = -Z^2 \times 4.3675 \times 10^{-18} \text{ J} = -Z^2 \times 27.2 \text{ eV} \quad (1.230)$$

Because this is a central force problem, the kinetic energy, T , is $-\frac{1}{2}V$.

$$T = \frac{Z^2 e^2}{8\pi\epsilon_0 a_H} = Z^2 \times 13.59 \text{ eV} \quad (1.231)$$

The same result can be obtained from $T = \frac{1}{2}m_e v_1^2$ and Eq. (1.47).

Alternatively, the kinetic energy, which is equal to the stored electric energy, E_{ele} , can be calculated from

$$T = E_{ele} = -\frac{1}{2}\epsilon_0 \int_{\infty}^{r_1} E^2 dv \quad (1.232)$$

where $|E| = -\frac{Ze}{4\pi\epsilon_0 r^2}$. Thus, as the orbitsphere shrinks from ∞ to r_1 ,

$$E_{ele} = -\frac{Z^2 e^2}{8\pi\epsilon_0 a_H} = -Z^2 \times 2.1786 \times 10^{-18} \text{ J} = -Z^2 \times 13.598 \text{ eV} \quad (1.233)$$

The calculated Rydberg constant is $109,677.58 \text{ cm}^{-1}$; the experimental Rydberg constant is $109,677.58 \text{ cm}^{-1}$. Furthermore, a host of parameters can be calculated for the hydrogen atom, as shown in Table 1.1.

Table 1.1. Some calculated parameters for the hydrogen atom ($n=1$).

radius	$r_1 = a_H$	$5.2918 \times 10^{-11} \text{ m}$
potential energy	$V = \frac{-e^2}{4\pi\epsilon_0 a_H}$	-27.196 eV
kinetic energy	$T = \frac{e^2}{8\pi\epsilon_0 a_H}$	13.598 eV
angular velocity (spin)	$\omega_1 = \frac{\hbar}{m_e r_1^2}$	$4.13 \times 10^{16} \text{ rads}^{-1}$
linear velocity	$v_1 = r_1 \omega_1$	$2.19 \times 10^6 \text{ ms}^{-1}$
wavelength	$\lambda_1 = 2\pi r_1$	$3.325 \times 10^{-10} \text{ m}$
spin quantum number	$s = \frac{1}{2}$	$\frac{1}{2}$
moment of Inertia	$I = m_e r_1^2 \sqrt{s(s+1)}$	$2.209 \times 10^{-51} \text{ kgm}^2$
angular kinetic energy	$E_{angular} = \frac{1}{2} I \omega_1^2$	11.78 eV
magnitude of the angular momentum	\hbar	$1.0545 \times 10^{-34} \text{ Js}$
projection of the angular momentum onto the S-axis	$S = \hbar \sqrt{s(s+1)}$	$9.133 \times 10^{-35} \text{ Js}$
projection of the angular momentum onto the z-axis	$S_z = \frac{\hbar}{2}$	$5.273 \times 10^{-35} \text{ Js}$
mass density	$\frac{m_e}{4\pi r_1^2}$	$2.589 \times 10^{-11} \text{ kgm}^{-2}$
charge-density	$\frac{e}{4\pi r_1^2}$	4.553 Cm^{-2}

Table 1.2 gives the radii and energies for some one-electron atoms. In addition to the energies, the wavelength, angular frequency, and the linear velocity can be calculated for any one-electron atom from Eqs. (1.46), (1.55), and (1.56). Values are given in Table 1.3.

Table 1.2. Calculated energies (non-relativistic) and calculated ionization energies for some one-electron atoms.

Atom	Calculated r_1^a (a_H)	Calculated Kinetic Energy ^b (eV)	Calculated Potential Energy ^c (eV)	Calculated Ionization Energy ^d (eV)	Experimental Ionization Energy ^e (eV)
<i>H</i>	1.000	13.60	-27.20	13.60	13.59
<i>He</i> ⁺	0.500	54.42	-108.84	54.42	54.58
<i>Li</i> ²⁺	0.333	122.44	-244.88	122.44	122.45
<i>Be</i> ³⁺	0.250	217.68	-435.36	217.68	217.71
<i>B</i> ⁴⁺	0.200	340.13	-680.26	340.13	340.22
<i>C</i> ⁵⁺	0.167	489.78	-979.56	489.78	489.98
<i>N</i> ⁶⁺	0.143	666.65	-1333.30	666.65	667.03
<i>O</i> ⁷⁺	0.125	870.73	-1741.46	870.73	871.39

a from Equation (1.229)

b from Equation (1.231)

c from Equation (1.230)

d from Equation (1.233)

e experimental

It is noteworthy that the potential energy is a constant (at a given n) because the electron is at a fixed distance, r_n , from the nucleus. And, the kinetic energy and velocity squared are constant because the atom does not radiate at r_n and the potential energy is constant.

Table 1.2. Calculated radii, angular frequencies, linear velocities, and wavelengths for the $n=1$ state of some one-electron atoms (non-relativistic).

Atom	r_1^a (a_0)	angular ^b velocity ($10^{17} \text{ rad s}^{-1}$)	linear ^c velocity (10^6 ms^{-1})	wavelength ^d (10^{-10} m)
<i>H</i>	1.000	0.413	2.19	3.325
<i>He</i> ⁺	0.500	1.65	4.38	1.663
<i>Li</i> ²⁺	0.333	3.72	6.56	1.108
<i>Be</i> ³⁺	0.250	6.61	8.75	0.831
<i>B</i> ⁴⁺	0.200	10.3	10.9	0.665
<i>C</i> ⁵⁺	0.167	14.9	13.1	0.554
<i>N</i> ⁶⁺	0.143	20.3	15.3	0.475
<i>O</i> ⁷⁺	0.125	26.5	17.5	0.416

^a from Equation (1.226)
^b from Equation (1.55)
^c from Equation (1.56)
^d from Equation (1.46)

It should be noted that the linear velocity is an appreciable percent of the velocity of light for some of the atoms in Table 1.2—5.9% for O^{7+} for example. Relativistic corrections must be applied before a comparison between the total energy and ionization energy (Table 1.2) is made.

APPENDIX I

NONRADIATION BASED ON THE ELECTROMAGNETIC FIELDS AND
THE POYNTING POWER VECTOR

A point charge undergoing periodic motion accelerates and as a consequence radiates according to the Larmor formula:

$$P = \frac{1}{4\pi\epsilon_0} \frac{2e^2}{3c^3} a^2 \quad (1)$$

where e is the charge, a is its acceleration, ϵ_0 is the permittivity of free space, and c is the speed of light. Although an accelerated *point* particle radiates, an *extended distribution* modeled as a superposition of accelerating charges does not have to radiate. An ensemble of charges, all oscillating at the same frequency, create a radiation pattern with a number of nodes. The same applies to current patterns in phased array antenna design [34]. It is possible to have an infinite number of charges oscillating in such a way as to cause destructive interference or nodes in all directions. In order to obtain the condition, if it exists, that the electron current distribution given by Eq. (11) must satisfy such that the electron does not radiate, the electromagnetic far field is determined from the current distribution. The vector potential in the Lorentz gauge satisfies

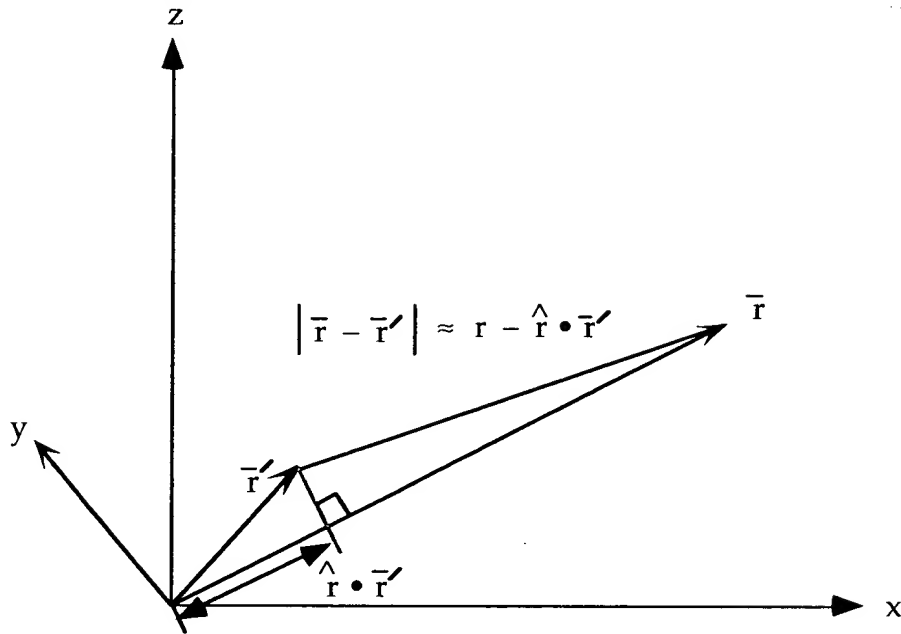
$$\nabla^2 \mathbf{A} + \omega^2 \mu_0 \epsilon_0 \mathbf{A} = -\mu_0 \mathbf{J} \quad (2)$$

where μ_0 is the permeability of free space, ω is the frequency of the time harmonic electron motion, \mathbf{J} is the current of the electron, and \mathbf{A} is the vector potential given by

$$\mathbf{A}(\mathbf{r}) = \frac{\mu_0}{4\pi} \int \frac{\mathbf{J}(\mathbf{r}', t - |\mathbf{r} - \mathbf{r}'|/c)}{|\mathbf{r} - \mathbf{r}'|} d^3 r' \quad (3)$$

where the coordinates are shown in Figure 1

Figure 1. Far field approximation.



The magnetic field is given by

$$\mathbf{H} = \frac{1}{\mu_0} \nabla \times \mathbf{A} \quad (4)$$

The electric field is given by

$$\mathbf{E} = \frac{1}{j\omega\epsilon_0} \nabla \times \mathbf{H} \quad (5)$$

The power density $S(t)$ is given by

$$S(t) = \mathbf{E} \times \mathbf{H} \quad (6)$$

The charge density functions of the electron orbitsphere in spherical coordinates plus time are given by Eqs. (1.64-1.65). For $\ell = 0$, $N = \frac{-e}{8\pi r_n^2}$, and the charge-density function is

$$\ell = 0$$

$$\rho(r, \theta, \phi, t) = \frac{e}{8\pi r^2} [\delta(r - r_n)] [Y_\ell^m(\theta, \phi) + Y_0^0(\theta, \phi)] \quad (7)$$

The equipotential, uniform or constant charge density function (Eq. (1.64) and Eq. (7)) further comprises a current pattern given in the ORBITSPIRE EQUATION OF MOTION FOR $\ell = 0$ section. It also corresponds to the nonradiative $n=1, \ell = 0$ state of atomic hydrogen and to the spin function of the electron. The current density function is given by multiplying Eq. (7) by the constant angular velocity ω . There is acceleration without radiation. In this case, centripetal acceleration. A

static charge distribution exists even though each point on the surface is accelerating along a great circle. Haus's condition predicts no radiation for the entire ensemble. The same result is trivially predicted from consideration of the fields and the radiated power. Since the current is not time dependent, the fields are given by

$$\nabla \times \mathbf{H} = \mathbf{J} \quad (8)$$

and

$$\nabla \times \mathbf{E} = 0 \quad (9)$$

which are the electrostatic and magnetostatic cases, respectively, with no radiation. Also see Daboul and Jensen [35].

In cases of orbitals of heavier elements and excited states of one electron atoms and atoms or ions of heavier elements which are not constant as given by Eq. (1.65), the constant spin function is modulated by a time and spherical harmonic function. The modulation or traveling charge density wave corresponds to an orbital angular momentum in addition to a spin angular momentum. These states are typically referred to as p, d, f, etc. orbitals and correspond to an ℓ quantum number not equal to zero. Haus's condition also predicts nonradiation for a constant spin function modulated by a time and spherically harmonic orbital function. However, in the case that such a state arises as an excited state by photon absorption, it is radiative due to a radial dipole term in its current density function since it possesses spacetime Fourier Transform components synchronous with waves traveling at the speed of light as given in the INSTABILITY OF EXCITED STATES section.

The nonradiation condition given by Eqs. (1.44-1.45) may be confirmed by determining the fields and the current distribution condition that is nonradiative based on Maxwell's equations.

For $\ell \neq 0$, $N = \frac{-e}{4\pi r_n^2}$. The charge-density functions including the time-function factor are

$$\ell \neq 0$$

$$\rho(r, \theta, \phi, t) = \frac{e}{4\pi r^2} [\delta(r - r_n)] \left[Y_0^0(\theta, \phi) + \text{Re} \left\{ Y_\ell^m(\theta, \phi) [1 + e^{i\omega_n t}] \right\} \right] \quad (10)$$

where

$\text{Re} \left\{ Y_\ell^m(\theta, \phi) [1 + e^{i\omega_n t}] \right\} = \text{Re} [Y_\ell^m(\theta, \phi) + Y_\ell^m(\theta, \phi) e^{i\omega_n t}] = P_\ell^m(\cos \theta) \cos m\phi + P_\ell^m(\cos \theta) \cos(m\phi + \omega_n t)$
and $\omega_n = 0$ for $m = 0$ (In the cases that $m \neq 0$, Eq. (1.65) and Eq. (10) is a traveling charge density wave that moves on the surface of the orbitsphere about the z-axis and modulates the orbitsphere corresponding to $\ell = 0$. Since the charge is moving time harmonically about the z-axis with frequency ω_n and the current-density function is given by the time derivative of the charge-density function, the current-

density function is given by the normalized product of the constant angular velocity and the charge-density function. The first current term of Eq. (10) is static. Thus, it is trivially nonradiative. The current due to the time dependent term is

$$\begin{aligned}
 \mathbf{J} &= \omega_n \frac{e}{4\pi r^2} N[\delta(r-r_n)] \text{Re}\{Y_\ell^m(\theta, \phi)[1 + e^{i\omega_n t}]\} \hat{\phi} \\
 &= \omega_n \frac{e}{4\pi r^2} N[\delta(r-r_n)] \text{Re}\{Y_\ell^m(\theta, \phi) + Y_\ell^m(\theta, \phi)e^{i\omega_n t}\} \hat{\phi} \\
 &= \omega_n \frac{e}{4\pi r^2} N[\delta(r-r_n)] (P_\ell^m(\cos\theta)\cos m\phi + P_\ell^m(\cos\theta)e^{im\phi}e^{i\omega_n t}) \hat{\phi} \\
 &= \omega_n \frac{e}{4\pi r^2} N[\delta(r-r_n)] (P_\ell^m(\cos\theta)\cos m\phi + P_\ell^m(\cos\theta)\cos(m\phi + \omega_n t)) \hat{\phi}
 \end{aligned} \tag{11}$$

where N is the normalization constant. Let $r_n = R$ in Eq. (11). Using the coordinate designation shown in Figure 1, the vector potential due to the time dependent term is given by

$$\mathbf{A}(\mathbf{r}, t) = e \frac{\omega_n}{2\pi} m \frac{2\ell+1}{2R^2} \frac{\mu_0}{4\pi} \int_0^{2\pi} \int_0^\pi \int_0^\infty Y_\ell^m(\theta, \phi) \frac{e^{i\omega_n(t-|\mathbf{r}-\mathbf{r}'|/c)}}{|\mathbf{r}-\mathbf{r}'|} \hat{\mathbf{u}} \times \hat{\mathbf{r}}' \delta(r-R) r^2 \sin\theta dr d\theta d\Phi \tag{12}$$

$$\mathbf{A}(\mathbf{r}, t) = e \frac{\omega_n}{2\pi} m \frac{2\ell+1}{2R^2} \frac{\mu_0}{4\pi} e^{i\omega_n t} \hat{\mathbf{u}} \times \int_0^{2\pi} \int_0^\pi \int_0^\infty \hat{\mathbf{r}}' Y_\ell^m(\theta, \phi) \frac{e^{-ik|\mathbf{r}-\mathbf{r}'|}}{|\mathbf{r}-\mathbf{r}'|} \delta(r-R) r^2 \sin\theta dr d\theta d\Phi \tag{13}$$

where " $\hat{\mathbf{u}}$ " denotes the unit vectors $\hat{\mathbf{u}} \equiv \frac{\mathbf{u}}{|\mathbf{u}|}$, and the current function is

normalized. The expansion of the Green function given by Jackson [36] is

$$\frac{e^{-ik|\mathbf{r}-\mathbf{r}'|}}{|\mathbf{r}-\mathbf{r}'|} = ik \sum_{\ell=0}^{\infty} j_\ell(kr_<) h_\ell^{(1)}(kr_>) \sum_{m=-\ell}^{\ell} Y_{\ell,m}^*(\theta', \phi') Y_{\ell,m}(\theta, \phi) \tag{14}$$

where

$$r_< \equiv \min(r, R), \quad r_> \equiv \max(r, R) \tag{15}$$

Since the modulation function $Y_{\ell,m}(\theta, \phi)$ is a traveling charge density wave that moves time harmonically on the surface of the orbitsphere about the z-axis with frequency ω_n , ϕ is a function of t . Substitution of Eq. (14) into Eq. (13) gives

$$\mathbf{A}(\mathbf{r}, t) = e \frac{\omega_n}{2\pi} m \left[\frac{2\ell+1}{2} \right] \frac{\mu_0}{4\pi} \int_0^{2\pi} \int_0^\pi e^{i(\omega_n t + m\phi)} \hat{\mathbf{u}} \times \int_0^\pi \hat{\mathbf{r}}' ik j_\ell(kr_<) h_\ell^{(1)}(kr_>) (P_\ell^m(\cos\theta))^2 \sin\theta d\theta d\Phi \tag{16}$$

$$\mathbf{A}(\mathbf{r}, t) = e \frac{m\omega_n}{2\pi} \frac{\mu_0}{4\pi} \int_0^{2\pi} e^{i\omega_n t} \hat{\mathbf{u}} \times \hat{\mathbf{r}}' ik j_\ell(kr_<) h_\ell^{(1)}(kr_>) \cos(m\phi) d\Phi \tag{17}$$

$$\mathbf{A}(\mathbf{r}, t) = e \frac{m\omega_n}{2\pi} \frac{\mu_0}{4\pi} \int_0^{vT_n} e^{i\omega_n t} \hat{\mathbf{u}} \times \hat{\mathbf{r}}' ik j_\ell(kr_<) h_\ell^{(1)}(kr_>) \cos(mks(t)) ds \tag{18}$$

where $s(t)$ is the angular displacement of the rotation modulation function during one period T_n and v is the linear velocity in the $\hat{\mathbf{u}} \times \hat{\mathbf{r}}'$ direction.

Thus,

$$\mathbf{A}(\mathbf{r}, t) = e \frac{\omega_n}{2\pi} \frac{\mu_0}{4\pi} i \left[e^{i\omega_n t} \hat{\mathbf{u}} \times \hat{\mathbf{r}} \right] j_\ell(kr_<) h_\ell^{(1)}(kr_>) \sin(mkvT_n) \quad (19)$$

$$\mathbf{A}(\mathbf{r}, t) = e \frac{\omega_n}{2\pi} \frac{\mu_0}{4\pi} i \left[e^{i\omega_n t} \hat{\mathbf{u}} \times \hat{\mathbf{r}} \right] j_\ell(kr_<) h_\ell^{(1)}(kr_>) \sin(mks) \quad (20)$$

In the case that k is the lightlike k^0 , then $k = \omega_n/c$, and Eq. (20) vanishes for

$$R = cT_n \quad (21)$$

$$RT_n^{-1} = c \quad (22)$$

$$Rf = c \quad (23)$$

Thus,

$$s = vT_n = R = r_n = \lambda_n \quad (24)$$

which is identical to the Haus condition for nonradiation given by Eq. (1.45).

The electric and magnetic fields and the power density as a function of time are given by Eq.(20) and Eqs. (4-6). The spherical components of the fields, are defined by

$$\mathbf{E} = E_r \hat{\mathbf{r}} + E_\phi \hat{\phi} + E_\theta \hat{\theta} \quad (25)$$

where

$$\hat{\phi} = \frac{\hat{\mathbf{u}} \times \hat{\mathbf{r}}}{|\hat{\mathbf{u}} \times \hat{\mathbf{r}}|} = \frac{\hat{\mathbf{u}} \times \hat{\mathbf{r}}}{\sin \theta} \quad (26)$$

$$\hat{\mathbf{u}} = \hat{\mathbf{z}} = \text{orbital axis} \quad (28)$$

$$\hat{\theta} = \hat{\phi} \times \hat{\mathbf{r}} \quad (29)$$

The fields inside of the electron orbitsphere ($r < R$) are

$$E_r = E_\theta = B_\phi = 0 \quad (30)$$

$$E_\phi = -\sqrt{\frac{\mu_0}{\epsilon_0}} k e \frac{\omega_n}{2\pi} \frac{1}{4\pi} h_\ell^{(1)}(kR) j_\ell(kr) \sin(mks) \sin \theta e^{i\omega_n t} \quad (31)$$

$$H_r = 2e \frac{\omega_n}{2\pi} \frac{1}{4\pi} i k \frac{h_\ell^{(1)}(kR)}{kr} j_\ell(kr) \sin(mks) \cos \theta e^{i\omega_n t} \quad (32)$$

$$H_\theta = -2e \frac{\omega_n}{2\pi} \frac{1}{4\pi} i k \frac{h_\ell^{(1)}(kR)}{kr} \frac{d}{dkr} (kr j_\ell(kr)) \sin(mks) \sin \theta e^{i\omega_n t} \quad (33)$$

The fields outside of the electron orbitsphere ($r > R$) are

$$E_r = E_\theta = B_\phi = 0 \quad (34)$$

$$E_\phi = -\sqrt{\frac{\mu_0}{\epsilon_0}} k e \frac{\omega_n}{2\pi} \frac{1}{4\pi} j_\ell(kR) h_\ell^{(1)}(kr) \sin(mks) \sin \theta e^{i\omega_n t} \quad (35)$$

$$H_r = 2e \frac{\omega_n}{2\pi} \frac{1}{4\pi} i k \frac{j_\ell(kR)}{kr} h_\ell^{(1)}(kr) \sin(mks) \cos \theta e^{i\omega_n t} \quad (36)$$

$$H_{\theta} = -2e \frac{\omega_n}{2\pi} \frac{1}{4\pi} ik \frac{j_{\ell}(kR)}{kr} \frac{d}{dkr} \left(kr h_{\ell}^{(1)}(kr) \right) \sin(mks) \sin \theta e^{i\omega_n t} \quad (37)$$

The power density $S(t)$ is given by substitution of Eqs. (35) and (37) into Eq. (6).

$$S(t) = - \sqrt{\frac{\mu_0}{\epsilon_0}} k e \frac{\omega_n}{2\pi} \frac{1}{4\pi} j_{\ell}(kR) h_{\ell}^{(1)}(kr) \sin(mks) \sin \theta e^{i\omega_n t} \hat{\phi} \quad (38)$$

$$\begin{aligned} & \times -2e \frac{\omega_n}{2\pi} \frac{1}{4\pi} ik \frac{j_{\ell}(kR)}{kr} \frac{d}{dkr} \left(kr h_{\ell}^{(1)}(kr) \right) \sin(mks) \sin \theta e^{i\omega_n t} \hat{\theta} \\ S(t) &= ik^2 2 \sqrt{\frac{\mu_0}{\epsilon_0}} \left(\frac{\omega_n}{2\pi} \frac{e}{4\pi} \right)^2 \frac{(j_{\ell}(kR))^2}{kr} h_{\ell}^{(1)}(kr) \frac{d}{dkr} \left(kr h_{\ell}^{(1)}(kr) \right) \sin^2(mks) \sin^2 \theta e^{i2\omega_n t} \hat{r} \end{aligned} \quad (39)$$

For the condition given by Eq. (24), the power density as a function of time $S(t)$ is zero. *There is no radiation.*

APPENDIX II

QUANTUM ELECTRODYNAMICS IS PURELY MATHEMATICAL AND HAS NO BASIS IN REALITY

The spin of the electron and the Lamb shift are calculated from first principles in closed form by Mills as shown in the Electron g Factor section and the Resonant Line Shape and Lamb Shift section, respectively. The spin angular momentum results from the motion of negatively charged mass moving systematically, and the equation for angular momentum, $\mathbf{r} \times \mathbf{p}$, can be applied directly to the wave function (a current density function) that describes the electron. The Lamb shift results from conservation of linear momentum of the photon. The Casimir effect is predicted by Maxwell's equations. These results demonstrate that QED has no basis in reality.

Quantum mechanics failed to predict the results of the Stern-Gerlach experiment which indicated the need for an additional quantum number. Quantum electrodynamics was proposed by Dirac in 1926 to provide a generalization of quantum mechanics for high energies in conformity with the theory of special relativity and to provide a consistent treatment of the interaction of matter with radiation. It relies on the unfounded notions of negative energy states of the vacuum, virtual particles, and gamma factors. From Weisskopf [37], "Dirac's quantum electrodynamics gave a more consistent derivation of the results of the correspondence principle, but it also brought about a number of new and serious difficulties." Quantum electrodynamics; 1.) does not explain nonradiation of bound electrons; 2.) contains an internal inconsistency with special relativity regarding the classical electron radius - the electron mass corresponding to its electric energy is infinite; 3.) it admits solutions of negative rest mass and negative kinetic energy; 4.) the interaction of the electron with the predicted zero-point field fluctuations leads to infinite kinetic energy and infinite electron mass; 5.) Dirac used the unacceptable states of negative mass for the description of the vacuum; yet, infinities still arise. In 1947, contrary to Dirac's predictions, Lamb discovered a 1000 MHz shift between the $^2S_{1/2}$ state and the $^2P_{1/2}$ state of the hydrogen atom [38]. This so called Lamb Shift

marked the beginning of modern quantum electrodynamics. In the words of Dirac [39], "No progress was made for 20 years. Then a development came initiated by Lamb's discovery and explanation of the Lamb Shift, which fundamentally changed the character of theoretical physics. It involved setting up rules for discarding ...infinities..." Renormalization is presently believed to be required of any fundamental theory of physics [40]. However, dissatisfaction with renormalization has been expressed at various times by many physicists including Dirac [41] who felt that, "This is just not sensible mathematics. Sensible mathematics involves neglecting a quantity when it turns out to be small - not neglecting it just because it is infinitely great and you do not want it!"

Throughout the history of quantum theory; wherever there was an advance to a new application, it was necessary to repeat a trial-and-error experimentation to find which method of calculation gave the right answers. Often the textbooks present only the successful procedure as if it followed from first principles; and do not mention the actual method by which it was found. In electromagnetic theory based on Maxwell's equations, one deduces the computational algorithm from the general principles. In quantum theory, the logic is just the opposite. One chooses the principle to fit the empirically successful algorithm. For example, we know that it required a great deal of art and tact over decades of effort to get correct predictions out of Quantum Electrodynamics (QED). The QED method of the determination of $(g-2)/2$ from the *postulated* Dirac equation is based on a *postulated* powers series of α/π where each *postulated* virtual particle is a source of *postulated* vacuum polarization that gives rise to a *postulated* term which is processed over decades using ad hoc rules to remove infinities from each term that arises from *postulated* scores of *postulated* Feynman diagrams. Mohr and Taylor reference some of the Herculean efforts to arrive at g using QED [42]:

"the sixth-order coefficient $A_1^{(6)}$ arises from 72 diagrams and is also known analytically after nearly 30 years of effort by many researchers [see Roskies, Remiddi, and Levine (1990) for a review of the early work]. It was not until 1996 that the last remaining distinct diagrams were calculated analytically, thereby completing the

theoretical expression for $A_1^{(6)}$ ".

For the right experimental numbers to emerge, one must do the calculation (i.e. subtract off the infinities) in one particular way and not in some other way that appears in principle equally valid. For example, Milonni [43] presents a QED derivation of the magnetic moment of the electron which gives a result of the wrong sign and requires the introduction of an

"upper limit K in the integration over $k=\omega/c$ in order to avoid a divergence."

A differential mass is arbitrarily added, then

"the choice $K=0.42mc/\hbar$ yields $(g-2)/2=\alpha/2\pi$ which is the relativistic QED result to first order in α . [...] However, the reader is warned not to take these calculations too seriously, for the result $(g-2)/2=\alpha/2\pi$ could be obtained by retaining only the first (radiation reaction) term in (3.112) and choosing $K=3mc/8\hbar$. It should also be noted that the solution $K\cong 0.42mc/\hbar$ of (3.112) with $(g-2)/2=\alpha/2\pi$ is not unique."

Such an ad hoc nonphysical approach makes incredulous:

" the cliché that QED is the best theory we have!" [44]

or the statement that:

"The history of quantum electrodynamics (QED) has been one of unblemished triumph" [45].

There is a corollary, noted by Kallen: from an inconsistent theory, any result may be derived.

The QED determination of the postulated power series in α/π is based on scores of Feynman diagrams corresponding to thousands of matrices with thousands of integrations per matrix requiring decades to reach a consensus on the "appropriate" algorithm to remove the intrinsic

infinities. Remarkably, $(g-2)/2$ may be derived in closed form from Maxwell's equations in a simple straight forward manner that yields a result with eleven figure agreement with experiment—the limit of experimental capability. The derivation from first principles without invoking virtual particles, zero point fluctuations of the vacuum, and negative energy states of the vacuum is given in the Electron g Factor section.

Furthermore, Oskar Klein pointed out a glaring paradox implied by the Dirac equation which was never resolved [46]. "Electrons may penetrate an electrostatic barrier even when their kinetic energy, $E - mc^2$ is lower than the barrier. Since in Klein's example the barrier was infinitely broad this could not be associated with wave mechanical tunnel effect. It is truly a paradox: Electrons too slow to surpass the potential, may still only be partially reflected. ...Even for an infinitely high barrier, i.e. $r_2 = 1$ and energies $\approx 1 \text{ MeV}$, (the reflection coefficient) R is less than 75%! From (2) and (3) it appears that as soon as the barrier is sufficiently high: $V > 2mc^2$, electrons may transgress the repulsive wall—seemingly defying conservation of energy. ...Nor is it possible by way of the positive energy spectrum of the free electron to achieve complete Einstein causality."

The Rutherford experiment demonstrated that even atoms are comprised of essentially empty space [47]. Zero-point field fluctuations, virtual particles, and states of negative energy and mass invoked to describe the vacuum are nonsensical and have no basis in reality since they have never been observed experimentally and would correspond to an essentially infinite cosmological constant throughout the entire universe including regions of no mass. As given by Waldrop [48], "What makes this problem into something more than metaphysics is that the cosmological constant is observationally zero to a very high degree of accuracy. And yet, ordinary quantum field theory predicts that it ought to be enormous, about 120 orders of magnitude larger than the best observational limit. Moreover, this prediction is almost inescapable because it is a straightforward application of the uncertainty principle, which in this case states that every quantum field contains a certain, irreducible amount of energy even in empty space. Electrons, photons, quarks--the quantum field of every particle contributes. And that

energy is exactly equivalent to the kind of pressure described by the cosmological constant. The cosmological constant has accordingly been an embarrassment and a frustration to every physicist who has ever grappled with it."

The Casimir effect is often touted as proof of that the vacuum is teeming with infinities of virtual particles. The experiment comprises a feeble force between two plates with precision machined surfaces that are brought within microns of contacting each other. The QED explanation of the weak force that is observed between the two plates is that the plates serve to limit the number of virtual particle modes between the plates as opposed to those outside the plates and the resulting imbalance in pressure between two infinite quantities gives rise to the feeble force [49].

The Casimir effect is predicted by Maxwell's equations and is not due to virtual particles. There is no reality to electromagnetic field zero point fluctuations and the implication that the Casimir force is an intrinsic property of space. The attractive force is due only to the interactions of the material bodies themselves. Lifshitz [50-51] first developed the theory of the attractive force between two plane surfaces made of a material with a general susceptibility. The Lifshitz calculation is developed from considerations of charge and current fluctuations in a material body. These fluctuations serve as a source term for Maxwell's equations, i.e. classical fields, subject to the boundary conditions presented by the body surfaces. In the limiting case of rarefied media, the van der Waals force of interaction between individual atoms is obtained.

APPENDIX III

MUON g FACTOR

The muon, like the electron, is a lepton with \hbar of angular momentum. The magnetic moment of the muon is given by Eq. (1.136) with the electron mass replaced by the muon mass. It is twice that from the gyromagnetic ratio as given by Eq. (2.36) of the Orbital and Spin Splitting section corresponding to the muon mass. As is the case with the electron, the magnetic moment of the muon is the sum of the component corresponding to the kinetic angular momentum, $\frac{\hbar}{2}$, and the component corresponding to the vector potential angular momentum, $\frac{\hbar}{2}$, (Eq. (1.132)).

The spin-flip transition can be considered as involving a magnetic moment of g times that of a Bohr magneton of the muon. The g factor (Eq. (1.196)) is

$$\frac{g}{2} = 1 + \frac{\alpha}{2\pi} + \frac{2}{3}\alpha^2 \left(\frac{\alpha}{2\pi} \right) - \frac{4}{3} \left(\frac{\alpha}{2\pi} \right)^2 \quad (1)$$

For $\alpha^{-1} = 137.03603(82)$ (Eq. 1.203)),

$$\frac{g}{2} = 1.001\,159\,652\,137 \quad (2)$$

The muon anomalous magnetic moment has been measured in a new experiment at Brookhaven National Laboratory (BNL) [29]. Polarized muons were stored in a superferric ring, and the angular frequency difference ω_a between the spin precession and orbital frequencies was determined by measuring the time distribution of high-energy decay positrons. The ratio R of ω_a to the Larmor precession frequency of free protons ω_p in the storage-ring magnetic field was measured. R is given by

$$R = \frac{\omega_a}{\omega_p} \quad (3)$$

The anomalous g value a_μ of the μ^+ was determined where the anomalous g value is related to the gyromagnetic ratio by

$$a_\mu = \frac{(g-2)}{2} \quad (4)$$

and

$$a_\mu = \frac{R}{\lambda - R} \quad (5)$$

where λ is the ratio of the muon and proton magnetic moments:

$$\lambda = \frac{\mu_\mu}{\mu_p} \quad (6)$$

According to Carey et al. [29], "For polarized muons moving in a uniform magnetic field \vec{B} , which is perpendicular to the muon spin direction and to the plane of the orbit, and with an electric quadrapole field \vec{E} for vertical focusing, the angular frequency difference, ω_a , between the spin precession frequency ω_s and the cyclotron frequency ω_c is given by

$$\bar{\omega}_a = -\frac{e}{m} \left[a_\mu \vec{B} - \left(a_\mu - \frac{1}{\gamma^2 - 1} \right) \vec{B} \times \vec{E} \right] \quad (7)$$

The dependence of ω_a on the electric field is eliminated by storing muons with the "magic" $\gamma=29.3$, which corresponds to a muon momentum $p=3.09 \text{ GeV}/c$. Hence measurement of ω_a and of B determines a_μ ."

Based on Lorentz covariance Jackson [30] gives the BMT equation which is the relativistic equation of motion for spin in uniform or slowly varying external fields. The rate of change of the component of spin s parallel to the velocity may be determined from the BMT equation. This is the longitudinal polarization or net helicity of the particle. If $\hat{\beta}$ is a unit vector in the direction of β , the longitudinal polarization is $\hat{\beta} \cdot s$. It changes in time because s changes and also β changes. The BMT equation in cgs units gives

$$\frac{d}{dt}(\hat{\beta} \cdot s) = -\frac{e}{mc} s_\perp \cdot \left[\left(\frac{g}{2} - 1 \right) \hat{\beta} \times \mathbf{B} + \left(\frac{g\beta}{2} - \frac{1}{\beta} \right) \mathbf{E} \right] \quad (8)$$

where s_\perp is the component of s perpendicular to the velocity. Eq. (8) demonstrates a remarkable property of a particle with $g=2$. In a purely magnetic field, the spin precesses in such a manner that the longitudinal polarization remains constant, whatever the motion of the particle. If the particle is relativistic ($\beta \rightarrow 1$), even the presence of an electric field causes the longitudinal polarization to change only very slowly, at a rate proportional to γ^{-2} times the electric field component perpendicular to v .

The "magic" γ given by Eq. (8) wherein the contribution to the change of the longitudinal polarization by the electric quadrapole focusing fields are eliminated occurs when

$$\frac{g_\mu \beta}{2} - \frac{1}{\beta} = 0 \quad (9)$$

where g_μ is the muon g factor which is required to be different from the electron g factor in the standard model due to the dependence of the mass dependent interaction of each lepton with vacuum polarizations due to virtual particles. For example, the muon is much heavier than the electron, and so high energy (short distance) effects due to strong and

weak interactions are more important here [26]. Also, according to the BNL collaboration [29]:

“The hadronic contribution and uncertainty are dominated by the single vacuum polarization loop with hadrons present, which is determined from a dispersion relationship using data from annihilation to hadrons and from hadronic decay. A contribution from higher order hadronic vacuum polarization and light-by-light scattering must be included”

The BNL Muon (g-2) Collaboration [29] used a “magic” $\gamma=29.3$ which satisfied Eq. (9) identically for $\frac{g_\mu}{2}$; however, their assumption that this condition eliminated the affect of the electrostatic field on ω_a is flawed as shown below. The relativistic factor γ is given by

$$\gamma = \frac{1}{\sqrt{1-\beta^2}} \quad (10)$$

where

$$\beta = \frac{v}{c} \quad (11)$$

Substitution of Eq. (9) into Eq. (10) gives

$$\gamma = \frac{1}{\sqrt{1-\frac{2}{g_\mu}}} \quad (12)$$

and

$$\beta_\mu = \sqrt{\frac{2}{g_\mu}} = \sqrt{1-\frac{1}{\gamma^2}} \quad (13)$$

From the BNL99 results and the average of the CERN and BNL97 results [29] an estimated value of $\frac{g_\mu}{2}$ is

$$\frac{g_\mu}{2} = 1.00116593 \quad (14)$$

Substitution of Eq. (14) into Eq. (12) gives the “magic” γ as

$$\gamma = 29.3033176 \quad (15)$$

and from Eq. (13),

$$\beta_\mu = 0.999417544 \quad (16)$$

As shown in the Electron g Factor section, in the case of an exact balance between the Lorentzian force (Eq. (1.151)) and the electric force corresponding to the Hall voltage (Eq. (1.152)), the superconducting condition is met when

$$\frac{E}{B} = v \quad (17)$$

which in cgs units is

$$E = \frac{Bv}{c} = B\beta_\mu \quad (18)$$

Consider the case that the g factor for the muon and the electron are the same and the “magic” $\gamma=29.3$ selected by the BNL Muon ($g-2$)

Collaboration which satisfied Eq. (9) identically for $\frac{g_\mu}{2}$ (Eq. (1.197)) does

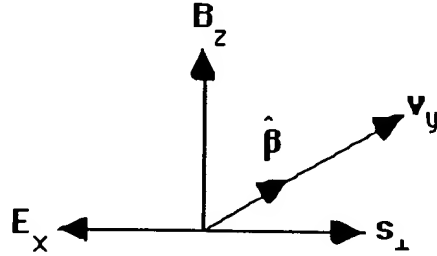
not satisfy Eq. (9) for $\frac{g_e}{2}$ given by the experimental value (Eq. (27)). In this case, the second term of Eq. (8) contributes to ω_a . With $g = g_e$ and $\beta = \beta_\mu$, the BMT equation is

$$\frac{d}{dt}(\hat{\beta} \cdot \mathbf{s}) = -\frac{e}{mc} \mathbf{s}_\perp \cdot \left[\left(\frac{g_e}{2} - 1 \right) \hat{\beta} \times \mathbf{B} + \left(\frac{g_e \beta_\mu}{2} - \frac{1}{\beta_\mu} \right) \mathbf{E} \right] \quad (19)$$

Since \mathbf{B} is parallel to $\mathbf{s}_\perp \times \hat{\beta}$ and since \mathbf{E} and \mathbf{s}_\perp are anti-parallel, the electric field from Eq. (18) is

$$\mathbf{E} = -\beta_\mu \hat{\beta} \times \mathbf{B} \quad (20)$$

Figure 1. Coordinate system of crossed electric field, \mathbf{E}_x , corresponding to the Hall voltage, magnetic flux, \mathbf{B}_z , due to the applied field, the velocity, \mathbf{v}_y , in the $\hat{\beta}$ direction, and \mathbf{s}_\perp where $|\mathbf{E}| = \beta B$.



Then

$$\frac{d}{dt}(\hat{\beta} \cdot \mathbf{s}) = -\frac{e}{mc} \mathbf{s}_\perp \cdot \left[\left(\frac{g_e}{2} - 1 \right) - \left(\frac{g_e \beta_\mu^2}{2} - 1 \right) \right] \hat{\beta} \times \mathbf{B} \quad (21)$$

$$= -\frac{e}{mc} \left[\frac{g_e}{2} - \frac{g_e \beta_\mu^2}{2} \right] \mathbf{s}_\perp \cdot (\hat{\beta} \times \mathbf{B}) \quad (22)$$

$$= -\frac{e}{mc} \left[\frac{g_e}{2} (1 - \beta_\mu^2) \right] \mathbf{s}_\perp \cdot (\hat{\beta} \times \mathbf{B}) \quad (23)$$

In the case that $g = g_\mu \neq g_e$, the term in \mathbf{E} of Eq. (8) vanishes and

$$\frac{d}{dt}(\hat{\beta} \cdot \mathbf{s}) = -\frac{e}{mc} \left[\frac{g_\mu}{2} - 1 \right] \mathbf{s}_\perp \cdot (\hat{\beta} \times \mathbf{B}) \quad (24)$$

A change in longitudinal polarization due to the finite electric term can be considered as an additional term to the electron g factor which gives rise to an effective g factor corresponding to $\frac{g_\mu}{2}$. Comparison of Eq. (23) and Eq. (24) gives the effective value of $\frac{g_\mu}{2}$ which is the predicted

experimental value for $\frac{g_\mu}{2}$:

$$\frac{g_\mu}{2} - 1 = \frac{g_e}{2} (1 - \beta_\mu^2) \quad (25)$$

$$\frac{g_\mu}{2} = 1 + \frac{g_e}{2} (1 - \beta_\mu^2) \quad (26)$$

Eq. (19) which gives the predicted experimental value for $\frac{g_\mu}{2}$ (Eq. (26))

corresponds to the experimental situation of the BNL measurement of $\frac{g_\mu}{2}$.

The experimental value of $\frac{g_e}{2}$ [24] is

$$\frac{g_e}{2} = 1.001\,159\,652\,188(4) \quad (27)$$

Substitution of $\frac{g_e}{2}$ and β_μ given by Eq. (27) and Eq. (16), respectively, into Eq. (26) gives the calculated effective muon g factor which is

$$\frac{g_\mu}{2} = 1.001\,165\,923 \quad (28)$$

The calculated result based on the equivalence of the muon and electron g factors is in agreement with the result of Carey et al. [29]:

$$\frac{g_\mu}{2} = 1.001\,165\,925\,(15) \quad (29)$$

Rather than indicating an expanded plethora of postulated supersymmetry virtual particles which make contributions such as smuon-neutralino and sneutrino-chargino loops as suggested by Brown et al.

[31], the deviation of the experimental value of $\frac{g_\mu}{2}$ from that of the

standard model prediction simply indicates that the muon g factor is identical to the electron g factor. This could have been spotted immediately had the objectivity of the experimental design been given precedence over the assumption of the validity of the standard model. Given the ad hoc nonphysical nature of QED (See Appendix II: Quantum Electrodynamics is Purely Mathematical and Has No Basis in Reality) and the internal inconsistency of the theoretical basis of this experiment regarding using the classical BMT equation in a test of nonclassical QED, more scrutiny was especially warranted.

From Eqs. (26), (27), and (16), the difference between $\frac{g_\mu}{2}$ and $\frac{g_e}{2}$ due to the finite electric term of Eqs. (8) and (19) with $g = g_e$ is

$$\frac{g_\mu}{2} - \frac{g_e}{2} = 1 - \frac{g_e}{2} \beta_\mu^2 = 0.0000062705 \quad (30)$$

With the equivalence of the muon g factor and the electron g factor, the possibilities are limited for the occurrence of internal consistency during the determination of $\frac{g_\mu}{2}$ using the BMT equation with the flawed

assumption that $\frac{g_\mu}{2} \neq \frac{g_e}{2}$. Consider the case of Eq. (9) with $g = g_e = g_\mu$ and $\beta = \beta_u$ with the corresponding “magic” γ given by Eqs. (10-13). An equation equivalent to Eq. (30) that gives rise to an internally consistent experimental observation of an effective muon g factor corresponding to $\beta = \beta_u$ is

$$\left[\frac{1}{\sqrt{\frac{2}{g_{\mu\gamma}}}} - \frac{g_e \sqrt{\frac{2}{g_{\mu\gamma}}}}{2} \right] \sqrt{\frac{2}{g_{\mu\gamma}}} = 0.0000062705 \quad (31)$$

$$1 - \frac{\frac{g_e}{2}}{\frac{g_{\mu\gamma}}{2}} = 0.0000062705 \quad (32)$$

where $g_{\mu\gamma}$ is the muon anomalous g factor selected before the experiment to fix the “magic” γ , 0.0000062705 given by Eq. (32) (also see Eq. (30)) is the difference between the projected experimental value of $\frac{g_\mu}{2}$ and the experimentally measured value of $\frac{g_e}{2}$. The experimental value of $\frac{g_e}{2}$ from Eq. (27) and the selected value of $\frac{g_{\mu\gamma}}{2}$ from Eq. (14) satisfy Eqs. (31-32)

and are in close agreement with the experimental value of $\frac{g_\mu}{2}$ determined by Carey et al. [29] (Eqs. (28-29)). The “magic” γ of BNL which gave an internally consistent but misinterpreted result was most likely arrived at by trial and error. Consider the following relationship between δ and $\frac{(g_{\mu\gamma}-2)}{2}$ of the “magic” γ that follows from Eq. (32):

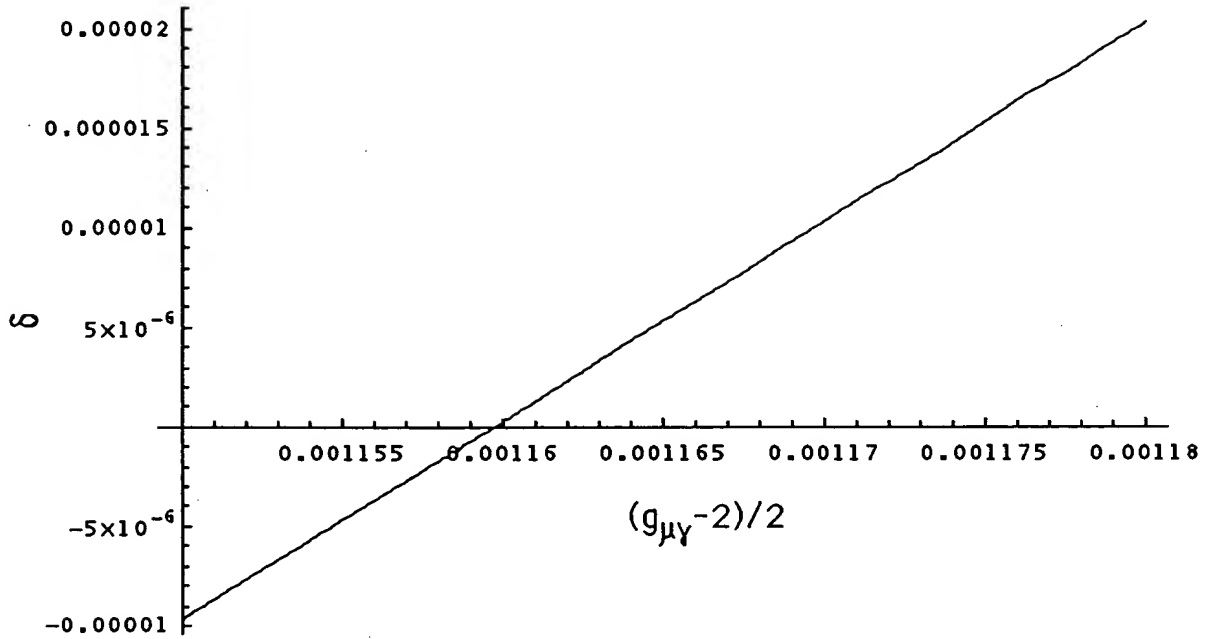
$$1 - \frac{\frac{g_e}{2}}{\frac{g_{\mu\gamma}}{2}} = \delta \quad (33)$$

where

$$\frac{(g_e-2)}{2} + \delta = \frac{(g_\mu-2)}{2} \quad (34)$$

and g_e is the experimentally measured electron anomalous g factor and g_μ is the projected experimental value of the muon anomalous g factor based on $g_{\mu\gamma}$, the selected value the muon anomalous g factor to fix the “magic” γ . A plot of δ versus $\frac{(g_{\mu\gamma}-2)}{2}$ from Eq. (33) is shown in Figure 2.

Figure 2. Plot of δ versus $\frac{(g_{\mu\gamma}-2)}{2}$ of the “magic” γ from Eq. (33).



Only a narrow range of values of $\frac{(g_{\mu\gamma}-2)}{2}$ about the value of $\frac{(g_{\mu}-2)}{2}$ measured by Carey et al. [29] are internally consistent.

Similar misinterpretations of data based on a bias towards quantum theory are described in the Schrödinger "Black" Cats section. For example, NIST claimed to have placed a ${}^9\text{Be}^+$ ion in two places at once when in reality an applied magnetic field and potential well were found which forced a resonance between an oscillatory and a Stern-Gerlach transition. And, the resulting interference pattern in the fluorescence emission was misinterpreted as indicating that the ion was in two widely separated positions simultaneously [52]. The BNL experiment should be repeated to determine the dependence of ω_a on the “magic” γ . The current BNL results and classical theory support the equivalence of the electron and muon g factors.

Experimental determination of the proper β [53]

The angular frequency difference between the spin procession frequency and the cyclotron frequency, [24], is

$$\bar{\omega}_a = -\frac{e}{mc} \left[a_{\mu} \bar{\mathbf{B}} - \left(a_{\mu} - \frac{1}{\gamma^2 - 1} \right) \bar{\mathbf{B}} \times \bar{\mathbf{E}} \right] \quad (35)$$

Introducing the velocity ratio, β , and g ,

$$\gamma^2 - 1 = \frac{\beta^2}{1 - \beta^2}, \quad a_\mu = \frac{g}{2} - 1 \quad (36)$$

yields

$$\bar{\omega}_a = -\frac{e}{mc} \left[\left(\frac{g}{2} - 1 \right) \bar{\mathbf{B}} - \left(\frac{g}{2} - \frac{1}{\beta^2} \right) \bar{\mathbf{B}} \times \bar{\mathbf{E}} \right] \quad (37)$$

The unique value of β for which the term in $\bar{\mathbf{E}}$ vanishes is β^* :

$$\frac{g}{2} = \frac{1}{\beta^{*2}} \quad (38)$$

For $\beta = \beta^*$

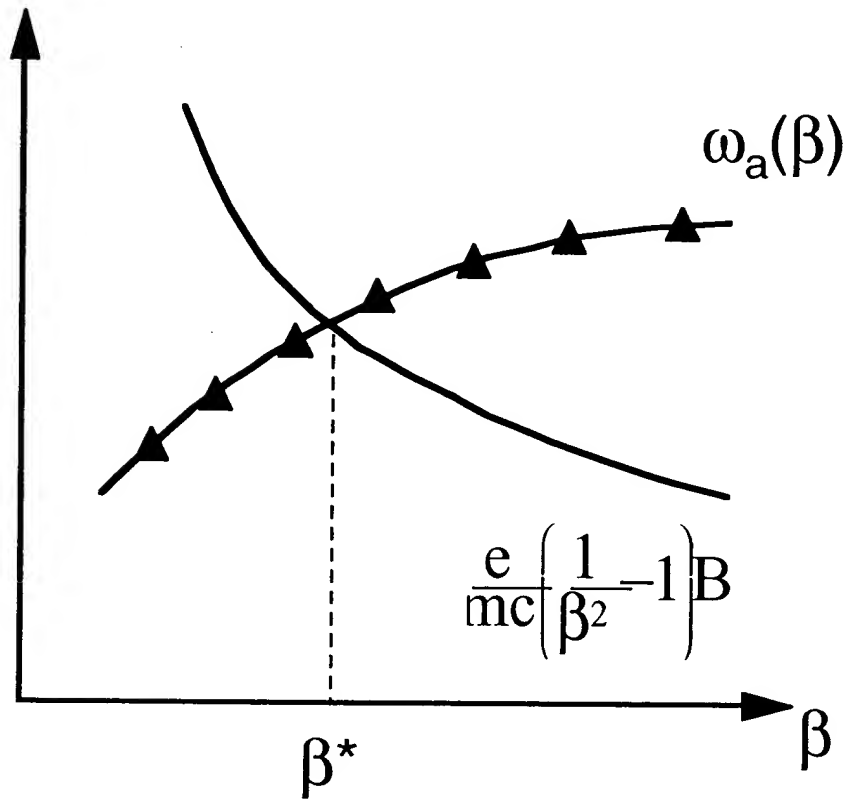
$$\bar{\omega}_a(\beta^*) = -\frac{e}{mc} \left(\frac{1}{\beta^{*2}} - 1 \right) \bar{\mathbf{B}} \quad (39)$$

Taking the magnitude results in

$$\omega_a(\beta^*) = \frac{e}{mc} \left(\frac{1}{\beta^{*2}} - 1 \right) B \quad (40)$$

The experimental measurement of the frequency difference for various β allows the graphical determination of β^* , (See Figure 3), with no assumption regarding g .

Figure 3. Plot of the experimental measurement of the frequency difference for various β which allows the graphical determination of β^* .



References

1. Haus, H. A., "On the radiation from point charges", American Journal of Physics, 54, (1986), pp. 1126-1129.
2. Jackson, J. D., Classical Electrodynamics, Second Edition, John Wiley & Sons, New York, (1962), p. 111.
3. Bracewell, R. N., The Fourier Transform and Its Applications, McGraw-Hill Book Company, New York, (1978), pp. 252-253.
4. Siebert, W. McC., Circuits, Signals, and Systems, The MIT Press, Cambridge, Massachusetts, (1986), p. 415.
5. Luke, Y. L., Integrals of Bessel Functions, McGraw-Hill, New York, (1962), p.22.
6. Abramowitz and Stegun (3rd Printing 1965), p. 366, eq. 9.1.10, and p. 255, eq. 6.1.6.
7. Luke, Y. L., Integrals of Bessel Functions, McGraw-Hill, New York, (1962), p.30.

8. Bateman, H., Tables of Integral Transforms, Vol. III, McGraw-Hill, New York, (1954), p. 33.
9. Bateman, H., Tables of Integral Transforms, Vol. III, McGraw-Hill, New York, (1954), p. 5.
10. Reynolds, G. O., DeVelis, J. B., Parrent, G. B., Thompson, B. J., The New Physical Optics Notebook, SPIE Optical Engineering Press, (1990).
11. Abbott, T. A., Griffiths, D. J., Am. J. Phys., Vol. 153, No. 12, (1985), pp. 1203-1211.
12. McQuarrie, D. A., Quantum Chemistry, University Science Books, Mill Valley, CA, (1983), pp. 206-221.
13. Jackson, J. D., Classical Electrodynamics, Second Edition, John Wiley & Sons, New York, (1962), p. 99.
14. Fowles, G. R., Analytical Mechanics, Third Edition, Holt, Rinehart, and Winston, New York, (1977), p. 196.
15. Pauling, Linus, Wilson, E., Bright, Introduction to Quantum Mechanics with Applications to Chemistry, McGraw-Hill Book Company, New York, (1935), pp. 118-121.
16. McQuarrie, D. A., Quantum Chemistry, University Science Books, Mill Valley, CA, (1983), pp. 238-241.
17. Jackson, J. D., Classical Electrodynamics, Second Edition, John Wiley & Sons, New York, (1962), p. 178.
18. Jackson, J. D., Classical Electrodynamics, Second Edition, John Wiley & Sons, New York, (1962), pp. 194-197.
19. Purcell, E. M., Electricity and Magnetism, McGraw-Hill, New York, (1965), pp. 370-375.
20. Das Sarma, S., Prange, R. E., Science, Vol. 256, (1992), pp. 1284-1285.
21. Jackson, J. D., Classical Electrodynamics, Second Edition, John Wiley & Sons, New York, (1962), pp. 582-584.
22. Jackson, J. D., Classical Electrodynamics, Second Edition, John Wiley & Sons, New York, (1962), pp. 758-763.
23. Robert C. Weast, CRC Handbook of Chemistry and Physics, 68 th Edition, CRC Press, Boca Raton, Florida, (1987-88), p. F-186 to p. F-187.
24. R. S. Van Dyck, Jr., P. Schwinberg, H. Dehmelt, "New high precision comparison of electron and positron g factors", Phys. Rev. Lett., Vol. 21, (1987), p. 26-29.
25. P. J. Mohr and B. N. Taylor, "CODATA recommended values of the fundamental physical constants: 1998", Reviews of Modern Physics, Vol. 72, No. 2, April, (2000), pp. 351-495.
26. G. P. Lepage, "Theoretical advances in quantum electrodynamics, International Conference on Atomic Physics, Atomic Physics; Proceedings, Singapore, World Scientific, Vol. 7, (1981), pp. 297-311.
27. E. R. Williams and P. T. Olsen, Phys. Rev. Lett. Vol. 42, (1979), p. 1575.

28. K. v. Klitzing et al., Phys. Rev. Lett. Vol. 45, (1980), p. 494.
29. R. M. Carey et al., Muon (g-2) Collaboration, "New measurement of the anomalous magnetic moment of the positive muon", Phys. Rev. Lett., Vol. 82, (1999), pp. 1632-1635.
30. Jackson, J. D., Classical Electrodynamics, Second Edition, John Wiley & Sons, New York, (1962), pp. 556-560.
31. H. N. Brown et al., Muon (g-2) Collaboration, "Precise measurement of the positive muon anomalous magnetic moment", Phys. Rev. D62, 091101 (2000).
32. Bueche, F., Introduction to Physics for Scientists and Engineers, McGraw-Hill, (1975), pp. 352-353.
33. Purcell, E. M., Electricity and Magnetism, McGraw-Hill, New York, (1965), pp. 170-199.
34. L. C. Shi, J. A. Kong, Applied Electromagnetism, Brooks/Cole Engineering Division, Monterey, CA, (1983), pp. 170-209.
35. J. Daboul and J. H. D. Jensen, Z. Physik, Vol. 265, (1973), pp. 455-478.
36. J. D. Jackson, Classical Electrodynamics, Second Edition, John Wiley & Sons, New York, (1962), pp. 739-742.
37. V. F. Weisskopf, Reviews of Modern Physics, Vol. 21, No. 2, (1949), pp. 305-315.
38. W. E. Lamb, R. C. Retherford, "Fine Structure of the Hydrogen Atom by a Microwave Method", R. C., Phys. Rev., Vol. 72, No. 3, August 1, (1947), pp. 241-243.
39. P. A. M. Dirac, From a Life of Physics, ed. A. Salam, et al., World Scientific, Singapore, (1989).
40. P. W. Milonni, The Quantum Vacuum, Academic Press, Inc., Boston, p. 90.
41. P. A. M. Dirac, Directions in Physics, ed. H. Hora and J. R. Shepanski, Wiley, New York, (1978), p. 36.
42. P. J. Mohr and B. N. Taylor, "CODATA recommended values of the fundamental physical constants: 1998", Reviews of Modern Physics, Vol. 72, No. 2, April, (2000), p. 474.
43. P. W. Milonni, The Quantum Vacuum An Introduction to Quantum Electrodynamics, Academic Press, Inc. Boston, pp. 107-111.
44. P. W. Milonni, The Quantum Vacuum An Introduction to Quantum Electrodynamics, Academic Press, Inc. Boston, p. 108.
45. G. P. Lepage, "Theoretical advances in quantum electrodynamics, International Conference on Atomic Physics, Atomic Physics; Proceedings, Singapore, World Scientific, Vol. 7, (1981), pp. 297-311.
46. H. Wergeland, "The Klein Paradox Revisited", Old and New Questions in Physics, Cosmology, Philosophy, and Theoretical Biology, A. van der Merwe, Editor, Plenum Press, New York, (1983), pp. 503-515.
47. Beiser, A., Concepts of Modern Physics, Fourth Edition, McGraw-Hill

- Book Company, New York, (1978), pp. 119-122.
48. M. M. Waldrop, Science, Vol. 242, December, 2, (1988), pp. 1248-1250.
49. P. W. Milonni, The Quantum Vacuum An Introduction to Quantum Electrodynamics, Academic Press, Inc. Boston, pp. 54-58.
50. E. M. Lifshitz, "The theory of molecular attractive forces between solids", Soviet Physics, Vol. 2, No. 1, January, (1956), pp. 73-83.
51. S. K. Lamoreaux, "CF-1: Casimir Force", Am. J. Phys. Vol. 67, No. 10, October, (1999), p. 850-861.
52. C. Monroe, D. M. Meekhof, B. E. King, D. J. Wineland, Science, Vol. 272, (1996), pp. 1131-1135.
53. M. Nansteel, BlackLight Power, Inc., Cranbury, NJ, Personal Communication, May, (2001).

ATOMIC COULOMB FIELD COLLAPSE - HYDRINO THEORY BLACKLIGHT PROCESS

BLACKLIGHT PROCESS

Certain atoms or ions serve as catalysts to release energy from hydrogen to produce an increased binding energy hydrogen atom called a *hydrino atom* having a binding energy of

$$\text{Binding Energy} = \frac{13.6 \text{ eV}}{n^2} \quad (5.1)$$

where

$$n = \frac{1}{2}, \frac{1}{3}, \frac{1}{4}, \dots, \frac{1}{p} \quad (5.2)$$

and p is an integer greater than 1, designated as $H\left[\frac{a_H}{p}\right]$ where a_H is the radius of the hydrogen atom. Hydrinos are predicted to form by reacting an ordinary hydrogen atom with a catalyst having a net enthalpy of reaction of about

$$m \cdot 27.2 \text{ eV} \quad (5.3)$$

where m is an integer. This catalysis releases energy from the hydrogen atom with a commensurate decrease in size of the hydrogen atom, $r_n = na_H$. For example, the catalysis of $H(n=1)$ to $H(n=1/2)$ releases 40.8 eV, and the hydrogen radius decreases from a_H to $\frac{1}{2}a_H$.

The excited energy states of atomic hydrogen are also given by Eq. (5.1) except that

$$n = 1, 2, 3, \dots \quad (5.4)$$

The $n=1$ state is the "ground" state for "pure" photon transitions (the $n=1$ state can absorb a photon and go to an excited electronic state, but it cannot release a photon and go to a lower-energy electronic state).

However, an electron transition from the ground state to a lower-energy state is possible by a nonradiative energy transfer such as multipole coupling or a resonant collision mechanism. These lower-energy states have fractional quantum numbers, $n = \frac{1}{\text{integer}}$. Processes that occur

without photons and that require collisions are common. For example, the exothermic chemical reaction of $H+H$ to form H_2 does not occur with the emission of a photon. Rather, the reaction requires a collision with a third body, M , to remove the bond energy- $H+H+M \rightarrow H_2+M^*$ [1]. The third body distributes the energy from the exothermic reaction, and the end result is the H_2 molecule and an increase in the temperature of the

system. Some commercial phosphors are based on nonradiative energy transfer involving multipole coupling. For example, the strong absorption strength of Sb^{3+} ions along with the efficient nonradiative transfer of excitation from Sb^{3+} to Mn^{2+} , are responsible for the strong manganese luminescence from phosphors containing these ions. Similarly, the $n=1$ state of hydrogen and the $n = \frac{1}{\text{integer}}$ states of hydrogen are nonradiative,

but a transition between two nonradiative states is possible via a nonradiative energy transfer, say $n=1$ to $n=1/2$. In these cases, during the transition the electron couples to another electron transition, electron transfer reaction, or inelastic scattering reaction which can absorb the exact amount of energy that must be removed from the hydrogen atom, a resonant energy sink called an **energy hole**. Thus, a **catalyst** is a source of an energy hole *infra*. because it provides a net positive enthalpy of reaction of $m \cdot 27.2 \text{ eV}$ (i.e. it absorbs or provides an energy sink of $m \cdot 27.2 \text{ eV}$). The reaction of hydrogen-type atoms to lower-energy states is referred to as a **transition reaction**. Certain atoms or ions serve as transition catalysts which resonantly accept energy from hydrogen atoms and release the energy to the surroundings to effect electronic transitions to fractional quantum energy levels.

An example of *nonradiative energy transfer* is the basis of commercial fluorescent lamps. Consider Mn^{2+} which when excited sometimes emits yellow luminescence. The absorption transitions of Mn^{2+} are spin-forbidden. Thus, the absorption bands are weak, and the Mn^{2+} ions cannot be efficiently raised to excited states by direct optical pumping. Nevertheless, Mn^{2+} is one of the most important luminescence centers in commercial phosphors. For example, the double-doped phosphor $Ca_5(PO_4)_3F:Sb^{3+},Mn^{2+}$ is used in commercial fluorescent lamps where it converts mainly ultraviolet light from a mercury discharge into visible radiation. When 2536 \AA mercury radiation falls on this material, the radiation is absorbed by the Sb^{3+} ions rather than the Mn^{2+} ions. Some excited Sb^{3+} ions emit their characteristic blue luminescence, while other excited Sb^{3+} ions transfer their energy to Mn^{2+} ions. These excited Mn^{2+} ions emit their characteristic yellow luminescence. The efficiency of transfer of ultraviolet photons through the Sb^{3+} ions to the Mn^{2+} ions can be as high as 80%. The strong absorption strength of Sb^{3+} ions along with the efficient transfer of excitation from Sb^{3+} to Mn^{2+} , are responsible for the strong manganese luminescence from this material.

This type of *nonradiative energy transfer* is common. The ion which emits the light and which is the active element in the material is called the *activator*; and the ion which helps to excite the activator and

makes the material more sensitive to pumping light is called the *sensitizer*. Thus, the sensitizer ion absorbs the radiation and becomes excited. Because of a coupling between sensitizer and activator ions, the sensitizer transmits its excitation to the activator, which becomes excited, and the activator may release the energy as its own characteristic radiation. The sensitizer to activator transfer is *not* a radiative emission and absorption process, rather a *nonradiative transfer*. The nonradiative transfer may be by electric or magnetic multipole interactions. In the transfer of energy between dissimilar ions, the levels will, in general, not be in resonance, and some of the energy is released as a phonon or phonons. In the case of similar ions the levels should be in resonance, and phonons are not needed to conserve energy.

Sometimes the host material itself may absorb (usually in the ultraviolet) and the energy can be transferred nonradiatively to dopant ions. For example, in $YVO_4:Eu^{3+}$, the vanadate group of the host material absorbs ultraviolet light, then transfers its energy to the Eu^{3+} ions which emit characteristic Eu^{3+} luminescence.

The catalysis of hydrogen involves the nonradiative transfer of energy from atomic hydrogen to a catalyst which may then release the transferred energy by radiative and nonradiative mechanisms. As a consequence of the nonradiative energy transfer, the hydrogen atom becomes unstable and emits further energy until it achieves a lower-energy nonradiative state having a principal energy level given by Eq. (5.1).

ENERGY HOLE CONCEPT

For a spherical resonator cavity, the nonradiative boundary condition and the relationship between the electron and the photon give the "allowed" hydrogen energy states which are quantized as a function of the parameter n . That is the nonradiative boundary condition and the relationship between an allowed radius and the photon standing wave wavelength Eq. (2.1) gives rise to Eq. (2.2), the boundary condition for allowed radii and allowed electron wavelengths as a function of the parameter n . Each value of n corresponds to an allowed transition effected by a resonant photon which excites the transition in the orbitsphere resonator cavity. In addition to the traditional integer values (1, 2, 3,...) of n , values of fractions are allowed by Eq. (2.2) which correspond to transitions with an increase in the central field (charge) and decrease in the radius of the orbitsphere. This occurs, for example, when the orbitsphere couples to another resonator cavity which can absorb energy. This is the ***absorption of an energy hole by the hydrogen-type atom***. The absorption of an energy hole destroys the

balance between the centrifugal force and the increased central electric force. Consequently, the electron undergoes a transition to a lower energy nonradiative state. Thus, the corresponding reaction from an initial energy state to a lower energy state requiring an energy hole is called a *transition reaction*.

From energy conservation, the energy hole of a hydrogen atom which excites resonator modes of radial dimensions $\frac{a_H}{m+1}$ is

$$m \times 27.2 \text{ eV}, \quad (5.5)$$

where $m = 1, 2, 3, 4, \dots$

After resonant absorption of the energy hole, the radius of the orbitsphere, a_H , shrinks to $\frac{a_H}{m+1}$ and after t cycles of transition, the radius

is $\frac{a_H}{mt+1}$. In other words, the radial ground state field can be considered as the superposition of Fourier components. The removal of negative Fourier components of energy $m \times 27.2 \text{ eV}$, where m is an integer increases the positive electric field inside the spherical shell by m times the charge of a proton. The resultant electric field is a time harmonic solution of Laplace's Equations in spherical coordinates. In this case, the radius at which force balance and nonradiation are achieved is $\frac{a_H}{m+1}$ where m is an integer. In decaying to this radius from the "ground" state, a total energy of $[(m+1)^2 - 1^2] \times 13.6 \text{ eV}$ is released. The process is hereafter referred to as the Atomic BlackLight Process. (See Mills International Patent Application [2]). An appropriate technical term is "Coulomb Field Collapse".

For the hydrogen atom, the radius of the ground state orbitsphere is a_H . This orbitsphere contains no photonic waves and the centripetal force and the electric force balance including the electrodynamic force which is included by using the reduced electron mass as given by Eqs. (1.223), (1.228), and (1.229) is

$$\frac{m_e v_1^2}{a_H} = \frac{e^2}{4\pi\epsilon_0 a_H^2} \quad (5.6)$$

where v_1 is the velocity in the "ground" state. It was shown in the Excited States of the One Electron Atom (Quantization) section that the electron orbitsphere is a resonator cavity which can trap electromagnetic radiation of discrete frequencies. The photon electric field functions are solutions of Laplace's equation. The "trapped photons" decrease the nuclear charge to $1/n$ and increase the radius of the orbitsphere to na_H . The new configuration is also in force balance.

$$\frac{\hbar^2}{m_e r_n^3} = \frac{Z_{eff} e^2}{4\pi\epsilon_0 r_n^2} \quad (5.12)$$

A transition occurs because the effective nuclear charge increases by an integer, m , when Eqs. (5.10-5.12) are satisfied by the introduction of an energy hole. The source of energy holes may not be consumed in the transition reaction; therefore it is a transition catalyst. The catalyst provides energy holes and affects the transition from the initial radius

$\frac{a_H}{p}$ and an effective nuclear charge of p to the second radius $\left[\frac{a_H}{p+m}\right]$ and

an effective nuclear charge of $p+m$. Energy conservation and the boundary condition that "trapped photons" must be a solution to Laplace's equation determine that the energy hole to cause a transition is given by Eq. (5.5). As a result of coupling, the hydrogen atom nonradiatively transfers $m \times 27.21 \text{ eV}$ to the catalyst. Stated another way, the hydrogen atom absorbs an energy hole of $m \times 27.21 \text{ eV}$. The energy hole absorption causes a standing electromagnetic wave ("photon") to be trapped in the hydrogen atom electron orbitsphere. Recall from the Excited States of the One Electron Atom (Quantization) section that electromagnetic radiation of discrete energy can be trapped in a resonator cavity. As shown previously, the photonic equation must be a solution of Laplace's equation in spherical coordinates. The "trapped photon" field comprises an electric field which provides force balance and a nonradiative orbitsphere. The solution to this boundary value problem of the radial photon electric field is given by

$$\begin{aligned} E_{r_{photon\ n,l,m}} &= \frac{e\left(\frac{a_H}{n}\right)^l}{4\pi\epsilon_0} \frac{1}{r^{(l+2)}} \left[-Y_0^0(\theta, \phi) + n \left[Y_0^0(\theta, \phi) + \text{Re} \left\{ Y_l^m(\theta, \phi) \left[1 + e^{i\omega_n t} \right] \right\} \right] \right] \\ \omega_n &= 0 \text{ for } m = 0 \\ n &= 2, 3, 4, \dots \\ l &= 1, 2, \dots, n-1 \\ m &= -l, -l+1, \dots, 0, \dots, +l \end{aligned} \quad (5.13)$$

And, the quantum numbers of the electron are n , l , m (m_l), and m_s as described previously. It is apparent from this equation that given an

initial radius of $\frac{a_H}{p}$ and a final radius of $\left[\frac{a_H}{p+m}\right]$ that the central field is

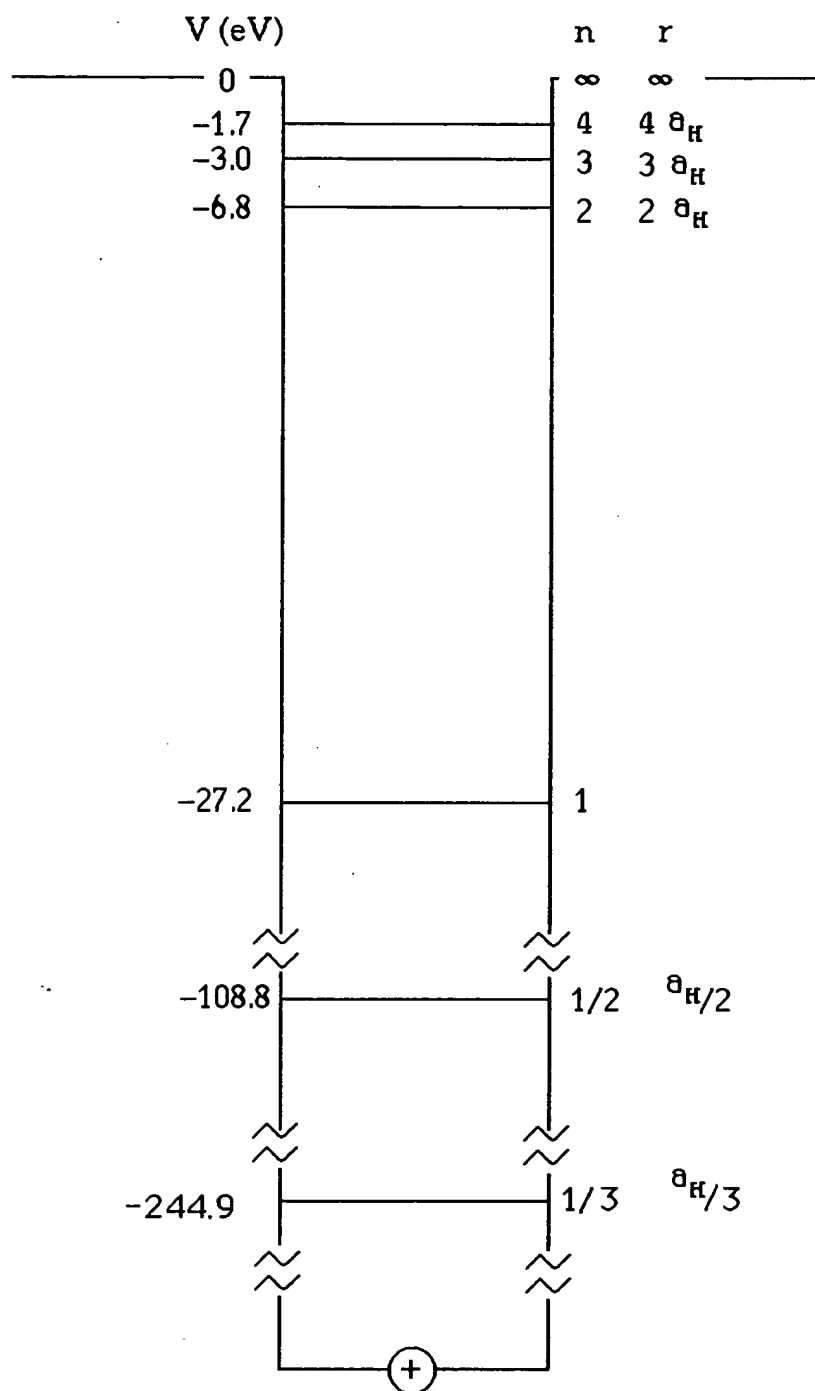
increased by m with the absorption of an energy hole of $m \times 27.2 \text{ eV}$. The potential energy decreases by this energy; thus, energy is conserved. However, the force balance equation is not initially satisfied as the effective nuclear charge increases by m . Further energy is emitted as force balance is achieved at the final radius. By replacing the initial radius with the final radius, and by increasing the charge by m in Eq.

(5.12).

$$[p+m]^3 \frac{\hbar^2}{m_e a_H^3} = [p+m]^2 \frac{((p+m)e)e}{4\pi\epsilon_0 a_H^2} \quad (5.14)$$

force balance is achieved and the orbitsphere is non-radiative. The energy balance for $m=1$ is as follows. An initial energy of 27.21 eV is transferred as the energy hole absorption event. This increases the effective nuclear charge by one and decreases the potential by 27.21 eV . More energy is emitted until the total energy released is $[(p+1)^2 - p^2] \times 13.6 \text{ eV}$. The potential energy diagram of the electron is given in Figure 5.1.

Figure 5.1. Potential Energy well of a Hydrogen Atom.



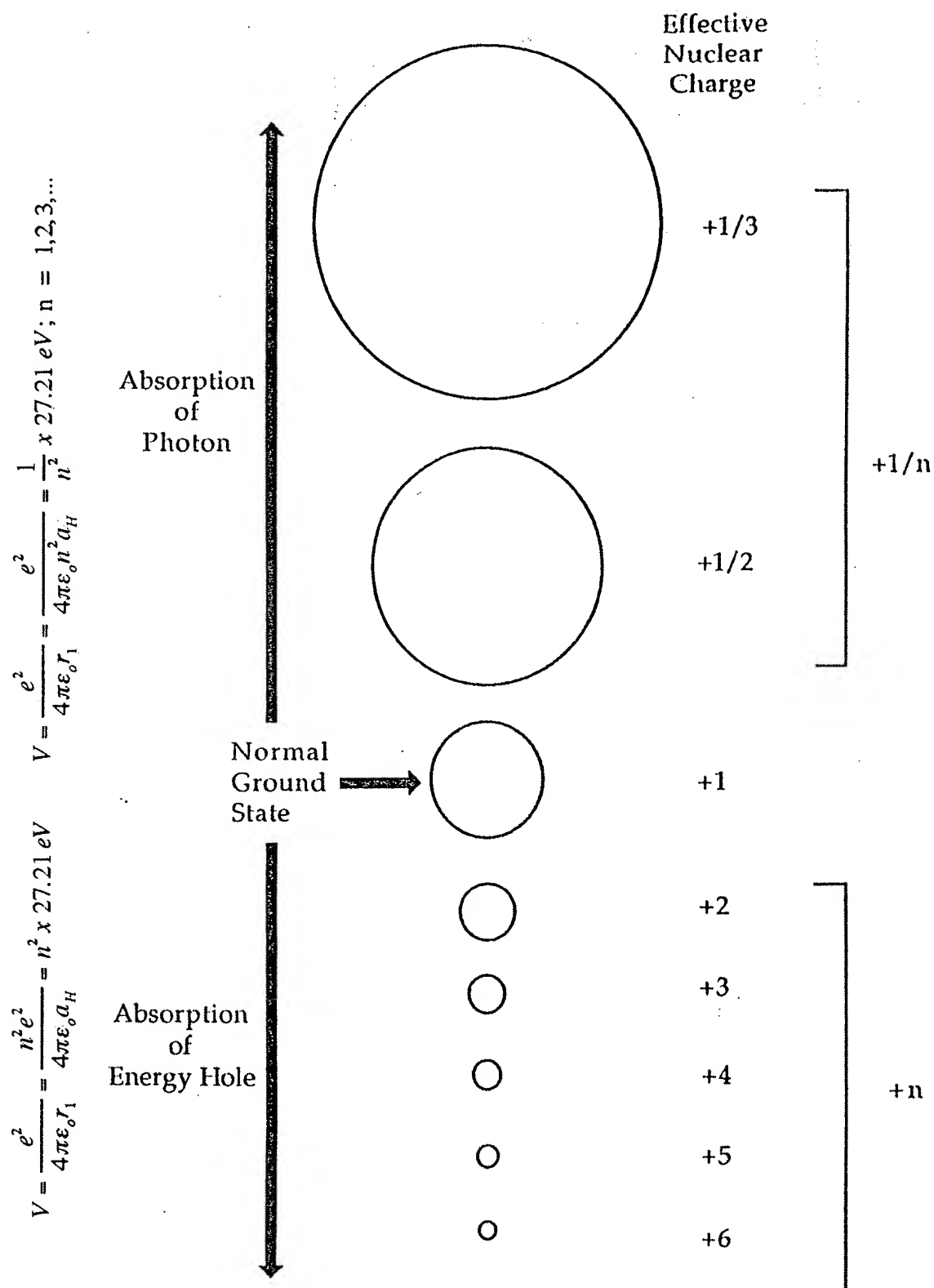
The energy hole ($m \times 27.21 \text{ eV}$) required to cause a hydrogen atom to undergo a transition reaction to form a given hydrino atom ($H\left(\frac{a_H}{m+1}\right)$) as well as the corresponding radius ($\frac{a_H}{m+1}$), effective nuclear charge ($m+1$) and energy parameters of several states of atomic hydrogen are given in Table 5.1.

Table 5.1. Principal quantum number, radius, potential energy, kinetic energy, effective nuclear charge, energy hole required to form the hydrino from atomic hydrogen ($n=1$), and hydrino binding energy, respectively, for several states of hydrogen.

$H(n)$	R	$V(\text{eV})$	$T(\text{eV})$	Z_{eff}	Energy Hole (eV)	Binding Energy (eV)
1	a_H	-27.2	13.6	1	0	13.6
$\frac{1}{2}$	$\frac{a_H}{2}$	-108.8	54.4	2	27.2	54.4
$\frac{1}{3}$	$\frac{a_H}{3}$	-244.9	122.4	3	54.4	122.4
$\frac{1}{4}$	$\frac{a_H}{4}$	-435.4	217.7	4	81.6	217.7
$\frac{1}{5}$	$\frac{a_H}{5}$	-680.2	340.1	5	108.8	340.1
$\frac{1}{6}$	$\frac{a_H}{6}$	-979.6	489.6	6	136.1	489.6
$\frac{1}{7}$	$\frac{a_H}{7}$	-1333.3	666.4	7	163.3	666.4
$\frac{1}{8}$	$\frac{a_H}{8}$	-1741.4	870.4	8	190.5	870.4
$\frac{1}{9}$	$\frac{a_H}{9}$	-2204.0	1101.6	9	217.7	1101.6
$\frac{1}{10}$	$\frac{a_H}{10}$	-2721.0	1360.5	10	244.9	1360.5

The size of the electron orbitsphere as a function of potential energy is given in Figure 5.2.

Figure 5.2. Quantized sizes of hydrogen atoms.



CATALYSTS

A catalytic system is provided by the ionization of t electrons from an atom each to a continuum energy level such that the sum of the ionization energies of the t electrons is approximately $m \times 27.2 \text{ eV}$ where m is an integer. One such catalytic system involves cesium. The first and second ionization energies of cesium are 3.89390 eV and 23.15745 eV , respectively [3]. The double ionization ($t=2$) reaction of Cs to Cs^{2+} , then, has a net enthalpy of reaction of 27.05135 eV , which is equivalent to $m=1$ in Eq. (5.5).

$$27.05135 \text{ eV} + \text{Cs}(m) + H\left[\frac{a_H}{p}\right] \rightarrow \text{Cs}^{2+} + 2e^- + H\left[\frac{a_H}{(p+1)}\right] + [(p+1)^2 - p^2] \times 13.6 \text{ eV} \quad (5.15)$$

$$\text{Cs}^{2+} + 2e^- \rightarrow \text{Cs}(m) + 27.05135 \text{ eV} \quad (5.16)$$

And, the overall reaction is

$$H\left[\frac{a_H}{p}\right] \rightarrow H\left[\frac{a_H}{(p+1)}\right] + [(p+m)^2 - p^2] \times 13.6 \text{ eV} \quad (5.17)$$

where $m=1$ in Eq. (5.17). The energy given off during catalysis is much greater than the energy lost to the catalyst. The energy released is large as compared to conventional chemical reactions. For example, when hydrogen and oxygen gases undergo combustion to form water



the known enthalpy of formation of water is $\Delta H_f = -286 \text{ kJ/mole}$ or 1.48 eV per hydrogen atom. By contrast, each ($n=1$) ordinary hydrogen atom undergoing catalysis releases a net of 40.8 eV . Moreover, further catalytic transitions may occur: $n = \frac{1}{2} \rightarrow \frac{1}{3}$, $\frac{1}{3} \rightarrow \frac{1}{4}$, $\frac{1}{4} \rightarrow \frac{1}{5}$, and so on. Once catalysis begins, hydrinos autocatalyze further in a process called disproportionation discussed in the Disproportionation of Energy States section. This mechanism is similar to that of an inorganic ion catalysis. But, hydrino catalysis should have a higher reaction rate than that of the inorganic ion catalyst due to the better match of the enthalpy to $m \cdot 27.2 \text{ eV}$.

Hydrogen catalysts capable of providing a net enthalpy of reaction of approximately $m \times 27.2 \text{ eV}$ where m is an integer to produce hydrino whereby t electrons are ionized from an atom or ion are given in Table 5.2. The atoms or ions given in the first column are ionized to provide the net enthalpy of reaction of $m \times 27.2 \text{ eV}$ given in the tenth column where m is given in the eleventh column. The electrons which are ionized are given with the ionization potential (also called ionization energy or binding energy). The ionization potential of the n th electron of the atom or ion is designated by IP_n and is given by the CRC [3]. That is for example, $\text{Cs} + 3.89390 \text{ eV} \rightarrow \text{Cs}^+ + e^-$ and $\text{Cs}^+ + 23.15745 \text{ eV} \rightarrow \text{Cs}^{2+} + e^-$. The first ionization potential, $IP_1 = 3.89390 \text{ eV}$, and the second ionization potential, $IP_2 = 23.15745 \text{ eV}$, are given in the second and third columns, respectively. The net enthalpy of reaction for the double ionization of Cs is 27.05135 eV as given in the tenth column, and $m=1$ in Eq. (5.5) as given in the eleventh column.

Table 5.2. Hydrogen Catalysts.

Catalyst	IP1	IP2	IP3	IP4	IP5	IP6	IP7	IP8	Enthalpy	m
Li	5.39172	75.6402							81.032	3
Be	9.32263	18.2112							27.534	1
K	4.34066	31.63	45.806						81.777	3
Ca	6.11316	11.8717	50.9131	67.27					136.17	5
Ti	6.8282	13.5755	27.4917	43.267	99.3				190.46	7
V	6.7463	14.66	29.311	46.709	65.2817				162.71	6
Cr	6.76664	16.4857	30.96						54.212	2
Mn	7.43402	15.64	33.668	51.2					107.94	4
Fe	7.9024	16.1878	30.652						54.742	2
Fe	7.9024	16.1878	30.652	54.8					109.54	4
Co	7.881	17.083	33.5	51.3					109.76	4
Co	7.881	17.083	33.5	51.3	79.5				189.26	7
Ni	7.6398	18.1688	35.19	54.9	76.06				191.96	7
Ni	7.6398	18.1688	35.19	54.9	76.06	108			299.96	11
Cu	7.72638	20.2924							28.019	1
Zn	9.39405	17.9644							27.358	1
Zn	9.39405	17.9644	39.723	59.4	82.6	108	134	174	625.08	23
As	9.8152	18.633	28.351	50.13	62.63	127.6			297.16	11
Se	9.75238	21.19	30.8204	42.945	68.3	81.7	155.4		410.11	15
Kr	13.9996	24.3599	36.95	52.5	64.7	78.5			271.01	10
Kr	13.9996	24.3599	36.95	52.5	64.7	78.5	111		382.01	14
Rb	4.17713	27.285	40	52.6	71	84.4	99.2		378.66	14
Rb	4.17713	27.285	40	52.6	71	84.4	99.2	136	514.66	19
Sr	5.69484	11.0301	42.89	57	71.6				188.21	7

Nb	6.75885	14.32	25.04	38.3	50.55				134.97	5
Mo	7.09243	16.16	27.13	46.4	54.49	68.8276			151.27	8
Mo	7.09243	16.16	27.13	46.4	54.49	68.8276	125.664	143.6	489.36	18
Pd	8.3369	19.43							27.767	1
Sn	7.34381	14.6323	30.5026	40.735	72.28				165.49	6
Te	9.0096	18.6							27.61	1
Te	9.0096	18.6	27.96						55.57	2
Cs	3.8939	23.1575							27.051	1
Ce	5.5387	10.85	20.198	36.758	65.55				138.89	5
Ce	5.5387	10.85	20.198	36.758	65.55	77.6			216.49	8
Pr	5.464	10.55	21.624	38.98	57.53				134.15	5
Sm	5.6437	11.07	23.4	41.4					81.514	3
Gd	6.15	12.09	20.63	44					82.87	3
Dy	5.9389	11.67	22.8	41.47					81.879	3
Pb	7.41666	15.0322	31.9373						54.386	2
Pt	8.9587	18.563							27.522	1
He+		54.4178							54.418	2
Na+		47.2864	71.6200	98.91					217.816	8
Rb+		27.285							27.285	1
Fe3+				54.8					54.8	2
Mo2+			27.13						27.13	1
Mo4+					54.49				54.49	2
In3+				54					54	2
Xe+		21.20979	32.1230						53.332792	

An additional catalytic system involving potassium metal is provided by the ionization of t electrons from a potassium atom each to a continuum energy level such that the sum of the ionization energies of the t electrons is approximately $mX27.2\text{ eV}$ where m is an integer. The first, second, and third ionization energies of potassium are 4.34066 eV , 31.63 eV , 45.806 eV , respectively [3]. The triple ionization ($t=3$) reaction of K to K^{3+} , then, has a net enthalpy of reaction of 81.7426 eV , which is equivalent to $m=3$ in Eq. (5.5).

$$81.7426\text{ eV} + K(m) + H\left[\frac{a_H}{p}\right] \rightarrow K^{3+} + 3e^- + H\left[\frac{a_H}{(p+3)}\right] + [(p+3)^2 - p^2]X13.6\text{ eV} \quad (5.19)$$

$$K^{3+} + 3e^- \rightarrow K(m) + 81.7426\text{ eV} \quad (5.20)$$

And, the overall reaction is

$$H\left[\frac{a_H}{p}\right] \rightarrow H\left[\frac{a_H}{(p+3)}\right] + [(p+3)^2 - p^2]X13.6\text{ eV} \quad (5.21)$$

Potassium ions can also provide a net enthalpy of a multiple of that

of the potential energy of the hydrogen atom. The second ionization energy of potassium is 31.63 eV ; and K^+ releases 4.34 eV when it is reduced to K . The combination of reactions K^+ to K^{2+} and K^+ to K , then, has a net enthalpy of reaction of 27.28 eV , which is equivalent to $m=1$ in Eq. (5.5).

$$27.28 \text{ eV} + K^+ + K^+ + H\left[\frac{a_H}{p}\right] \rightarrow K + K^{2+} + H\left[\frac{a_H}{(p+1)}\right] + [(p+1)^2 - p^2] \times 13.6 \text{ eV} \quad (5.22)$$

$$K + K^{2+} \rightarrow K^+ + K^+ + 27.28 \text{ eV} \quad (5.23)$$

The overall reaction is

$$H\left[\frac{a_H}{p}\right] \rightarrow H\left[\frac{a_H}{(p+1)}\right] + [(p+1)^2 - p^2] \times 13.6 \text{ eV} \quad (5.24)$$

Rubidium ions can also provide a net enthalpy of a multiple of that of the potential energy of the hydrogen atom. The second ionization energy of rubidium is 27.28 eV . The reaction Rb^+ to Rb^{2+} has a net enthalpy of reaction of 27.28 eV , which is equivalent to $m=1$ in Eq. (5.5).

$$27.28 \text{ eV} + Rb^+ + H\left[\frac{a_H}{p}\right] \rightarrow Rb^{2+} + e^- + H\left[\frac{a_H}{(p+1)}\right] + [(p+1)^2 - p^2] \times 13.6 \text{ eV} \quad (5.25)$$

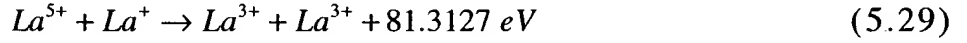
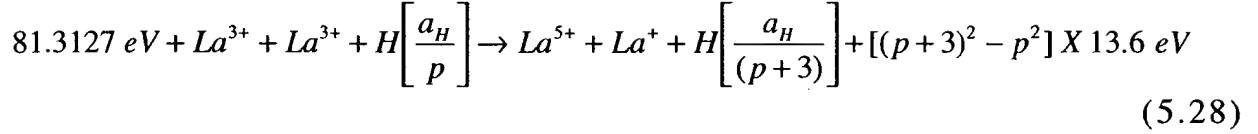
$$Rb^{2+} + e^- \rightarrow Rb^+ + 27.28 \text{ eV} \quad (5.26)$$

The overall reaction is

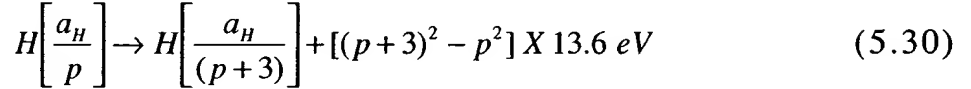
$$H\left[\frac{a_H}{p}\right] \rightarrow H\left[\frac{a_H}{(p+1)}\right] + [(p+1)^2 - p^2] \times 13.6 \text{ eV} \quad (5.27)$$

In another example, a catalytic system transfers two electrons from one ion to another such that the sum of the total ionization energy of the electron donating species minus the total ionization energy of the electron accepting species equals approximately $m \times 27.2 \text{ eV}$ where m is an integer. One such catalytic system involves lanthanum. The only stable oxidation state of lanthanum is La^{3+} . The fourth and fifth ionization energies of lanthanum are 49.95 eV and 61.6 eV , respectively. The third and second ionization energies of lanthanum are 19.1773 eV and 11.060 eV , respectively [3]. The combination of reactions La^{3+} to La^{5+} and La^{3+} to La^+ , then, has a net enthalpy of reaction of 81.3127 eV , which is

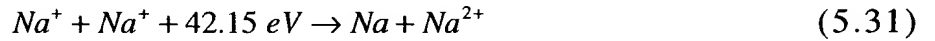
equivalent to $m=3$ in Eq. (5.5).



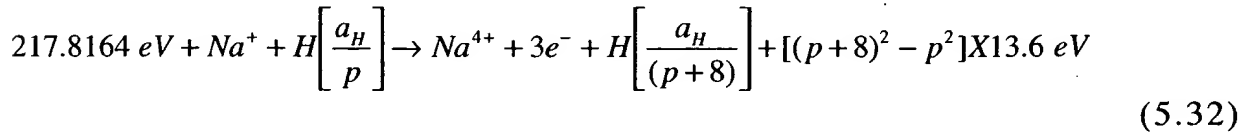
The overall reaction is



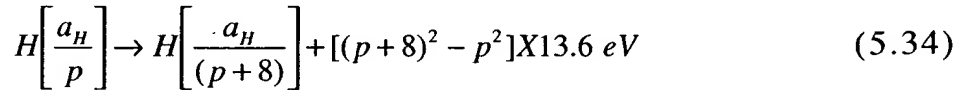
For sodium, no electrocatalytic reaction of approximately 27.21 eV is possible by the transfer of an electron between two Na^+ ions as is the case with K^+ . For example, 42.15 eV of energy is absorbed by the reverse of the reaction given in Eq. (5.23) where Na^+ replaces K^+ :



However a catalytic system is provided by the ionization of 3 electrons from Na^+ to a continuum energy level such that the sum of the ionization energies of the 3 electrons is approximately $m \times 27.2 \text{ eV}$ where m is an integer. The second, third, and fourth ionization energies of sodium are 47.2864 eV, 71.6200 eV, and 98.91 eV, respectively [3]. The triple ionization reaction of Na^+ to Na^{4+} , then, has a net enthalpy of reaction of 217.8164 eV, which is equivalent to $m=8$ in Eq. (5.5).

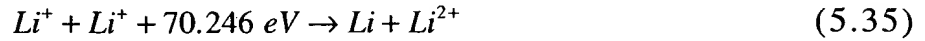


And, the overall reaction is



For lithium, no electrocatalytic reaction of approximately 27.21 eV is possible by the transfer of an electron between two Li^+ ions as is the case

with K^+ . For example, 70.246 eV of energy is absorbed by the reverse of the reaction given in Eq. (5.23) where Li^+ replaces K^+ :



However, lithium metal is a catalyst as shown in Table 5.2.

DISPROPORTIONATION OF ENERGY STATES

Lower-energy hydrogen atoms, **hydrinos**, can act as a source of energy holes because each of the metastable excitation, resonance excitation, and ionization energy of a hydrino atom is $m \times 27.2\text{ eV}$ (Eq. (5.5)). The transition reaction mechanism of a first hydrino atom affected by a second hydrino atom involves the resonant coupling between the atoms of m degenerate multipoles each having 27.21 eV of potential energy. (See the Energy Hole as a Multipole Expansion section). The energy transfer of $m \times 27.2\text{ eV}$ from the first hydrino atom to the second hydrino atom causes the central field of the first to increase by m and the electron of the first to drop m levels lower from a radius of $\frac{a_H}{p}$ to a

radius of $\frac{a_H}{p+m}$. The second lower-energy hydrogen is excited to a metastable state, excited to a resonance state, or ionized by the resonant energy transfer. The resonant transfer may occur in multiple stages. For example, a nonradiative transfer by multipole coupling may occur wherein the central field of the first increases by m , then the electron of the first drops m levels lower from a radius of $\frac{a_H}{p}$ to a radius of $\frac{a_H}{p+m}$ with further resonant energy transfer. The energy transferred by multipole coupling may occur by a mechanism that is analogous to photon absorption involving an excitation to a virtual level. Or, the energy transferred by multipole coupling during the electron transition of the first hydrino atom may occur by a mechanism that is analogous to two photon absorption involving a first excitation to a virtual level and a second excitation to a resonant or continuum level [4-6]. The transition energy greater than the energy transferred to the second hydrino atom may appear as a photon in a vacuum medium.

For example, $H\left[\frac{a_H}{4}\right]$ may serve as a source of energy holes to form $H\left[\frac{a_H}{5}\right]$. The transition of $H\left[\frac{a_H}{4}\right]$ to $H\left[\frac{a_H}{5}\right]$ induced by a resonance transfer of 27.21 eV , $m=1$ in Eq. (5.5) with a metastable state excited in $H\left[\frac{a_H}{4}\right]$ is

represented by

$$27.2 \text{ eV} + H\left[\frac{a_H}{4}\right] + H\left[\frac{a_H}{4}\right] \rightarrow H^*\left[\frac{a_H}{4}\right] + H\left[\frac{a_H}{5}\right] + 27.2 \text{ eV} + 95.2 \text{ eV} \quad (5.36)$$

$$H^*\left[\frac{a_H}{4}\right] \rightarrow H\left[\frac{a_H}{4}\right] + 27.2 \text{ eV} \quad (5.37)$$

$$H\left[\frac{a_H}{4}\right] \rightarrow H\left[\frac{a_H}{5}\right] + 95.2 \text{ eV} + 27.2 \text{ eV} \quad (5.38)$$

$H\left[\frac{a_H}{4}\right]$ may serve as both a source of energy holes and a reactant to form $H\left[\frac{a_H}{3}\right]$ and $H\left[\frac{a_H}{6}\right]$. The transition of $H\left[\frac{a_H}{4}\right]$ to $H\left[\frac{a_H}{6}\right]$ induced by a multipole resonance transfer of 54.4 eV , $m=2$ in Eq. (5.5) and a transfer of 40.8 eV with a resonance state of $H\left[\frac{a_H}{3}\right]$ excited in $H\left[\frac{a_H}{4}\right]$ is represented by

$$H\left[\frac{a_H}{4}\right] + H\left[\frac{a_H}{4}\right] \rightarrow H\left[\frac{a_H}{6}\right] + H\left[\frac{a_H}{3}\right] + 176.8 \text{ eV} \quad (5.39)$$

In general, the transition of $H\left[\frac{a_H}{p}\right]$ to $H\left[\frac{a_H}{p+m}\right]$ induced by a resonance transfer of $m \cdot 27.21 \text{ eV}$ (Eq. (5.5)) with a metastable state excited in $H\left[\frac{a_H}{p'}\right]$ is represented by

$$m \cdot 27.2 \text{ eV} + H\left[\frac{a_H}{p'}\right] + H\left[\frac{a_H}{p}\right] \rightarrow H^*\left[\frac{a_H}{p'}\right] + H\left[\frac{a_H}{p+m}\right] + [(p+m)^2 - p^2] \times 13.6 \text{ eV} \quad (5.40)$$

$$H^*\left[\frac{a_H}{p'}\right] \rightarrow H\left[\frac{a_H}{p'}\right] + m \cdot 27.2 \text{ eV} \quad (5.41)$$

And, the overall reaction is

$$H\left[\frac{a_H}{p}\right] \rightarrow H\left[\frac{a_H}{p+m}\right] + [(p+m)^2 - p^2] \times 13.6 \text{ eV} \quad (5.42)$$

where p , p' , and m are integers and the asterisk represents an excited metastable state.

The transition of $H\left[\frac{a_H}{p}\right]$ to $H\left[\frac{a_H}{p+m}\right]$ induced by a multipole

resonance transfer of $m \cdot 27.21 \text{ eV}$ (Eq. (5.5)) and a transfer of $[(p')^2 - (p' - m')^2] \times 13.6 \text{ eV} - m \cdot 27.2 \text{ eV}$ with a resonance state of $H\left[\frac{a_H}{p' - m'}\right]$

excited in $H\left[\frac{a_H}{p'}\right]$ is represented by

$$H\left[\frac{a_H}{p'}\right] + H\left[\frac{a_H}{p}\right] \rightarrow H\left[\frac{a_H}{p' - m'}\right] + H\left[\frac{a_H}{p + m}\right] + [((p + m)^2 - p^2) - (p'^2 - (p' - m')^2)] \times 13.6 \text{ eV} \quad (5.43)$$

where p , p' , m , and m' are integers.

The second lower-energy hydrogen may be ionized by the resonant energy transfer. For an example, the equation for the absorption of an energy hole of 27.21 eV , $m=1$ in Eq. (5.5), during the transition cascade for the third cycle of the hydrogen-type atom, $H\left[\frac{a_H}{3}\right]$, with the hydrogen-type atom, $H\left[\frac{a_H}{2}\right]$, that is ionized as the source of energy holes that causes the transition is represented by

$$27.21 \text{ eV} + H\left[\frac{a_H}{2}\right] + H\left[\frac{a_H}{3}\right] \rightarrow H^+ + e^- + H\left[\frac{a_H}{4}\right] + [4^2 - 3^2] \times 13.6 \text{ eV} - 27.21 \text{ eV} \quad (5.44)$$

$$H^+ + e^- \rightarrow H\left[\frac{a_H}{1}\right] + 13.6 \text{ eV} \quad (5.45)$$

And, the overall reaction is

$$H\left[\frac{a_H}{2}\right] + H\left[\frac{a_H}{3}\right] \rightarrow H\left[\frac{a_H}{1}\right] + H\left[\frac{a_H}{4}\right] + [4^2 - 3^2 - 4] \times 13.6 \text{ eV} + 13.6 \text{ eV} \quad (5.46)$$

The general equation for the absorption of an energy hole of 27.21 eV , $m=1$ in Eq. (5.5), during the transition cascade for the p th cycle of the hydrogen-type atom, $H\left[\frac{a_H}{p}\right]$, with the hydrogen-type atom, $H\left[\frac{a_H}{m'}\right]$, that is ionized as the source of energy holes that causes the transition is represented by

$$27.21 \text{ eV} + H\left[\frac{a_H}{m'}\right] + H\left[\frac{a_H}{p}\right] \rightarrow H^+ + e^- + H\left[\frac{a_H}{(p+1)}\right] + [(p+1)^2 - p^2] \times 13.6 \text{ eV} - (m'^2 - 2) \times 13.6 \text{ eV} \quad (5.47)$$

$$H^+ + e^- \rightarrow H\left[\frac{a_H}{1}\right] + 13.6 \text{ eV} \quad (5.48)$$

And, the overall reaction is

$$H\left[\frac{a_H}{m'}\right] + H\left[\frac{a_H}{p}\right] \rightarrow H\left[\frac{a_H}{1}\right] + H\left[\frac{a_H}{(p+1)}\right] + [2p+1-m'^2] \times 13.6 \text{ eV} + 13.6 \text{ eV} \quad (5.49)$$

Transitions to nonconsecutive energy levels involving the absorption of an energy hole of an integer multiple of 27.21 eV are possible. Lower-energy hydrogen atoms, **hydrinos**, can act as a source of energy holes that can cause transition reactions with the absorption of energy holes each of $m \times 27.2 \text{ eV}$ (Eq. (5.5)). Thus, the transition cascade for the p th cycle of the hydrogen-type atom, $H\left[\frac{a_H}{p}\right]$, with the hydrogen-type atom, $H\left[\frac{a_H}{m'}\right]$, that is ionized as the source of energy holes that causes the transition is represented by

$$m \times 27.21 \text{ eV} + H\left[\frac{a_H}{m'}\right] + H\left[\frac{a_H}{p}\right] \rightarrow H^+ + e^- + H\left[\frac{a_H}{(p+m)}\right] + [(p+m)^2 - p^2 - (m'^2 - 2m)] \times 13.6 \text{ eV} \quad (5.50)$$

$$H^+ + e^- \rightarrow H\left[\frac{a_H}{1}\right] + 13.6 \text{ eV} \quad (5.51)$$

And, the overall reaction is

$$H\left[\frac{a_H}{m'}\right] + H\left[\frac{a_H}{p}\right] \rightarrow H\left[\frac{a_H}{1}\right] + H\left[\frac{a_H}{(p+m)}\right] + [2pm + m^2 - m'^2] \times 13.6 \text{ eV} + 13.6 \text{ eV} \quad (5.52)$$

Disproportionation may be the predominant mechanism of hydrogen electronic transitions to lower energy levels of interstellar hydrogen and hydrinos. Hydrogen transitions to electronic energy levels below the "ground" state corresponding to fractional quantum numbers exactly match the spectral lines of the extreme ultraviolet background of interstellar space. This assignment given in the Spectral Data of Hydrinos from the Dark Interstellar Medium and Spectral Data of Hydrinos, Dihydrinos, and Hydrino Hydride Ions from the Sun section resolves the paradox of the identity of dark matter and accounts for many celestial observations such as: diffuse H α emission is ubiquitous throughout the

Galaxy, and widespread sources of flux shortward of 912 \AA are required [7]. The energy of the emission line for the transition given by Eqs. (5.44-5.46) involving the absorption of an energy hole of 27.21 eV , $m=1$ in Eq. (5.5), is 40.8 eV .

$$H\left[\frac{a_H}{3}\right] \xrightarrow{H\left[\frac{a_H}{2}\right]} H\left[\frac{a_H}{4}\right] \quad (5.53)$$

The energy of the emission line for the transition given by Eqs. (5.50-5.52) where $m=2$, $m'=2$, and $p=1$ involving the absorption of an energy hole of $2 \times 27.21 \text{ eV}$, $m=2$ in Eq. (5.5), is 54.4 eV .

$$H\left[\frac{a_H}{1}\right] \xrightarrow{H\left[\frac{a_H}{2}\right]} H\left[\frac{a_H}{3}\right] \quad (5.54)$$

Stars are sources of lower-energy hydrogen for reactants for interstellar disproportionation reactions given by Eqs. (5.47-5.49). The source of energy holes in stellar production are hydrogen and singly ionized helium, He^+ . The ionization energy of hydrogen is 13.6 eV . Disproportionation can occur between three hydrogen atoms whereby two atoms provide an energy hole of 27.21 eV for the third hydrogen atom. Thus, the transition cascade for the p th cycle of the hydrogen-type atom, $H\left[\frac{a_H}{p}\right]$, with two hydrogen atoms, $H\left[\frac{a_H}{1}\right]$, as the source of energy holes that causes the transition is represented by

$$27.21 \text{ eV} + 2H\left[\frac{a_H}{1}\right] + H\left[\frac{a_H}{p}\right] \rightarrow 2H^+ + 2e^- + H\left[\frac{a_H}{(p+1)}\right] + [(p+1)^2 - p^2] \times 13.6 \text{ eV} \quad (5.55)$$

$$2H^+ + 2e^- \rightarrow 2H\left[\frac{a_H}{1}\right] + 27.21 \text{ eV} \quad (5.56)$$

And, the overall reaction is

$$H\left[\frac{a_H}{p}\right] \rightarrow H\left[\frac{a_H}{(p+1)}\right] + [(p+1)^2 - p^2] \times 13.6 \text{ eV} \quad (5.57)$$

Helium II is one of the catalysts that can cause a transition reaction because the second ionization energy is 54.4 eV , $m=2$ in Eq. (5.5). Thus, the transition cascade for the p th cycle is represented by

$$54.4 \text{ eV} + He^+ + H\left[\frac{a_H}{p}\right] \rightarrow He^{2+} + e^- + H\left[\frac{a_H}{(p+2)}\right] + [(p+2)^2 - p^2] \times 13.6 \text{ eV} \quad (5.58)$$

$$He^{2+} + e^- \rightarrow He^+ + 54.4 \text{ eV} \quad (5.59)$$

And, the overall reaction is

$$H\left[\frac{a_H}{p}\right] \rightarrow H\left[\frac{a_H}{(p+2)}\right] + [(p+2)^2 - p]X13.6 \text{ eV} \quad (5.60)$$

Also, Helium II is a catalyst that can cause a transition reaction with the absorption of an energy hole of 27.21 eV, $m=1$ in Eq. (5.5). Thus, the transition cascade for the p th cycle is represented by

$$27.21 \text{ eV} + He^+ + H\left[\frac{a_H}{p}\right] \rightarrow He^{2+} + e^- + H\left[\frac{a_H}{(p+1)}\right] + [(p+1)^2 - p^2]X13.6 \text{ eV} - 27.21 \text{ eV} \quad (5.61)$$

$$He^{2+} + e^- \rightarrow He^+ + 54.4 \text{ eV} \quad (5.62)$$

And, the overall reaction is

$$H\left[\frac{a_H}{p}\right] \rightarrow H\left[\frac{a_H}{(p+1)}\right] + [(p+1)^2 - p]X13.6 \text{ eV} \quad (5.63)$$

The majority of the solar power can be attributed to disproportionation reactions as given in the Spectral Data of Hydrinos from the Dark Interstellar Medium and Spectral Data of Hydrinos, Dihydrinos, and Hydrino Hydride Ions from the Sun section. This assignment resolves the solar neutrino problem and the mystery of the cause of sunspots and other solar activity and why the Sun emits X-rays. It also provides the reason for the abrupt change in the speed of sound and transition from "radiation zone" to "convection zone" at a radius of 0.7 the solar radius, $0.7R_s$.

INTERSTELLAR DISPROPORTIONATION RATE

Disproportionation may be the predominant mechanism of hydrogen electronic transitions to lower energy levels of interstellar hydrogen and hydrinos. The reaction rate is dependent on the collision rate between the reactants and the coupling factor for resonant energy transfer. The collision rate can be calculated by determining the collision frequency. The collision frequency, f , and the mean free path, ℓ , for a gas containing n_u spherical particles per unit volume, each with radius r and velocity v is given by Bueche [8].

$$f = 4\pi\sqrt{2}n_ur^2v \quad (5.64)$$

$$\ell = \frac{1}{4\pi\sqrt{2}n_u r^2} \quad (5.65)$$

The average velocity, v_{avg} , can be calculated from the temperature, T , [8].

$$\frac{1}{2}m_H v_{avg}^2 = \frac{3}{2}kT \quad (5.66)$$

where k is Boltzmann's constant. Substitution of Eq. (5.66) into Eq. (5.64) gives the collision rate, $f_H\left[\frac{a_H}{p}\right]$, in terms of the temperature, T , the number of hydrogen or hydrino atoms per unit volume, n_H , and the radius of each hydrogen atom or hydrino, $\frac{a_H}{p}$.

$$f_H\left[\frac{a_H}{p}\right] = 4\pi\sqrt{2}n_H\left(\frac{a_H}{p}\right)^2\sqrt{\frac{3kT}{m_H}} \quad (5.67)$$

The rate constant of the disproportionation reaction, $k_{m,m',p}$, to the transition reaction, Eqs. (5.44-5.52), is given by the product of the collision rate per atom, Eq. (5.67), and the coupling factor for resonant energy transfer, $g_{m,m',p}$.

$$k_{m,m',p} = g_{m,p}4\pi\sqrt{2}n_H\left(\frac{a_H}{p}\right)^2\sqrt{\frac{3kT}{m_H}} \quad (5.68)$$

The coupling factor for resonant energy transfer, $g_{m,m',p}$, can be determined from the experimental results of Labov and Bowyer [7]. Consider the case that $m=1$, $m'=2$, and $p=3$ in Eqs. (5.50-5.52); $T=50\text{ K}$, and the column density of hydrogen and hydrino atoms is estimated from typical values of the column density of H in diffuse hydrogen regions along the sight-line at $b=48$ deg. The intensity is calculated as the rate constant times the column density and equated to the experimental intensity of the 304 \AA line which is assigned in the Spectral Data of Hydrinos from the Dark Interstellar Medium and Spectral Data of Hydrinos, Dihydrinos, and Hydrino Hydride Ions from the Sun section as the $1/3 \rightarrow 1/4 H$ transition. This yields a value of $g_{m,m',p}$ in the range of 1 which is consistent with the efficiencies of dipole-dipole resonant energy transfers [9-12]. Thus, an estimate of the rate constant of the disproportionation reaction, $k_{m,m',p}$, to cause the transition reaction, Eqs. (5.44-5.52), is given by substitution of $g_{m,m',p}=1$ into Eq. (5.68).

$$k_{m,m',p} = 4\pi\sqrt{2}n_H\left(\frac{a_H}{p}\right)^2\sqrt{\frac{3kT}{m_H}} \text{ sec}^{-1} \quad (5.69)$$

The rate of the disproportionation reaction, $r_{m,m',p}$, to cause the transition reaction, Eqs. (5.44-5.52), is given by the product of the rate constant, $k_{m,m',p}$ given by Eq. (5.69), and the total number of hydrogen or hydrino

atoms, N_H .

$$r_{m,m',p} = N_H 4\pi \frac{1}{2} \sqrt{2} n_H \left(\frac{a_H}{p} \right)^2 \sqrt{\frac{3kT}{m_H}} \frac{\text{transitions}}{\text{sec}} \quad (5.70)$$

The factor of one half in Eq. (5.70) corrects for double counting of collisions [13]. The power, $P_{m,m',p}$, is given by the product of the rate of the transition, Eq. (5.70), and the energy of the transition, Eq. (5.49)

$$P_{m,m',p} = \frac{N_H^2}{V} \frac{4\pi}{\sqrt{2}} \left(\frac{a_H}{p} \right)^2 \sqrt{\frac{3kT}{m_H}} [2mp + m^2 - m'^2 + 1] \times 2.2 \times 10^{-18} \text{ W} \quad (5.71)$$

where V is the volume.

COULOMBIC ANNIHILATION FUSION (CAF)

The electric field of a hydrogen atom is zero for $r > r_n$, where r_n is the radius of the orbitsphere of the electron (See Figure 1.9). Thus, as the orbitsphere shrinks with transitions to lower-energy states, approaching nuclei experience a smaller electric barrier and the internuclear distance (between two deuterium or tritium atoms, for example) shrinks as well. As the internuclear separation decreases, fusion is more probable. In muon catalyzed fusion, for example, the internuclear separation is reduced by about 200 (the muon to electron mass ratio) and the fusion rate increases by about 80 orders of magnitude. In a catalytic system that produces energy holes of 27.21 eV, deuterium atoms can be repeatedly shrunk and the internuclear separation can be much smaller than the muon reduction. These smaller internuclear distances yield much higher fusion rates. The cold fusion process is hereafter referred to as Coulombic Annihilation Fusion (CAF).

It is important to note that the products of CAF are tritium, ^3H , and protons, ^1H . In hot fusion, deuterium nuclei collide randomly and produce about 50% ^3H plus ^1H and about 50% ^3He plus a neutron. In CAF, however, the nuclei are moving slowly and will collide in the most favored Coulombic arrangement—with the two protons as far from each other as possible. Thus, for CAF significantly more ^3H will be produced than ^3He .

NEW "GROUND" STATE

Hydrogen atoms can undergo transitions to energy states below the $n=1$ state until the potential energy of the proton is converted to relativistically corrected kinetic energy and total energy (the negative of the binding energy) and a state is formed which is stable to both radiation and nonradiative energy transfer. The potential energy V of the electron and the proton separated by the radial distance radius r_1 is,

$$V = \frac{-e^2}{4\pi\epsilon_0 r_1} \quad (5.72)$$

where the radius r_1 is the proton radius given by Eq. (28.1)

$$r_p = 1.3 \times 10^{-15} \text{ m} \quad (5.73)$$

Substitution of Eq.(5.73) into Eq.(5.72) gives the total potential energy V of the electron and the proton

$$V = \frac{-e^2}{4\pi\epsilon_0 r_p} = 1.1 \times 10^6 \text{ eV} \quad (5.74)$$

Without considering the relativistic mass, in the present case of an inverse squared central field, the binding energy and the kinetic energy are each equal to one half the potential energy [14]. Lorentzian transformations of special relativity apply for inertial frames moving at constant rectilinear relative velocity, and the relativistic correction applies only to the direction of relative motion, not the perpendicular direction. Mass in a circular orbit is constantly accelerating. The projection of the motion along each of the Cartesian axes is time harmonic with a $\frac{\pi}{2}$ relative phase shift. In this case, mass is not in constant

rectilinear motion. The relativistic invariance of the charge of the electron of e and the angular momentum of the electron of \hbar may be used to characterize the limiting $v=c$ case. Considering the consequences of special relativity, the size of a hydrogen atom in the true ground state is significantly larger than the size of a muonic atom and is limited not to be less than λ , the electron Compton wavelength bar,

$$\lambda = \frac{\hbar}{m_e c} = \alpha a_0 \quad (5.75)$$

since the tangential electron velocity (Eq. (1.56)) is the speed of light at this radius. As shown in the "SPACETIME FOURIER TRANSFORM OF THE ELECTRON FUNCTION" section, at light speed, there can be no motion transverse to the radius. The radial projection of the time harmonic motion of a point charge of a great circle becomes equivalent to a time harmonic oscillator moving along an axis of distance $2r_n$ in the direction of r . No radiation is possible. This result is also analogous to the case of a nonradiative harmonically expanding and contracting sphere as given by Abbott and Griffiths [15], Schott [16] and Pearle [17-18]. Nonradiative energy transfer is also forbidden since this requires conservation of angular momentum of the electron and the photon standing wave, and also no coupling mechanism exists in this case. Electronic transitions below the $H\left[\frac{a_H}{\alpha^{-1}}\right]$ state are not possible since no energy transfer mechanism is possible.

However, for this electronic state, it may be possible for the proton

to decay to gamma rays with the capture the electron. With electron capture, the electron orbitsphere superimposes that of the proton, and a neutral particle is formed that is energy deficient with respect to the neutron. To conserve spin, electron capture requires the concurrent capture of an electron antineutrino with decay to a photon and an electron neutrino as given in the Gravity section. Disproportionation reactions to the lowest-energy states of hydrogen followed by electron capture with gamma ray emission may be a source of nonthermal γ -ray bursts from interstellar regions [19]. Hydrinos present in neutron stars may effect Coulombic Annihilation Fusion. This may be the mechanism of principally gamma emission by neutron stars. With sufficient energy/mass release, a chain reaction of neutron decay to release electron antineutrinos which react with hydrinos according to Eq. (23.173) may be the cause of γ -ray bursts. Another more likely mechanism based on a particle of the Planck Mass is given in the Gravity section.

References

1. N. V. Sidgwick, The Chemical Elements and Their Compounds, Volume I, Oxford, Clarendon Press, (1950), p.17.
2. R. L. Mills, International Application Number: PCT/US96/07949, Lower-Energy Hydrogen Methods and Structures, January, 26, 1996; R. L. Mills, International Application Number: PCT/US98/14029, Inorganic Hydrogen Compounds, Separation Methods, and Fuel Applications, July 7, 1998.
3. David R. Linde, CRC Handbook of Chemistry and Physics, 79 th Edition, CRC Press, Boca Raton, Florida, (1998-9), p. 10-175.
4. Thompson, B. J., Handbook of Nonlinear Optics, Marcel Dekker, Inc., New York, (1996), pp. 497-548.
5. Shen, Y. R., The Principles of Nonlinear Optics, John Wiley & Sons, New York, (1984), pp. 203-210.
6. B. de Beauvoir, F. Nez, L. Julien, B. Cagnac, F. Biraben, D. Touahri, L. Hilico, O. Acef, A. Clairon, and J. J. Zondy, Physical Review Letters, Vol. 78, No. 3, (1997), pp. 440-443.
7. Labov, S., Bowyer, S., "Spectral observations of the extreme ultraviolet background", The Astrophysical Journal, 371, (1991), pp. 810-819.
8. Bueche, F. J., Introduction to Physics for Scientists and Engineers, McGraw-Hill Book Company, New York, (1986), pp. 261-265.
9. Morawetz, H., Science, 240, (1988), pp. 172-176.
10. Schnepf, O., Levy, M., J. Am. Chem. Soc., 84, (1962), pp. 172-177.
11. Wilkinson, F., Luminescence in Chemistry, Edited by E. J. Bowen, D.

- Van Nostrand Co. Ltd., London, (1968), pp. 155-182.
12. Förster, Th., Comparative Effects of Radiation, Report of a Conference held at the University of Puerto Rico, San Juan, February 15-19, (1960), sponsored by the National Academy of Sciences; National Research Council, Edited by Milton Burton, J. S. Kirby-Smith, and John L. Magee, John Wiley & Sons, Inc., New York pp. 300-325.
 13. Levine, I., Physical Chemistry, McGraw-Hill Book Company, New York, (1978), pp. 420-421.
 14. Fowles, G. R., Analytical Mechanics, Third Edition, Holt, Rinehart, and Winston, New York, (1977), pp. 154-156.
 15. T. A. Abbott and D. J. Griffiths, Am. J. Phys., Vol. 153, No. 12, (1985), pp. 1203-1211.
 16. G. A. Schott, Philos. Mag. Vol. 7, (1933), P. 752.
 17. P. Pearle, "Classical Electron Models", Electromagnetism: Paths to Research, Edited by D. Teplitz, Plenum, New York, (1982), Chp. 7.
 18. P. Pearle, Found. of Phys. Vol. 7, (1977), p. 931.
 19. Hurley, K., et. al., Nature, 372, (1994), pp. 652-654.